UNITED NATIONS EDUCATIONAL, SCIENTIFIC AND CULTURAL ORGANIZATION
INTERNATIONAL ATOMIC ENERGY AGENCY
INTERNATIONAL CENTRE FOR THEORETICAL PHYSICS
I.C.T.P., P.O. BOX 586, 34100 TRIESTE, ITALY, CABLE: CENTRATOM TRIESTE

SMR.998c - 12

Research Workshop on Condensed Matter Physics
30 June - 22 August 1997
MINIWORKSHOP ON
PATTERN FORMATION AND SPATIO-TEMPORAL CHAOS
28 JULY - 8 AUGUST 1997

"Numerical Experiments"

R. TORAL
Instituto Mediterraneo de Estudios Avanzados
Universitat de les Illes Balears
IMEDEA CSIC/UIB
Departament de Fisica
Facultat de Ciences
07071 Palma de Mallorca
SPAIN

These are preliminary lecture notes, intended only for distribution to participants.

NUMERICAL EXPERIMENTS

Raúl Toral

INSTITUTO MEDITERRANEO DE ESTUDIOS
AVANZADOS IMEDEA (CSIC–UIB)
CAMPUS UNIVERSITAT ILLES BALEARS
Palma de Mallorca (Spain)

Chris van den Broeck
Amitabha Chakrabarti
Roberto Deza
Rafael Gallego
Jordi Garcia-Ojalvo
James Gunton
Juan M. Gonzalez Parrondo
Ryoichi Kawai
Ana Lacasta
Sergio Mangioni
Catalina Mayol
Claudio Mirasso
Maxi San Miguel
Jose M. Sancho
Horacio Wio
...

OUTLINE

Phase Separation Dynamics

$$\Phi(\vec{r},t) = \rho_A(\vec{r},t) - \rho_B(\vec{r},t)$$

Conservation law:

$$m \equiv \frac{1}{V}\int_V d\vec{r}\Phi(\vec{r},t) \longrightarrow \frac{dm}{dt} = 0$$

Continuity equation:

$$\frac{\partial\Phi(\vec{r},t)}{\partial t} + \vec{\nabla}\cdot\vec{J}(\vec{r},t) = 0$$

Fick's law plus random thermal fluctuations:

$$\vec{J}(\vec{r},t) = -\Gamma\vec{\nabla}\mu + \vec{\eta}(\vec{r},t)$$

Γ is the *mobility*
Chemical potential μ:

$$\mu(\vec{r},t) = \frac{\delta\mathcal{H}([\Phi])}{\delta\Phi(\vec{r},t)}$$

Gaussian "noise" variables $\vec{\eta} = (\eta_1,\ldots,\eta_d)$

$$\langle\eta_k(\vec{r},t)\eta_{k'}(\vec{r}',t')\rangle = 2k_BT\delta_{k,k'}\delta(r-r')\delta(t-t')$$

Cahn-Hilliard-Cook (CHC) equation or model B

$$\frac{\partial\Phi(\vec{r},t)}{\partial t} = \nabla^2\left(\Gamma\frac{\delta\mathcal{H}([\Phi])}{\delta\Phi(\vec{r},t)}\right) + \xi(\vec{r},t)$$

where $\xi(\vec{r},t) = \vec{\nabla}\cdot\vec{\eta}(\vec{r},t)$

$$\beta\mathcal{H}([\Phi]) = \int d\vec{r}\left[\frac{-b}{2}\Phi(\vec{r})^2 + \frac{u}{4}\Phi(\vec{r})^4 + \frac{K}{2}|\vec{\nabla}\Phi(\vec{r})|^2\right]$$

$$\frac{\partial\Phi(\vec{r},t)}{\partial t} = \Gamma k_BT\nabla^2\left(-b\Phi + u\Phi^3 - K\nabla^2\Phi\right) + \xi(\vec{r},t)$$

Stochastic, nonlinear, partial differential equation.
Calls for numerical treatment.
Deterministic case: Euler method:

$$\Phi_i(t+h) = \Phi_i(t) + h\frac{\partial\Phi_i(t)}{\partial t}$$

Runge-Kutta methods.
Semi–implicit methods.

But need to deal with stochastic terms.
Dynamical Scaling

$$G(\vec{r},t) = \langle\Phi(\vec{r},t)\Phi(\vec{r}+\vec{r}',t)\rangle,$$

or, rather, its circular average:

$$G(r,t) = \frac{\int d\Omega G(\vec{r},t)}{\int d\Omega}$$

$$G(r,t) = g(r/R(t))$$

$$R(t) \sim t^a$$

Kardar, Parisi and Zhang (KPZ) model for surface growth.

$$\frac{\partial h(\vec{r},t)}{\partial t} = \nu\nabla^2 h(\vec{r},t) + \frac{\lambda}{2}(\nabla h)^2 + \eta(\vec{r},t)$$

$$\langle\eta(\vec{r},t)\eta(\vec{r}',t')\rangle = 2D\delta(\vec{r}-\vec{r}')\delta(t-t')$$

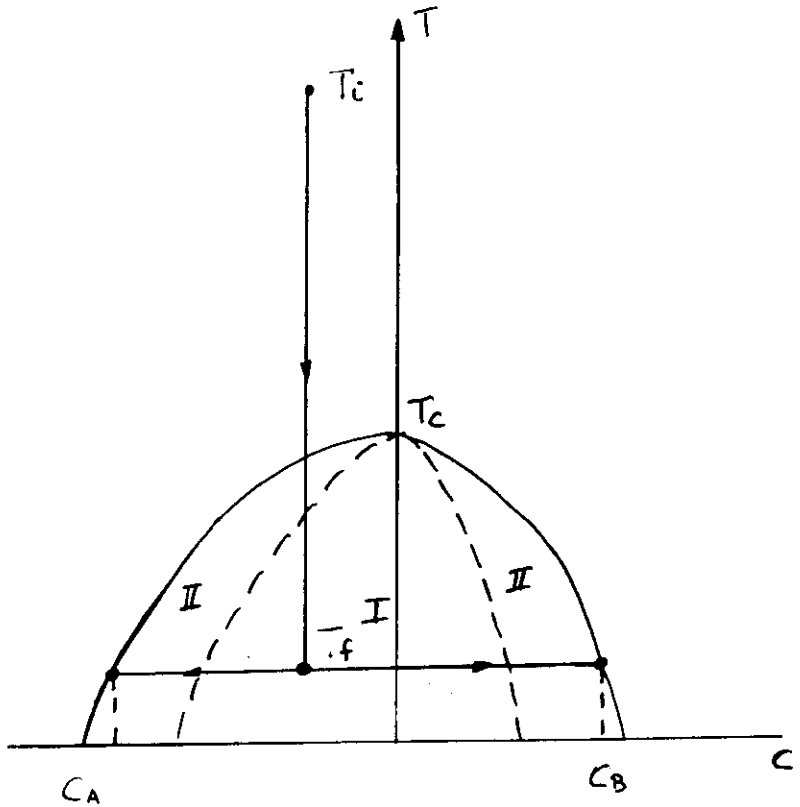

• SUDDEN QUENCH

I - SPINODAL DECOMPOSITION

II - NUCLEATION

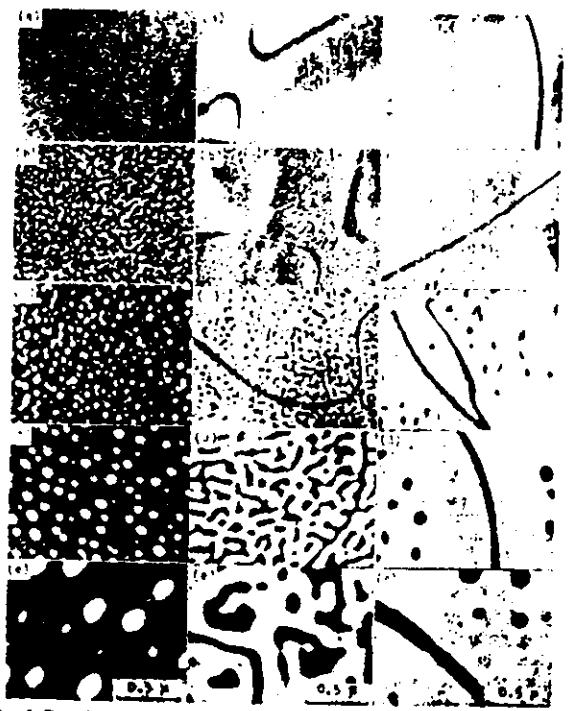

FIG. 3. Domain structures imaged with B_2 superlattice reflection in 23.0, 24.7 and 24.9 at% Al alloys, from left to right. The samples are quenched from 630 °C and annealed at 570 °C in the case of 23.0 and 24.7 at% Al alloys and at 568 °C in the case of 24.9 at% Al alloy. (a) As quenched; (b) annealed for 15 min in 23.0 and 24.9 at% Al and for 10 min in 24.7 at% Al alloy; (c) 100 min; (d) 1000 min; (e) 10000 min. (From Oki *et al.*, 1977.)

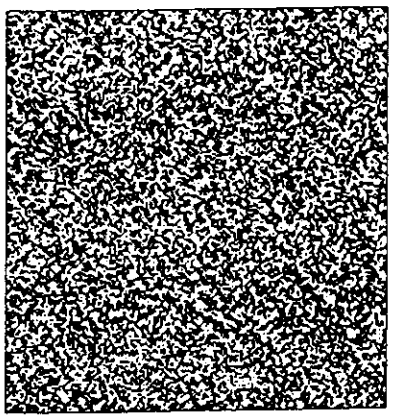

t = 0

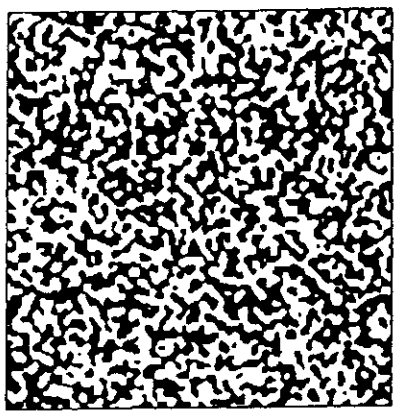

t = 1

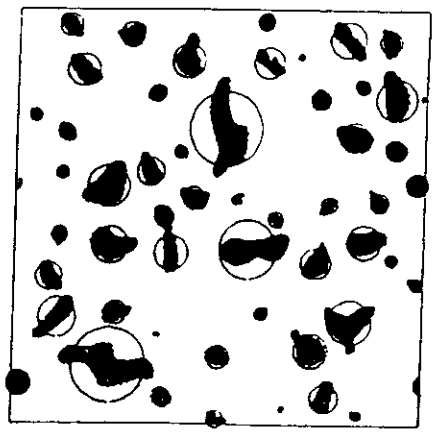

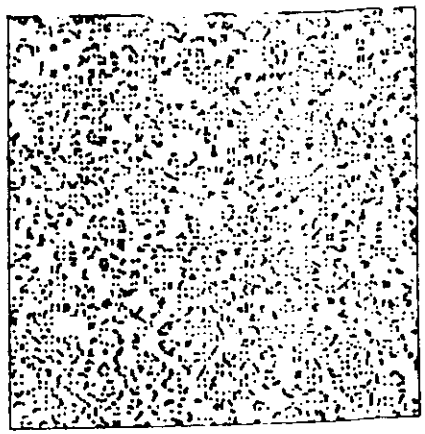

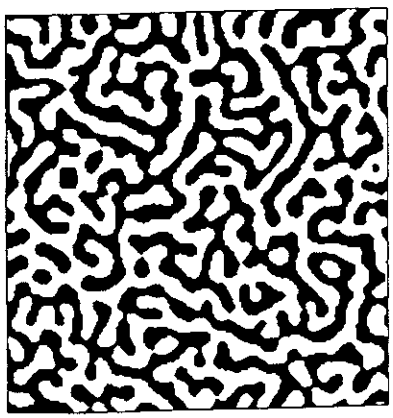

t = 40

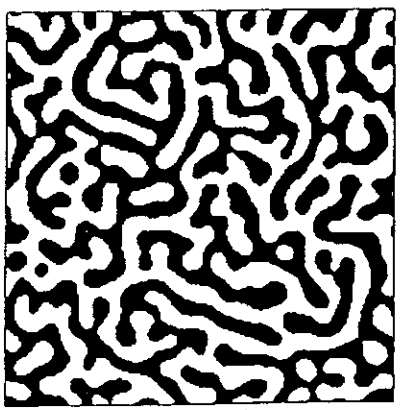

t = 80

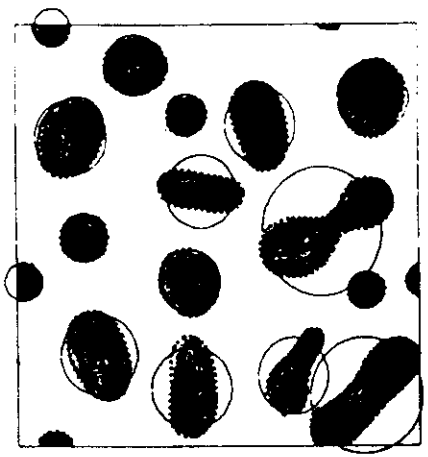

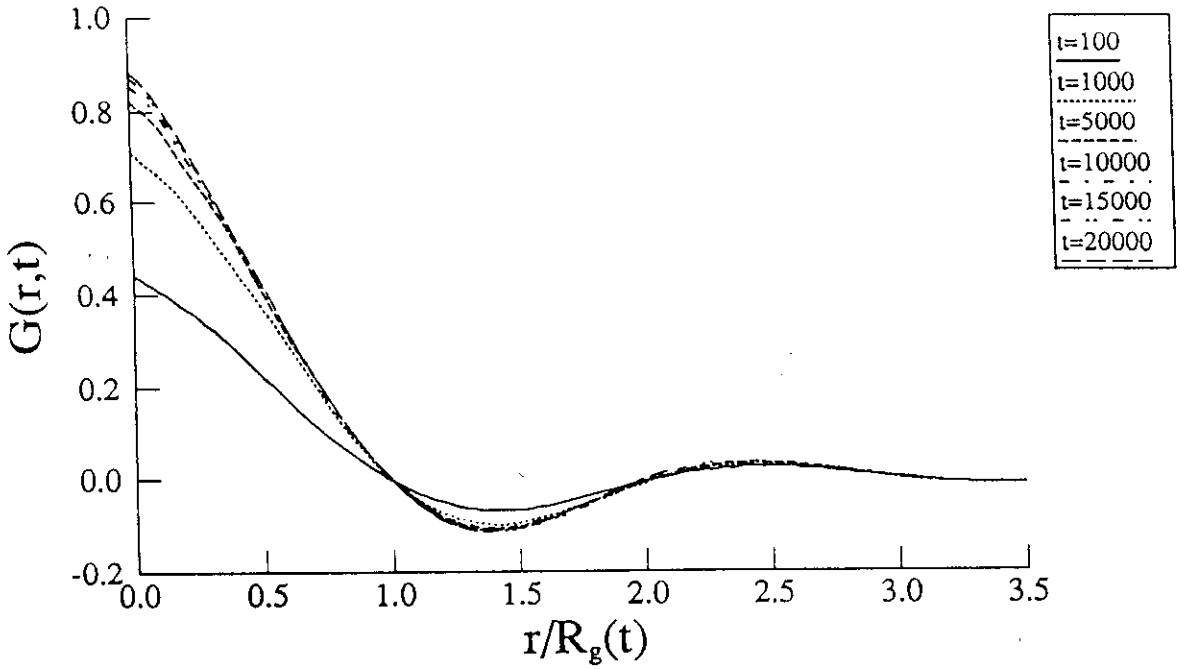
1.0
0.8
0.6
0.4
0.2
0.0
-0.2
G(r,t)
0.0
0.5
1.0
1.5
2.0
2.5
3.0
3.5
r/R_g(t)
t=100
t=1000
t=5000
t=10000
t=15000
t=20000

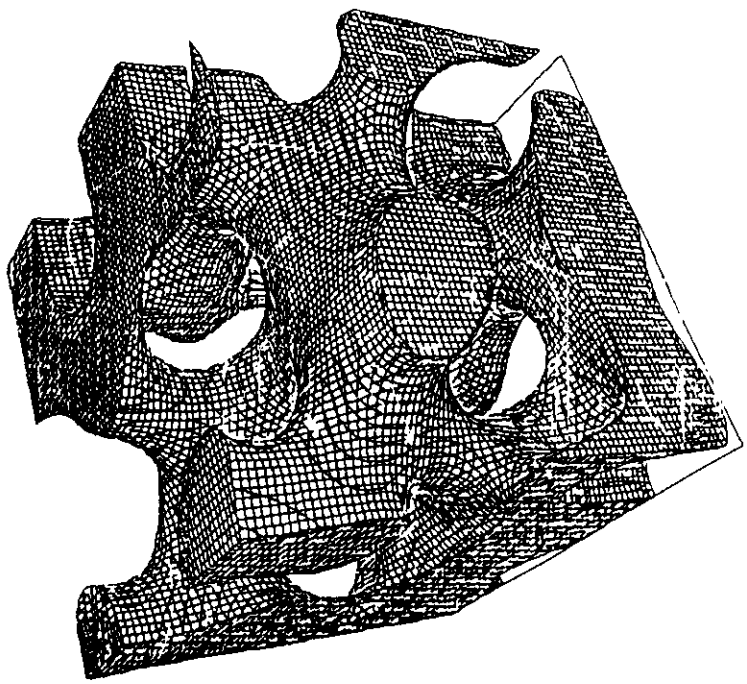

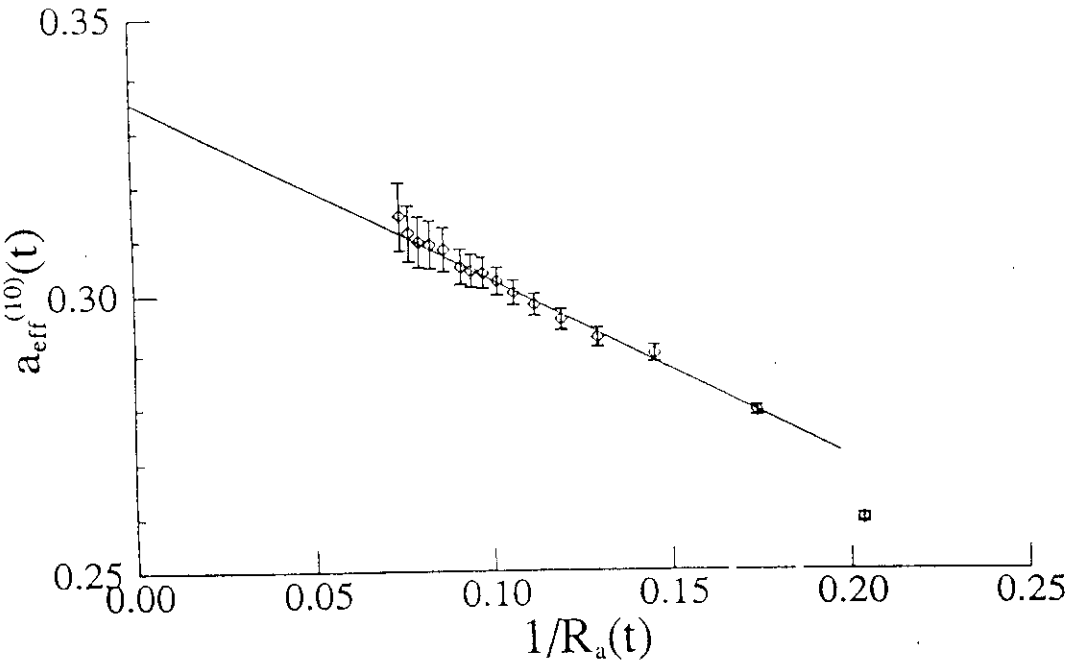
0.35
0.30
0.25
$a_{eff}^{(10)}(t)$
0.00
0.05
0.10
0.15
0.20
0.25
$1/R_a(t)$

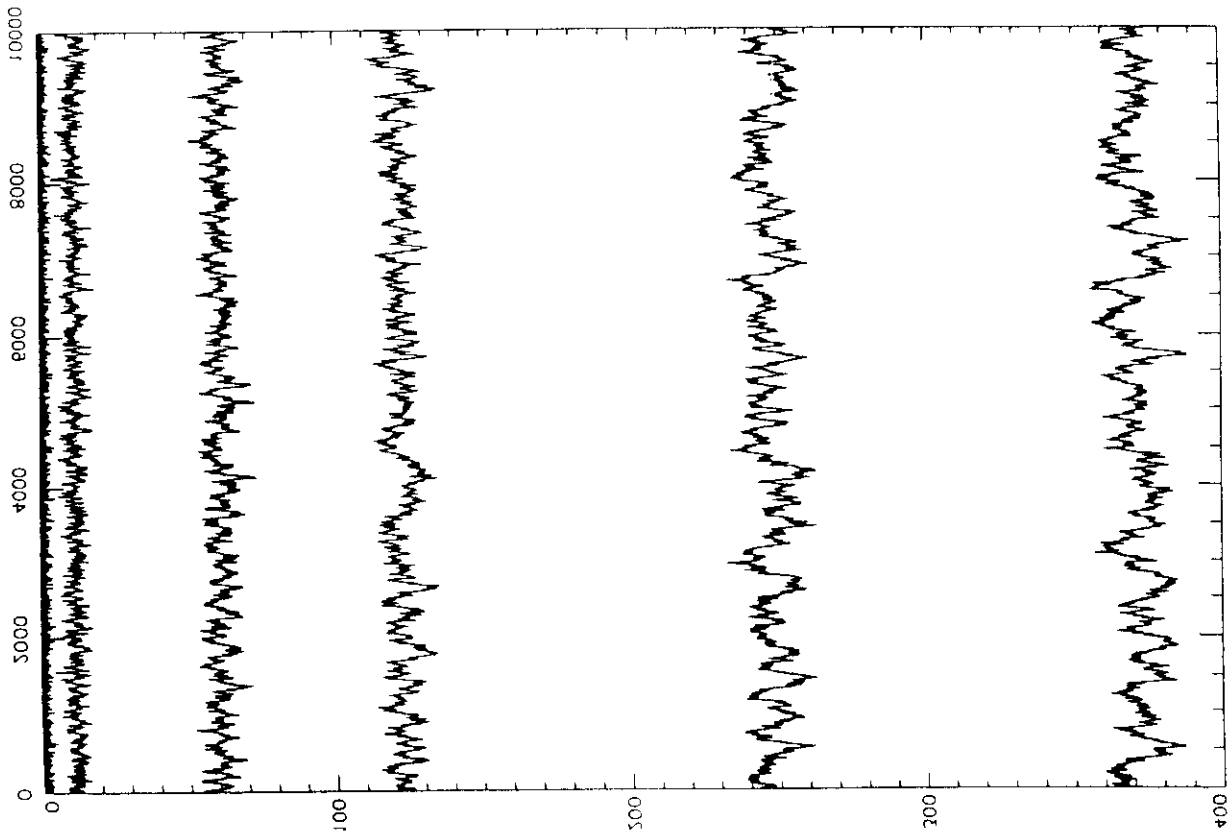
0
4000
8000
12000
0
100
500
700
900

Surface roughness:

$$w(t,L) = \sqrt{\bar{h}^2 - \bar{h}^2}$$

Dynamical scaling:

$$w(t,L) = t^{\beta} F(tL^{-\varsigma/\beta})$$

long time behaviour (infinite system):

$$w(t,\infty) \sim t^{\beta}$$

For $d = 1$ $\beta = 1/3$. Systems with absorbing states;

$$\frac{\partial \vec{n}(\vec{r},t)}{\partial t} = -b\vec{n} - u\vec{n}|n^2] + |\vec{n}|\xi(t)$$

Küppers-Lorz tinstability for a rotating fluid.
The complex Ginzburg–Landau Equation
Dynamics of liquid crystals in the nematic phase
Single mode laser (class A and clas B)
Excitable systems: Fizugh–Naguno Model
Lotka–Volterra models for expecies competition

$$\dot{x}_i = f_i(x) + \sum_{j=1}^{N} g_{ij}\xi_j(t)$$

How should we perform and what can we learn from "numerical experiments"?

Deterministic dynamics

Real dynamical variables: $x \equiv (x_1, \ldots, x_N)$

$$\frac{dx_i}{dt} = f_i(x_1, \ldots, x_N), \qquad i = 1, \ldots, N$$

Fixed points $\bar{x}$ of the dynamical system

$$\left.\frac{dx_i}{dt}\right|_{x=\bar{x}} = 0, \qquad i = 1, \ldots, N$$

$$f_i(\bar{x}_1, \ldots, \bar{x}_N) = 0, \qquad i = 1, \ldots, N$$

Stability and asymptotic stability.

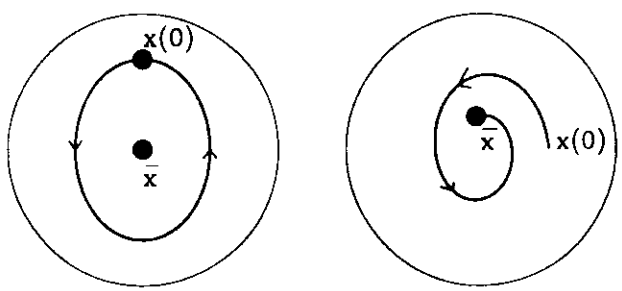

stable asymptotically stable

Lyapunov function (potential) $L(x)$:

$$(a)\ \ L(x) > L(\bar{x}) \qquad \text{for } x \neq \bar{x}$$

$$(b)\ \ \frac{dL}{dt} = \sum_{i=1}^{N} \frac{\partial L}{\partial x_i}\frac{dx_i}{dt} \leq 0 \quad \text{for } x \neq \bar{x}$$

$$(b')\ \ \frac{dL}{dt} \leq 0 \qquad \text{for } x \neq \bar{x}$$

$L(x)$ gives information about global stability.
$L(\bar{x}^{(2)}) < L(\bar{x}^{(1)}) \to \bar{x}^{(2)}$ is the stable fixed point and that $\bar{x}^{(1)}$ is a metastable fixed point.

1.- Relaxational Gradient Flow
2.- Relaxational Non–Gradient Flow
3.- Non–Relaxational Potential Flow
4.- Non–Potential Flow

(1) Relaxational Gradient Flow.
potential $V(x) = V(x_1, \ldots, x_N)$

$$\frac{dx_i}{dt} = -\frac{\partial V}{\partial x_i}$$

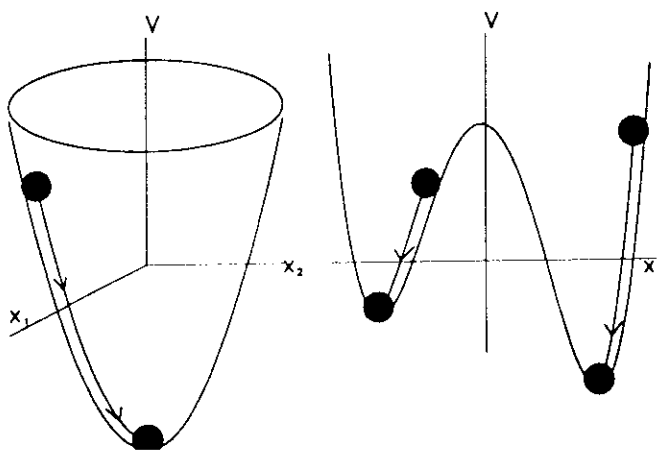

$$\frac{dV}{dt} = \sum_{i=1}^{N} \frac{\partial V}{\partial x_i}\frac{dx_i}{dt} = -\sum_{i=1}^{N}\left(\frac{\partial V}{\partial x_i}\right)^2 \leq 0$$

Model A of critical phenomena

(2) Relaxational Non–Gradient Flow

$$\frac{dx_i}{dt} = -\sum_{j=1}^{N} S_{ij}\frac{\partial V}{\partial x_j}$$

where $S_{ij}(x)$ is a real, symmetric, positive definite matrix.

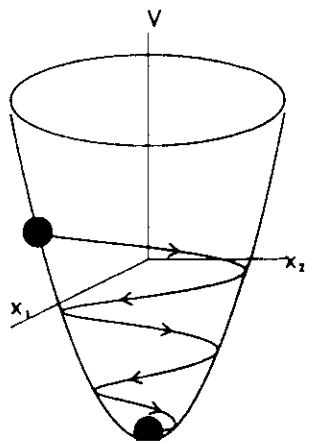

$$\frac{dV}{dt} = \sum_{i=1}^{N} \frac{\partial V}{\partial x_i}\frac{dx_i}{dt} = -\sum_{i,j=1}^{N} S_{ij}\frac{\partial V}{\partial x_i}\frac{\partial V}{\partial x_j} \leq 0$$

Cahn-Hilliard model: $S = -\nabla^2$

(3) Non–Relaxational Potential flow

$$\frac{dx_i}{dt} = f_i \equiv -\sum_{j=1}^{N} S_{ij}\frac{\partial V}{\partial x_j} + v_i$$

$v_i(x)$:the residual dynamics after the relaxational part has acted.
If V is a Lyapunov potential:

$$\frac{dV}{dt} = -\sum_{i,j=1}^{N} S_{ij}\frac{\partial V}{\partial x_i}\frac{\partial V}{\partial x_j} + \sum_{i=1}^{N} v_i\frac{\partial V}{\partial x_i} \leq 0$$

$$\sum_{i=1}^{N} v_i\frac{\partial V}{\partial x_i} = 0$$

$$\sum_{i=1}^{N}\left(f_i + \sum_{j=1}^{N} S_{ij}\frac{\partial V}{\partial x_j}\right)\frac{\partial V}{\partial x_i} = 0$$

This is verified for:

$$v_i = -\sum_{j=1}^{N} A_{ij}\frac{\partial V}{\partial x_j}$$

with $A_{ij} = -A_{ji}$ or

$$\frac{dx_i}{dt} = -\sum_{j=1}^{N} D_{ij}\frac{\partial V}{\partial x_j}$$

$$D = S + A\begin{cases} S = \frac{1}{2}(D + D^T) \\ A = \frac{1}{2}(D - D^T) \end{cases}$$

S positive definite matrix.
Küppers-Lortz instability
Single mode laser dynamics

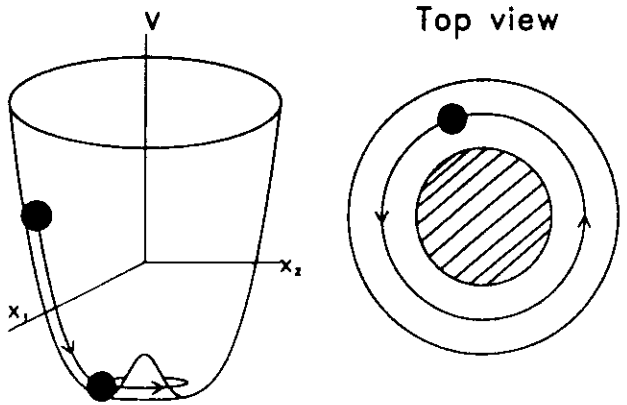

(4) Non–Potential flow.
The only solution is $V = 0$, $v_i = f_i$.

Examples:
The complex Ginzburg–Landau equation (CGLE)
$A(\vec{r},t) = X(\vec{r},t) + \mathrm{i}Y(\vec{r},t)$:

$$\frac{\partial A}{\partial t} = \mu A + \gamma\nabla^2 A - \beta|A|^2 A$$

$\mu = \mu_R + \mathrm{i}\mu_I$, $\beta = \beta_R + \mathrm{i}\beta_I$ and $\gamma = \gamma_R + \mathrm{i}\gamma_I$

$$\frac{\partial A}{\partial t} = -\frac{\delta\Phi}{\delta A^*}$$

$$\Phi\{A, A^*\} = \int d\vec{r}\left[-\mu|A|^2 + \gamma|\vec{\nabla}A|^2 + \frac{\beta}{2}|A|^4\right]$$

Is it possible to find V such that?:

$$\left.\begin{aligned}\frac{\partial X}{\partial t} &= -\frac{\delta V}{\delta X}\\ \frac{\partial Y}{\partial t} &= -\frac{\delta V}{\delta Y}\end{aligned}\right\}$$

$$\frac{\delta}{\delta Y}\left(\frac{\partial X}{\partial t}\right) = \frac{\delta}{\delta X}\left(\frac{\partial Y}{\partial t}\right)$$

$$\mu = \mu^* \qquad \gamma = \gamma^* \qquad \beta = \beta^*$$

$\Phi(A, A^*) = \Phi_R(X, Y) + \mathrm{i}\Phi_I(X, Y)$ the variation of the real part is:

$$\begin{aligned}\frac{d\Phi_R}{dt} &= -\tfrac{1}{2}\int d\vec{r}\left[\left(\tfrac{\delta\Phi_R}{\delta X}\right)^2 + \left(\tfrac{\delta\Phi_I}{\delta Y}\right)^2\right] + \\ &\quad 2(\gamma_I\beta_R - \beta_I\gamma_R)\int d\vec{r}(X^2+Y^2)\vec{\nabla}(Y\vec{\nabla}X - X\vec{\nabla}Y)\end{aligned}$$

Φ_R is a Lyapunov if:

$$\gamma_I\beta_R - \beta_I\gamma_R = 0$$

$$\begin{pmatrix}\frac{\partial X}{\partial t}\\ \frac{\partial X}{\partial t}\end{pmatrix} = -\begin{pmatrix}2 & 0\\ 0 & 2\end{pmatrix}\begin{pmatrix}\frac{\delta\Phi_R}{\delta X}\\ \frac{\delta\Phi_R}{\delta Y}\end{pmatrix} + 2\begin{pmatrix}\frac{\delta\Phi_I}{\delta Y}\\ -\frac{\delta\Phi_I}{\delta X}\end{pmatrix}$$

Orthogonality condition:

$$\left(\frac{\delta\bar{\Phi}_I}{\delta Y}, -\frac{\delta\bar{\Phi}_I}{\delta X}\right)\begin{pmatrix}\frac{\delta\Phi_R}{\delta X}\\ \frac{\delta\Phi_R}{\delta Y}\end{pmatrix} = 0$$

After a change of variables $A(\vec{r}, t) \to \mathrm{e}^{i\alpha}A(\vec{r}, t)$:

$$\frac{\partial A}{\partial t} = -(1+i)\frac{\delta\bar{\Phi}_R}{\delta A^*}$$

Stil, approximations to the potential exist in the general case.

Potentials and Stationary Distributions

$$\dot{x}_i = f_i(x) + \sum_{j=1}^{N} g_{ij}\xi_j(t)$$

$\xi_j(t)$ Gaussian variables (white noise):

$$\begin{aligned}\langle\xi_i(t)\rangle &= 0\\ \langle\xi_i(t)\xi_j(t')\rangle &= 2\epsilon\delta_{ij}\delta(t-t')\end{aligned}$$

ϵ is the noise intensity.
Probability distribution function $P(x, t)$ satisfies Fokker–Planck eq.:

$$\frac{\partial P(x,t)}{\partial t} = \sum_{i=1}^{N}\frac{\partial}{\partial x_i}\left[-f_iP + \epsilon\sum_{j=1}^{N}\frac{\partial}{\partial x_j}(G_{ij}P)\right]$$

$$G = g\cdot g^T$$

$$f_i = -\sum_{j=1}^{N} S_{ij}\frac{\partial V}{\partial x_j} + v_i$$

(i) S is a constant matrix,
(ii) $G = S$ (fluctuation–dissipation)
(iii) v_i satisfies the orthogonality condition.
(iv) v_i is divergence free: $\sum_i \frac{\partial v_i}{\partial x_i} = 0$

Satisfied for $v_i = -\sum_j A_{ij}\partial_{x_j} V$

$$P_{st}(x) = N \exp\left\{-\frac{V(x)}{\epsilon}\right\}$$

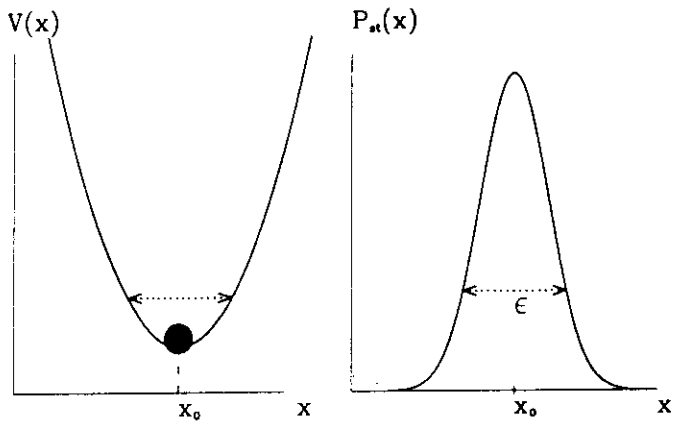

Thermal fluctuations: $\epsilon = k_B T$.
For a non–relaxational potential flow (i.e. the orthogonality condition is satisfied) and the fluctuation–dissipation relation $S = G$ holds, in the small noise limit, we have

$$V(x) = \lim_{\epsilon \to 0} -\epsilon \ln P_{st}(x)$$

In those case the potential $V(x)$ is given also the name of "Graham potential",

Küppers-Lortz instability Rayleigh–Bénard convection in a rotating fluid:

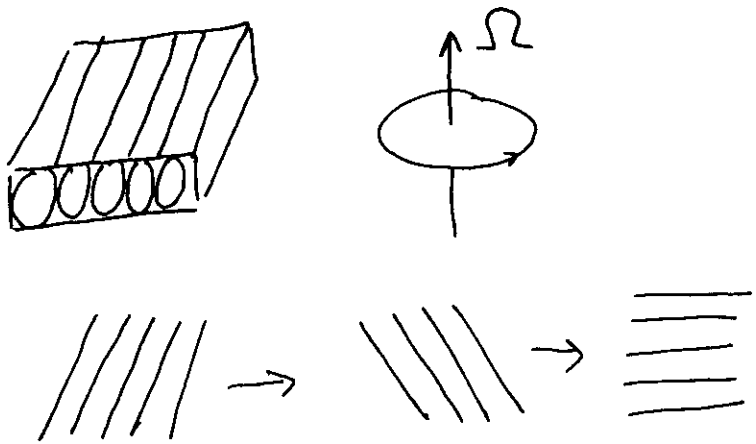

A_1, A_2, A_3, follow the evolution equations:

$$\begin{aligned}
\dot{A}_1 &= A_1\left(1 - |A_1|^2 - (1+\mu+\delta)|A_2|^2 - (1+\mu-\delta)|A_3|^2\right)\\
\dot{A}_2 &= A_2\left(1 - |A_2|^2 - (1+\mu+\delta)|A_3|^2 - (1+\mu-\delta)|A_1|^2\right)\\
\dot{A}_3 &= A_3\left(1 - |A_3|^2 - (1+\mu+\delta)|A_1|^2 - (1+\mu-\delta)|A_2|^2\right)
\end{aligned}$$

Species competition

$$\frac{dN}{dt} = rN(1 - \alpha N)$$

Gause–Lotka–Volterra form

$$\begin{cases}
\dot{N}_1 &= r_1 N_1\left(1 - N_1 - \alpha N_2 - \beta N_3\right)\\
\dot{N}_2 &= r_2 N_2\left(1 - N_2 - \alpha N_3 - \beta N_1\right)\\
\dot{N}_3 &= r_3 N_3\left(1 - N_3 - \alpha N_1 - \beta N_2\right)
\end{cases}$$

Stationary solutions

(a) Roll solutions
One non-vanishing amplitude, for instance:
$(A_1, A_2, A_3) = (1, 0, 0)$
is a roll solution with rolls parallel to the $\hat{e}_1$ direction.

(b) Hexagon solutions.
The three amplitudes are different from 0
$A_1^2 = A_2^2 = A_3^2 = \frac{1}{3+2\mu}$.
Stability diagram

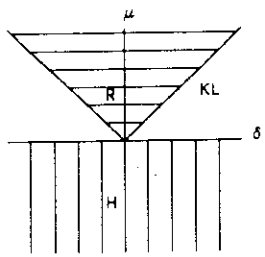

Küppers-Lortz instability:

$$(1,0,0) \to (0,1,0) \to (0,0,1) \to (1,0,0) \to (0,1,0) \ldots$$

Potential description:

$$V(A_1, A_2, A_3) = \frac{-1}{2}(A_1^2 + A_2^2 + A_3^2) + \frac{1}{4}(A_1^4 + A_2^4 + A_3^4) + \frac{1+\mu}{2}(A_1^2A_2^2 + A_2^2A_3^2 + A_3^2A_1^2)$$

$$\frac{dA_i}{dt} = -\frac{\partial V}{\partial A_i} + v_i$$

$$v_1 = \delta A_1(-A_2^2 + A_3^2)$$
$$v_2 = \delta A_2(-A_3^2 + A_1^2)$$
$$v_3 = \delta A_3(-A_1^2 + A_2^2)$$

$\delta = 0$ Relaxational Gradient Flow. Orthogonality condition:

$$\delta\mu = 0$$

NUMERICAL METHODS

OUTLINE

Stationary distributions

Integration Schemes (white noise)

Colored noise

Runge–Kutta methods

Partial Differential Equations

Spacial structure of noise

Stochastic Differential Equations (SDE)

$$\dot{x}_i = f_i(x) + \sum_{j=1}^{N} g_{ij}\xi_j(t) \qquad i = 1, \ldots, N$$

$\xi_j(t)$ Gaussian variables (white noise):

$$\begin{aligned} \langle \xi_i(t) \rangle &= 0 \\ \langle \xi_i(t)\xi_j(t') \rangle &= 2\epsilon\delta_{ij}\delta(t-t') \end{aligned}$$

Probability distribution function $P(x,t)$. Fokker–Planck eq.:

$$\frac{\partial P(x,t)}{\partial t} = \sum_{i=1}^{N} \frac{\partial}{\partial x_i} \left[-f_i P + \epsilon \sum_{j=1}^{N} \frac{\partial}{\partial x_j} (G_{ij} P) \right]$$

$$G = g \cdot g^T$$

Interested on:

$$\langle x_i(t)^n \rangle \qquad \langle x_i(t) x_j(t) \rangle$$

$$\langle x_i(t)^n \rangle = \int dx P(x,t) x_i(t)^n$$

$$\langle x_i(t)^n \rangle = \frac{1}{M} \sum_{k=1}^{M} [x_i(t)^{(k)}]^n$$

How to generate $x(t)^{(k)}$?
Under certain conditions:

$$P_{st}(x) = \lim_{t\to\infty} P(x,t) = Z^{-1} \exp(-V(x)/\epsilon)$$

Best way to sample P_{st} is Monte-Carlo

NO systematic errors
Statistical errors $\sim M^{-1/2}$
Propose (random) change $x \to x'$
Accept with probability:

$$p = \min[1, \exp(-(V(x') - V(x))/\epsilon)]$$

Alternative (bad): Integrate SDE up to $t =$"∞"
Best use Hybrid Monte Carlo:
Molecular dynamics with random velocities for $x \to x'$
Uses same integration algorithm of the SDE

Time dependent properties:
Simplest example:

$$\begin{aligned} \dot{x}(t) &= f(t) + \xi(t) \\ \langle \xi(t)\xi(t') \rangle &= \delta(t - t') \end{aligned}$$

Exact solution:

$$x(t) = x(0) + \int_0^t f(s)\, ds + \int_0^t \xi(s)\, ds \equiv x(0) + F(t) + W(t)$$

$W(t)$ = Wiener process (Gaussian):

$$\begin{aligned} \langle W(t) \rangle &= 0 \\ \langle W(t)W(t') \rangle &= \min(t, t') \end{aligned}$$

$x(t)$ is also Gaussian:

$$\begin{aligned} \langle x(t) \rangle &= x(0) + F(t) \\ \langle x(t)x(t') \rangle &= (x(0) + F(t))(x(0) + F(t')) + \min(t, t') \end{aligned}$$

Can not use standard algorithms: $\xi(t)$ is not differentiable.

$$\begin{aligned} x(t+h) &= x(t) + \int_t^{t+h} \dot{x}(s)\, ds \\ &= x(t) + \int_t^{t+h} f(s)\, ds + \int_t^{t+h} \xi(s)\, ds \\ &\equiv x(t) + f_h(t) + w_h(t) \end{aligned}$$

$$\langle w_h(t) \rangle = \int_t^{t+h} \langle \xi(s) \rangle\, ds = 0$$

$$\begin{aligned} \langle w_h(t)w_h(t') \rangle &= \int_t^{t+h} ds \int_{t'}^{t'+h} du \langle \xi(s)\xi(u) \rangle \\ &= \int_t^{t+h} ds \int_{t'}^{t'+h} du \delta(s - u) \end{aligned}$$

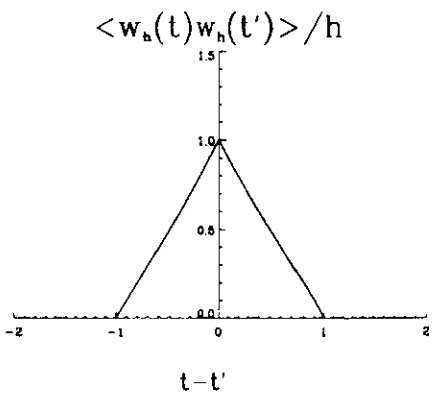

$$\begin{aligned} \langle w_h(t)^2 \rangle &= h \\ \langle w_h(t_i)w_h(t_j) \rangle &= h\delta_{ij} \end{aligned}$$

$$w_h(t) = h^{1/2} u(t)$$

Generation of Independent Gaussian random numbers.

$$\langle u(t)\rangle = 0 \ , \ \langle u(t^2)\rangle = 1$$
$$\langle u(t)u(t')\rangle = 0 \ , \ t \neq t'$$

Box–Muller–Wiener algorithm: r_1, r_2 uniform $(0,1)$ random numbers (free).

$$g_1 = \sqrt{-2\ln(r_1)}\cos(2\pi r_2)$$
$$g_2 = \sqrt{-2\ln(r_1)}\sin(2\pi r_2)$$

Can be improved (numerical inversion method).

$$x(t=0) = x_0$$
$$x(t+h) = x(t) + f_h(t) + h^{1/2}\,u(t)$$

More difficult case:

$$\dot{x}(t) = q(x) + g(x)\xi(t)$$

$$x(t+h) - x(t) = \int_t^{t+h} q(x(s))\,ds + \int_t^{t+h} g(x(s))\xi(s)\,ds$$

$$q(x(s)) = q(x(t)) + \left.\frac{dq}{dx}\right|_{x(t)} (x(s) - x(t)) + O[(x(s) - x(t))^2]$$

$$g(x(s)) = g(x(t)) + \left.\frac{dg}{dx}\right|_{x(t)} (x(s) - x(t)) + O[(x(s) - x(t))^2]$$

$$\begin{aligned} x(t+h) - x(t) &= hq(x(t)) + hO[x(s) - x(t)] + w_h(t)g(x(t)) \\ &\quad + w_h(t)O[x(s) - x(t)] \end{aligned}$$

$$w_h(t) = \int_t^{t+h} ds\ \xi(s) = h^{1/2}\,u(t)$$

Need to go one step further

$$x(s) - x(t) = g(x(t)) \int_t^s dv\ \xi(v) = O[h^{1/2}]$$

$$g'(x(t)) \int_t^{t+h} ds\ (x(s) - x(t))\xi(s) + O[x(s) - x(t)]^2 w_h(t) =$$
$$g'(x(t))g(x(t)) \int_t^{t+h} ds \int_t^s dv\ \xi(s)\xi(v) + O[h^{3/2}]$$

$$\int_t^{t+h} ds \int_t^s dv\ \xi(s)\xi(v) = \frac{1}{2}[w_h(t)]^2$$

Milshtein algorithm:

$$\begin{aligned} x(t+h) &= x(t) + h^{1/2}g(x(t))u(t) + \\ &\quad h\left[q(x(t)) + \frac{1}{2}g(x(t))g'(x(t))u(t)^2\right] + O[h^{3/2}] \end{aligned}$$

For additive noise (Euler algorithm):

$$x(t+h) = x(t) + hq(x(t)) + g(x(t))h^{1/2}u(t) + O[h^{3/2}]$$

Another "Euler algorithm" (modified Milshtein)

$$\begin{aligned} x(t+h) &= x(t) + g(x(t))h^{1/2}u(t) + \\ &\quad h[q(x(t)) + \frac{1}{2}g(x(t))g'(x(t))] + O[h^{3/2}] \end{aligned}$$

Stochastic convergence for the trajectories:

$$\begin{aligned} \bar{x}(t+h) &= x(t) + h^{1/2}g(x(t))u(t) + \\ &\quad h\left[q(x(t)) + \frac{1}{2}g(x(t))g'(x(t))u(t)^2\right] \end{aligned}$$

$$\langle(\bar{x}(t+h) - x(t+h))^2\rangle = O[h^3]$$

Stochastic convergence for the moments:

$$D_n(h) \equiv \langle \bar{x}(t+h)^n \rangle - \langle x(t+h)^n \rangle$$

$$D_n(h) = O[h^2]$$

$$\langle x(t)^n \rangle = \langle \bar{x}(t)^n \rangle + O[h]$$

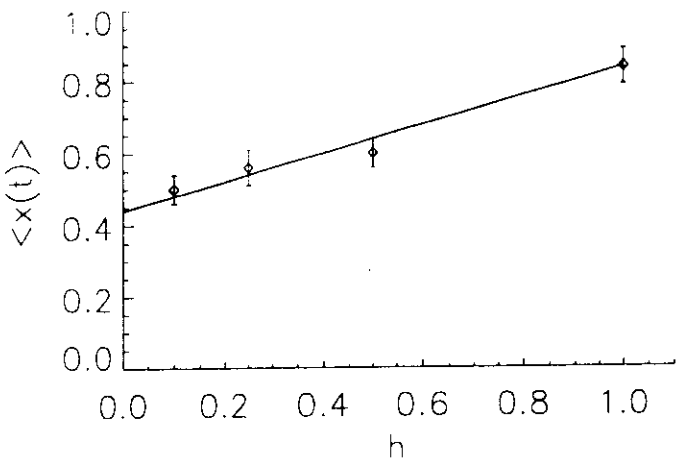

Rümelin Theorem. It is not possible to write:

$$x(t+h) = x(t) + C_1 w_h(t) + C_2 h + C_3 w_h(t)^2 + C_4 h w_h(t) + C_5 w_h(t)^3 + \ldots$$

Milshtein method is also valid for

$$\dot{x}(t) = q(t,x) + g(t,x)\xi(t)$$

Finite Correlation time

Ornstein-Uhlenbeck noise, ξ_{OU} Gaussian Markov process characterized by:

$$\langle \xi_{OU}(t) \rangle = 0$$

$$\langle \xi_{OU}(t)\xi_{OU}(t') \rangle = \frac{1}{2\tau} e^{-|t-t'|/\tau}$$

(i) Non zero correlation time τ, but

$$\lim_{\tau \to 0} \xi_{OU}(t) = \xi(t)$$

$$\langle \xi(t)\xi(t') \rangle = \delta(t-t')$$

(ii) The OU-noise is, up to a change of variables, the only Gaussian, Markov, *stationary* process.
The OU-noise is the solution of the SDE:

$$\frac{d\xi_{OU}}{dt} = -\frac{1}{\tau}\xi_{OU}(t) + \frac{1}{\tau}\xi(t)$$

$\xi_{OU}(0)$ is Gaussian of mean 0 and variance $(2\tau)^{-1}$.

$$\xi_{OU}(t+h) = \xi_{OU}(t)e^{-h/\tau} + H_h(t)$$

$$H_h(t) = \tau^{-1} e^{-(t+h)/\tau} \int_t^{t+h} ds\, \xi(s) e^{s/\tau}$$

$$\begin{aligned} \langle H_h(t) \rangle &= 0 \\ \langle H_h(t_i) H_h(t_j) \rangle &= (2\tau)^{-1} \left[1 - e^{-2h/\tau} \right] \delta_{ij} \end{aligned}$$

$$H_h(t) = \sqrt{(1 - e^{-2h/\tau})/(2\tau)}\, u(t)$$

$$\begin{cases} \xi_{OU}(0) = \sqrt{(2\tau)^{-1}}\, u(0) \\ \xi_{OU}(t+h) = \xi_{OU}(t)e^{-h/\tau} + \sqrt{(1 - e^{-2h/\tau})/(2\tau)}\, u(t+h) \end{cases}$$

Example:

$$\frac{dx(t)}{dt} = f(t) + \xi_{OU}(t)$$

$$\begin{aligned} x(t+h) &= x(t) + \int_t^{t+h} ds\ f(s) + \int_t^{t+h} ds\ \xi_{OU}(s) \equiv \\ & x(t) + f_h(t) + g_h(t) \end{aligned}$$

$$\begin{aligned} \langle g_h(t) \rangle &= 0 \\ \langle g_h(t) g_h(t') \rangle &= \tau \left[\cosh\left(\tfrac{h}{\tau}\right) - 1 \right] \exp\left(-\tfrac{|t-t'|}{\tau} \right) \end{aligned}$$

To lowest order in h:

$$\langle g_h(t) g_h(t') \rangle = \frac{h^2}{2\tau} \exp\left(-\frac{|t-t'|}{\tau} \right) + O[h^3]$$

or

$$g_h(t) = h\xi_{OU}(t)$$

$$x(t+h) = x(t) + f_h(t) + h\xi_{OU}(t) + O[h^2]$$

It is possible to generate exactly the process $g_h(t)$:

$$G(t) = \int_0^t ds\ \xi_{OU}(s)$$

$$g_h(t) = G(t+h) - G(t)$$

$$\begin{aligned} \tfrac{d^2G(t)}{dt^2} + \tfrac{1}{\tau}\tfrac{dG(t)}{dt} &= \tfrac{1}{\tau}\xi(t) \\ G(0) &= 0 \\ \tfrac{dG(t)}{dt}|_{t=0} &= \xi_{OU}(0) \equiv \xi_0 \end{aligned}$$

$$G(t) = \tau\xi_0 - \tau\xi_0 \mathrm{e}^{-t/\tau} + \int_0^t ds\ \xi(s) - \mathrm{e}^{-t/\tau} \int_0^t ds\ \mathrm{e}^{s/\tau} \xi(s)$$

$$g_h(t+h) = p g_h(t) - p f_1(t) + f_1(t+h) - f_2(t) + f_2(t+h)$$

$$\begin{aligned} p &= \mathrm{e}^{-h/\tau} \\ f_1(t) &= \int_t^{t+h} ds\ \xi(s) \\ f_2(t) &= -p\mathrm{e}^{-t/\tau} \int_t^{t+h} ds\ \mathrm{e}^{s/\tau} \xi(s) \end{aligned}$$

$$\begin{aligned} \langle f_1(t_i) \rangle &= 0 \\ \langle f_2(t_i) \rangle &= 0 \\ \langle f_1(t_i) f_1(t_j) \rangle &= h\delta_{ij} \\ \langle f_2(t_i) f_2(t_j) \rangle &= \tfrac{\tau(1-p^2)}{2}\delta_{ij} \\ \langle f_1(t_i) f_2(t_j) \rangle &= -\tau(1-p)\delta_{ij} \end{aligned}$$

$$\begin{aligned} f_1(t) &= \alpha_1 u_1(t) \\ f_2(t) &= \beta_1 u_1(t) + \beta_2 u_2(t) \end{aligned}$$

$$\begin{aligned} \alpha_1 &= \sqrt{h} \\ \beta_1 &= -\tfrac{\tau(1-p)}{\sqrt{h}} \\ \beta_2 &= \sqrt{\tfrac{\tau(1-p)}{2}\left[1 - \tfrac{2\tau}{h} + p\left(1 + \tfrac{2\tau}{h}\right)\right]} \end{aligned}$$

More general case:

$$\frac{dx}{dt} = q(t,x) + g(t,x)\xi_{OU}(t)$$

Recursion relation:

$$x(t+h) = x(t) + hq(t,x(t)) + g_h(t)g(t,x(t)) + O[h^2]$$

Runge–Kutta methods

Reminder:

$$\dot{x}(t) = q(t,x)$$

$$x(t+h) = x(t) + hq(t,x(t)) + O[h^2]$$

$$x(t+h) = x(t) + \frac{h}{2}[q(t,x(t)) + q(t+h, x(t+h))]$$

$$x(t+h) = x(t) + \frac{h}{2}[q(t,x(t)) + q(t+h, x(t) + hq(t,x(t)))] + O[h^3]$$

This is usually written as:

$$\begin{aligned} k &= hq(t,x(t)) \\ x(t+h) &= x(t) + \tfrac{h}{2}[q(t,x(t)) + q(t+h, x(t)+k)] \end{aligned}$$

Same idea applied to SDE:

$$\dot{x}(t) = q(t,x) + g(t,x)\xi(t)$$

Modify Euler algorithm:

$$x(t+h) = x(t) + hq(t,x(t)) + g(t,x(t))h^{1/2}u(t)$$

to obtain

$$\begin{aligned} x(t+h) &= x(t) + \tfrac{h}{2}[q(t,x(t)) + q(t+h, x(t+h)] + \\ &\quad \tfrac{h^{1/2}u(t)}{2}[g(t,x(t)) + g(t+h, x(t+h))] \end{aligned}$$

Heun method

$$\begin{aligned} k &= hq(t,x(t)) \\ l &= h^{1/2}u(t)g(t,x(t)) \\ x(t+h) &= x(t) + \tfrac{h}{2}[q(t,x(t)) + q(t+h, x(t)+l+k)] + \\ &\quad \tfrac{h^{1/2}u(t)}{2}[g(t,x(t)) + g(t+h, x(t)+k+l)] \end{aligned}$$

Same algorithm applies for colored noise:

$$\begin{aligned} k &= hq(t,x(t)) \\ l &= g_h(t)g(t,x(t)) \\ x(t+h) &= x(t) + \tfrac{h}{2}[q(t,x(t)) + q(t+h, x(t)+k+l)] + \\ &\quad \tfrac{g_h(t)}{2}[g(t,x(t)) + g(t+h, x(t)+k+l)] \end{aligned}$$

Convergence of the stochastic part same as Milshtein.
Deterministic part more stable.
Hint: use exact generation of $g_h(t)$ and it will tend smoothly to the white–noise limit.

Multivariate Case

$$\dot{x}_i = q_i(x) + \sum_{j=1}^{N} g_{ij}(x)\xi_j(t) \qquad i = 1, \ldots, N$$

$x \equiv (x_1, \ldots, x_N)$
Generally valid: Milshtein algorithm

$$x_i(t+h) = x_i(t) + h^{1/2}\sum_j g_{ij}(x(t))u_j(t) + h\left[q_i(x(t)) + \frac{1}{2}\sum_{j,k} g_{jk}(x(t))\frac{\partial g_{ik}(x(t))}{\partial x_j(t)}\right]$$

$$\langle u_i(t)\rangle = 0 \ , \ \langle u_i(t)u_j(t)\rangle = \delta_{ij}$$
$$\langle u_i(t)u_j(t')\rangle = 0 \ , \ t \neq t'$$

Case of diagonal noise: $g_{ij}(x) = g_i(x_i)\delta_{ij}$

$$\dot{x}_i = q_i(x) + g_i(x_i)\xi_i(t) \qquad i = 1, \ldots, N$$

Milshtein method reads:

$$\begin{aligned} z_i(t+h) &= x_i(t) + g_i(x_i(t))h^{1/2}u_i(t) + \\ & \quad h\left[q_i(x(t)) + \frac{1}{2}g_i(x_i(t))g'_i(x_i(t))u_i(t)^2\right] \end{aligned}$$

Heun method:

$$\begin{aligned} k_i &= hq_i(x(t)) \\ l_i &= h^{1/2}u_i(t)g_i(x(t)) \\ x_i(t+h) &= x_i(t) + \tfrac{h}{2}[q_i(x(t)) + q_i(x(t)+l+k)] + \\ & \quad \tfrac{h^{1/2}u_i(t)}{2}[g_i(x_i(t)) + g_i(x_i(t)+k_i+l_i)] \end{aligned}$$

And similar expressions for colored noise.

Stochastic Partial Differential Equations Field $A(\vec{r},t)$:

$$\frac{\partial A}{\partial t} = G[A, \vec{\nabla}A, \nabla^2 A, \ldots; \xi(\vec{r},t)]$$

$$\langle \xi(\vec{r},t)\xi(\vec{r}\,',t')\rangle = \delta(\vec{r}-\vec{r}\,')\delta(t-t')$$

Discretize space: Regular d–dimensional lattice.

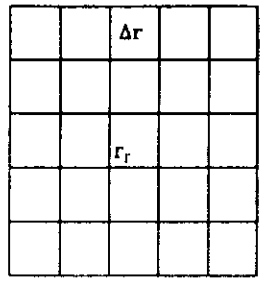

Number of lattice points: $N = L^d$.
Periodic boundary conditions (pbc). Traslational invariance
Lattice spacing Δr. Volume $V = N(\Delta r)^d$.
Space vectors

$$\vec{r}_j \equiv j = (j_1, \ldots, j_d)\Delta r$$

$$\begin{aligned} j_\mu &\in [-L/2+1, L/2] \\ j_\mu &\in [0, L-1], \qquad (\mu = 1, \ldots, d) \end{aligned}$$

Field discretization:

$$A(\vec{r}_i, t) \to A_i(t)$$

Noise discretization:

$$\xi(\vec{r}_i, t) \to (\Delta r)^{-d/2}\xi_i(t)$$

$$\langle \xi_i(t)\xi_j(t')\rangle = \delta_{ij}\delta(t-t')$$

$$\int d\vec{r} \int d\vec{r}\,' \langle \xi(\vec{r},t)\xi(\vec{r}\,',t')\rangle = V\delta(t-t')$$

$$\left[(\Delta r)^d \sum_{i=1}^{N}\right]\left[(\Delta r)^d \sum_{j=1}^{N}\right]\langle\left[(\Delta r)^{-d/2}\xi_i(t)\right]\left[(\Delta r)^{-d/2}\xi_j(t')\right]$$

$$= N(\Delta r)^d \delta(t-t')$$

The derivatives are approximated by finite differences (lattice derivatives):

$$\nabla^2 A(\vec{r}_i, t) \approx \nabla_L^2 A_i(t) \equiv (\Delta r)^{-2} \sum_{j \in n(i)} [A_j(t) - A_i(t)]$$

$$\frac{dA_i(t)}{dt} = G_i(A_1(t), \ldots, A_N(t); \xi_1(t), \ldots, \xi_N(t)), \quad i = 1, \ldots, N$$

Langevin form:

$$\frac{dA_i(t)}{dt} = q_i(A) + \sum_j g_{ij}(A)\xi_j(t)$$

Fourier methods for the partial derivatives:

$$\mathcal{F}[\nabla^2 A(\vec{r}, t)] = -k^2 \mathcal{F}[A(\vec{r}, t)]$$

$$\nabla^2 A(\vec{r}, t) = \mathcal{F}^{-1}[-k^2 \mathcal{F}[A(\vec{r}, t)]]$$

Use Fast Fourier Routines.

$$\hat{A}(\vec{k}) \equiv \mathcal{F}[A(\vec{r})] = L^{-d/2} \sum_{\vec{r}} \mathrm{e}^{\mathrm{i}\vec{r}\vec{k}} A(\vec{r})$$

and the inverse relation:

$$A(\vec{r}) = L^{-d/2} \sum_{\vec{k}} \mathrm{e}^{-\mathrm{i}\vec{r}\vec{k}} \hat{A}(\vec{k})$$

Reciprocal lattice $\vec{k}$
Periodic boundary conditions.
First Brillouin zone: $\vec{k} = \frac{2\pi}{L\Delta r}(k_1, \ldots, k_d)$
k_q integer numbers in the interval $[-L/2+1, L/2]$.

Semi-implicit methods:

$$\dot{A} = -bA - A^3 + \nabla^2 A + \xi$$

Milshtein method (explicit):

$$A_i(t+h) = A_i(t) + h[-bA_i(t) - A_i(t)^3 + \nabla_L^2 A_i(t)] + h^{1/2} u_i(t) +$$

Semi-implicit:

$$A_i(t+h) = A_i(t) + h[-bA_i(t+h) - A_i(t)^3 + \nabla_L^2 A_i(t)] + h^{1/2} u_i(t)$$

$$A_i(t+h) = (1+bh)^{-1} \left[A_i(t) - h[A_i(t)^3 + \nabla_L^2 A_i(t)] + h^{1/2} u_i(t) \right]$$

Absorbing state:

$$\dot{n} = un - n^3 + \nabla^2 n + n\xi$$

Respect positivity.
Modified Milshtein:

$$n_i(t+h) = n_i(t) + h[-\tilde{u} n_i(t) + n_i(t)^3 + \nabla_L^2 n_i(t)] + n_i h^{1/2} u_i(t)$$

$$\begin{aligned} n_i(t+h) &= \frac{1}{2} \left[n_i(t) + 2h[-\tilde{u} n_i(t) + n_i(t)^3] + 2n_i h^{1/2} u_i(t) \right] + \\ &\quad \frac{1}{2} \left[n_i(t) + 2h\nabla_L^2 n_i(t) \right] \end{aligned}$$

$$\begin{aligned} n_i(t+h) &= \frac{1}{2} n_i(t) \exp \left[2h[-\tilde{u} + n_i(t)^2] + 2h^{1/2} u_i(t) \right] + \\ &\quad \frac{1}{2} \left[n_i(t) + 2h\nabla_L^2 n_i(t) \right] \end{aligned}$$

Finite correlation length

Generate d-dimensional real Gaussian field $h(\vec{r})$

$$\begin{aligned} \langle h(\vec{r}) \rangle &= 0 \\ \langle h(\vec{r}) h(\vec{r}\,') \rangle &= C(\vec{r}, \vec{r}\,') = C(\vec{r} - \vec{r}\,') \end{aligned}$$

Numerically

$$C^{(s)}(\vec{r}) = \frac{1}{N}\sum_{\vec{r}\,'} h^{(s)}(\vec{r}\,')h^{(s)}(\vec{r}+\vec{r}\,')$$

Perform an ensemble average over M (preferably a large number) realizations:

$$C(\vec{r}) \equiv \langle C^{(s)}(\vec{r})\rangle \equiv \frac{1}{M}\sum_{s=1}^{M} C^{(s)}(\vec{r})$$

Constructive sequential algorithm (Schmidt's ortonormalization process).
Generate a set $\{u_j\}$, $j = 1, \ldots, N$, of independent Gaussian variables of zero mean and variance one.

$$h_1 = \beta_{11}u_1$$

$\beta_{11} = (C_{1,1})^{1/2}$

$$h_2 = \beta_{21}u_1 + \beta_{22}u_2$$

$$\begin{aligned}\langle h_2^2\rangle &= C_{2,2}\\ \langle h_1 h_2\rangle &= C_{1,2}\end{aligned}$$

In general, we write

$$h_j = \sum_{i=1}^{j}\beta_{ji}u_i$$

$$\langle h_j h_i\rangle = C_{i,j}, \qquad i = 1, \ldots, j$$

Useful when the number N of variables is small.

For large N, use Fourier transform. Fourier Filtering Method.

$$S(\vec{k}) = L^{-d/2}\sum_{\vec{r}} e^{i\vec{r}\vec{k}}C(\vec{r})$$

satisfies exactly:

$$S(\vec{k}) = L^{-d}|\hat{h}^{(s)}(\vec{k})|^2$$

To generate realizations $h^{(s)}(\vec{r})$, $s = 1, \ldots, M$ of the field $h(\vec{r}\,)$, the FFM proceeds in the following way:
(i) Given $C(\vec{r}\,)$, compute $S(\vec{k}\,)$
(ii) Generate a set of independent Gaussian random variables $u^{(s)}(\vec{r})$ of mean zero and variance one.
(iii) Compute the Fourier transform $\hat{u}^{(s)}(\vec{k})$ of $u^{(s)}(\vec{r})$.
(iv) Generate the Fourier transform of the field as:

$$\hat{h}^{(s)}(\vec{k}) = L^{d/2}S(\vec{k})^{1/2}\hat{u}^{(s)}(\vec{k})$$

(v) Compute the required field $h^{(s)}(\vec{r})$ as the inverse Fourier transform of $\hat{h}^{(s)}(\vec{k})$.
Step (i) needs to be done only once for each function $C(\vec{r}\,)$
Step (iii) can be avoided by generating directly the random field $u^{(s)}(\vec{k})$ in Fourier space
Respect the symmetries of the field $u^{(s)}(\vec{k})$, namely:
$u^{(s)}(-\vec{k}) = [u^{(s)}(\vec{k})]^*$.
Power-law correlations:

$$C(\vec{r}) \sim r^{-\gamma} \text{ for } r \to \infty$$

$S(k) \sim k^{\gamma-d}$ for $k \to 0$.
To be precise $(d = 1)$

$$C_i = \begin{cases} i^{-\gamma} & \text{if} \quad 0 < i \leq L/2 - 1 \\ (L-i)^{-\gamma} & \text{if} \quad L/2 \leq i \leq L-1 \\ 1 & \text{if} \quad i = 0, \end{cases}$$

$S_{min}(k) < 0$!!

minimal substraction procedure.

Substracting the minimum value $S_0(k) = S(k) - S_{min}$.

$S_0(k)$ is used instead of $S(k)$

$C(0)$ is no longer equal to 1 .

$C(0, L = 2^{21}) \sim 1.01$ $C(0, L = 2^6) \sim 1.17$

Another possibility:

$$C_j = (1 + j^2)^{-\gamma/2} \quad \text{if} \quad -L/2 + 1 \leq j \leq L/2$$

$$S(k) = \frac{2\pi^{1/2}}{\Gamma(\beta + 1)} \left(\frac{k}{2}\right)^{\beta} K_\beta(k)$$

$K_\beta(k)$ is the modified Bessel function of order $\beta = (\gamma - 1)/2$.

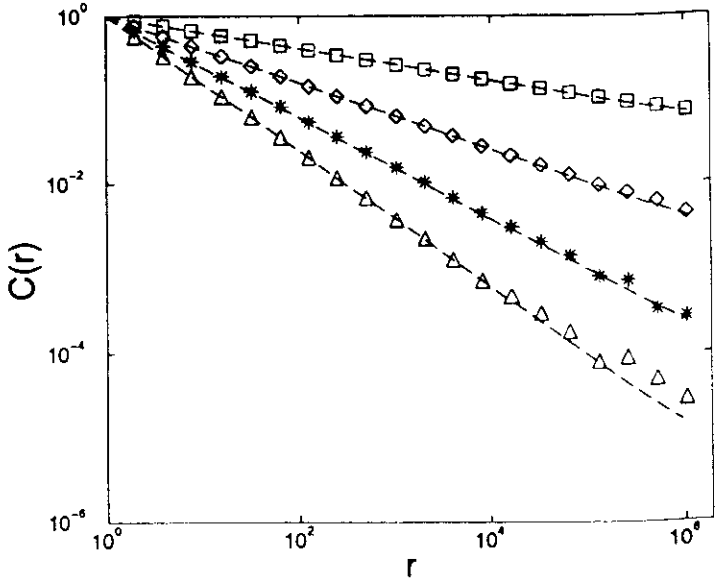

KÜPPERS-LORTZ INSTABILITY

OUTLINE

Busse–Heikes model

Potential description

Role of noise

Küppers-Lortz instability Rayleigh–Bénard convection in a rotating fluid:

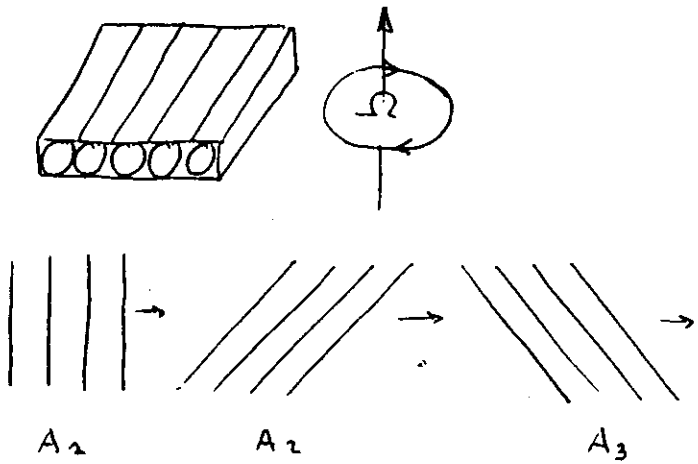

The angle between rolls directions is nearly 60^o
Busse and Heikes introduced a 3-mode approximation (BH)
The complex amplitudes of the three modes, A_1, A_2, A_3, follow the evolution equations:

$$\begin{aligned}
\dot{A}_1 &= A_1\left(1-|A_1|^2-(1+\mu+\delta)|A_2|^2-(1+\mu-\delta)|A_3|^2\right)\\
\dot{A}_2 &= A_2\left(1-|A_2|^2-(1+\mu+\delta)|A_3|^2-(1+\mu-\delta)|A_1|^2\right)\\
\dot{A}_3 &= A_3\left(1-|A_3|^2-(1+\mu+\delta)|A_1|^2-(1+\mu-\delta)|A_2|^2\right)
\end{aligned}$$

Turns out to be equal to a model for 3 species competition (May and Leonard)
Single species (Verhulst model)

$$\frac{dN}{dt} = rN(1-\alpha N)$$

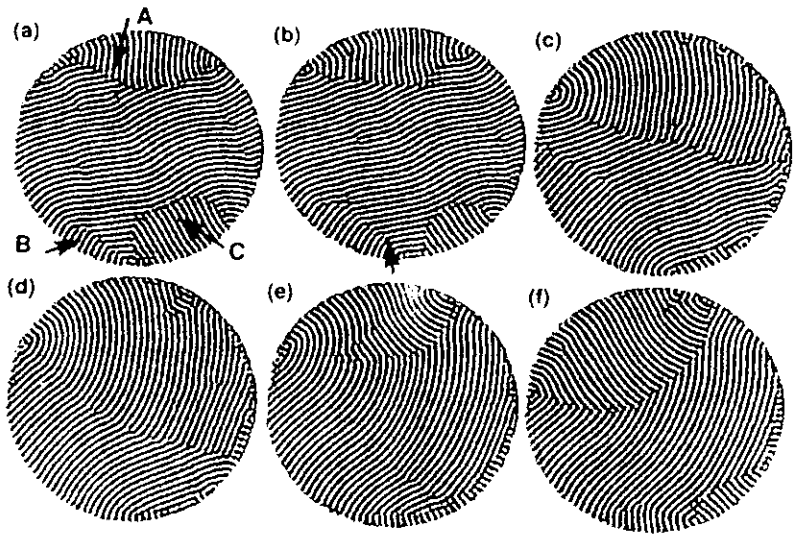

Figure 7.9: Time sequence of Küppers-Lortz instability mixed with skewed-varicose instability at $\epsilon \approx 0.06$ and $\Omega = 8.8$. The images are $37.5\,\tau_v$ apart. A, B, and C in (a) designate 3 different fronts. The arrow in (b) points to a line of defects.

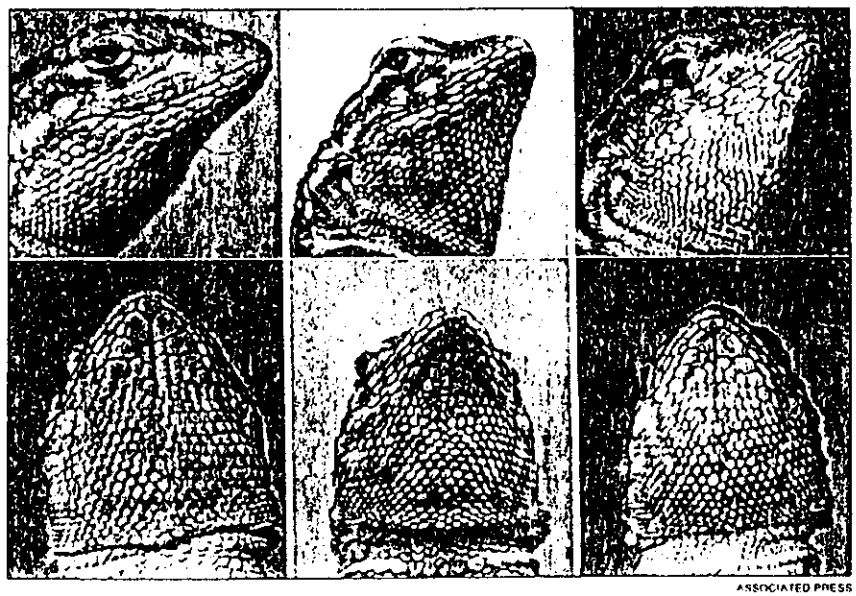

ASSOCIATED PRESS

Los lagartos de cuello naranja (izquierda), azul (centro) y amarillo (derecha) siguen diferentes pautas de apareamiento.

BIOLOGÍA ▶ COMPORTAMIENTO ANIMAL

Lagartos de tres colores compiten con tres estrategias de apareamiento

E. L. (NATURE), Londres

Encontrar pareja no es tarea fácil, sino que exige una estrategia eficaz, primero, para atraer al sexo opuesto, y segundo, para mantener a distancia la atención de machos rivales. Especies diferentes utilizan estrategias diferentes. En algunos casos, una estrategia se generaliza gracias a su éxito a lo largo de generaciones. En otros casos, como en el del lagarto ocelado, los miembros masculinos exhiben toda una gama de técnicas para competir por la atención de las hembras.

En una zona montañosa de California (EE UU) vive una población de estos iguánidos ocelados. Un estudio publicado en el último número de *Nature* revela las ingeniosas técnicas empleadas por machos de diferente coloración para atraer y mantener a las hembras.

Los lagartos ocelados macho, *Uta stansburiana*, parecen pequeñas iguanas y pueden ser de tres clases diferentes, que se distinguen por el color de la garganta: los machos de garganta naranja son muy agresivos y defienden grandes territorios con muchas hembras; los de garganta azul son menos agresivos y defienden territorios más pequeños, a menudo, con sólo una hembra; los de garganta a rayas amarillas no defienden ningún territorio, pero utilizan su parecido con las hembras para introducirse en los territorios de otros machos y aparearse con las hembras.

B. Sinervo y C. M. Lively, de la Universidad de Indiana en Bloomington (EE UU), observaron a estos iguánidos durante seis años. Cuando iniciaron su estudio, los machos de garganta azul eran los más numerosos, pero fueron rápidamente tomados por un número menor de machos más agresivos, con la garganta naranja, aferrados a su estrategia de controlar grandes territorios con varias hembras en cada uno.

Al año siguiente, los descendientes de los machos de garganta naranja llenaban la zona, pero se infiltraron los de rayas amarillas y se apoderaron rápidamente de las hembras; dominaron durante el tercer y cuarto años de observación, pero en el quinto año su falta de defensa adecuada dio paso a la conquista de los lagartos de garganta azul. Luego volvieron a dominar los naranjas.

El color de la garganta y el comportamiento asociado están determinados genéticamente: los machos de garganta naranja tienden a producir más machos de esta coloración y lo mismo sucede con los de garganta azul o amarilla. El lagarto ocelado tiene un ciclo de apareamiento anual y el número de los diferentes tipos de machos en la población fluctúa considerablemente de un año para otro.

Sinervo y Lively han descubierto que la fluctuación no es fortuita ni debida a influencias medioambientales, sino que sigue un ciclo debido a las pautas de comportamiento heredadas. Esta estrategia cíclica es un caso rarísimo en la evolución.

Competing species: Gause–Lotka–Volterra model

$$\begin{aligned}\dot{N}_1 &= r_1 N_1 (1 - N_1 - \alpha N_2 - \beta N_3)\\ \dot{N}_2 &= r_2 N_2 (1 - N_2 - \alpha N_3 - \beta N_1)\\ \dot{N}_3 &= r_3 N_3 (1 - N_3 - \alpha N_1 - \beta N_2)\end{aligned}$$

which is equivalent to BH if $N_i = |A_i|^2 \equiv a_i$

Stationary solutions

(a) Roll solutions

One non-vanishing amplitude, for instance: $(A_1, A_2, A_3) = (1, 0, 0)$ is a roll solution with rolls parallel to the $\hat{e}_1$ direction.

(b) Hexagon solutions.

The three amplitudes are different from 0, $A_1^2 = A_2^2 = A_3^2 = \frac{1}{3+2\mu}$.

Linear stability diagram

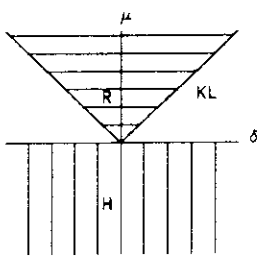

Küppers-Lortz instability shows up in the rotation of convective rolls:

$$(1,0,0) \to (0,1,0) \to (0,0,1) \to (1,0,0) \to (0,1,0) \ldots$$

Numerical integration using a Runge-Kutta scheme gives that rotation period increases with time against experiments

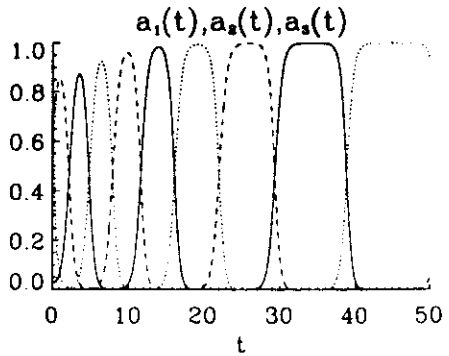

Several modifications have been proposed to fix this feature:

(i) Add noise

(ii) Consider spatial depending terms

Aim: understand the dynamics of the BH model in terms of Lyapunov potentials

A_i can be considered real

Potential description:

$$\frac{dA_i}{dt} = -\frac{\partial V}{\partial A_i} + v_i$$

$$\begin{aligned}V(A_1, A_2, A_3) &= \frac{-1}{2}(A_1^2 + A_2^2 + A_3^2) + \frac{1}{4}(A_1^4 + A_2^4 + A_3^4) + \\ &\quad \frac{1+\mu}{2}(A_1^2 A_2^2 + A_2^2 A_3^2 + A_3^2 A_1^2)\end{aligned}$$

$$\begin{aligned}v_1 &= \delta A_1(-A_2^2 + A_3^2)\\ v_2 &= \delta A_2(-A_3^2 + A_1^2)\\ v_3 &= \delta A_3(-A_1^2 + A_2^2)\end{aligned}$$

Non-rotating Rayleigh-Bénard, $\delta = 0$, Relaxational Gradient Flow.

Relative stability of rolls and hexagons can be determined

$$V_R = \frac{-1}{4} \qquad \text{Roll solution}$$

$$V_H = \frac{-3}{4(3+2\mu)} \qquad \text{Hexagon solution}$$

$$V_R < V_H \rightarrow \mu > 0$$

Is V a Lyapunov when $\delta \neq 0$?
Orthogonality condition:

$$\sum_{i=1}^{3} v_1 \frac{\partial V}{\partial A_i} = 0$$

$$\delta\mu \left(A_1^4(A_2^2 - A_3^2) + A_2^4(A_3^2 - A_1^2) + A_3^4(A_1^2 - A_2^2) \right) = 0$$

Verified if:

$$\delta\mu = 0$$

Focus on $\mu = 0$ which is "close" to the K-L instability
use $a_i = A_i^2$, $t \rightarrow t/2$

$$\begin{aligned}
\dot{a}_1 &= a_1(1 - a_1 - 1 + \mu(a_2 + a_3) - \delta(a_2 - a_3)) \\
\dot{a}_2 &= a_2(1 - a_1 - 1 + \mu(a_2 + a_3) - \delta(a_3 - a_1)) \\
\dot{a}_3 &= a_3(1 - a_1 - 1 + \mu(a_2 + a_3) - \delta(a_1 - a_2))
\end{aligned}$$

New variables

$$\begin{aligned}
x(t) &= a_1(t) + a_2(t) + a_3(t) \\
y(t) &= a_1(t)a_2(t) + a_2(t)a_3(t) + a_3(t)a_1(t)
\end{aligned}$$

$$\dot{x} = x(1 - x) - 2\mu y$$

For $\mu = 0$:

$$x(t) = \frac{1}{\left(\frac{1}{x_0} - 1\right) e^{-t} + 1}$$

Asymptotically (transient of order $t \sim O(1)$

$$x(t) = a_1(t) + a_2(t) + a_3(t) \rightarrow 1$$

Elliminate $a_1 = 1 - a_2 - a_3$

$$\begin{aligned}
\dot{a}_2 &= -\delta a_2(1 - a_2 - 2a_3) \\
\dot{a}_3 &= -\delta a_3(1 - 2a_2 - a_3)
\end{aligned}$$

Which have a Hamiltonian form

$$\begin{pmatrix} \dot{a}_2 \\ \dot{a}_3 \end{pmatrix} = \begin{pmatrix} 0 & \delta \\ -\delta & 0 \end{pmatrix} \begin{pmatrix} \frac{\partial \dot{\mathcal{H}}}{\partial a_2} \\ \frac{\partial \dot{\mathcal{H}}}{\partial a_3} \end{pmatrix}$$

$$\begin{cases} \dot{a}_2 = \delta \frac{\partial \dot{\mathcal{H}}}{\partial a_3} \\ \dot{a}_2 = -\delta \frac{\partial \dot{\mathcal{H}}}{\partial a_2} \end{cases}$$

$$\dot{\mathcal{H}} = a_2 a_3(1 - a_2 - a_3)$$

Relaxational gradient decay towards the minima of V

$$A_1^2 + A_2^2 + A_3^2 = a_1 + a_2 + a_3 = 1$$

Residual (conservative) movement after minima of V have been reached

$$\mathcal{H}(a_2, a_3) = E$$

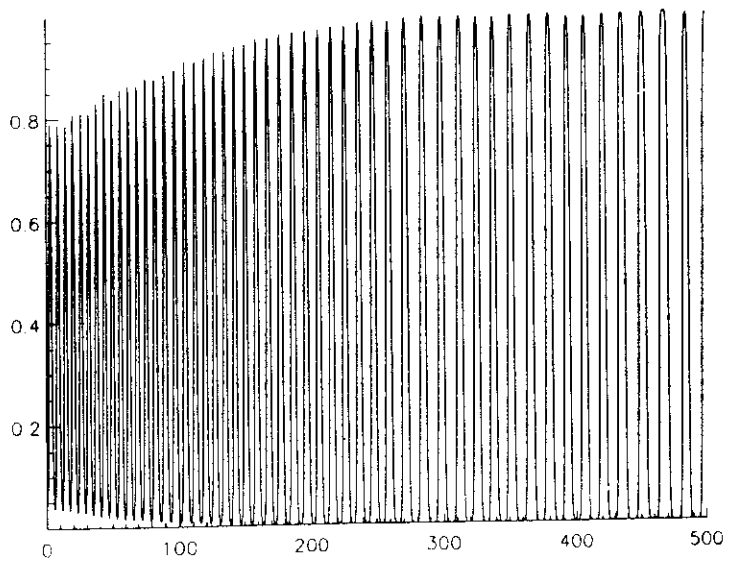

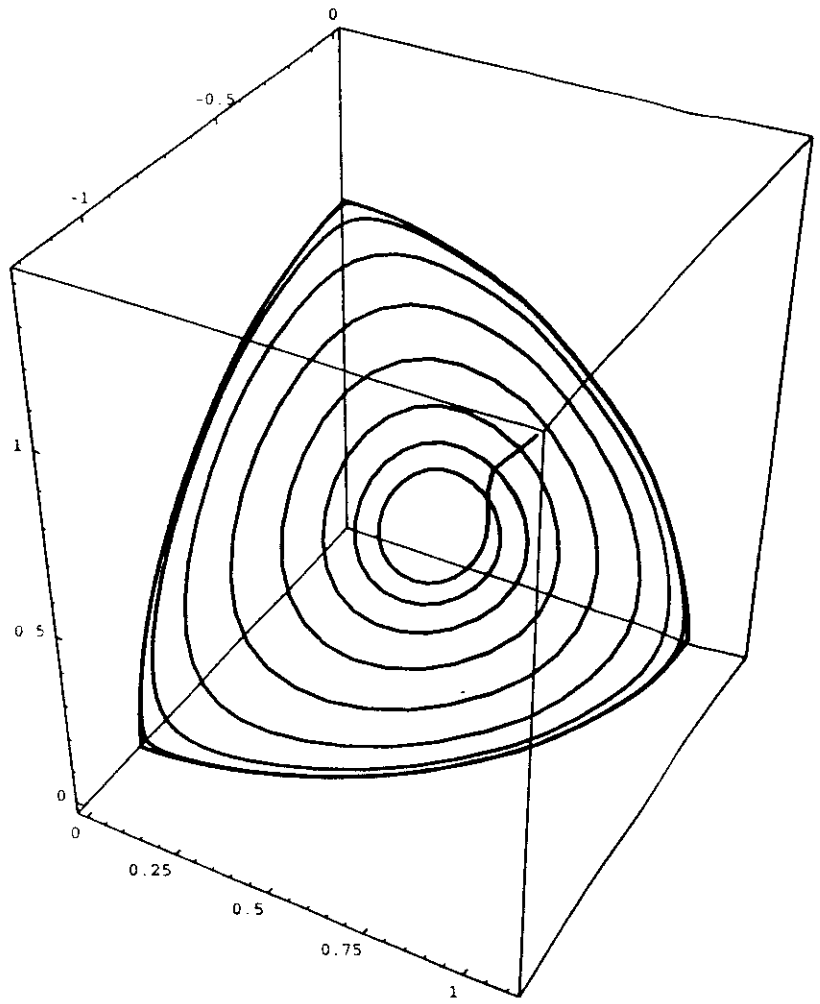

Out[317]=

-Graphics3D-

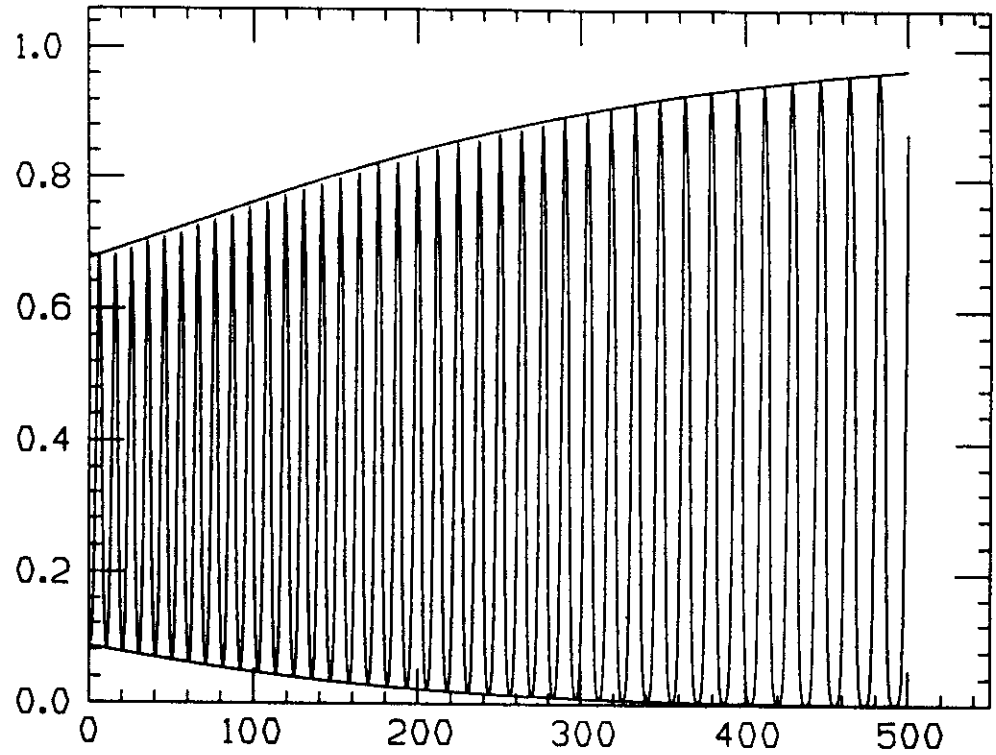

$\eta = 1.01$

$\eta = 1.01$

$\sigma = 1.32$

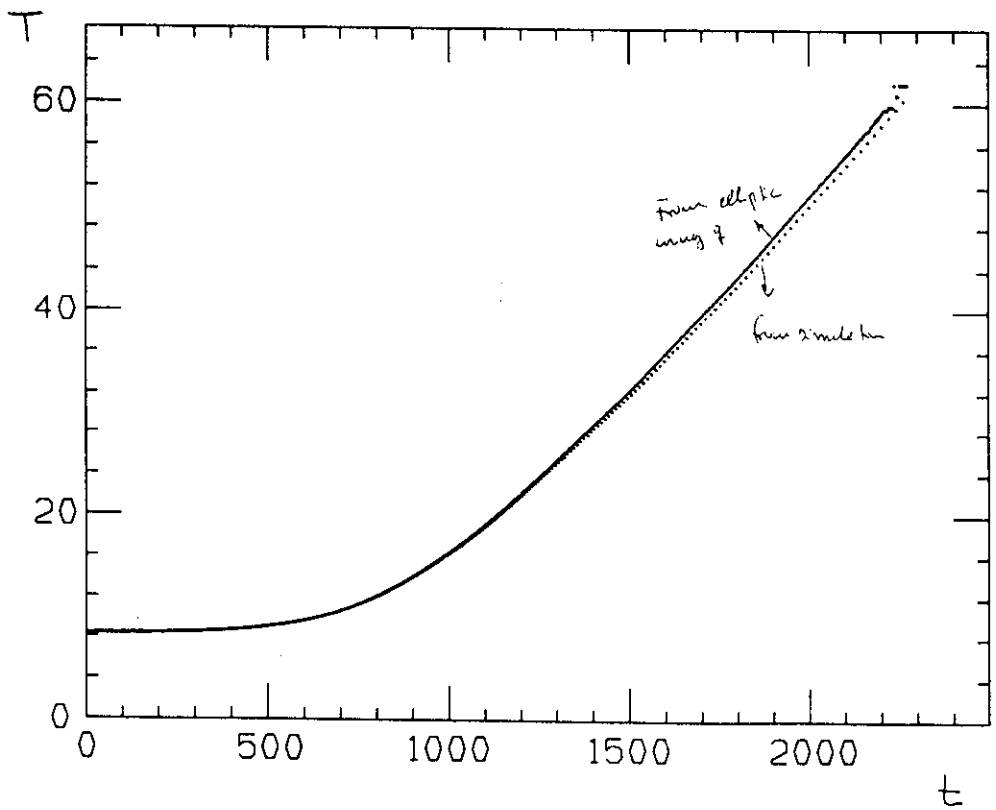

$\eta = 1.0$

$X(t) = a_1(t) + a_2(t) + a_3(t)$

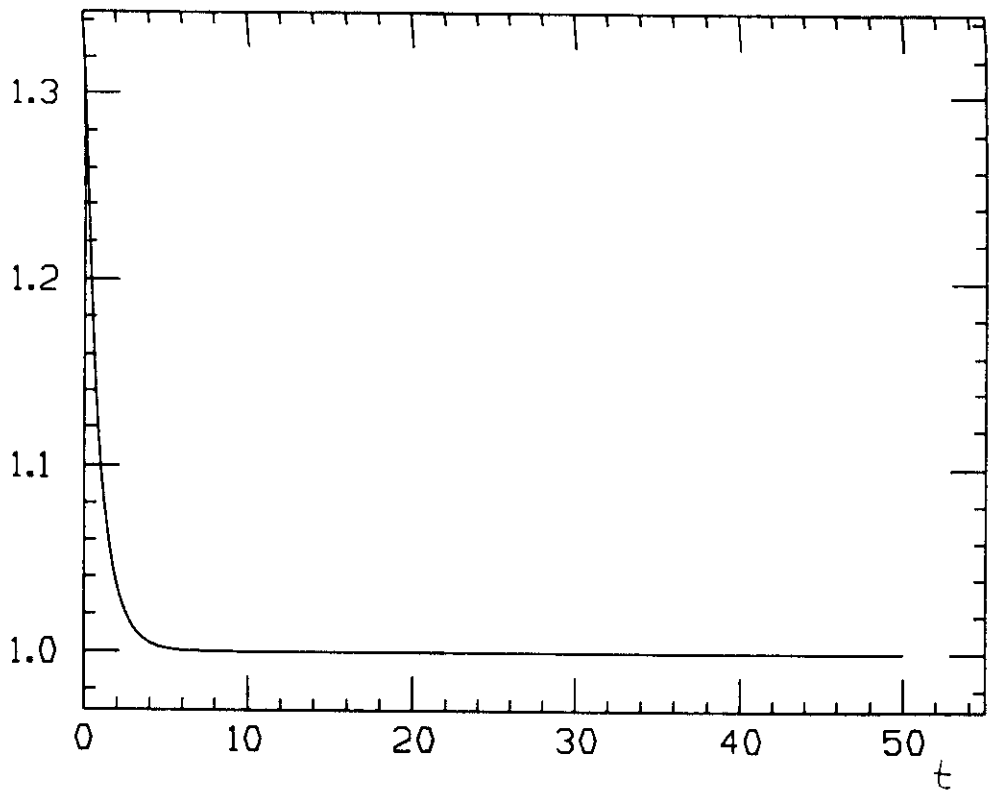

$\eta = 1.01$

$X(t)$

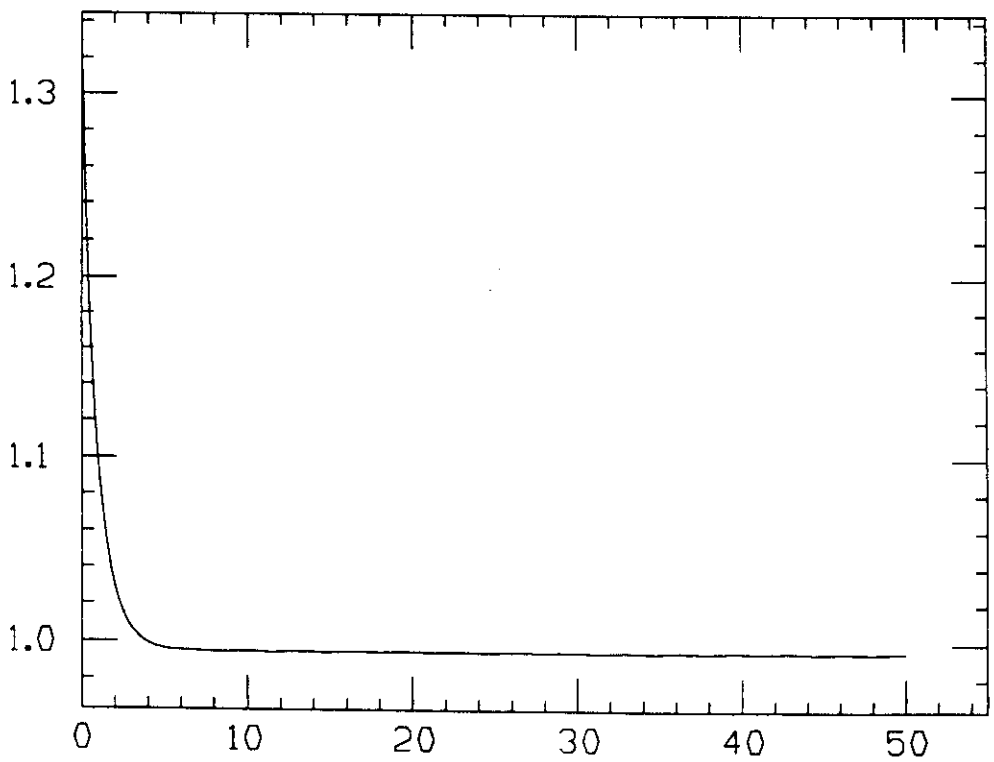

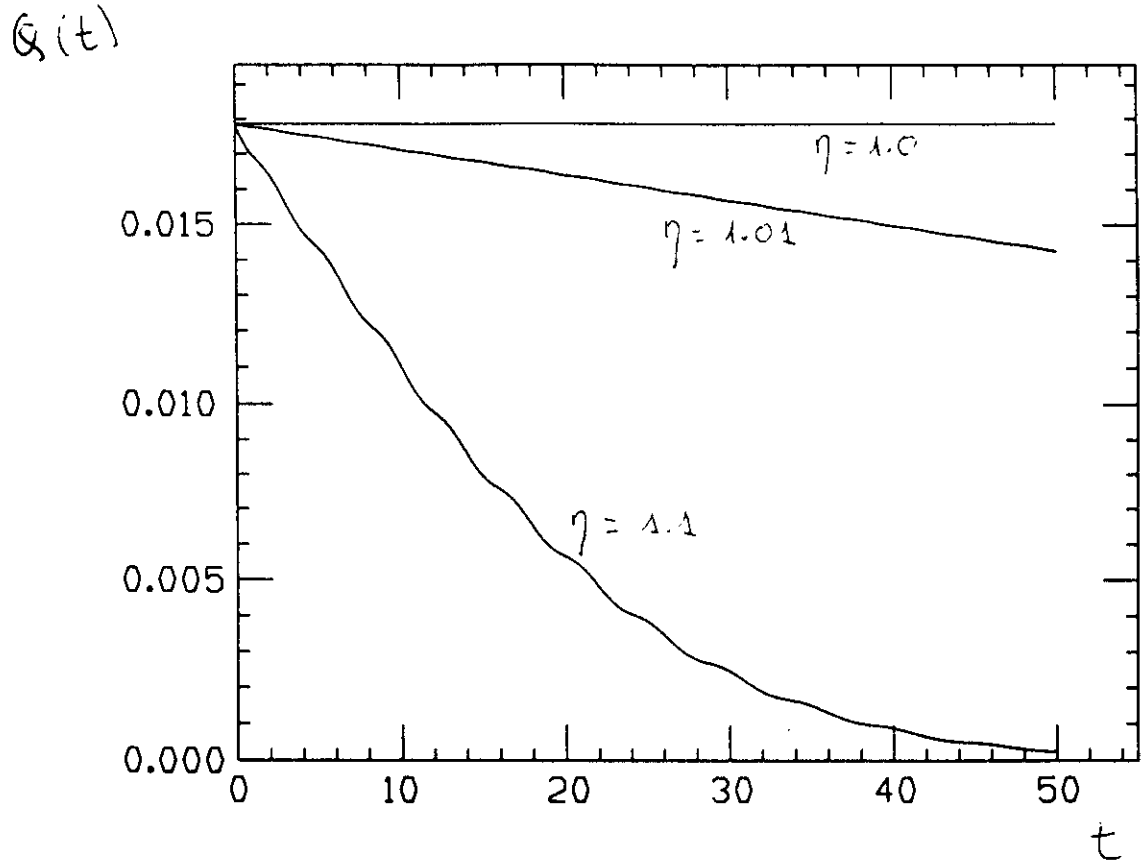
G(t)
η = 1.0
η = 1.01
η = 1.1
0.015
0.010
0.005
0.000
0
10
20
30
40
50
t

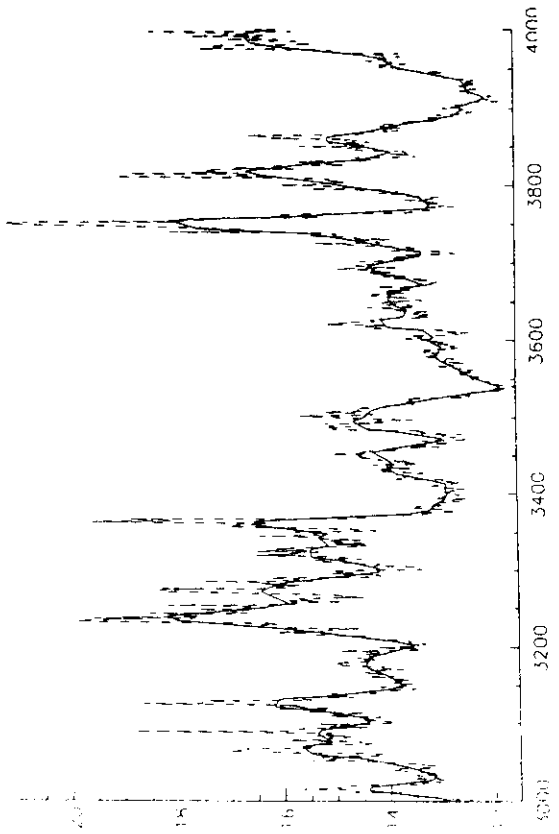
4000
3800
3600
3400
3200

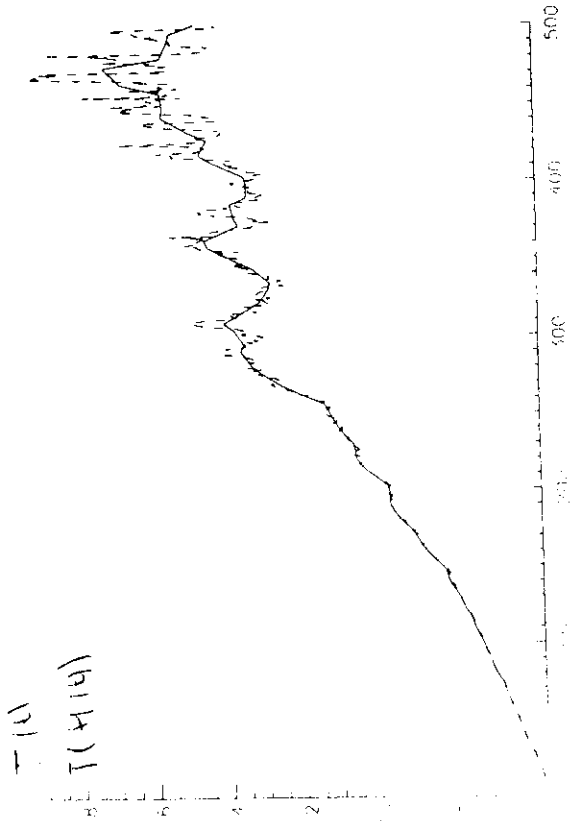
500

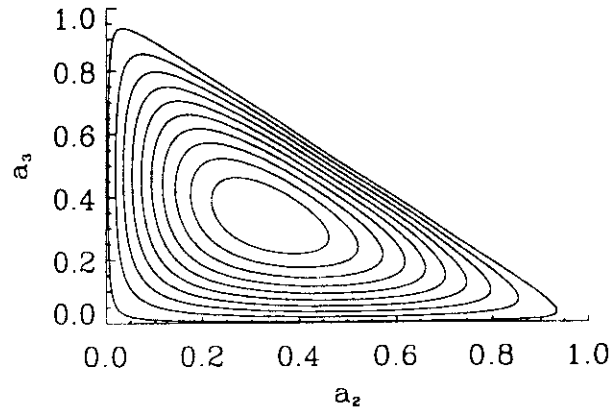

Periodic movement. Effective time scale δ^{-1}

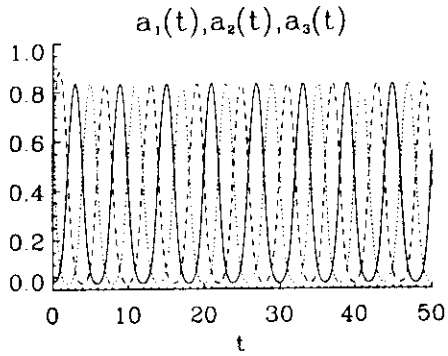

Chosen level curve, E, will depend on initial conditions

$$\mathcal{H} = a_1 a_2 a_3$$

$$\mathcal{H}^{-1}\frac{d\mathcal{H}}{dt} = 3 - (3 + 2\mu)x$$

$$\mathcal{H}(t) = \mathcal{H}_0 \left[(1 - x_0)e^{-t} + x_0\right]^{-3}$$

with $\mathcal{H}_0 = \mathcal{H}(t = 0) = a_1(0)a_2(0)a_3(0)$. The asymptotic value for $\mathcal{H}$ is

$$E = \lim_{t\to\infty} \mathcal{H}(t) = \mathcal{H}_0 x_0^{-3} = \frac{a_1(0)a_2(0)a_3(0)}{(a_1(0) + a_2(0) + a_3(0))^3}$$

The period depends on energy (on initial conditions)

$$\dot{a}_3 = \pm\delta\sqrt{a_3^2(1 - a_3)^2 - 4Ea_3}$$

$a_3(t)$ fis a periodic function (Elliptic integrals).

$$T(E) = \frac{4\delta^{-1}}{\sqrt{(a - c)b}} K\left(\sqrt{\frac{(b - c)a}{(a - c)b}}\right)$$

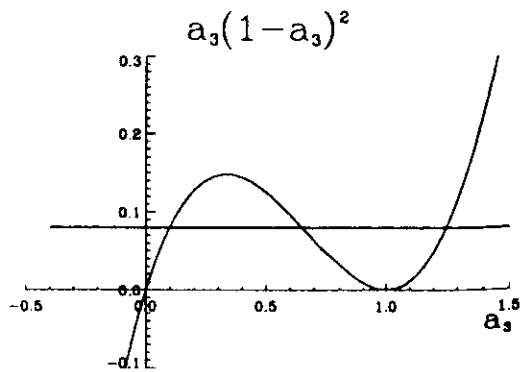

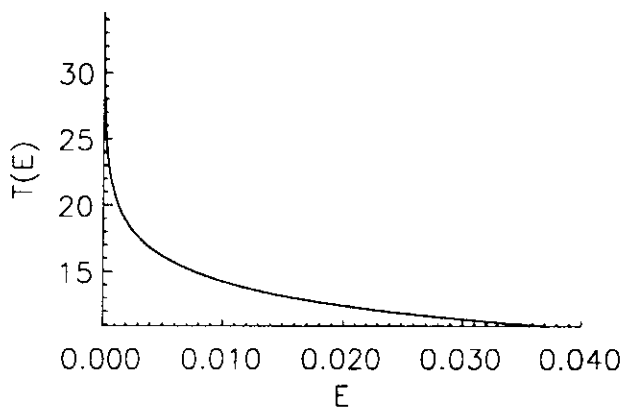

For $\mu \neq 0$ small

$$E(t) = \frac{a_1(t)a_2(t)a_3(t)}{(a_1(t)+a_2(t)+a_3(t))^3}$$

Exact evolution equation:

$$\frac{dE}{dt} = -2\mu E\left(x - \frac{3y}{x}\right) \equiv -2\mu f(t)E$$

$$E(t) = E(0)\mathrm{e}^{-2\mu F(t)}$$

$$F(t) = \int_0^t f(t)\,dt \sim t, \qquad t \to \infty$$

Exponential Decrease of $E(t)$ with a characteristic time scale μ^{-1}

Decrease of energy $E(t) \to$ increase of period T

$$T(t) = T(E(t))$$

Constant (mean) period independent on initial conditions

Add noise-dependent terms (talk by R. Gallego)
Add noise (Busse-Heikes)
Choose simplest (additive, complex, white noise) in amplitude equations

$$\begin{aligned}
\dot{A}_1 &= A_1\left(1 - |A_1|^2 - (1+\mu+\delta)|A_2|^2 - (1+\mu-\delta)|A_3|^2\right) + \xi_1(t)\\
\dot{A}_2 &= A_2\left(1 - |A_2|^2 - (1+\mu+\delta)|A_3|^2 - (1+\mu-\delta)|A_1|^2\right) + \xi_2(t)\\
\dot{A}_3 &= A_3\left(1 - |A_3|^2 - (1+\mu+\delta)|A_1|^2 - (1+\mu-\delta)|A_2|^2\right) + \xi_3(t)
\end{aligned}$$

$$\langle \xi_i(t)\xi_j(t')\rangle = 2\epsilon\delta(t-t')\delta_{ij}$$

For the modulus (population number)

$$\begin{aligned}
\dot{a}_1 &= a_1(1 - a_1 - (1+\mu)(a_2+a_3) - \delta(a_2-a_3)) + \sqrt{a_1}\xi_1(t)\\
\dot{a}_2 &= a_2(1 - a_1 - (1+\mu)(a_2+a_3) - \delta(a_3-a_1)) + \sqrt{a_2}\xi_2(t)\\
\dot{a}_3 &= a_3(1 - a_1 - (1+\mu)(a_2+a_3) - \delta(a_1-a_2)) + \sqrt{a_3}\xi_3(t
\end{aligned}$$

But more complicated to simulate beacuse of positivity
Small levels of noise produce a periodic behaviour

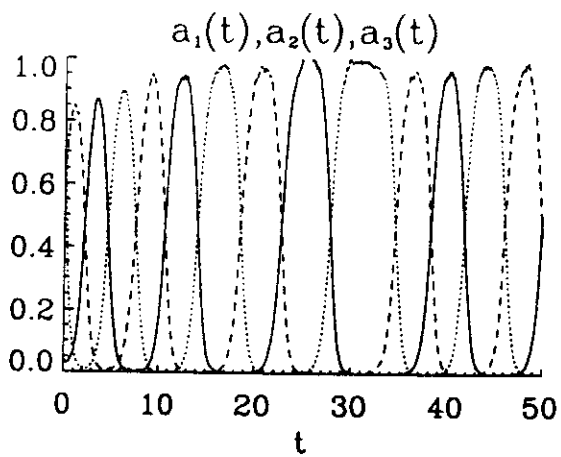

Choice for noise satisfies fluctuation–dissipation

$$g = \begin{pmatrix} 1 & 0 & 0 \\ 0 & 1 & 0 \\ 0 & 0 & 1 \end{pmatrix} = S$$

Stationary distribution (for small ϵ)

$$P_{st}(A_1, A_2, A_3) \propto \mathrm{e}^{-V(A_1,A_2,A_3)/\epsilon}$$

Mean period can be computed as a function of mean energy

$$\langle T(\epsilon) \rangle = T(\langle E \rangle)$$

where

$$\langle E \rangle = \frac{\int \mathcal{H} \mathrm{e}^{-V/\epsilon}}{\int \mathrm{e}^{-V/\epsilon}}$$

η	ϵ	$\langle T \rangle$	$T(\langle H \rangle)$
1.01	10^{-6}	16.2	14.7
1.01	10^{-8}	21.7	20.4
1.01	10^{-10}	27.6	26.3
1.1	10^{-6}	17.6	16.6

4.- NOISE-INDUCED ORDERING EFFECTS

OUTLINE

Noise-induced transitions

Noise-induced phase transitions

Effect of colored noise

Noise-induced phase separation

Noise usually creates disorder
Stochastic Resonance
Shifts in critical points
Pattern forming transition in convection
Noise–induced transitions

ϕ^4 model of Phase transitions (model A)

$$\dot{x}_i = -\frac{\partial V(x)}{\partial x_i} + \xi_i(t)$$

$$\begin{aligned} V(x) &= \sum_{i=1}^{N} \left[-\frac{b}{2}x_i^2 + \frac{1}{4}x_i^4 + \frac{1}{2}|\vec{\nabla} x_i|^2 \right] \\ &= \sum_{i=1}^{N} \left[V_0(x_i) + \frac{1}{2}|\vec{\nabla} x_i|^2 \right] \end{aligned}$$

$$\dot{x}_i = -\frac{dV_0(x_i)}{dx_i} + \sum_{j \in n(i)} [x_j - x_i] + \xi_i(t)$$

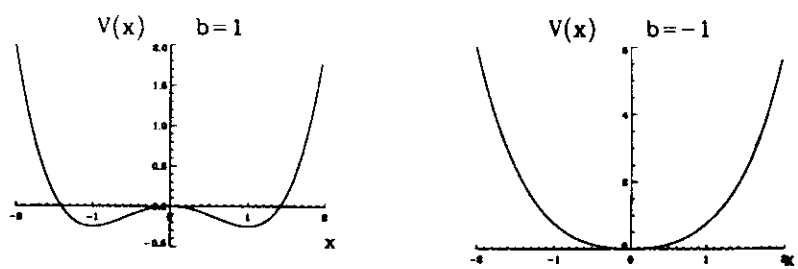

Extrema of V_0

$$m = \begin{cases} 0 & b < 0 \ , T > T_0 \\ \pm\sqrt{b} & b > 0 \ , T < T_0 \end{cases}$$

Local probability distribution changes from unimodal to bimodal
It is not a phase transition
Noise restores symmetry

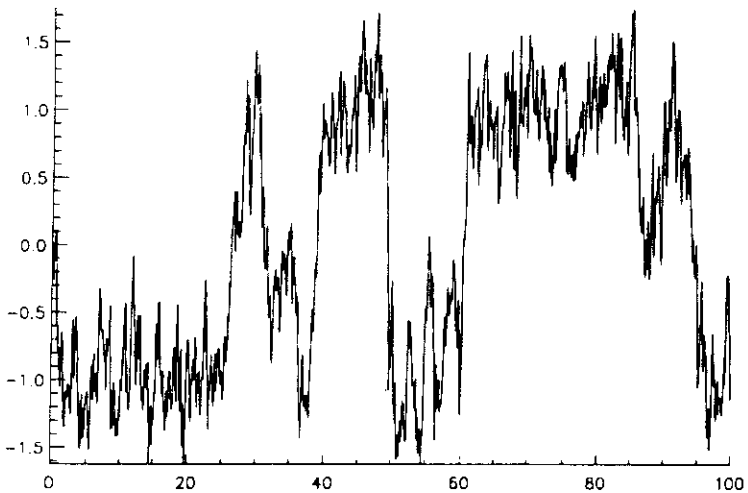

Coupling ($N \to \infty$) breaks the symmetry
Mean field (Landau) theory
Fluctuation–dissipation relation:

$$\langle \xi_i(t)\xi_j(t')\rangle = 2k_B T\delta_{ij}\delta(t-t')$$

the stationary distribution is given by:

$$P_s t(x) = Z^{-1}\exp[-V(x)/k_B T]$$

Z being a normalization constant (the partition function).
Noise makes the ordered region smaller

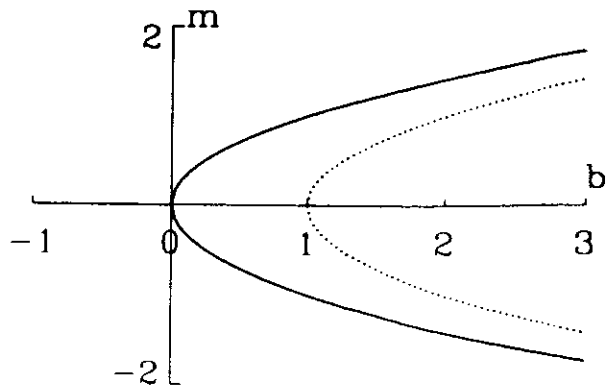

Consider the SDE (Stratonovich sense):

$$\dot{x} = f(x) + g(x)\xi(t)$$

$$\langle \xi(t)\xi(t')\rangle = \sigma^2\delta(t-t')$$

The Fokker–Planck equation:

$$\partial_t P(x,t) = -\partial_x[f(x)P(x,t)] + \frac{\sigma^2}{2}\partial_x\left\{g(x)\partial_x[g(x)P(x,t)]\right\}$$

Stationary solution:

$$P_{st}(x) = C\exp\left\{\int_0^x dy \frac{f(y) - \frac{\sigma^2}{2}g(y)g'(y)}{\frac{\sigma^2}{2}g^2(y)}\right\}$$

Extrema of $P_{st}(x)$:

$$f(\bar{x}) - \frac{\sigma^2}{2}g(\bar{x})g'(\bar{x}) = 0$$

New "stationary states" might appear as a consequence of the

noise term. Example:

$$\dot{x} = -x + \lambda x(1-x^2) + (1-x^2)\xi(t)$$

for $|x| < 1$ and $\lambda < 1$. It can be put in the form:

$$\dot{x} = -\frac{\partial V}{\partial x} + (1-x^2)\xi(t)$$

with

$$V(x) = \frac{1-\lambda}{2}x^2 + \frac{\lambda}{4}x^4$$

For $\sigma = 0$, $\bar{x} = 0$. Writing

$$P_{st}(x) \sim \exp(-V_{st}(x)/\sigma^2)$$

$$V_{st}(x) = (\sigma^2 + \lambda)\ln(1-x^2) + \frac{1}{1-x^2}$$

Extrema:

$$\begin{aligned} \bar{x} &= 0 \quad \text{if} \quad \sigma^2 < 1-\lambda \\ \bar{x} &= \pm\sqrt{(\sigma^2+\lambda-1)/(\sigma^2+\lambda)} \quad \text{if} \quad \sigma^2 > 1-\lambda \end{aligned}$$

Generic behaviour if

$$\begin{aligned} f(x) &= -ax + o(x) \\ g(x) &= 1 - bx^2 + o(x^2) \end{aligned}$$

Again is not a symmetry breaking transition.

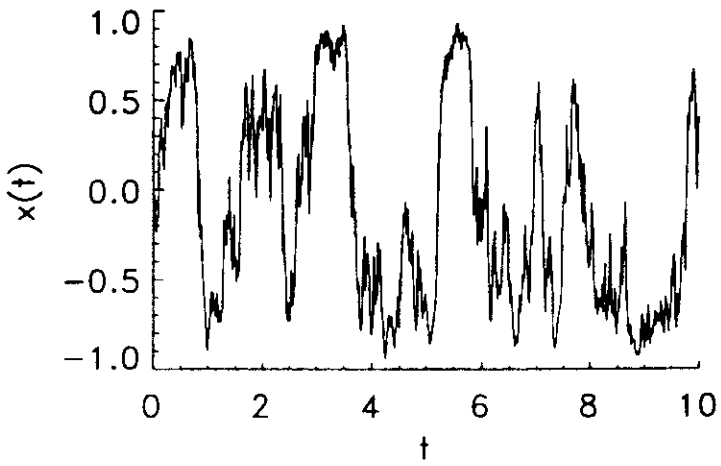

Coupling would produce a symmetry breaking state

$$\dot{x}_i = f(x_i) + \frac{D}{2d}\sum_{j\in n(i)}(x_j - x_i) + g(x_i)\xi_i(t)$$

$$\langle \xi_i(t)\xi_j(t')\rangle = \sigma^2\delta_{ij}\delta(t-t')$$

Wrong!!
Mean–field theory

$$\frac{\partial}{\partial x_i}\left[-f(x_i) + D[x_i - \langle x_{n(i)}|x_i\rangle] + \frac{\sigma^2}{2}g(x_i)\frac{\partial}{\partial x_i}g(x_i)\right]P_{st}(x_i) =$$

$$\langle x_{n(i)}|x_i\rangle = \langle x_i\rangle$$

$$P_{st}(x) = Z^{-1}\exp\left[\int^x dy \frac{f(y) - \frac{\sigma^2}{2}g(y)g'(y) - D(y - \langle x\rangle)}{\frac{\sigma^2}{2}g^2(y)}\right]$$

Consistency relation:

$$\langle x \rangle = \int dx P_{st}(x)$$

In the large coupling limit $D \to \infty$

$$f(\langle x \rangle) + \frac{\sigma^2}{2} g(\langle x \rangle) g'(\langle x \rangle) = 0$$

which is related to the short time evolution of the maxima of $P(x,t)$

$$\frac{d\bar{x}}{dt} = f(\bar{x}) + \frac{\sigma^2}{2} g(\bar{x}) g'(\bar{x})$$

What we need to have non-vanishing order-parameter states is

$$g(x) = 1 + x^2$$

Long–time behaviour is linked to short–time instability.

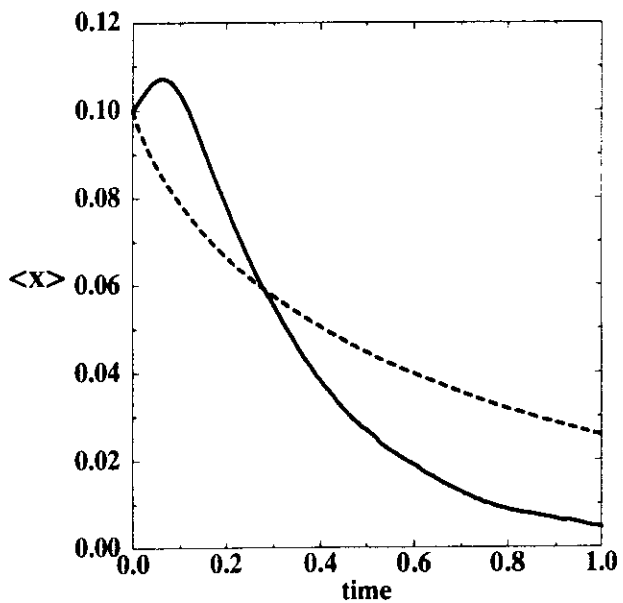

Specific example

$$\dot{x}_i = f(x_i) + \frac{D}{2d} \sum_{j \in n(i)} (x_j - x_i) + g(x_i)\xi_i(t)$$

$$\begin{aligned} f(x) &= -x(1+x^2)^2 = -\frac{\partial V}{\partial x}, \qquad V(x) = \tfrac{1}{3}(1+x^2)^3 \\ g(x) &= 1 + x^2 \end{aligned}$$

Regions of order/disorder

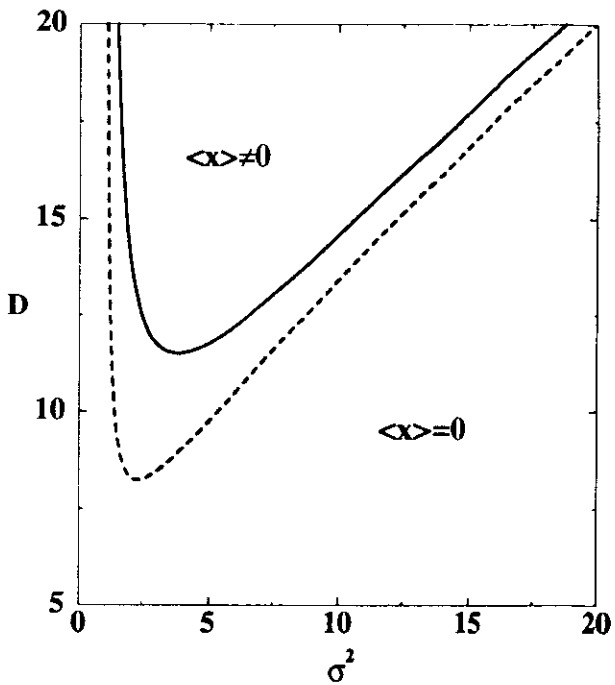

Large D limit

$$m = \langle x \rangle = \pm\sqrt{\sigma^2 - 1}$$

Phse diagram shows reentrance:
Numerical integration using Heun method (diagonal noise)
(hundred's of hours on a Connection Machine)

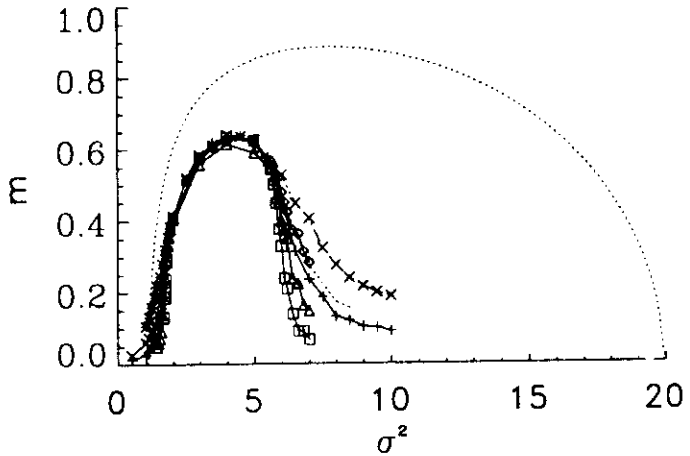

Is it a true phase transition?
Divergence of fluctuations (susceptibility):

$$\hat{\chi} \equiv \frac{\langle m^2 \rangle - \langle m \rangle^2}{N\sigma^2}$$

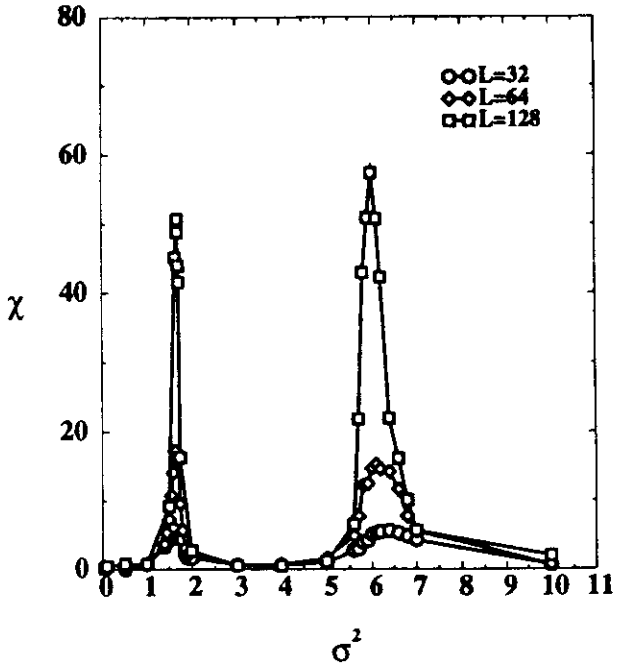

Are there finite size scaling relations?
location of critical points: second order cumulant:

$$\kappa_2 = \frac{\langle m^2 \rangle}{\langle m \rangle^2}$$

$$\kappa_2(\sigma^2, L) = \tilde{\kappa}_2(\epsilon L^{-\nu})$$

$$\epsilon = 1 - \sigma^2/\sigma_c^2$$

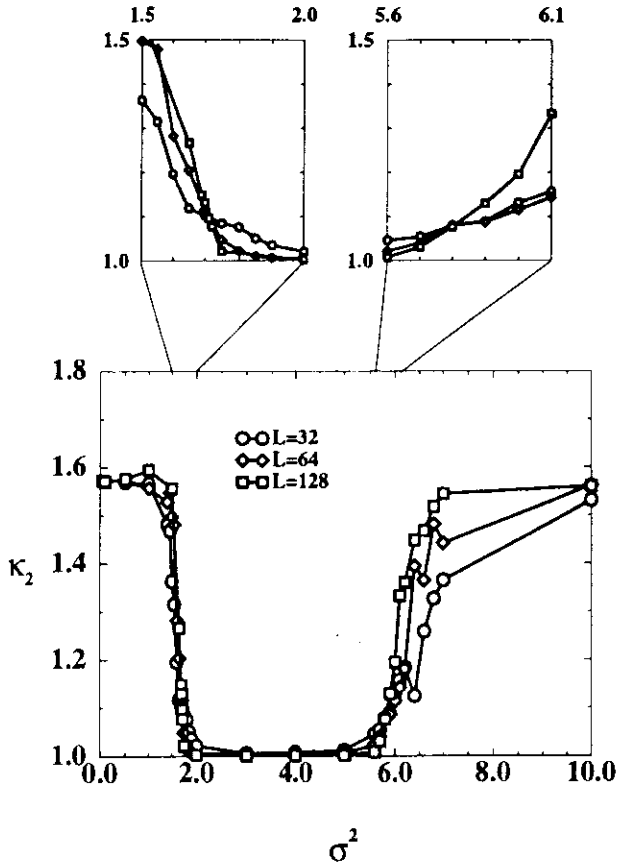

Finite size scaling for order parameter

$$m = |\frac{1}{N}\sum_{i=1}^{N} x_i|$$

Two averages are performed: time and ensemble averages:

$$m = \left\langle \left\langle | \frac{1}{N}\sum_{i=1}^{N} x_i | \right\rangle_{\text{time}} \right\rangle_{\text{ensemble}}$$

$$\langle m(\sigma^2, L)\rangle = L^{-\beta/\nu} m(\epsilon L^{1/\nu})$$

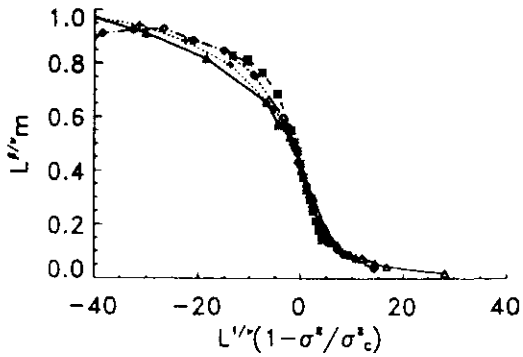

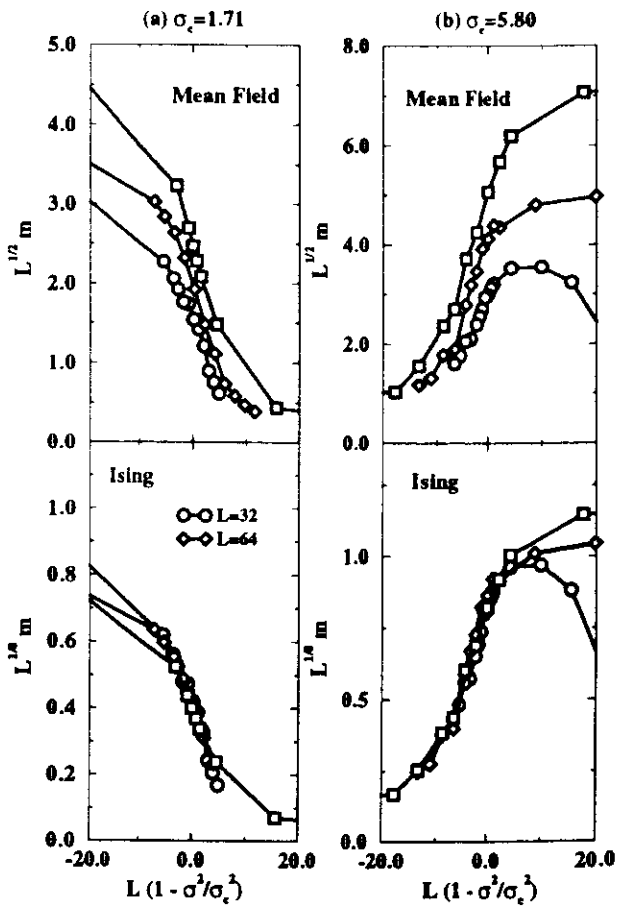

Finite size scaling for susceptiblity

$$\chi(\sigma^2, L) = L^{2-2\nu}\tilde{\chi}(\epsilon L^{-1/\nu})$$

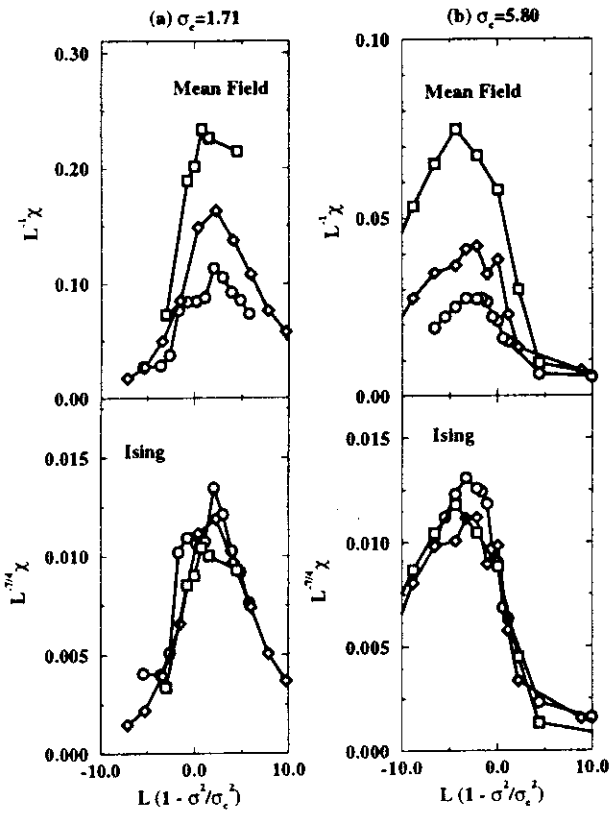

Are there long-range correlations?

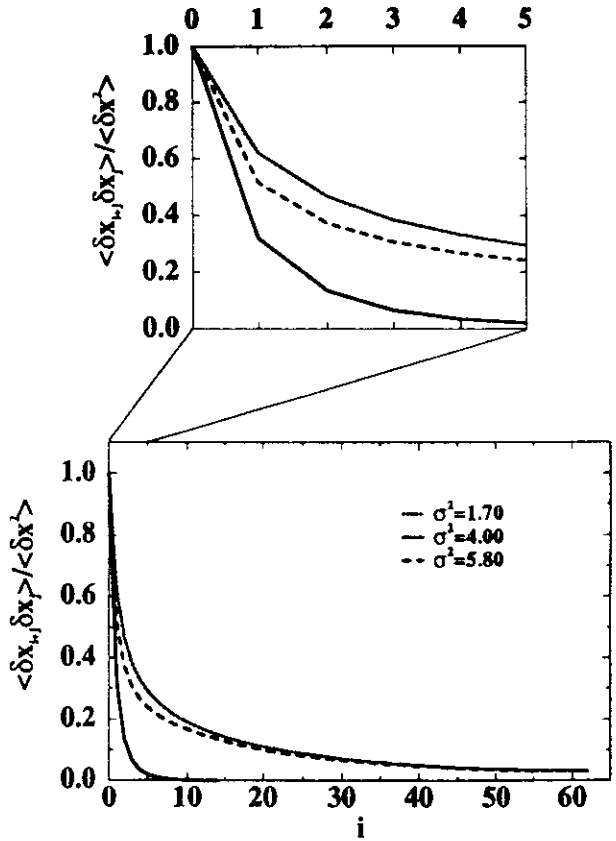

Critical slowing down?

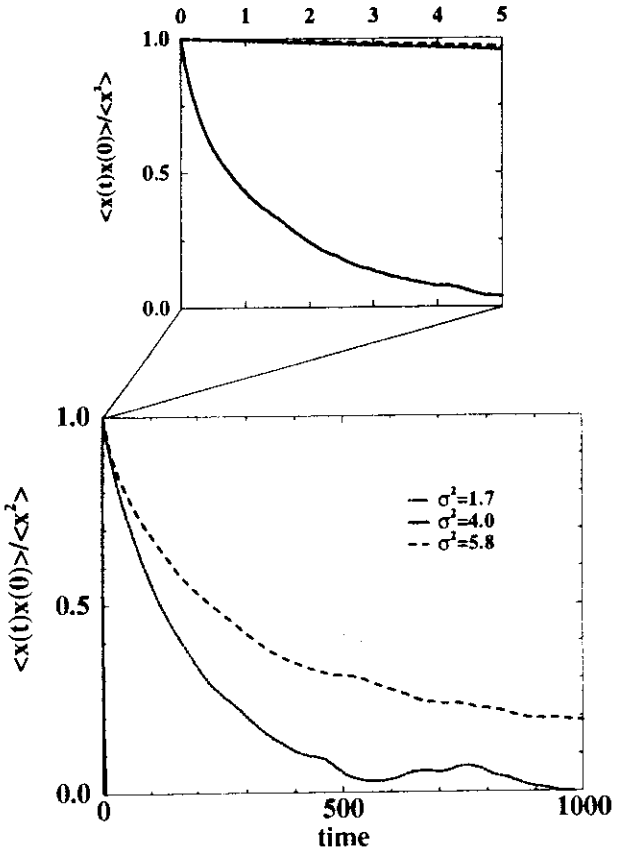

Effect of colored noise

$$\dot{x}_i = f(x_i) + g(x_i)\eta_i + \frac{D}{2d}\sum_{j\in n(i)}(x_j - x_i)$$

$$f(x) = -x(1+x^2)^2 \text{ and } g(x) = 1 + x^2$$

Ornstein-Uhlenbeck noise

$$\langle \eta_i(t)\eta_j(t')\rangle = \delta_{ij}\frac{\sigma^2}{2\tau}\exp(-\frac{|t-t'|}{\tau})$$

$$\tau\dot{\eta}_i = -\eta_i + \sigma\xi_i$$

$\langle \xi_i(t)\xi_j(t')\rangle = \delta_{ij}\delta(t-t')$.

Approximations:

(i) Set $\ddot{x}_i = (\dot{x}_i)^2 = 0$ (UCNA)

(ii) Replace neighbors x_j of x_i by a common value $\langle x\rangle$ mean field)

(iii) Use consistency relation

$$\langle x\rangle = \int_{-\infty}^{\infty} dx\, x P^{st}(x)$$

Regions of order/disorder (Fixed D):

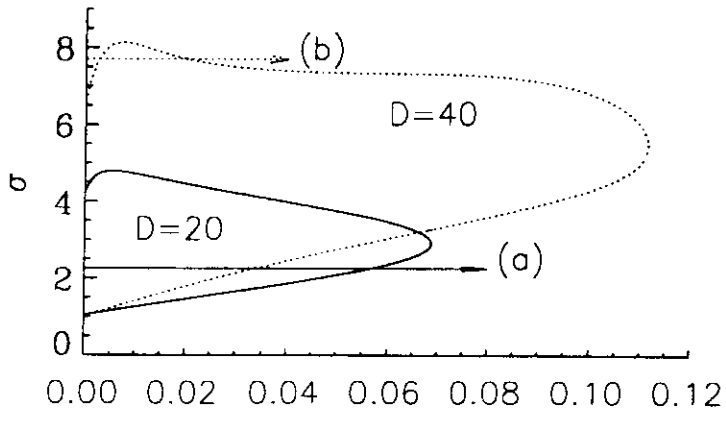

Regions of order/disorder (Fixed τ):

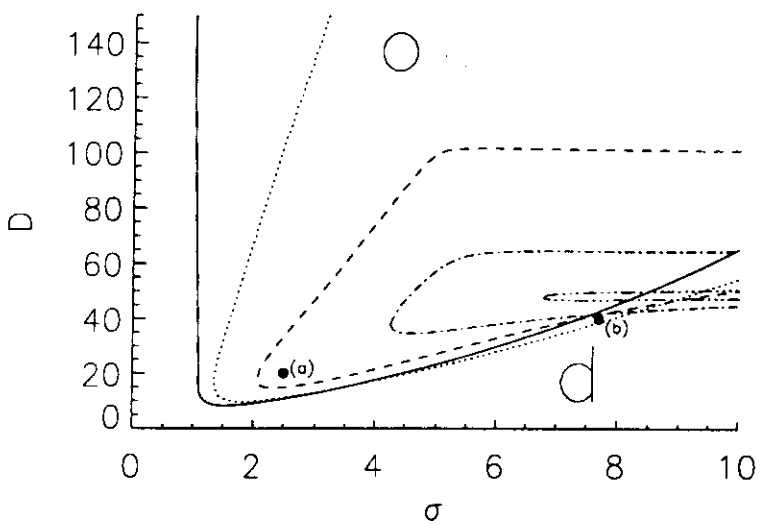

Order parameter (fixed D):

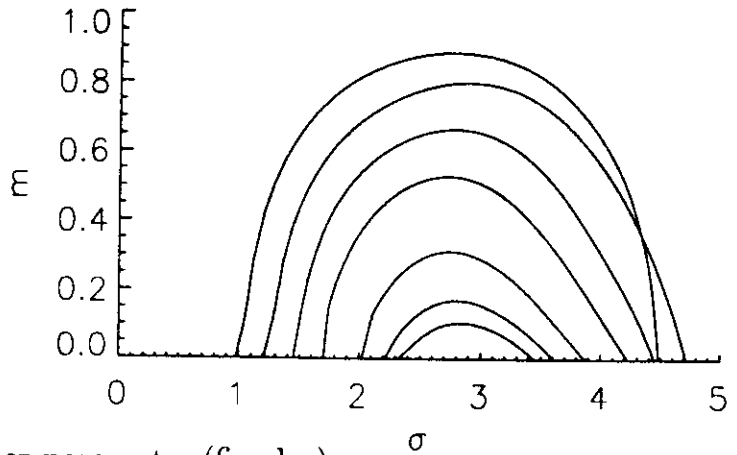

Order parameter (fixed τ):

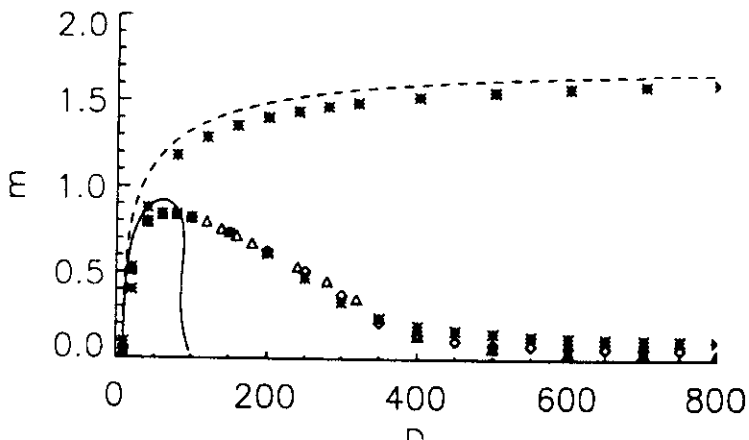

Order is destroyed by increasing the coupling intensity
Linear analysis:

$$\langle \dot{x} \rangle = -\frac{1+\tau D-\sigma^2}{1+\tau D}$$

$\tau D+1>\sigma^2$,disordered phase $\langle x \rangle = 0$ is stable
$\tau D+1<\sigma^2$, Ordered phase $\langle x \rangle \neq 0$is stable

Phase separation induced by multiplicative noise

Cahn-Hilliard-Cook model

$$\frac{\partial\psi(\vec{x},t)}{\partial t} = \nabla^2\left(\frac{\delta\mathcal{F}}{\delta\psi}\right) + \xi(\vec{x},t)$$

Additive noise satisfies fluctuation-dissipation relation:

$$\langle\xi(\vec{x},t)\xi(\vec{x}',t')\rangle = -2\varepsilon\nabla^2\delta(t-t')\delta(\vec{x}-\vec{x}')$$

$\varepsilon = k_BT$. Ginzburg-Landau free energy

$$\mathcal{F} = \int d\vec{x}\left[\frac{r}{2}\psi^2 + \frac{1}{4}\psi^4 + \frac{K}{2}|\vec{\nabla}\psi|^2\right]$$

In the absence of additive (thermal) noise, phase separation occurs for $r < r_c = 0$.
External fluctuations:

$$r \to r + \eta(\vec{x},t)$$

Finite correlation length, λ

$$\langle\eta(\vec{x},t)\eta(\vec{x}\,',t')\rangle = 2\sigma^2\delta(t-t')g(\vec{x}-\vec{x}\,')$$

$$g(\vec{x}-\vec{x}\,') = \frac{1}{(\lambda\sqrt{2\pi})^d}\exp\left(-\frac{|\vec{x}-\vec{x}\,'|^2}{2\lambda^2}\right),$$

$$\hat{g}_k = \exp\left(-\frac{\lambda^2}{2}\left(\sin(k_x/2)^2 + \sin(k_y/2)^2\right)\right)$$

Final equations:

$$\dot{\psi}_i = -\mathcal{L}_L(r\psi_i + \eta_i\psi_i + \psi_i^3 - K\nabla_L^2\psi_i) + \xi_i\,,$$

Linear analysis

$$\text{model } A: \quad r_c = \sigma^2 g_0$$
$$\text{model } B: \quad r_c = -\sigma^2\nabla_L^2 g_0 = \sigma^2 2d(g_0 - g_1)$$

Phase searation will appear when $r_{eff} > 0$

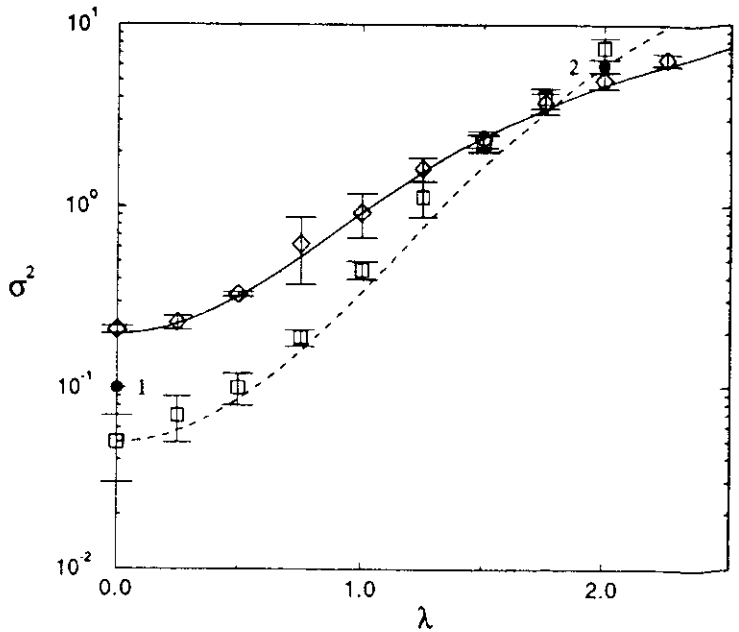

Phase Separation Driven by External Fluctuations

J. García–Ojalvo
Departament de Física i Enginyeria Nuclear, Universitat Politècnica de Catalunya, Colom 11, E-08222 Terrassa, Spain

A.M. Lacasta
Departament de Física Aplicada, Universitat Politècnica de Catalunya, Av. Dr. Gregorio Marañón, 50, E-08028 Barcelona, Spain

J.M. Sancho
Institute for Nonlinear Science, Department 0407, University of California, San Diego, 9500 Gilman Drive, La Jolla, California 92093-0407 and Departament d'Estructura i Constituents de la Matèria, Universitat de Barcelona, Av. Diagonal 647, E-08028 Barcelona, Spain

R. Toral
Departament de Física, Universitat de les Illes Balears and Instituto Mediterráneo de Estudios Avanzados (UIB-CSIC), E-07071 Palma de Mallorca, Spain

The influence of external fluctuations in phase separation processes is analysed. These fluctuations arise from random variations of an external control parameter. A linear stability analysis of the homogeneous state shows that phase separation dynamics can be induced by external noise. The spatial structure of the noise is found to have a relevant role in this phenomenon. Numerical simulations confirm these results. A comparison with order-disorder noise induced phase transitions is also made.

PACS numbers: 05.40+j, 47.20.Ky, 47.20.Hw

The role of noise as an ordering agent has been broadly studied in recent years in the context of both temporal and spatiotemporal dynamics. In the temporal case, which was the one to be addressed earlier, external fluctuations were found to produce and control transitions (known as *noise-induced transitions*) from monostable to bistable stationary distributions in a large variety of physical, chemical and biological systems [1]. Spatiotemporal systems have been faced much more recently. In these cases, the combined effects of the spatial coupling and the noise terms acting upon the system variables may produce an ergodicity breaking of a bistable state, leading to phase transitions between spatially homogeneous and inhomogeneous phases. Results obtained in this field include critical-point shifts in standard models of phase transitions [2–4], pure *noise-induced phase transitions* [5–7], stabilization of propagating fronts [8], and noise-driven structures in pattern-formation processes [9–12]. In all these cases, the qualitative (and somewhat counterintuitive) effect of noise is to enlarge the domain of existence of the ordered phase in parameter space. It is the purpose of this Letter to analyse the role of fluctuations in a radically different type of spatiotemporal process, namely in phase separation dynamics. It will be shown that external noise can induce the phase separation process and that this effect is determined by the spatial correlation of the noise terms. An important conclusion is that phase separation does not occur, necessarily, for the same range of parameters for which the system presents a phase ordering process.

The dynamics of a large class of spatially-extended systems can be described in a general way by the following standard model [13]:

$$\frac{\partial \psi(\vec{x},t)}{\partial t} = -\mathcal{L}(\nabla)\left(\frac{\delta \mathcal{F}}{\delta \psi}\right) + \xi(\vec{x},t) \qquad (1)$$

where $\psi(\vec{x},t)$ is a dynamical field that describes the state of the system, $\mathcal{F}$ is a free energy functional, and $\xi(\vec{x},t)$ is a space-dependent stochastic process that accounts for thermal fluctuations. Thermal equilibrium at temperature T is reached at long times if the fluctuation–dissipation relation holds:

$$\langle \xi(\vec{x},t)\xi(\vec{x}',t')\rangle = 2\varepsilon\mathcal{L}(\nabla)\delta(t-t')\delta(\vec{x}-\vec{x}') \qquad (2)$$

with $\varepsilon = k_B T$. The system is usually characterised by the behavior of the spatial average of the field ψ, which plays the role of an order parameter. The operator $\mathcal{L}(\nabla)$ does not alter the equilibrium state of the system ($\sim \exp(-\mathcal{F}/k_B T)$), but only its transient dynamics. Two forms of $\mathcal{L}$ are usually adopted: for $\mathcal{L} = 1$ (the so-called *model A*) the system evolves towards its equilibrium state without any constraint on the value of the order parameter; for $\mathcal{L}(\nabla) = -\nabla^2$ (*model B*) the order

parameter is conserved throughout the dynamical evolution. Model A is a prototype of ferromagnetic ordering, and model B of phase separation dynamics following a quench from a high temperature homogeneous phase to a low temperature state. In this latter case, according to the value of the order parameter and the quench location, the evolution might proceed either by spinodal decomposition or by nucleation [14].

Far from the critical point, the dynamics is not qualitatively affected by the presence of the thermal noise term $\xi(\vec{x},t)$. Instead, we will consider the situation in which there is an additional source of noise, $\eta(\vec{x},t)$. This happens, for instance, when one of the externally controlled system parameters is subjected to fluctuations. As these fluctuations are external, they do not usually verify the fluctuation–dissipation relation (2) and the system is no longer at equilibrium. We will show that, in the case of model B, these external fluctuations can induce a phase separation in the system. Although this is a reminiscence of noise–induced phase transitions reported earlier for model A [2,4,15] (and, in what follows, we will make a comparison between the effect of external noise in both models), an unexpected and notorious feature is that the nature of the destabilizing terms due to the noise is intrinsically different for model A and model B. We conclude that phase separation does not necessarily occur in the conserved order–parameter model B at the same values for which model A shows a noise–induced phase transition. It follows that, in contrast with what happens at equilibrium, both models have now different stationary distributions. Furthermore, a relevant result of our analysis is that the spatial structure of the noise plays an important and distinct role for both models. We assume the following correlation for the external noise with a characteristic correlation length λ:

$$\langle \eta(\vec{x},t)\eta(\vec{x}\,',t')\rangle = 2\sigma^2\delta(t-t')g(|\vec{x}-\vec{x}\,'|/\lambda) \qquad (3)$$

where g is a (short–ranged) spatial correlation function. It is expected, and will be confirmed in what follows, that since model B represents a domain-growth process, this correlation length will play a role far beyond the intuitive intensity-reduction effect of space-time noise correlation [3]. Correlation time of the noise should not have a parallel influence, since all time scales of the system are larger than those of the noise. Therefore, it seems that a finite (non-zero) correlation time of the noise would not differentiate between models A and B, and will not be considered here (the time dependence of the correlation of $\eta(\vec{x},t)$ will be assumed to be a Dirac delta, as shown in Eq.(3)).

Although our results are quite general, we shall work, for the sake of clarity, with the well known Ginzburg–Landau free energy

$$\mathcal{F} = \int d\vec{x}\left[\frac{r}{2}\psi^2 + \frac{1}{4}\psi^4 + \frac{K}{2}|\vec{\nabla}\psi|^2\right] \qquad (4)$$

In the absence of additive (thermal) noise, phase separation occurs for $r < r_c = 0$. If additive noise is present, the transition occurs at $r_c < 0$. We will consider $r > 0$, so that order will not appear spontaneously. The control parameter r will be assumed to be subjected to external fluctuations, *i.e.* $r \to r + \eta(\vec{x},t)$. The spatial correlation function g is chosen to be a Gaussian of width λ:

$$g\left(\frac{|\vec{x}-\vec{x}\,'|}{\lambda}\right) = \frac{1}{(\lambda\sqrt{2\pi})^d}\,\exp\left(-\frac{|\vec{x}-\vec{x}\,'|^2}{2\lambda^2}\right), \qquad (5)$$

(d is the $\vec{x}$-space dimension) which becomes a delta function in the limit $\lambda \to 0$. It is simpler to analyze the role of noise by using a lattice discretization in which the space vectors $\vec{x}$ take values x_i $(i = 1,\ldots,N)$, defined on regular lattice of linear cell size $\Delta x = 1$. The field $\psi(\vec{x},t)$ then becomes a discrete set of variables $\psi_i(t)$ and similar notation is used for the random fields $\eta_i(t)$ and $\xi_i(t)$. Under these considerations, the lattice version of model (1) with the Ginzburg–Landau free energy (4) is:

$$\dot{\psi}_i = -\mathcal{L}_L(r\psi_i + \eta_i\psi_i + \psi_i^3 - K\nabla_L^2\psi_i) + \xi_i\,, \qquad (6)$$

where $\mathcal{L}_L = 1$ for model A and $\mathcal{L}_L = -\nabla_L^2$ for model B. ∇_L^2 is the lattice Laplacian operator. Finally, in this version, the external noise has a correlation function $g_{|i-j|}$ which is the discrete inverse Fourier transform of $\hat{g}_k$, the corresponding lattice version of the Fourier transform of (5), namely (in two dimensions):

$$\hat{g}_k = \exp\left(-\frac{\lambda^2}{2}\left(\sin(k_x/2)^2 + \sin(k_y/2)^2\right)\right) \qquad (7)$$

There is no closed analytical form for $g_{|i-j|}$ and the desired values g_0 and g_1 (see later) must be obtained numerically.

The transition towards an ordered state can be analyzed by studying the stability of the homogeneous phase $\psi_i = 0$. The early time evolution of the statistical moments of ψ_i in Fourier space can be obtained in a linear approximation. For example, the second moment (structure function) is defined as $S_k(t) = \frac{1}{N}\langle\hat{\psi}_k\hat{\psi}_{-k}\rangle$, where N is the number of points of the system. Making use of the Stratonovich calculus and Novikov's theorem, its evolution equation is [11]:

$$\frac{dS_k(t)}{dt} = -2\,\omega(k)S_k(t) + \frac{1}{N}\,f(k)\sum_k \hat{g}_k S_k(t) + 2\varepsilon \qquad (8)$$

Hence the second moment equation contains a term which globally couples Fourier modes and a constant term due to thermal noise. The particular values of the dispersion relation $\omega(k)$ and of the mode-coupling coefficient $f(k)$ differ for models A and B. For model A, the result is well known [4]

$$\omega^A(k) = r^A_{eff} + Kk^2, \qquad f^A(k) = 1 \qquad (9)$$

with an effective control parameter $r^A_{eff} = r - \sigma^2 g_0$. For model B the situation is drastically different:

$$\omega^B(k) = r^B_{eff} k^2 + K^B_{eff} k^4, \qquad f^B(k) = k^2 \qquad (10)$$

with effective control parameter $r^B_{eff} = r + \sigma^2 \nabla^2_L g_0$ and effective diffusion coefficient $K^B_{eff} = K - \sigma^2 g_1$. Two main differences are observed with respect to model A: the diffusion coefficient K is also renormalized by the correlated external noise, and the noise-induced shift of the control parameter r depends now, through the Laplace operator ∇^2_L, on the spatial structure of the noise correlation, i.e. not only on the same–site correlation g_0, but also on the nearest–neighbor correlation g_1. These differences will reveal itself in the position of the transition point where the homogeneous state loses stability and phase separation appears.

When neglecting the mode–coupling terms in Eq.(8), it is readily seen that perturbations grow when $w(k)^{A,B} < 0$ for some interval of k values. We have checked, by means of a numerical integration of Eq. (8), that mode-coupling terms hardly influence the position of the transition curves. Hence the transition point is characterised by $r_{eff} = 0$ for both model A and model B. The critical value of the control parameter r and its dependence on the spatial structure of the noise is, however, different in the two cases:

$$\begin{aligned} &\text{model } A: \quad r_c = \sigma^2 g_0 \\ &\text{model } B: \quad r_c = -\sigma^2 \nabla^2_L g_0 = \sigma^2 2d(g_0 - g_1) \end{aligned} \qquad (11)$$

Figure 1 shows the transition curves between homogenous and inhomogeneous states in the (λ, σ^2) plane for models A and B for a fixed value, $r = 0.2$, of the control parameter and spatial dimension $d = 2$. All points located above the curves shown in this phase diagram are in an inhomogeneous state, which corresponds to an ordered phase in model A (solid curve) and to phase separation in model B (dashed curve). The λ–dependence of the model-A curve is merely due to the natural "softening" effect of noise correlation [3,11]. In the case of model B, on the other hand, additional, non-trivial dependence on the correlation length is introduced via the Laplace operator. As a consequence, for small λ, the transition in model B occurs *sooner* in model B than in model A, whereas the situation is the opposite for large values of λ. A crossing of the two transition curves occurs for an intermediate value of $\lambda \approx 1.8$. We stress again that the presence of ordered regions in the phase diagram of figure 1 is due to the presence of a multiplicative noise on the model, since we are taking $r = 0.2$ which is larger than the mean–field critical value $r_c = 0$.

The lines drawn in the phase diagram of Fig. 1 have been obtained in a linear approximation (11). It is presumable that this linear stability analysis will provide the position of the transition points up to leading order of approximation [4]. In order to corroborate the results obtained by means of the linear stability analysis, equations (6) have been integrated numerically for models A and B in dimension $d = 2$. A standard stochastic algorithm is used in order to handle both the additive and multiplicative noise terms [16]. Gaussianly-distributed random vectors are generated by means of a numerical inversion method, optimised to efficiently produce large quantities of Gaussian random numbers [17]. According to the previous discussion, the spatially correlated external noise is generated in Fourier space with the desired correlation function (7), and transformed back to real space at each integration time step [11].

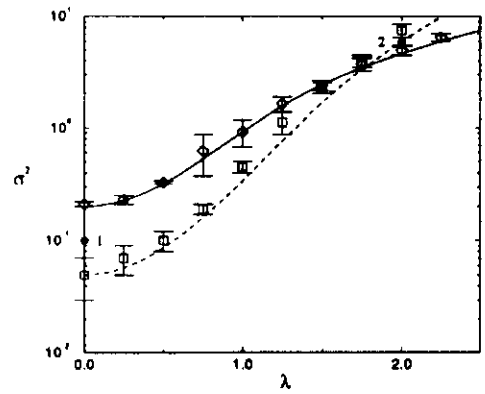

FIG. 1. Phase diagram in the (λ, σ^2) plane for model A (solid line) and model B (dashed line), obtained from a linear stability analysis (8). Points correspond to numerical simulations of the full model (6), (diamonds: model A, squares: model B) ($r = 0.2$, $K = 1$, and $\epsilon = 10^{-4}$).

A unified criterion for the existence of an ordered phase in model A and of phase separation in model B is the growth of the averaged second moment of ψ in real space (the averaged first moment is not useful for model B because this model conserves the order parameter). We define this quantity as $J(t) = \frac{1}{N}(\sum_i \psi_i^2(t))$ or, alternatively, as $J(t) = \sum_k S_k(t)$. The instability point is thus defined so that, below it, $J(t)$ decays to a thermal-noise background at large times and, above it, it grows to a non-zero steady-state value J_{st}. In this way, one can determine numerically the phase diagram of the system. The numerical results are represented in Fig. 1 as diamonds (model A) and squares (model B). It can be observed that the simulations of the full nonlinear models reasonably adjust to the predictions of the linear analysis. The agreement starts to fail at high values of λ and σ^2. In fact, according to previous observations in model A [15] and other models [5,6], the transition curves might be expected to exhibit, for higher values of the noise intensity, a reentrant branch towards the $\lambda = 0$ axis. These reentrant transitions are hard to observe numerically be-

cause of the large noise intensities involved.

Fig. 2 shows two patterns of a system evolving according to model B, for point 1 in the phase diagram of Fig. 1. Depending on the initial conditions we get spinodal decomposition (Fig. 2a, with $\langle\psi(\vec{x},0)\rangle = 0$), or nucleation (Fig. 2b, with $\langle\psi(\vec{x},0)\rangle = 0.1$). For the same values of the noise parameters a homogeneous phase is obtained for model A.

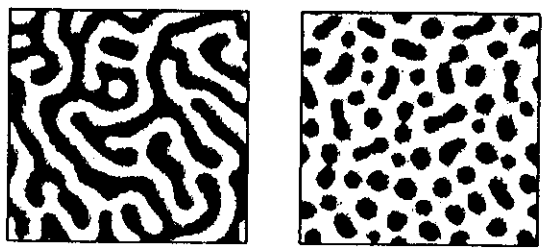

(a) (b)

FIG. 2. Spatial patterns of model B: a) Spinodal decomposition and b) Nucleation. ($t = 2500$, $\lambda = 0$, $\sigma^2 = 0.1$ and $\epsilon = 10^{-4}$)

For larger values of the noise parameters a reverse situation is found. Fig. 3 shows a spatial pattern of model A for point 2 in the phase diagram of Fig. 1. Now the homogeneous phase corresponds to model B.

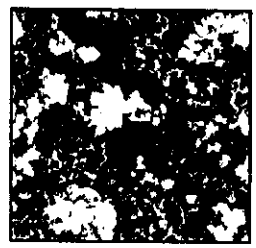

FIG. 3. Spatial pattern of model A. ($t = 100$, $\lambda = 2$, $\sigma^2 = 6$ and $\epsilon = 10^{-4}$.)

In conclusion, we have demonstrated for the first time the ordering role of external noise in processes of phase separation. The study has concentrated on the conserved time-dependent Ginzburg-Landau model, although our results are not restricted to this particular model. External noise is found to enhance the phase separation process, and this effect is observed to be modified by spatial correlation of the noise, which increases the efficiency of fluctuations for small correlation lengths and decreases it for large correlation lengths. Future work on this issue should analyse the important effect of external noise on the dynamical scaling of the phase separation process. Additional theoretical analysis such as a mean-field approach [2,5,6] could be useful in determining whether a reentrant transition should be expected in this model.

We acknowledge financial support from the Dirección General de Investigación Científica y Técnica (Spain), under projects PB96-0421, PB94-1167 and PB94-1172), and computing support from Fundació Catalana per a la Recerca.

[1] W. Horsthemke and R. Lefever, *Noise-Induced Transitions* (Springer-Verlag, Berlin, 1984).
[2] C. Van den Broeck, J.M.R. Parrondo, J. Armero, and A. Hernández-Machado, Phys. Rev. E **49**, 2639 (1994).
[3] J. García-Ojalvo and J.M. Sancho, Phys. Rev. E **49**, 2769 (1994).
[4] A. Becker and L. Kramer, Phys. Rev. Lett. **73**, 955 (1994); Physica D **90**, 408 (1995).
[5] C. Van den Broeck, J.M.R. Parrondo, and R. Toral, Phys. Rev. Lett. **73**, 3395 (1994).
[6] C. Van den Broeck, J.M.R. Parrondo, R. Toral, and R. Kawai, Phys. Rev. E **55**, 4084 (1997).
[7] S.H. Park and S. Kim, Phys. Rev. E **53**, 3425 (1996).
[8] J. Armero, J.M. Sancho, J. Casademunt, A.M. Lacasta, L. Ramírez-Piscina, and F. Sagués, Phys. Rev. Lett. **76**, 3045 (1996).
[9] J. García-Ojalvo, A. Hernández-Machado, and J.M. Sancho, Phys. Rev. Lett. **71**, 1542 (1993).
[10] J.M.R. Parrondo, C. Van den Broeck, J. Buceta, and F.J. de la Rubia, Physica A **224**, 153 (1996).
[11] J. García-Ojalvo and J.M. Sancho, Phys. Rev. E **53**, 5680 (1996).
[12] G.D. Lythe, Phys, Rev. E **53**, R4271 (1996).
[13] P.C. Hohenberg and B.I. Halperin, Rev. Mod. Phys. **49**,435 (1977).
[14] J.D. Gunton, M. San Miguel and P. Sahni, in *Phase Transitions and Critical Phenomena*, vol. 8, edited by C. Domb and J.L. Lebowitz, Academic, New York (1983).
[15] J. García-Ojalvo, J.M.R. Parrondo, J.M Sancho, and C. Van den Broeck, Phys. Rev. E **54**, 6918 (1996).
[16] T.C. Gard, *Introduction to Stochastic Differential Equations* (Marcel Dekker, New York, 1987).
[17] R. Toral and A. Chakrabarti, Comp. Phys. Commun. **74**, 327 (1993).

A General Class of

Hybrid Monte–Carlo Methods

Raúl Toral
Departament de Física, Universitat de les Illes Balears,
Palma de Mallorca, Spain

Antonio Luis Ferreira
Departamento de Física, Universidade de Aveiro
Aveiro, Portugal

-64-

~alf/papers/lugano_talk.tex

Multidimensional integrals:

$$\langle \mathcal{O} \rangle = \frac{\int_{-\infty}^{\infty} d\phi_1 \ldots \int_{-\infty}^{\infty} d\phi_N \mathcal{O}(\phi_1, \ldots, \phi_N) e^{-\mathcal{H}(\phi_1,\ldots,\phi_N)}}{\int_{-\infty}^{\infty} d\phi_1 \ldots \int_{-\infty}^{\infty} d\phi_N e^{-\mathcal{H}(\phi_1,\ldots,\phi_N)}}$$

$N \sim 10^2 - 10^8$ Monte–Carlo

$$\phi = (\phi_1, \ldots, \phi_N)$$

$$\langle \mathcal{O} \rangle = \int d\phi \mathcal{O}(\phi) f(\phi)$$

$$f(\phi) = \frac{e^{-\mathcal{H}}}{\mathcal{Z}}$$

Generate "configurations" $\phi^{(k)}$

$$< \mathcal{O} >= \frac{1}{M} \sum_{k=1}^{M} \mathcal{O}(\phi^{(k)}) \pm \epsilon$$

Statistical error:

$$\epsilon = \frac{\sigma_{\mathcal{O}}}{\sqrt{M}} (2\tau_{\mathcal{O}} + 1)$$

$$\sigma_{\mathcal{O}}^2 = \frac{1}{M} \sum_{k=1}^{M} \mathcal{O}(\phi^{(k)})^2 - \left(\frac{1}{M} \sum_{k=1}^{M} \mathcal{O}(\phi^{(k)}) \right)^2$$

$\tau_{\mathcal{O}}$: Correlation time

Independent configurations imply $\tau_{\mathcal{O}} = 0$.

Generation of configurations:

$$\phi^{(n)} \longrightarrow \phi^{(n+1)} \longrightarrow \phi^{(n+2)} \ldots$$

Proposal/acceptance scheme

Propose a transition $\phi \to \phi'$ with probability $g(\phi'|\phi)$

Accept the proposed ϕ' with probability $h(\phi'|\phi)$

Great freedom in choosing $g(\phi'|\phi)$, $h(\phi'|\phi)$

Satisfy *detailed balance*:

$$g(\phi'|\phi)h(\phi'|\phi)f(\phi) = g(\phi|\phi')h(\phi|\phi')f(\phi')$$

Metropolis algorithm. $g(\phi'|\phi)$ changes only one variable

$$\begin{array}{rcl} \phi & \to & \phi' \\ (\phi_1, ..., \phi_{i-1}, \phi_i, \phi_{i+1}, ..., \phi_N) & \to & (\phi_1, ..., \phi_{i-1}, \phi_i', \phi_{i+1}, ..., \phi_N) \end{array}$$

With $\phi_i' \in (\phi_i - \Delta, \phi_i + \Delta)$.

$$g(\phi'|\phi) = g(\phi|\phi')$$

Metropolis solution:

$$h(\phi'|\phi) = \min(1, e^{-\Delta\mathcal{H}}) \in (0, 1)$$

$$\Delta\mathcal{H} = \mathcal{H}(\phi') - \mathcal{H}(\phi)$$

Unit of time: 1 MC step = N trials

Highly correlated configurations

At critical point:

$$\tau \sim L^z \qquad z \approx 2$$

Requires computation of $\mathcal{H}$ every proposal

Need proposal $g(\phi'|\phi)$ with big change in configuration, but small change in energy $\mathcal{H}$

A clue is given by Molecular Dynamics:

Auxiliary momenta variables $P = (P_1, \ldots, P_N)$

Add "kinetic energy" to Hamiltonian:

$$\hat{\mathcal{H}}(\phi, P) = \mathcal{H}(\phi) + \frac{P^2}{2} = \mathcal{H}(\phi) + \sum_{i=1}^{N} \frac{P_i^2}{2}$$

From statistical point of view the new variables are Gaussian

distributed independent variables

$$e^{-\hat{\mathcal{H}}} = e^{-\mathcal{H}} \prod_{i=1}^{N} e^{-\frac{P_i^2}{2}}$$

Numerical integration of Hamilton equations:

$$\frac{d\phi_i}{dt} = P_i$$

$$\frac{dP_i}{dt} = F_i = -\frac{\partial \mathcal{H}}{\partial \phi_i}$$

using, for instance, the *leap–frog* algorithm:

$$\begin{aligned} \phi_i(t+\delta t) &= \phi_i(t) + \delta t \left(P_i(t) + \tfrac{\delta t}{2} F_i(t)\right) \\ P_i(t+\delta t) &= P_i(t) + \tfrac{\delta t}{2} \left(F_i(t) + F_i(t+\delta t)\right) \end{aligned}$$

$$\begin{pmatrix} \phi(0) \\ P(0) \end{pmatrix} \overset{\delta t}{\to} \begin{pmatrix} \phi(\delta t) \\ P(\delta t) \end{pmatrix} \overset{\delta t}{\to} \quad n \quad \overset{\delta t}{\to} \begin{pmatrix} \phi(\Delta t) \\ P(\Delta t) \end{pmatrix}$$

Two interesting properties of the leap–frog algorithm

(i) Area preserving:

$$J\left(\frac{\phi(\Delta t), P(\Delta t)}{\phi(0), P(0)}\right) = 1$$

(ii) Time reversible:

$$P(\Delta t) \to -P(\Delta t) \Longrightarrow \phi(2\Delta t) = \phi(0), P(2\Delta t) = -P(0)$$

There is an energy error $\Delta\hat{\mathcal{H}} = o(N\delta t^m)$

(i) Generate P from a Gaussian distribution

Take $\phi(0) = \phi, P(0) = P$

(ii) Integrate numerically using a time reversal, area preserving

algorithm

(iii) Accept $\phi' = \phi(\Delta t)$ with probability $\min(1, e^{-\Delta\hat{\mathcal{H}}})$

Unit of time $\Delta t = 1 \equiv nMC$ steps

Global updating

Only one calculation of $\dot{\mathcal{H}}$ per unit of time

Not much success in reducing critical slowing down

Relation to Langevin dynamics:

$$\frac{\partial \phi_i}{\partial \tau} = -\frac{\partial \mathcal{H}}{\partial \phi_i} + \xi_i(\tau) = F_i(\tau) + \xi_i(\tau)$$

$$< \xi_i(\tau)\xi_j(\tau') >= 2\delta_{ij}\delta(\tau - \tau')$$

The stationary solution of this equation is: $P_{st}(\phi) = \frac{e^{-\mathcal{H}}}{\mathcal{Z}}$ Numerical solution, Euler algorithm:

$$\phi_i(\tau + \delta\tau) = \phi_i(\tau) + \delta\tau F_i(\tau) + \sqrt{2\delta\tau}\eta_i(\tau)$$

Compare with one step leap–frog

$$\phi_i(t + \delta t) = \phi_i(t) + \frac{\delta t^2}{2} F_i(t) + \delta t P_i(t)$$

Same evolution algorithm with: $\delta\tau = \delta t^2/2$

With the addition of an acceptance/rejection MC step

systematic errors are elliminated

Matrix–time–step solution of Langevin equation

(Batrouni et al.):

$$\phi_i(\tau + \delta\tau) = \phi_i(\tau) + \sum_j \left[-\delta\tau\epsilon_{ij}\frac{\delta\mathcal{H}}{\delta\phi_j} + \sqrt{2\delta\tau}\sqrt{\epsilon}_{ij}\eta_j \right]$$

Where ϵ_{ij} is an arbitrary matrix

Incorporate this scheme into Hybrid Monte–Carlo

Dynamics: Assign $D - dimensional$ vector momenta

$P = (\vec{P}_1, \ldots, \vec{P}_N)$. $\vec{P}_i = (P_i^1, \ldots, P_i^D)$

$$\frac{d\phi_i}{dt} = \sum_{s=1}^{D}\sum_{j=1}^{N}(\mathcal{A}^s)_{ij}P_j^s$$

$$\frac{dP_i^s}{dt} = \sum_{j=1}^{N}(\mathcal{A}^s)_{ji}F_j \qquad s = 1, \ldots, D$$

compact vector notation:

$$\frac{d\phi}{dt} = \sum_{s=1}^{D} \mathcal{A}^s P^s$$

$$\frac{dP^s}{dt} = (\mathcal{A}^s)^\top F \qquad s = 1, \ldots, D$$

$\mathcal{A}^s$ arbitrary mattrices

Standard HMC: $D = 1$, $\mathcal{A} = \mathcal{I}$

Proposed dynamics exactly conserves energy:

$$\hat{\mathcal{H}}(\phi, P) = \mathcal{H}(\phi) + \frac{P^2}{2} = \mathcal{H}(\phi) + \sum_{i=1}^{N} \sum_{s=1}^{D} \frac{(P_i^s)^2}{2}$$

$$\frac{d\hat{\mathcal{H}}}{dt} = 0$$

Leap-frog scheme:

$$\phi(t + \delta t) = \phi + \delta t \sum_{s=1}^{D} \mathcal{A}^s P^s(t) + \frac{(\delta t)^2}{2} \sum_{s=1}^{D} \mathcal{A}^s (\mathcal{A}^s)^\top F(t)$$

$$P'^s = P^s + \frac{\delta t}{2} (\mathcal{A}^s)^\top (F(t) + F(t + \delta t))$$

Still:

(i) Area preserving:

$$J\left(\frac{\phi(\Delta t), P(\Delta t)}{\phi(0), P(0)}\right) = 1$$

(ii) Time reversible:

$$P(\Delta t) \to -P(\Delta t) \Longrightarrow \phi(2\Delta t) = \phi(0), P(2\Delta t) = -P(0)$$

There is an energy error $\Delta\hat{\mathcal{H}} = o(N\delta t^m)$

Matrix time step methods recovered by:

$$D = 1 \qquad (\delta t)^2/2 = \delta\tau \qquad \mathcal{A}\mathcal{A}^\top = \epsilon.$$

The generalized HMC method makes exact (in the sense that averages are not biased by the choice of the time step) the numerical integration of the Langevin equation using a matrix time step.

Systems with conserved order parameter

Can introduce conservation law

$$\sum_i \phi_i = \sum_i \phi'_i$$

in the proposal $g(\phi'|\phi)$ via the matrices $\mathcal{A}^s$

Choose $D = d$ (the system dimensionality)

$\mathcal{A}^s : s - th$ component of lattice gradient operator $-\vec{\nabla}_L$

Leap–frog evolution equations:

$$\phi' = \phi - \frac{(\delta t)^2}{2}\Delta_L F(t) + \delta t\ \vec{\nabla}_L \cdot \vec{P}$$

$$\vec{P}' = \vec{P} - \frac{\delta t}{2}\vec{\nabla}_L^{\top} \cdot (F(t) + F(t + \delta t))$$

exactly conserve the order parameter

Langevin equivalence: Cahn–Hilliard-Cook equation

$$\frac{\partial \phi_i(\tau)}{\partial \tau} = -\Delta F_i(\tau) + \xi_i(\tau)$$

$$\langle \xi_i(\tau)\xi_j(\tau')\rangle = -2\Delta\delta_{ij}\delta(\tau - \tau')$$

Method to obtain unbiased averages on the stationary states

of the Cahn–Hilliard–Cook equation

Can be used to compute surfce tension

Fourier acceleratior

Choose $\mathcal{A}$ diagonal in Fourier space

Gaussian model:

$$\mathcal{H} = \sum_{i=1}^{N} \left[\frac{\mu}{2} \phi_i^2 + \frac{1}{2} \mid \vec{\nabla}_L \phi_i \mid^2 \right]$$

$d = 2$ square lattice, periodic boundary conditions

Fourier space:

$$\hat{\mathcal{H}} = \sum_{k=1}^{N} \left[\frac{\omega_k^2}{2} |\hat{\phi}_k|^2 + \frac{1}{2} |\hat{P}_k|^2 \right]$$

$\omega_k^2 = \mu + 4(\sin^2(k_x/2) + \sin^2(k_y/2))$

$\mathcal{A}$ diagonal matrix in Fourier space of elements $\hat{A}_k$

leap-frog algorithm in Fourier space reads:

$$\omega_k \hat{\phi}_k(\delta t) = (1 - \frac{c_k^2}{2})\ \omega_k \hat{\phi}_k(0) + c_k\ \hat{P}_k(0)$$

$$\hat{P}_k(\delta t) = -\frac{c_k}{2}(2 - \frac{c_k^2}{2})\ \omega_k \hat{\phi}_k(0) + (1 - \frac{c_k^2}{2})\ \hat{P}_k(0)$$

where $c_k = \hat{A}_k \omega_k \delta t$

Optimal choice: $\hat{A}_k = 1/\omega_k$

Reduces completely critical slowing down, $z = 0$.

Computational effort $n \sim L^{d/4}$.

Conclusions

- Developed a General class of Hybrid Monte–Carlo methods, characterized by arbitrary matrices $\mathcal{A}^s$.
- Make exact, in the sense that averages are not biased by the integration time step, matrix–time–step Langevin integration methods
- Allows an implementation of Fourier acceleration
- Might lead to other acceleration schemes
- Allows to study systems with a conserved order parameter

Computational Field Theory and Pattern Formation

Raúl Toral

Departament de Física,
Universitat de les Illes Balears,
07071-Palma de Mallorca, Spain

1. Monte Carlo Methods

1.1. Introduction

In many occasions we need to compute the value of a high-dimensional integral of the form:

$$\int_{-\infty}^{\infty} dx_1 \ldots \int_{-\infty}^{\infty} dx_N f_x(x_1,\ldots,x_N) G(x_1,\ldots,x_N) \equiv \int dX f_x(X) G(X) \quad (1.1)$$

here N is a *large* number and we have denoted by X the set $(x_1,\ldots,x_N)$ of real variables. The function $f_x(X)$ is non-negative and normalised, i.e.:

$$\begin{aligned} &(i) \qquad f_x(X) \geq 0 \\ &(ii) \qquad \int f_x(X)\, dX \equiv \int_{-\infty}^{\infty} dx_1 \ldots \int_{-\infty}^{\infty} dx_N f_x(x_1,\ldots,x_N) = 1 \end{aligned} \quad (1.2)$$

In next chapters we will give specific examples of when one needs to perform this type of calculation. If the above integral cannot be computed by analytical methods (which happens more often than desired), one has to resource to numerical methods. One must realize, however, that a simple extension of the standard methods used in small-N numerical integration (Simpson rules, Gauss integration, etc. (Faires and Burden, 1993)) to compute numerically the value of the integral will fail for very high-dimensional integrals. For instance, let us take $N = 100$ (and this is a rather small number for typical applications) and suppose we want to use Simpson methods. We need to generate a grid in the X space and sum up all the values of $G(X)$ on the points of this grid. If we choose, say, a grid of 10 points per every coordinate, we will have 10^{100} terms to add in the Simpson rule. If every addition takes 10^{-12} s (and today's computers take much longer than that) the time needed for the calculation exceeds any astronomical unit of time (including the age of the universe). The situation does not improve by diminishing the number of points in the integration grid. Even 2 points per integration variable is beyond the capability of any present (or future) computer.

Third Granada Lectures in Computational Physics
Proceedings, Granada (Spain) 1994
Pedro L. Garrido and Joaquín Marro, eds.
Springer Lecture Notes in Physics, vol.448

The solution to this problem is given by application of the Monte Carlo techniques (Kalos and Whitlock, 1986; Binder, 1992; Heermann, 1986). For our particular example, they consist in interpreting $f_{\hat{x}}(X)$ as a probability density function of some random variable $\hat{x}$ and, consequently, the integral is nothing but the average value of the function $G(X)$,

$$\langle G \rangle = \int dX f_{\hat{x}}(X) G(X) \tag{1.3}$$

The key idea behind Monte Carlo integration is to approximate the previous average by a sample average:

$$\langle G \rangle \approx \mu_M[G] = \frac{1}{M} \sum_{k=1}^{M} G(X^{(k)}) \tag{1.4}$$

where $X^{(k)}$, $k = 1, \ldots, M$ are values of the N-dimensional variable X distributed according to the probability density function $f_{\hat{x}}(X)$. This is called the technique of **importance sampling**. The basic principle of sampling is the same one that allows politicians to have an accurate knowledge of the election results before election day by making random polls amongst a representative sample of the electors.

A more precise statement on the relation between the average $\langle G \rangle$ and the sample average $\mu_M[G]$ is given by the *central limit theorem* (Feller, 1971). This theorem states that, if the values of $X^{(k)}$ are statistically independent, then the sample average μ_M tends in the limit $M \to \infty$ to a Gaussian distribution of mean $\langle G \rangle$ and variance $\sigma^2[\mu_M]$ given by:

$$\sigma^2[\mu_M] = \frac{1}{M} \sigma^2[G] = \frac{1}{M} \left[\langle G^2 \rangle - \langle G \rangle^2 \right] \tag{1.5}$$

It is usual to express the relation between $\mu_M[G]$ and $\langle G \rangle$ as:

$$\langle G \rangle = \mu_M[G] \pm \sigma[\mu_M] \tag{1.6}$$

which is to be interpreted in the usual statistical sense for the Gaussian distribution, i.e. that there is a 95.45% probability that $\langle G \rangle$ lies in the interval $(\mu_M[G] - 2\sigma[\mu_M], \mu_M[G] + 2\sigma[\mu_M])$, 99.73% in the interval $(\mu_M[G] - 3\sigma[\mu_M], \mu_M[G] + 3\sigma[\mu_M])$, etc. In practice, the unknown variance $\sigma^2[G]$ can be replaced by the sample variance:

$$\sigma^2[G] \approx \frac{1}{M} \sum_{k=1}^{M} G(X^{(k)})^2 - \left(\frac{1}{M} \sum_{k=1}^{M} G(X^{(k)}) \right)^2 \tag{1.7}$$

According to relation (1.5) the error in a Monte Carlo integration decreases as the inverse square root of the number of samplings M. In the case that the values $X^{(k)}$ are not independent, two major modifications are needed:

(a) The variance of the sample average is given by:

Meakin, P., Ramanlal, P., Sander, L.M., Ball, R.C. (1986): Phys. Rev. **A34**, 5091.

Mehlig, B., Ferreira, A.L. and Heermann, D.W. (1992a): Phys. Lett. **B291** 151.

Mehlig, B., Heermann, D.W. and Forrest, B.M. (1992b): Phys. Rev. **B 45** 679.

Metropolis, N., Rosenbluth, A.W., Rosenbluth, M.N., Teller, A.H., Teller, E. (1953): J. Chem. Phys. **21**, 917.

Milchev, A., Heermann, D. and Binder, K. (1986): J. Stat. Phys. **44**, 749.

Milshtein, G.N. (1974): Theory. Prob. Appl. **19**, 557; (1978): *ibid* **23**, 396.

Moser, K., Kertész, J., and Wolf, D.E. (1991): Physica A **178**, 215.

Parisi, G. (1984): in *Progress in Gauge Field Theory* (Cargese lectures), ed. G't Hooft et al., Plenum Press (reproduced in Parisi, G. (1992), *Field theory, disorder and simulations*, World Scientific.

Parisi, G. (1988):*Statistical Field Theory*, Addison Wesley.

Pathria, R.K. (1972):*Statistical Mechanics*, Pergamon Press.

Press, W.H., Flannery, B.P., Teulolsky, S.A. and Vetterling, W. (1986): "Numerical Recipes". Cambridge University Press.

Rubinstein, R.Y. (1981): *Simulation and the Monte Carlo method*, John Wiley & Sons.

Sander, L. (1991): in*Solids Far From Equilibrium: Growth, Morphology and Defects*, edited by C. Godrèche, Cambridge Univ. Press, Cambridge, England.

Sexton, J.C., Weingarten, D.W. (1992): Nuc. Phys. **B380** 665.

Sokal, A.D. (1991): Nuclear Physics B (Proc. Suppl.) **20** 55.

Thomas, T.R. (1982):*Rough Surfaces* (Longman, London).

Toral, R., Chakrabarti, A. (1990): Phys. Rev. **B 42**, 2445.

Toral, R., Chakrabarti, A. and Gunton, J.D. (1989): Phys. Rev. B **39**, 901; (1992): Phys. Rev. A **45**, R2147.

Toral, R., Chakrabarti, A. (1993): Comp. Phis. Comm. **74**, 327.

Toral, R. and Ferreira, A.L. (1994) *Proceeding fo the Conference Physics Computing, '94*, p. 265, R.Gruber, M. Tomasini, editors.

Valls, O.T. and Mazenko, G.F. (1986): Phys. Rev. B **34**, 7941.

van Kampen (1981): *Stochastic Processes in Physics and Chemistry*, North-Holland.

Vicsek, T. (1989):*Fractal growth phenomena*, World Scientific, Singapore.

Zinn-Justin, J. (1989): *Quantum Field Theory and Critical phenomena*, Oxford. U. Press.

Ferrenberg, A.M. and Swendsen, R.H. (1989): Comp. in Phys. Sept/Oct, 101.
Forrest, B.M. and Toral, R. (1993): J.Stat.Phys. 70, 703.
Forrest, B.M. and Toral, R. (1994): J.Stat Phys. 77, 473.
Fratzl, P. and Lebowitz, J.L , (1989): Acta Metall. 37, 3245; Fratzl, P. (1991): J. Appl. Cryst.24, 593.
Gard, T.C. (1987): "Introduction to Stochastic Differential Equations", Marcel Dekker inc, vol 114 of "Monographs and Textbooks in Pure and Applied Mathematics".
Gardiner, C.W. (1985): *Handbook of Stochastic Methods*, Springer-Verlag, Berlin.
Glauber, R.J. (1963): J. Math. Phys. 4, 294.
Grant, M., San Miguel, M., Viñals, J. and Gunton, J.D. (1985): Phys. Rev. B 31, 3027.
Greiner, A., Strittmatter, W. and Honerkamp, J. (1988): J. Stat. Phys. 51, 95.
Grimmett, G.R. and Stirzaker, D.R. (1982):*Probability and Random Processes*, Oxford U. Press.
Gunton, J.D., San Miguel, M. and Sahni, P.S. (1983): in *Phase Transitions and Critical Phenomena*, Vol. 8, edited by C. Domb and J. L. Lebowitz (Academic, London).
Gunton, J.D. and Droz, M. (1983): *Introduction ot the Theory of Metastable and Unstable States*, Springer-Verlag.
Gupta, S. (1992): Nuc. Phys. B 370 741.
Heermann 1986: *Computer Simulation Methods*, Springer-Verlag.
Hohenberg, P.C. and Halperin, B, (1977): Rev. Mod. Phys. 49, 435.
Irback, A. (1994): J. Chem.Phys. 101 1661.
James, F. (1990): Comp. Phis. Comm. 60, 329.
Jullien, R. and Botet, R. (1985): J. Phys. A 18, 2279.
Kalos, M.H. and Whitlock, P.A. (1986): *Monte Carlo Methods*, John Wiley and Sons.
Kardar, M., Parisi, G. and Zhang, Y.C. (1986): Phys. Rev. Lett. 56, 889.
Kawasaki, K. (1972): in *Phase Transitions and Critical Phenomena*, vol. 2, edited by C. Domb and M.S.Green, Academic Press.
Kennedy A.D. and Pendleton B. (1991), Nucl.Phys. B (Proc. Suppl). 20, 118.
Kim, J.M. and Kosterlitz, J.M. (1989): Phys. Rev. Lett. 62, 2289.
Kloeden, P.E. and Platen, E. (1992):*Numerical Solution of Stochastic Differential Equations*, Springer-Verlag.
Knuth, D.E. (1981): "The Art of Computer Programming, vol 2 Seminumerical Algorithms", Addison-Wesley Pub. Co.
Krug, J. and Spohn, H. (1991): in *Solids Far From Equilibrium: Growth, Morphology and Defects*, edited by C. Godrèche, Cambridge Univ. Press, Cambridge, England.
Lacasta, A.M., Sancho, J.M., Hernández-Machado, A. and Toral, R. (1992): Phys. Rev. B 45, 5276; (1993): Phys. Rev. B 48, 6854.
Lagally M. (ed.) (1990):*Kinetics of Ordering and Growth at Surfaces*, (Plenum, New York), and references therein.
Landau, L.D. and Lifshitz, E.M. (1980):*Statistical Physics*, Pergamon Press.
Langer, J.S. (1971): Ann.Phys. 65, 53.
Langer, J.S., Bar-on, B. and Miller, H.D. (1975): Phys. Rev. A 11, 1417.
Lebowitz, J.L., Marro, J. and Kalos, M.H. (1982): Act. Metall. 30, 290 and references therein.

$$\sigma^2[\mu_M] = \frac{\sigma^2[G]}{M}(2\tau_G + 1) \tag{1.8}$$

where the *autocorrelation time* τ_G is given (in the limit of large M) by:

$$\tau_G = \sum_{k=1}^{\infty} \rho_G(k) \tag{1.9}$$

here the *normalised autocorrelation function* $\rho_G(k)$ is defined as:

$$\rho_G(k) = \frac{\langle G(X^{(k')})G(X^{(k+k')})\rangle - \langle G\rangle^2}{\sigma^2[G]} \tag{1.10}$$

The situation for non zero autocorrelation time can arise, for instance, when the value $X^{(k)}$ depends on the value $X^{(k-1)}$. In our poll example, this can occur if the k–th person to be questioned lives in the neighbourhood of the $(k-1)$–th person, such that their social classes are likely to be similar. Intuitively, τ_G measures the number of values of the sample $X^{(k)}, X^{(k+1)}, \ldots, X^{(k+\tau_G)}$ that we have to discard in order to consider that $X^{(k)}$ and $X^{(k+\tau_G)}$ are independent of each other. A problem of Monte Carlo methods is that, in many cases of interest, τ_G becomes very large and grows with the number of variables N.

(b) The relation $\langle G\rangle = \mu_M[G] \pm \sigma[\mu_M]$ has to be interpreted now according to Chebichev's theorem (Feller, 1971):

$$P(|\mu_M[G] - \langle G\rangle| > k\sigma[\mu_M]) > 1 - \frac{1}{k^2} \tag{1.11}$$

i.e. the probability that $\langle G\rangle$ lies in the interval $(\mu_M[G] - 2\sigma[\mu_M], \mu_M[G] + 2\sigma[\mu_M])$ is *at least* 75%, that it lies in $(\mu_M[G] - 3\sigma[\mu_M], \mu_M[G] + 3\sigma[\mu_M])$, *at least* 88.89%, etc.

The above Monte Carlo importance sampling procedure is one of the most powerful methods available to compute high-dimensional integrals. In order to completely specify the method, though, we need a procedure to generate the values of the samples $X^{(k)}$ that appear in the above formulae. These should be values of the N–dimensional variable $(x_1, \ldots, x_N)$ distributed according to the probability density function $f_E(X)$. There are several methods devised to generate the required values $X^{(k)}$. Before we can explain the very powerful methods available we need to study in detail some simpler cases.

1.2. Uniform sampling

Let us start with a simple example. Consider the one–dimensional (N=1) integral:

$$I = \int_0^1 dx \cos(x) \tag{1.12}$$

this is a particular case of Eq.(1.1) in which the function $f_x(x)$ is equal to 1 in the interval $(0,1)$ and 0 otherwise. The name **uniform sampling** comes from the fact that the variable x is equally likely to take any value in the interval $(0,1)$ (or, generally speaking, in any finite interval (a,b)). Although one could, in principle, devise some physical process that would produce values of a variable x uniformly distributed in the interval $(0,1)$, it is preferable, for many reasons, to use simple algorithms that can be programmed on a computer and that produce "random-type" (or *pseudo-random*) numbers uniformly distributed in the interval $(0,1)$. We will not discuss in these lectures the interesting topic of pseudo-random number generation. An excellent exposition can be found in references (Knuth, 1981) and (James, 1990). Let us simply assume that there exists a fortran function, which we will call *ran_u()*, which returns an independent random number uniformly distributed in the interval $(0,1)$. By using such a function, we can implement very easily the algorithm of uniform sampling:

```
      m=1000
      r=0.0
      s=0.0
      do 99 k=1,m
      x=ran_u()
      gk=g(x)
      r=r+gk
      s=s+gk*gk
99    continue
      r=r/m
      s=s/m-r*r
      s=sqrt(s/m)
      write(6,*) r,'+/-',s
      end
      function g(x)
      g=cos(x)
      return
      end
```

The reader should find out the name given to the function *ran_u()* in his own computer and run the above program checking that the error in the output value scales as the inverse square root of the number of samples M.

1.3. Importance sampling for N=1

In the N=1 case, when the variable $X = x$ has only one component, a simple and important theorem allows to generate $x^{(i)}$ very easily. Recall that the probability distribution function $F_x(x)$ is defined by integration of the probability density function $f_x(x)$ as:

$$F_x(x) = \int_{-\infty}^{x} f_x(y)\, dy \qquad (1.13)$$

References

Abramowitz, M. and Stegun, I.A. (1972): *Handbook of Mathematical Functions*, Dover Publications.

Ahrens, J.H., Dieter, U. (1972): Comm. of the ACM, 15 873; (1988): 31 1331.

Allen, M.P., Tildesley, D.J. (1987): *Computer Simulation of Liquids*, Clarendon Press.

Amit, D.J. (1984):*Field Theory, the Renormalisation Group and Critical Phenomena*, World Scientific.

Barber, M. (1983):*Phase Transitions and Critical Phenomena*, vol. 8, edited by C. Domb and J.Lebowitz, Academic Press.

Batrouni, G.G., Kats, G.R., Kronfled, A.S., Lepage, G.P., Svetitsky, B., Wilson, K.G. (1985): Phys. Rev. D 32 2736.

Binder, K., and Stauffer, D. (1974): Phys. Rev. Lett. 33, 1006.

Binder, K. and Heermann, D.W. (1988): *Monte Carlo simulations in Statistical Physics*, Springer, Berlin, Heidelberg.

Binder, K. (1990):*Materials Science and Technology, Vol. 5 : Phase Transformation in Materials*, ed. P. Haasen, VCH (Weinheim, Germany), p-405.

Binder, K. (ed) (1992):*The Monte Carlo Method in Condensed Matter Physics*, Topics App. Phys. Vol 71 (Springer, Berlin, Heidelberg).

Box, G.E.P. and Muller, M.E. (1958): Ann. Math. Statist. 29, 610.

Bruce, A.D. (1980): Adv. Phys. 29, 111.

Bruce, A.D. and Cowley, R. (1980): Adv. Phys. 29, 219.

Bruce, A.D. (1985): J.Phys. A 18, L873.

Cahn, J.W. and Hilliard, J. E., (1958): J. Chem. Phys. 28, 258.

Cardy, J.L., editor (1988):*Finite Size Scaling*, North-Holland.

Chakrabarti, A., (1992): Phys. Rev. B 45, 9620.

Chakrabarti, A., Toral, R. and Gunton, J.D., (1991): Phys. Rev. A 44, 12133; (1993): Phys. Rev. E 47, 3025.

Cook, H. (1970): Acta. Metall. 18 297 (1970).

Cowley, R. (1980): Adv. Phys. 29, 1.

Duane, S., Kennedy, A.D., Pendleton, B.J., and Roweth, D. (1987): Phys. Lett. B 195 216.

Eden, M. (1958):*Symposium on Information Theory in Biology*, edited by H. P. Yockey (Pergamon Press, New York), p.359.

Edwards, S.F. and Wilkinsons, D.R. (1982): Proc. R. Soc. Lon. A 381 17.

Faires, J. and Burden, R. (1993): *Numerical Methods*, PWS Publishing Company, Boston.

Family, F. and Vicsek, T. (1985): J. Phys. A 18, L75.

Family, F. and Vicsek, T. (eds.) (1991): *Dynamics of Fractal Surfaces*, World Scientific, Singapore.

Feller, W. (1971):*An introduction to probability theory and its applications*, vols. 1,2. John Wiley & Sons.

Ferreira, A.L. and Toral, R. (1993): Phys. Rev. E 47 R3848.

for $t \simeq 6000$. The moral of the story is that if one wants to avoid finite size effects one has to take systems at least as large as the ones needed in the linear case, as it is sustained by a perturbative solution of the KPZ equation (Forrest at al., 1993).

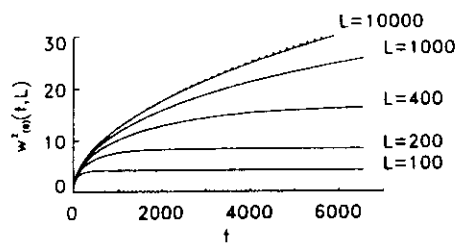

Fig. 19. Dependence with L of the square of the surface roughness, $w^2_{(0)}(t, L)$ for the linear solution of the KPZ equation, Eq.(5.31).

In fact, the finite size effects show up in a very determined way. It is now well established (Family and Vicsek, 1985; Jullien and Botet, 1985) that the roughness $w(L,t)$, for a finite substrate length L, follows an asymptotic scaling description in terms of both time t and L:

$$w(t, L) = t^{\beta} F(tL^{-\zeta/\beta}) \tag{5.32}$$

(ζ is the so-called *roughness exponent*) In principle, this relation can also be used to compute the exponent β. Again, the difficulty is that this relation is also valid for the linear case, $\lambda = 0$ *with different values for the exponents*, namely $w(t, L) = t^{1/4} F(tL^{-2})$ and one has to be careful enough to ensure that the non-linearity has fully developed. It is not strange, then, that the most powerful available computers have been used in this problem of computing precisely the exponents of the KPZ equation.

Financial support from the DGICYT, project number PB-92-0046 is acknowledged.

-19-

Theorem 1 *If $f_x(x)$ is a one-variable probability distribution function, then the variable $u = F_x(x)$ is uniformly distributed in the interval $(0, 1)$.*

As a consequence, we have the

Corollary 1 *If u is uniformly distributed in the interval $(0, 1)$, then $x = F_x^{-1}(u)$ is distributed according to $f_x(x)$.*

(The proof of this theorem is left as an exercise for the reader). This theorem reduces the problem of generating random numbers according to a given distribution $f_x(x)$ to the inversion of the corresponding probability distribution function. If, for instance, we want to use the method of importance sampling to compute the integral

$$I = \int_0^{\infty} dx e^{-x} x^2 \tag{1.14}$$

we can take $f_x(x) = e^{-x}$ if $x \geq 0$, and $G(x) = x^2$. This choice for $f_x(x)$ respects positivity and normalization. To generate values of $x^{(k)}$ according to $f_x(x)$ we need to invert $F_x(x)$, which in this case can be done analytically:

$$F_x(x) = \int_0^x dy e^{-y} = 1 - e^{-x} = u \rightarrow x = F_x^{-1}(u) = -\log(1-u) \tag{1.15}$$

Since $1-u$ is also uniformly distributed in the interval $(0, 1)$ we can write simply:

$$x = -\log(u) \tag{1.16}$$

which is equivalent to $x = -\log(1-u)$ from the statistical point of view. A program to compute integral (1.14) can be:

```
      m=1000
      r=0.0
      s=0.0
      do 99 k=1,m
      x=ran_1()
      gk=g(x)
      r=r+gk
      s=s+gk*gk
99    continue
      r=r/m
      s=s/m-r*r
      s=sqrt(s/m)
      write(6,*) r,'+/-',s
      end
      function g(x)
      g=x*x
      return
      end
```

```
function ran_f()
ran_f=-log(ran_u())
return
end
```

A technical point is that, in some cases, the function $F_x^{-1}(u)$ is not expressible in terms of elementary functions and some kind of approximative methods (such as numerical interpolation) might be needed to compute it. It is important to realize that the decomposition of a given integral in $f_x(x)$ and $G(x)$ to put it in the form of Eq.(1.3) might not be unique. In the previous example, Eq.(1.14), we could have taken as well $f_x(x) = xe^{-x}$ and $G(x) = x$. This choice, however, makes the probability distribution function $F_x(x)$ difficult to invert.

An important case in which the function $F_x^{-1}(u)$ is not easily calculable is that of Gaussian random numbers (of mean zero and variance 1) for which the probability density function is:

$$f_x(x) = \frac{1}{\sqrt{2\pi}} e^{-x^2/2} \tag{1.17}$$

(random numbers y of mean μ and variance σ^2 are easily obtained by the linear transformation $y = \sigma x + \mu$). The inverse probability distribution function is

$$x = \sqrt{2}\ \mathrm{erf}^{-1}(2u - 1) \tag{1.18}$$

where $\mathrm{erf}^{-1}(z)$ is the inverse error function (Abramowitz and Stegun, 1972; Valls and Mazenko, 1986). The inverse error function does not usually belong to the set of predefined functions in a programming language, although some libraries (for example, the NAG library) do include it in their list of functions. An alternative to the generation of Gaussian distributed random numbers is the algorithm of Box-Muller-Wiener (Box and Muller, 1958; Ahrens and Dieter, 1972; 1988) which is based on a change of variables to polar coordinates. Namely,

$$\begin{aligned} x_1 &= \sqrt{\rho}\cos(\theta) \\ x_2 &= \sqrt{\rho}\sin(\theta) \end{aligned} \tag{1.19}$$

If x_1 and x_2 are independent Gaussian variables, it is easy to prove that ρ and θ are independent variables. ρ follows an exponential distribution and θ a uniform distribution, so that their inverse distribution functions can be expressed in terms of elementary functions. Namely,

$$f_\rho(\rho) = \frac{1}{2}e^{-\rho/2} \rightarrow F_\rho(\rho) = 1 - e^{-\rho/2}, \quad \rho \geq 0$$

$$f_\theta(\theta) = \frac{1}{2\pi} \rightarrow F_\theta(\theta) = \frac{\theta}{2\pi}, 0 \leq \theta \leq 2\pi \tag{1.20}$$

The resulting algorithm is:

$$\begin{aligned} x_1 &= \sqrt{-2\log(u)}\cos(2\pi v) \\ x_2 &= \sqrt{-2\log(u)}\sin(2\pi v) \end{aligned} \tag{1.21}$$

$$w(t, L) = \sqrt{\langle \bar{h}^2 - \bar{h}^2 \rangle} \tag{5.29}$$

Where the bar denotes a spatial average $\bar{h} = L^{-1}\sum_{i=1}^{L} h_i$ and the angular brackets denote an average over initial conditions and realizations of the noise. It is important to characterize the time evolution of $w(t, L)$. The self-similar character of the surface implies that the late-time behaviour for a system of infinite size must be given by a power-law relation of the form:

$$w(t, \infty) \sim t^{\beta} \tag{5.30}$$

This relation has been well verified in computer simulations and the exact value for β can be obtained theoretically for 1-d systems ($\beta = 1/3$, see Familly et al., 1991). The reader could think that the verification of this simple law should be an easy task. Not at all! In the rest of these notes, we just want to point out which are the main difficulties in trying to verify directly the, innocent looking, power-law given by Eq.(5.30).

The first and most obvious difficulty comes from the fact that solving numerically a set of stochastic differential equations is *always* difficult. One has to average over a large number of realizations to have small statistical errors and also make sure that results do not depend on the time step chosen for the numerical integration.

The second problem is that expression (5.30) is an asymptotic result, i.e. strictly valid only in the limit $t \rightarrow \infty$. However, earlier time regimes can also be described by a relation of the same functional form with an *effective* exponent $\beta_{eff} \neq \beta$. For example, at very early times, the noise term dominates (remember that it gives a contribution of order $\sqrt{\Delta t}$) and the roughness grows as the square root of time, $w(t, L) \sim t^{1/2}$. For intermediate times, the linear term dominates. It is not difficult to solve this linear case ($\lambda = 0$, the so-called Edwards-Wilkinson model (Edwards and Wilkinsons, 1982)) and show that the roughness grows as $w(t) \sim t^{1/4}$. It is only at the very late stages that the effect of the non-linearity fully develops and one obtains the true asymptotic regime $w(t) \sim t^{1/3}$. But it is very difficult to be sure that one is in the asymptotic regime and that the exponent obtained from a, say, log-log plot of $w(t)$ versus t is giving indeed the true asymptotic exponent instead of an asymptotic exponent corresponding to smaller times.

Another problem concerns finite size effects. The result (5.30) is valid only in the limit of an infinite system. If the system size L is finite (as it is bound to be in a numerical simulation), the surface roughness can saturate to an asymptotic value $w(t \rightarrow \infty, L) \sim L^{\zeta}$ ($\zeta = 3/2$ in 1-d) and one might never enter the time regime in which relation (5.30) holds. The dramatic effect of the finite size effects can be shown in detail for the linear case, $\lambda = 0$. In this case, the solution can be found as:

$$w^2_{(0)}(t, L) = \frac{1}{L}\sum_{k=1}^{L-1} \frac{1 - \exp(-8\sin^2(\pi k/L)t)}{4\sin^2(\pi k/L)}. \tag{5.31}$$

The strong L dependence of this linear solution can be seen in Fig. [19]. Looking at the figure, we can say that only for $L \gtrsim 10^4$ there is a relative error $w_{(0)} < 1\%$

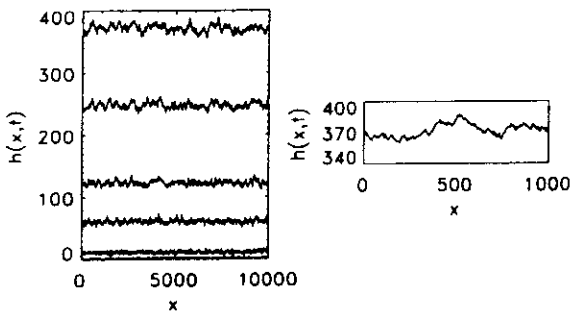

Fig. 18. Plot of the height field $h(x,t)$ from a numerical simulation of the KPZ equation in one-dimensional substrate for increasing times. We can see in this figure that the surface grows rough and that the roughness increases with time. The right figure shows a detail of the surface for the latest time.

(periodic boundary conditions are considered). The lattice spacing is usually taken equal to 1, $a_0 = 1$. The numerical integration of the previous set of stochastic differential equations can proceed by any of the methods explained in Chapter 3, although the Heun method is particularly well suited in this case since it allows to use much larger values for the integration step Δt than the one allowed in the Euler method (Forrest and Toral, 1993). If we write the previous equations in the general vector form:

$$\frac{\partial h(t)}{\partial t} = F(h(t)) + \eta(t), \tag{5.27}$$

The Heun method uses the following recurrence relation (see Eqs.(3.39)):

$$\begin{aligned} g_1 &= F(h(t)) \\ g_2 &= F(h(t) + \Delta t g_1 + \sqrt{\Delta t} u) \\ h(t+\Delta t) &= h(t) + \frac{\Delta t}{2}(g_1 + g_2) + \sqrt{\Delta t} u \end{aligned} \tag{5.28}$$

Where $u = (u_1, \ldots, u_N)$ are independent Gaussian variables of mean zero and variance unity.

In Figure 18 we can see the evolution of the field for a 1-d substrate of length L. It is clear from this figure that the surface grows rough, similarly to the case of the microscopic Eden model. A quantitative measure of the surface roughness is given by the quantity $w(t, L)$

Where u and v are independent random variables uniformly distributed in the interval $(0,1)$. The main advantage of this Box-Muller-Wiener algorithm is that it is exact, yielding two independent Gaussian variables, x_1, x_2 from two independent uniform variables, u, v. Its main disadvantage, though, is that it is extremely slow since it involves the calculation of trigonometric, logarithm and square root functions. In most of the applications a linear interpolation approximation to the inverse error function does produce sufficiently good quality Gaussian random numbers at a considerable gain in speed (Toral and Chakrabarti, 1993). A possible implementation of the Box-Muller-Wiener algorithm is the following:

```
function ran_g()
data is /-1/
is=-is
if (is.eq.1) then
      a=sqrt(-2.0*log(ran_u()))
      b=6.2831853072*ran_u()
      ran_g=a*cos(b)
      x2=a*sin(b)
      return
endif
ran_g=x2
return
end
```

(a practical note: it might be necessary to tell the compiler that the two functions *ran_u*() that appear in the previous program produce different values and need to be computed separately, sometimes compilers are too clever).

Another important case that deserves being considered explicitly, in despite of its simplicity, concerns the generation of events with a given probability. Imagine we want to simulate tossing a biased coin, with a $p = 0.6$ probability for heads (and 0.4 for tails). We need to generate a variable that takes some value (1, for example) 60% of the times and another value (0), 40% of the times. This can be done by comparing a random number u uniformly distributed in the interval $(0,1)$ with the given probability p. If $u \leq p$ then we take $x = 1$, otherwise we take $x = 0$. This is achieved by the program:

```
if (ran_u().lt.p) then
                  x=1
            else
                  x=0
endif
```

For N-dimensional variables $(x_1, \ldots, x_N)$, the situation is much more complex. The equivalent of Theorem 1 states that in order to generate values of the N-dimensional variable $(x_1, \ldots, x_N)$ we need (Rubinstein, 1981): (i) generate N-independent random numbers $(u_1, \ldots, u_N)$ uniformly distributed in the interval $(0,1)$ (this is the easy part) and (ii) solve the following set of equations:

$$\begin{aligned} F_{x_1}(x_1) &= u_1 \\ F_{x_2}(x_2|x_1) &= u_2 \\ &\cdots\cdots \\ F_{x_N}(x_N|x_1,\ldots,x_{N-1}) &= u_N \end{aligned} \tag{1.22}$$

Where, for example, $F_{x_2}(x_2|x_1)$ is the conditional probability distribution function of the variable x_2 given that x_1 has taken a particular value, and so on. The calculation of the conditional probability distribution functions is generally at least as complicated as the calculation of the original integral we wanted to compute numerically and the above procedure is of little practical use. In order to develop alternative methods suitable for the generation of N-dimensional variables we need first to introduce the so-called rejection methods for 1 variable.

1.4. Rejection method for N=1

In those cases that the inverse probability distribution function is difficult to compute, the rejection method offers a very convenient alternative. Also, it is the basis of the N-dimensional methods which we will develop later. The method is based on the fact that the probability density function $f_x(x)$ is proportional to the probability that the variable x takes a particular value. If, for example, $f_x(x_1) = 2f_x(x_2)$, we can affirm that the value x_1 is twice as probable as the value x_2. The rejection method (in its simplest version) proposes the values x_1 and x_2 with the same probability and then accepts the proposed value x with a probability $h(x)$ proportional to $f_x(x)$, such that, in our example, x_1 will be accepted twice as many times as x_2. Consequently, x_1 will appear twice as many times as x_2, which is equivalent to saying that x_1 is twice as probable as x_2 as desired. We will illustrate the method by an example. Let us consider the probability density function:

$$f_x(x) = 6x(1-x), \qquad x \in (0,1) \tag{1.23}$$

Which has the shape indicated in Fig.1.

We propose a value of x uniformly in the interval $(0,1)$. The proposed value has to be accepted with a probability $h(x)$ proportional to $f_x(x)$, $h(x) = \alpha f_x(x)$. The constant α is arbitrary but the resulting function $h(x)$ has to be interpreted as a probability, which means that we have to keep the bounds $0 \le h(x) \le 1$. This yields $\alpha \le \frac{1}{\max_x f_x(x)}$. Obviously, the rejection method is more efficient when the acceptance probability is high, which means that one has to take the maximum possible value for α. In our example, the maximum for $f_x(x)$ is at $x = 0.5$, $f_x(0.5) = 1.5$, so that we take $\alpha = 2/3$ and, consequently, $h(x) = 4x(1-x)$, see Fig.1. The acceptance process is done as explained in the previous section by comparing the probability $h(x)$ with a random number uniformly distributed in $(0,1)$. The whole process is repeated until the proposed value is accepted. The final algorithm can be coded as:

```
function ran_f()
h(x)=4.0*x*(1.0-x)
```


the height h_i in lattice site i. The presence of a surface tension is simulated by rejecting the addition of particles that produce a difference in the height between two nearest neighbours in the lattice larger that some fixed amount (Kim and Kosterlitz, 1989).

One of the most successful field theory models to study surface growth is that of Kardar, Parisi and Zhang (KPZ) (Kardar et al., 1986). In the KPZ model one defines a field $h(r,t)$ giving the surface height at location r on a $(d-1)$–dimensional substrate at time t. Several physical processes contribute to the time evolution of this field.

(i) Tendency to grow normal to the surface. A simple geometrical argument shows that in this case the evolution is given by:

$$\frac{\partial h(r,t)}{\partial t} = \lambda\sqrt{1+(\nabla h)^2} \approx \frac{\lambda}{2}(\nabla h)^2$$

to the lowest order in the gradient of the surface field. Here λ is the surface mean growth velocity.

(ii) Particle diffusion on the surface.

$$\nu\nabla^2 h$$

ν is a constant related to the surface tension.

(iii) Random variations of the incident flux. These are modeled by a stochastic, noise type term:

$$\eta(r,t)$$

Adding the contribution of the three terms we get the celebrated KPZ equation:

$$\frac{\partial h(r,t)}{\partial t} = \nu\nabla^2 h(r,t) + \frac{\lambda}{2}(\nabla h)^2 + \eta(r,t) \tag{5.22}$$

The $\eta(r,t)$ noise is assumed to be Gaussian distributed of mean zero and correlations:

$$\langle \eta(r,t)\eta(r',t')\rangle = 2D\delta(r-r')\delta(t-t') \tag{5.23}$$

Some of the parameters of this equation, λ, ν, D are redundant. One can reparametrize the field $h \to (\nu/2D)^{1/2}h$ and the time $t \to \nu t$ to obtain a simpler equation:

$$\frac{\partial h(r,t)}{\partial t} = \nabla^2 h(r,t) + \frac{\lambda}{2}(\nabla h)^2 + \eta(r,t) \tag{5.24}$$

where

$$\langle \eta(r,t)\eta(r',t')\rangle = \delta(r-r')\delta(t-t') \tag{5.25}$$

Although many exact results are known of this stochastic non-linear partial differential equation, an explicit solution is still missing. Numerical studies have played an important role in characterizing the solutions of the KPZ equation (Moser et al., 1991). In the numerical studies in a one-dimensional substrate one typically uses the following discretization of the KPZ equation:

$$\frac{dh_j(t)}{dt} = \frac{h_{j+1}+h_{j-1}-2h_j}{a_0^2} + \frac{\lambda}{2}\left(\frac{h_{j+1}-h_{j-1}}{2a_0}\right)^2 + \eta_j(t), \tag{5.26}$$

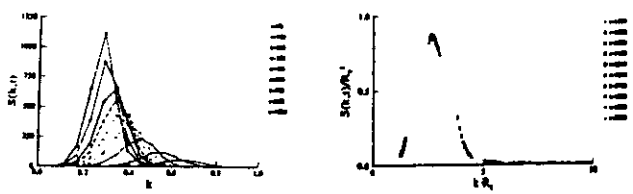

Fig. 16. Raw data (left figure) for the structure factor for the time evolution of the three-dimensional CHC in the case of a critical quench ($m = 0$). In the right figure we have rescaled the date according to Eq.(5.21) to show that dynamical scaling holds reasonably well for this system at the times studied.

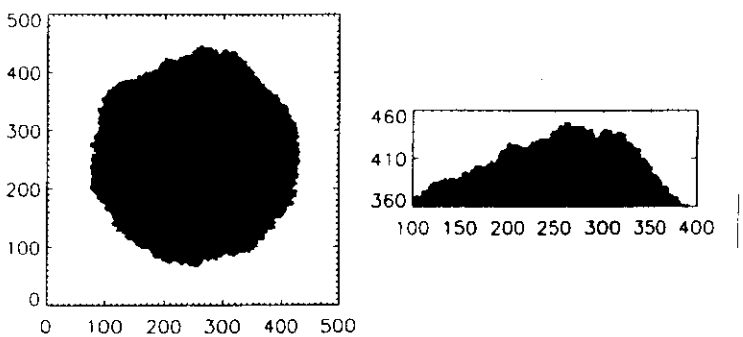

Fig. 17. A cluster grown by the Eden model rules (see text). The right figure is a detail of the cluster boundary to show that it is a rough surface.

roughness with time and with the linear dimensions of the Eden cluster can be described by a power-law with some characteristic exponents.

Another kind of models aim to mimic the evolution of a surface that grows by external flux of particles (Meakin et al., 1986). In the simplest *solid on solid* model particles are added to a regular lattice. The incident particles add to

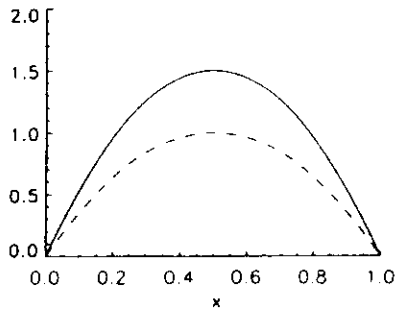

Fig. 1. Probability density function $f_x(x) = 6x(1-x)$ (solid line) and acceptance probability $h(x) = 4x(1-x)$ (dashed line)

```
1     x=ran_u()
      if (ran_u().gt.h(x)) goto 1
      ran_f=x
      return
      end
```

We will now consider a more general version of the rejection method in which a value is proposed according to some probability distribution function $g_x(x)$ and then accepted according to some probability $h(x)$. The probability distribution function of the joint process "propose the value x and accept it" is $g_x(x)h(x)$. According to the Bayes theorem, the probability density function of the variable x *given that it has been accepted* is (Grimmett and Stirzaker, 1982):

$$f_x(x) = \frac{g_x(x)h(x)}{\int_{-\infty}^{\infty} dx g_x(x)h(x)} \tag{1.24}$$

One interesting thing to notice is that the previous expression is properly normalized. This is very important in those cases where the normalization constant for $f_x(x)$ is not known explicitly. Looking at Eq.(1.24) one can see that there is some freedom in choosing the functions $g_x(x)$ and $h(x)$. The only requirement is that its product $g_x(x)h(x)$ be proportional to the function $f_x(x)$ we want to generate. An important constraint is that the proposal $g_x(x)$ must be normalized and that the acceptance function $h(x)$ must be bound in the interval $(0,1)$. For instance, in the example of Eq.(1.23), we could have considered $g_x(x) = 2x$. The function $h(x)$ should then be proportional to $3(1-x)$. Since $0 \leq h(x) \leq 1$ one takes simply $h(x) = 1-x$. The generation of $g_x(x) = 2x$ is straightforward since the inverse probability distribution function is $G_x^{-1}(u) = \sqrt{u}$. The pro-

posed value is accepted with probability $1-x$, i.e. rejected with probability x. This can be coded as:

```
      function ran_f()
1     x=sqrt(ran_u())
      if(ran_u().lt.x) goto 1
      ran_f=x
      return
      end
```

An efficient method is one that requires, on average, a small average number of proposals before acceptance. This average number is given by the inverse of the overall acceptance probability, p_a which is nothing but the denominator of expression (1.24):

$$p_a \equiv p(accept) = \int_{-\infty}^{\infty} dx g_x(x) h(x) \tag{1.25}$$

It is easy to show that of the two methods developed for the function (1.23) the first algorithm is more efficient than the second.

Let us consider yet another example: to generate numbers distributed according to

$$f_x(x) = C \exp\left[-\frac{x^2}{2} - x^4\right] \tag{1.26}$$

the obvious choice is (notice that the precise value of C is not needed):

$$\begin{aligned} g_x(x) &= \frac{1}{\sqrt{2\pi}} e^{-\frac{x^2}{2}} \\ h(x) &= e^{-x^4} \end{aligned} \tag{1.27}$$

Here $g_x(x)$ is nothing but a Gaussian distribution, and $h(x)$ is the optimal choice, given the choice for $g_x(x)$, since $\max_x h(x) = 1$. The overall acceptance probability is, according to Eq.(1.25):

$$p_a = \int_{-\infty}^{\infty} dx \frac{1}{\sqrt{2\pi}} e^{-\frac{x^2}{2}} e^{-x^4} \approx 0.62028 \tag{1.28}$$

And the average number of trials needed to accept a value is $1/0.62028 \approx 1.6$.

1.5. Rejection with repetition

There is a modification of the rejection method consisting in the following: if the proposed value is not accepted then, instead of proposing a new one, the previous value is repeated. This method obviously produces correlated values (some of them will be equal to the previous ones) but, however, can be very efficient for vector computers in which the usual structure of the rejection method prevents vectorization. We still have to prove that the values generated with this method do follow the required distribution $f_x(x)$. According to Bayes theorem,

This expresses again the idea that the system at two different times t_1, t_2 will look similar if a space rescaling of magnitude λ for the system at time t_1 is performed such that $\lambda R(t_1) = R(t_2)$ or, according to the previous expression, $\lambda = (t_2/t_1)^a$. Another important feature of the dynamical scaling description is that of the universality of the scaling function $g(x)$ and the scaling exponent a. The value $a = 1/3$ seems to hold for the CHC and Kawasaki models independently of dimension and the quench location. The function $g(x)$ does depend on dimension and quench location (Chakrabarti et al., 1991; 1993), although it seems that its variation is very small for quenches close to the critical concentration (Toral et al., 1989; Fratzl and Lebowitz, 1989).

Dynamical scaling is usually checked in terms of the experimentally accessible structure function $S(k,t)$, defined as the Fourier transform of the pair correlation function $G(r,t)$. The scaling relation for $S(k,t)$ is obtained from the one holding for $G(r,t)$ as:

$$S(k,t) = R(t)^d \mathcal{F}(kR(t)) \tag{5.21}$$

$\mathcal{F}(x)$ is the scaling function, d is the system dimensionality. In Figure 16 we plot the time evolution of the angularly averaged structure factor $S(k,t)$ from a numerical solution of the CHC equation in 3 dimensions in the case of a critical quench. We can see that the structure factor starts from a rather flat shape and, as time goes on, develops a maximum whose location k_m moves towards smaller values of k and whose intensity increases. The presence of this maximum signals the phase separation process and the location of the peak is related to the inverse typical linear length of the domains. In Figure 16 we also plot $S(k,t)R(t)^{-d}$ versus $kR(t)$ to check the scaling relation (5.21). One concludes that scaling is well satisfied at the times studied. Similar results hold for other dimensions and models, as well as for experiments (Binder, 1990).

5.2. Growth of rough surfaces

Many surfaces in nature grow roughly. Examples include such diverse systems as biological tumors, mountain ranges, sand piles, a fluid flowing through a porous medium and many others (Lagally, 1990; Thomas, 1982). To study this widespread phenomenon, scientists have developed microscopic models and field models [1].

The simplest of the microscopic models is one due to Eden (Eden, 1958). The Eden model can be used to study the spread of epidemics. In this model one considers a regular lattice in which a site is initially marked as "infected". At a given time a randomly selected infected site infects one of its nearest neighbours, again chosen at random. After some time, the infected area is rather compact with a rough surface, see Fig.17. From a careful analysis of this figure one can deduce that the surface has fractal properties and that the dependence of the

[1] Recent reviews on kinetic roughening in surface growth models can be found in: Family and Vicsek, (1991); Krug and Spohn, (1991); Sander, (1991); Wolf, (1990); Family, (1990) and Vicsek, (1989)

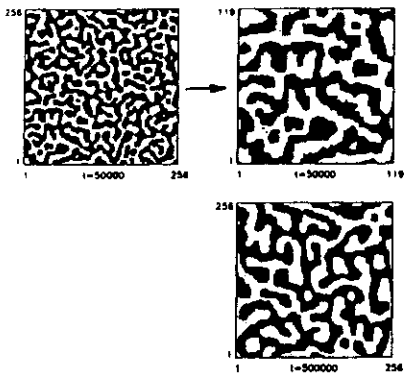

Fig. 15. Self similarity after rescaling of configurations for the two-dimensional CHC model in the case of a critical quench $m = 0$. A snapshot of the configuration at time $t_1 = 50,000$ (upper row, left) is magnified by a factor 256/119 *approx*2.15. The resulting figure is very similar (from the statistical point of view) to a snapshot of the same system at time $t_2 = t_1 \times 2.15^3 \approx 500,000$, showing that the dynamical exponent in Eq.(5.20) is close to 1/3.

$$G(r,t) = \langle \Phi(r,t)\Phi(r+r',t) \rangle, \tag{5.17}$$

or, rather, its circular average:

$$G(r,t) = \frac{\int d\Omega G(r,t)}{\int d\Omega} \tag{5.18}$$

(Ω denotes the angular variables), which, in principle, is a two variable function, depends only on a combination of them, namely:

$$G(r,t) = g(r/R(t)) \tag{5.19}$$

where the *scaling function* $g(x)$ is a one variable function of the scaling variable $x = r/R(t)$. $R(t)$ is a measure of the typical domain size and can be defined, for instance, as the first zero of the pair correlation function. The time behaviour of $R(t)$ is described by a power-law:

$$R(t) \sim t^a \tag{5.20}$$

the probability density function $f_{x_n}(x)$ generated at the n-proposal step will have two different contributions corresponding to the acceptance or rejection, respectively, of the proposed value

$$f_{x_n}(x) = f_{x_n}(x|accept)p(accept) + f_{x_n}(x|reject)p(reject) \tag{1.29}$$

The first term of the right hand side can be written as the probability of acceptance given x (which is the function $h(x)$) times the probability density function of proposing x (which is $g_x(x)$):

$$f_{x_n}(x) = h(x)g_x(x) + f_{x_n}(x|reject)(1-p_a) \tag{1.30}$$

If x has been rejected, the previous value is repeated which means that the probability density function at the n-step in the case of rejection is the same that the one at the $(n-1)$-step:

$$f_{x_n}(x) = h(x)g_x(x) + f_{x_{n-1}}(x)\left[1 - \int_{-\infty}^{\infty} dx h(x)g_x(x)\right] \tag{1.31}$$

where we have substituted p_a as given by Eq.(1.25). The solution of this linear recurrence relation is:

$$f_{x_n}(x) = (1-p_a)^n \left[f_{x_0}(x) - \frac{h(x)g_x(x)}{\int_{-\infty}^{\infty} dx h(x)g_x(x)}\right] + \frac{h(x)g_x(x)}{\int_{-\infty}^{\infty} dx h(x)g_x(x)} \tag{1.32}$$

We can write this result in terms of the desired distribution $f_x(x)$, Eq. (1.24):

$$f_{x_n}(x) = (1-p_a)^n [f_{x_0}(x) - f_x(x)] + f_x(x) \tag{1.33}$$

Given that $0 < p_a \leq 1$, one concludes that the solution tends to the desired distribution in the limit $n \to \infty$ independently of the initial distribution f_{x_0}:

$$lim_{n\to\infty} f_{x_n}(x) = f_x(x) \tag{1.34}$$

If the initial proposed numbers x_0 are distributed according to $f_x(x)$, i.e. if $f_{x_0}(x) = f_x(x)$, then we would have $f_{x_n}(x) = f_x(x)$, $\forall n$ and the numbers we obtain are distributed according to the desired distribution from the beginning. However, if the initial numbers are not distributed according to $f_x(x)$ (as it is usually the case) we can still affirm that, thanks to the factor $(1-p)^n$, the initial condition will be lost after a number sufficiently large of proposals. This process of rejecting the, say, M_0 initial values produced because they are not distributed yet according to the required distribution is called *thermalization*. The initial time needed for thermalization can be computed from the non-linear correlation function (Binder and Heermann, 1988):

$$\rho_x^{NL}(k) = \frac{\langle x^{(k)} \rangle - \langle x \rangle}{\langle x^{(0)} \rangle - \langle x \rangle} \tag{1.35}$$

The time M_0 can be measured as a characteristic time for the decay of the above function towards the stationary value 0. For the method of rejection with

repetition the non-linear correlation function coincides with the auto-correlation function (see later):

$$\rho_x^{NL}(k) = (1 - p_a)^k \tag{1.36}$$

The thermalization time M_0 can be defined as the time it takes the above function to reach a small value ϵ

$$M_0 = \frac{\ln \epsilon}{\ln(1 - p_a)} \tag{1.37}$$

If, for instance, $\epsilon = 10^{-6}$, $p_a = 0.5$, we have $M_0 \approx 27$.

We can illustrate now the enhancement of the errors due to the correlations. In this method of rejection with repetition, one can compute the correlation function of the variable x as (see Eq.(1.10)):

$$\rho_x(k) = \lim_{k' \to \infty} \frac{\langle x^{(k)} x^{(k+k')} \rangle - \langle x \rangle^2}{\langle x^2 \rangle - \langle x \rangle^2} = (1 - p_a)^k \tag{1.38}$$

From Eq.(1.9) we deduce that the autocorrelation time is:

$$\tau_x = \sum_{k=1}^{\infty} \rho_x(k) = \frac{1 - p}{p} \tag{1.39}$$

Remember that, according to Eq.(1.8) the statistical error gets enhanced by the factor $(2\tau_x + 1)^{1/2}$.

We finally mention that it is possible to interpret this algorithm of rejection with repetition as a Markov succession (Grimmett and Stirzaker, 1982). Indeed, Eq.(1.31) can be cast in the form:

$$f_{k_n}(x) = \int_{-\infty}^{\infty} f(x|y) f_{k_{n-1}}(y)\, dy \tag{1.40}$$

where the transition probability is:

$$f(x|y) = h(x) g_k(x) + \left[1 - \int_{-\infty}^{\infty} dx\, h(x) g_k(x)\right] \delta(x - y) \tag{1.41}$$

1.6. The algorithm of Metropolis et al.

Although it is very powerful, the rejection method can fail if the distribution is very peaked around an (unknown) value x_0 (see Fig.2). If our proposal does not take into account that only a very small part of the variable space (that around x_0) is important, we are bound to have a extremely high rejection probability yielding the rejection method completely useless. The solution comes by making a proposal that does not differ much of the present value of the random variable we are sampling, i.e by having the transition probabilities of the Markov succession depend explicitly on the present value, say y, of the variable. This implies that the functions $h(x)$ and $g_k(x)$ depend on y and become two-variable

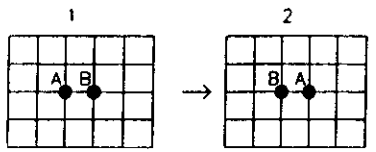

Fig. 14. Kawasaki exchange model basic process

The transition rate for the process $1 \to 2$ (see Fig. 14) is taken in Kawasaki formulation as:

$$P(1 \to 2) = \frac{1}{2\tau}\left[1 - \tanh\left(\frac{\Delta\mathcal{H}}{2k_B T}\right)\right] \tag{5.16}$$

Where $\Delta\mathcal{H}$ is the change in energy required to go from state 1 to state 2. τ simply fixes the unit of time. The previous expression is chosen by mathematical simplicity, but any function of the form $P(1 \to 2) = \exp\left(-\frac{\Delta\mathcal{H}}{k_B T}\right)\omega\left(\frac{\Delta\mathcal{H}}{k_B T}\right)$ where $\omega(z) = \omega(z^{-1})$ will satisfy detailed balance for the master equation and hence will ensure the correct equilibrium state (see discussion in section 1.6).

The Kawasaki exchange model and the Cahn–Hilliard–Cook model exhibit many common features. In fact, it is possible to obtain, using some approximations, the Cahn–Hilliard–Cook model by means of a coarse–graining of the Kawasaki exchange model (Langer, 1971; Gunton et al., 1983b). In Fig.13 we show the evolution of the CHC and Kawasaki models for the case of a quench of critical concentration. Observe the great similarity between the evolution of the two models.

5.1.3 Dynamical Scaling

An important property of the late stages of the dynamics of phase separation process is that of *dynamical scaling* (Binder and Stauffer, 1974; Lebowitz et al., 1982). This scaling description is suggested by the fact that systems at different times look similar provided a space rescaling is performed. More precisely: if we take a snapshot of a configuration of the system at a given time t_1 and make it larger by a factor λ it turns out that the resulting figure is *statistically indistinguishable* of a snapshot of the same system at a later time $t_2 = \lambda^{1/a} t_1$, a being a dynamical scaling exponent (see Fig.15). This dynamical scaling description is based on the physical assumption that, at the late stages of the evolution, only one length, related to the typical domain size, is relevant. Mathematically, the scaling description implies that the pair correlation function $G(r, t)$:

$$\mathcal{H} = \sum_{i,j} [J_{i,j}(AA)C_i^A C_j^A + J_{i,j}(BB)C_i^B C_j^B + J_{i,j}(AB)C_i^A C_j^B] \qquad (5.12)$$

Writing the occupation variable C_i^A and C_i^B in terms of the spin variables S_i one gets, apart from a constant factor:

$$\mathcal{H} = -\sum_{i,j} J_{i,j} S_i S_j \qquad (5.13)$$

Where $J_{i,j}$ is some linear combination of the interaction strengths $J_{i,j}(AA)$, $J_{i,j}(BB)$ and $J_{i,j}(AB)$. We take now the approximation that the forces between atoms are of short range nature, such that the only relevant interactions are the ones between nearest neighbour sites on the lattice and we further assume that they are all equal to a constant value J. In this case, the Hamiltonian reduces to:

$$\mathcal{H} = -J \sum_{<i,j>} S_i S_j \qquad (5.14)$$

where the sum runs over the nearest neighbour pairs on the lattice. This is nothing but the Hamiltonian of the celebrated Ising model. In our binary mixture model, though, there is the restriction that $N^{-1}\sum_i S_i = m$ must be a fixed constant. One can prove (Pathria, 1972) that the grand canonical partition function of the binary mixture model is equal to the canonical partition function of the standard Ising model. Many equilibrium properties of the binary mixture, such as the phase diagram, can thus be obtained from the corresponding ones of the Ising model.

Our model for a binary mixture is indeed too simplified and it is absent of many realistic features present in real materials, such as defects in the lattice, no perfect symmetry between A and B compounds leading to asymmetric phase diagrams, vacancies, etc. One can not pretend, then, to reproduce all of the features present in these substances. In fact our hamiltonian is so simple that it is absent of any "natural" dynamics such as the one given by Hamilton equations. Kawasaki introduced an *stochastic* dynamics for the binary mixture model in the same spirit that Glauber dynamics for the Ising model (Glauber, 1963). The thermal fluctuations, mediated by the lattice phonons, induce random transitions in which atoms exchange positions in the lattice, see Fig.14 (in the ordinary Glauber dynamics, spins flip randomly their value, this is forbidden here due to the conservation law). This exchange process aims to mimic, in a very crude way, the diffusion process occurring in real materials.

In order to ensure that the system will asymptotically reach the correct equilibrium state given by the Gibbs distribution, Kawasaki assigns a probability to the microscopic exchange process. The equation governing the evolution of the system is a master equation for the probability density of configurations $P([S_1,\ldots,S_N];t)$:

$$\frac{d}{dt}P([S];t) = -P([S];t)\sum_{[S']} P([S]\to[S']) + \sum_{[S']} P([S';t)P([S']\to[S]) \qquad (5.15)$$

functions, $g_x(x|y)$, $h(x|y)$. The transition probability Eq.(1.41) then becomes also a two variable function

$$f(x|y) = h(x|y)g_x(x|y) + \left[1 - \int_{-\infty}^{\infty} h(z|y)g_x(z|y)\,dz\right]\delta(x-y) \qquad (1.42)$$

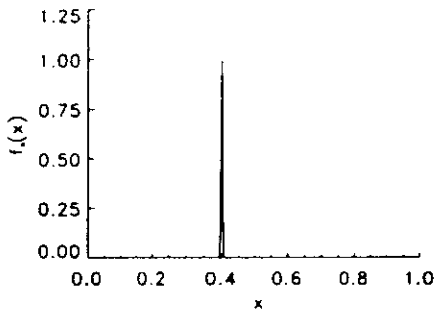

Fig. 2. Function $f_x(x)$ for which the rejection method can fail

The equation giving the evolution of the probability density function at the n-step is still Eq. (1.40), but now the recursion equation for $f_{x_n}(x)$ does not tell us in a straight way which is the stationary ($n \to \infty$) distribution. We would like to have $f_x(x)$ as stationary solution of the recursion equation, i.e:

$$f_x(x) = \int_{-\infty}^{\infty} f(x|y)f_x(y)\,dy \qquad (1.43)$$

By using the normalization condition $\int_{-\infty}^{\infty} f(y|x)\,dy = 1$ and the definition (1.42) for the transition probability $f(x|y)$, one gets easily:

$$\int dy\,[g_x(x|y)h(x|y)f_x(y) - g_x(y|x)h(y|x)f_x(x)] = 0 \qquad (1.44)$$

A sufficient condition to fulfill this relation is given by the *detailed balance condition*:

$$g_x(x|y)h(x|y)f_x(y) = g_x(y|x)h(y|x)f_x(x) \qquad (1.45)$$

to be satisfied by the proposal $g_x(x|y)$ and the acceptance probability $h(x|y)$. Let us remark that if the detailed balance condition is satisfied and if $f_{x_n}(x) = f_x(x)$ then $f_{x_n}(x) = f_x(x)$, $\forall n$. Also, if the transition probabilities satisfy the condition of *ergodicity*, which, roughly speaking, means that any value for the random variable can be achieved starting from any other value after a sufficient number of steps, then we can assure that $f_x(x)$ is the only stationary solution of the

Markov succession and that $\lim_{n\to\infty} f_{x_n}(x) = f_x(x)$, independently of the value of $f_{x_0}(x)$ (see Kalos and Whitlock, 1986).

It is important to stress that any functions $g_x(x|y)$ and $h(x|y)$ that satisfy ergodicity and the detailed balance condition are suitable to use in this rejection method. The most widely used solution is the one given by the the **Metropolis algorithm** (Metropolis et al., 1953) in which $g_x(x|y)$ is a given function usually of the form:

$$g_x(x|y) = \frac{1}{2\Delta}, \qquad \text{if} \quad |x-y| \leq \Delta \tag{1.46}$$

i.e. x is sample uniformly from the interval $(y-\Delta, y+\Delta)$. Once the value of x has been proposed one looks for acceptance probabilities $h(x|y)$ verifying the detailed balance condition:

$$\frac{h(x|y)}{h(y|x)} = \frac{g_x(y|x)f_x(x)}{g_x(x|y)f_x(y)} \equiv q(x|y) \tag{1.47}$$

When searching for solutions of these equations one has to remember that $h(x|y)$ is a probability and must also satisfy the condition $0 \leq h(x|y) \leq 1$. A possible solution is the *Metropolis solution*:

$$h(x|y) = \min(1, q(x|y)) \tag{1.48}$$

Another widely used solution is the *Glauber solution* (Glauber, 1963):

$$h(x|y) = \frac{q(x|y)}{1+q(x|y)} \tag{1.49}$$

A family of solutions is obtained by:

$$h(x|y) = \sqrt{q(x|y)}\,\omega\,(q(x|y)) \tag{1.50}$$

where $\omega(x)$ is any function satisfying

$$\omega(x) = \omega(x^{-1}) \tag{1.51}$$

In particular, the Metropolis solution is recovered taking:

$$\omega(x) = \min(x, x^{-1}) \tag{1.52}$$

and the Glauber solution taking

$$\omega(x) = \frac{1}{x^{1/2}+x^{-1/2}} \tag{1.53}$$

Before we use the Metropolis algorithm to study some models of field theory, we want to finish this section by showing the use of the Metropolis algorithm with a simple example in a one variable case. We will consider the Gaussian distribution:

$$f_x(x) = Ae^{-x^2/2} \tag{1.54}$$

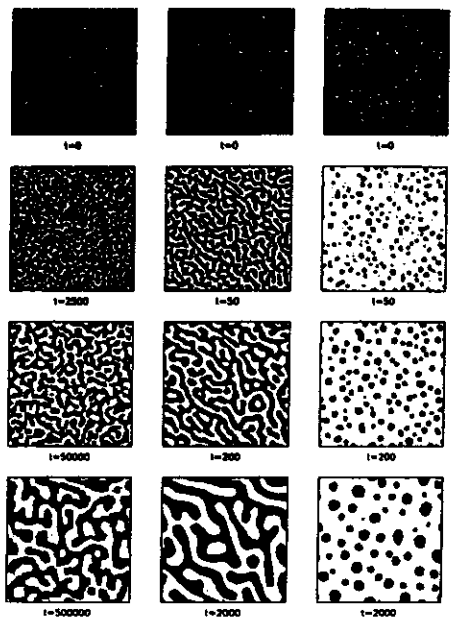

Fig. 13. Time evolution of the Kawasaki model and the Cahn-Hilliard-Cook (CHC) model. Positive (negative) values for the fields or the spins are indicated by white (black) regions. Notice the similarity between the Kawasaki model (left column) and the CHC (center column) both at critical concentration ($m = 0$). In these two cases, the system evolves by spinodal decomposition. In the right column, we plot a solution of the CHC model for an off-critical quench (in this case $m = 0.2$). Notice that evolution proceeds via the formation of nuclei of the minority phase that coarsen and grow.

S_i is an Ising type variable taking the value $+1$ (-1) if in site i there is a A-atom (B-atom). Let us denote by $J_{i,j}(AA)$, $J_{i,j}(BB)$, $J_{i,j}(AB)$ the strength of the interaction between AA, BB and AB atoms, respectively, at locations i and j in the lattice. The Hamiltonian is:

$$\frac{d\phi_i(t)}{dt} = \nabla_L^2 \left(-\theta b \phi_i + \gamma \phi_i^3 - \nabla_L^2 \phi_i\right) + \zeta_i(t) \tag{5.8}$$

with correlations

$$\langle \zeta_i(t)\zeta_j(t')\rangle = -2\delta(t-t')\nabla_L^2 \delta_{i,j} \tag{5.9}$$

The Cahn-Hilliard-Cook equation is a very complicated stochastic, nonlinear, partial differential equation that has so far defied an exact analytical treatment. Very successful systematic approximations valid for early times have been developed (Grant et al., 1985). For the late stages of the dynamics the most successful theory is that of Langer, Bar-on and Miller (Langer et al., 1975), based on some approximative mode decoupling. This theory, however, is very difficult to improve upon due to its non-perturbative nature. It seems at this stage that it is necessary to resource to numerical studies to analyze the long-time behaviour of the equation. One can integrate the CHC equation using any of the stochastic numerical methods developed in section 3.3. In Figure 13 we have plotted configurations resulting of a numerical integration using the simple Euler method. In this figure we observe that the evolution depends on the location of the quench point in phase diagram. For critical ($m = 0$) or near critical concentrations, (region I of the phase diagram in Fig.12), the system is unstable against long wavelength, small amplitude fluctuations. This generates initially a highly interconnected pattern that coarsens with time. The system is said to evolve by *spinodal decomposition*. If, on the other hand, the system is in region II, between the so-called spinodal line and the coexistence curve, the system is unstable against the formation of nuclei of the minority phase. These nuclei evolve in time in such a way that large droplets grow at the expense of small droplets. This is the evolution for *nucleation and growth*. Although this simple picture is thought to be of general validity, it is not possible to sharply separate the domains in the phase diagram where the two processes dominate (Binder, 1990; Chakrabarti, 1992).

5.1.2 The Kawasaki model

A more microscopic approach to the dynamics of phase separation is the one given by the Kawasaki dynamical version of the Ising model (Kawasaki, 1972). In each site of a regular lattice A we define two occupation variables, C_i^A and C_i^B, such that C_i^A takes the value 1 (0) if in site i there is (there is not) an A-atom. C_i^B is defined in a similar way. If we consider the situation in which every site of the lattice is occupied by either A-atoms or B-atoms, i.e. that there are no vacancies, C_i^A and C_i^B verify $C_i^A + C_i^B = 1$. We define a new variable S_i as:

$$S_i = C_i^A - C_i^B \tag{5.10}$$

from where it is easy to deduce:

$$C_i^A = \frac{1+S_i}{2} \qquad C_i^B = \frac{1-S_i}{2} \tag{5.11}$$

the normalization constant A is irrelevant for the Metropolis method. The proposal will be a value belonging to the interval $(y-\Delta, y+\Delta)$. Notice that this choice (Eq.(1.46)) satisfies the symmetry relation $g_\Delta(x|y) = g_\Delta(y|x)$. This proposal will be accepted with a probability given, for example, by the Metropolis solution Eq.(1.48):

$$h(x|y) = \min(1, q(x|y)) = \min(1, e^{(y^2-x^2)/2}) \tag{1.55}$$

i.e if $|x| \leq |y|$ accept with probability 1, otherwise accept with probability $e^{(y^2-x^2)/2}$. The Metropolis algorithm can be coded as:

```
function ran_g(y,delta)
x=y+delta*(2*ran_u()-1)
if(abs(x).gt.abs(y)) then
    if (exp(0.5*(y-x)*(y+x)).lt.ran_u()) then
                ran_g=y
                return
    endif
endif
y=x
ran_g=y
return
end
```

Intuitively, the effect of this algorithm is to accept with a larger probability those proposals which tend towards the origin, where the probability has a maximum.

An important warning concerns the fact that we must keep the old value of the variable if the new one has been rejected. We can not keep proposing until a value is accepted (at variance with what happened in the ordinary rejection method in which the two procedures were correct). If one does not keep the old value, a reasoning similar to the one used in the rejection method, section 1.4, leads to the following transition probabilities, see Eq.(1.24):

$$f(x|y) = \frac{h(x|y)g(x|y)}{\int_{-\infty}^{\infty} dz h(z|y)g(z|y)} \tag{1.56}$$

and:

$$f(y|x) = \frac{h(y|x)g(y|x)}{\int_{-\infty}^{\infty} dz h(z|x)g(z|x)} \tag{1.57}$$

Now it is very difficult to satisfy the detailed balance conditions, Eq.(1.45), namely:

$$\frac{h(x|y)g(x|y)}{\int_{-\infty}^{\infty} dz h(z|y)g(z|y)} f_\Delta(y) = \frac{h(y|x)g(y|x)}{\int_{-\infty}^{\infty} dz h(z|x)g(z|x)} f_\Delta(x) \tag{1.58}$$

since the integrals are generally difficult to compute (in particular, the Metropolis solution does not satisfy this condition). The reader can test the following modification of the Metropolis algorithm for the Gaussian distribution:

```
      function ran_g(y,delta)
1     x=y+delta*(2*ran_u()-1)
      if(abs(x).gt.abs(y)) then
         if (exp(0.5*(y-x)*(y+x)).lt.ran_u()) goto 1
      endif
      y=x
      ran_g=y
      return
      end
```

and check that it does not produce Gaussian random numbers (it is worse for large Δ).

For efficiency of the Metropolis algorithm Δ must be chosen such that the autocorrelation time of the algorithm, τ, takes its minimum value. It is easy to understand why there must be a minimum of τ as a function of Δ. If Δ is very small, the new proposal will be very close to the old one (hence highly correlated), τ will be large and $h(x|y)$ will be very close to 1 such that the acceptance will be also close to 1. On the other hand, if Δ is large, the acceptance probability will be small and the proposed value will be often rejected, such that the new value will be equal to the old one (again highly correlated). A rule of thumb tells us that Δ must be chosen such that the acceptance probability is neither too high, neither too small, i.e. of the order of 50%.

1.7. Rejection method in the N-dimensional case

We really do not need to develop any new concepts. The nice thing about the Metropolis algorithm is that is easily generalizable to the N-dimensional case. Simply replace x and y in the above expressions by the N-dimensional variable vectors $(x_1, \ldots, x_N)$ and $(y_1, \ldots, y_N)$, respectively, and all of the above formulae and concepts will still apply. In order to keep the acceptance probability within reasonable limits, the proposal can not be too different from the old value. This is achieved by changing only one of the N variables at one time. The variable to be updated can be chosen randomly amongst the set of the N variables or sequentially. If chosen randomly the function $g_x(x|y)$ is explicitly given by:

$$g_x(x|y) = \frac{1}{N}\sum_{i=1}^{N}\frac{1}{2\Delta}\prod_{j\neq i}\delta(x_j - y_j) \tag{1.59}$$

Since it verifies the symmetry condition $g_x(x|y) = g_x(y|x)$, the function $q(x|y)$ is simply $q(x|y) = f_x(x)/f_x(y)$. The acceptance probability can be chosen as the Metropolis solution $h(x|y) = \min(1, q(x|y))$ or other solution.

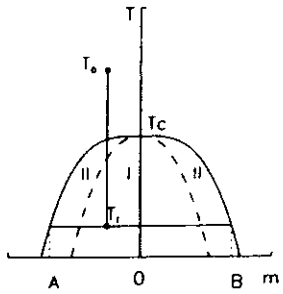

Fig. 12. Schematic phase diagram of a binary mixture $A - B$. The system is homogeneous at temperature T_0. After quenching at temperature T_f below T_c the system phase separates. At sufficiently late times, phase A and B coexist. The evolution proceeds differently if the quench is in region I or II, separated by the spinodal line (dashed line).

$$J(r,t) = -\Gamma\nabla\mu + \eta(r,t) \tag{5.3}$$

Γ is a positive coefficient called *mobility*. The noise variables $\eta = (\eta_1, \ldots, \eta_d)$ are Gaussian distributed, of mean zero and correlations:

$$\langle\eta_k(r,t)\eta_{k'}(r',t')\rangle = 2k_BT\delta_{k,k'}\delta(r-r')\delta(t-t') \tag{5.4}$$

The chemical potential is obtained as the derivative of $\mathcal{H}$ with respect to the field:

$$\mu(r,t) = \frac{\delta\mathcal{H}([\Phi])}{\delta\Phi(r,t)} \tag{5.5}$$

Combining Eqs.(5.2) to (5.5), we reobtain model B equation, which in the context of phase separation is called the Cahn-Hilliard-Cook (CHC) equation (Cahn and Hilliard, 1958; Cook, 1970):

$$\frac{\partial\Phi(r,t)}{\partial t} = \nabla^2\left(\Gamma\frac{\delta\mathcal{H}([\Phi])}{\delta\Phi(r,t)}\right) + \xi(r,t) \tag{5.6}$$

where $\xi(r,t) = \nabla\cdot\eta(r,t)$. If we adopt expression (2.1) for the Hamiltonian we arrive at the following lattice form for the CHC equation:

$$\frac{d\Phi_i(t)}{dt} = \Gamma k_BT\nabla_L^2\left(-b\Phi_i + u\Phi_i^3 - K\nabla_L^2\Phi_i\right) + \xi_i(t) \tag{5.7}$$

If we perform the same field and time rescaling than in the section 3.2 for model A, we obtain the simpler equation:

We can now answer the question of which is the optimal choice for matrix A. If we choose the following values for the diagonal elements of A in Fourier space:

$$A_k = 1/\omega_k = \left[\mu + 4\sum_{j=1}^{d}\sin^2(k_j/2)\right]^{-1/2} \tag{4.37}$$

the evolution matrices M_k^n become independent of μ and k such all the modes evolve with the same effective time step $A_k\omega_k\delta t = \delta t$. This choice for $\hat{A}_k$ reduces completely critical slowing down because correlation times (which are related to the eigenvalues of M_k^n) become independent of the mass μ even when μ tends to zero and the model becomes critical.

5. Applications in Domain Growth

5.1. Dynamics of first order phase transitions

5.1.1. The Cahn-Hilliard-Cook Equation

Many binary (A-B) mixtures which are homogeneous at high temperature T_0, phase separate when quenched below a certain critical value (T_c) of the temperature. In the final equilibrium configuration two phases coexist: the A and B phases, each one rich in the A and B material respectively (see Fig.12). We assume that the equilibrium properties of such mixture are given by the Gibbs distribution at the final temperature T_f and we are concerned here with the way the mixture reaches this thermal equilibrium, i.e. with the dynamical process of phase separation (Gunton et al., 1983; Binder, 1990). In many occasions the relevant equations of motion are those of model B defined in a previous chapter, equations that we now justify from a more physical point of view.

The relevant field Φ in this case is a scalar field representing the local concentration difference of the two components of the mixture $\Phi(\mathbf{r},t) = \rho_A(\mathbf{r},t) - \rho_B(\mathbf{r},t)$. This field obviously follows a conservation law:

$$m \equiv \frac{1}{V}\int_V d\mathbf{r}\Phi(\mathbf{r},t) \longrightarrow \frac{dm}{dt} = 0 \tag{5.1}$$

(V is the system volume). This global conservation law can be expressed in local terms by means of a continuity equation:

$$\frac{\partial\Phi(\mathbf{r},t)}{\partial t} + \nabla\cdot\mathbf{J}(\mathbf{r},t) = 0 \tag{5.2}$$

The conservation current $\mathbf{J}(\mathbf{r},t)$ provides the driving force for field diffusion. Equilibrium is reached when the chemical potentials of the two substances are equal and uniform. Thus, we write the current $\mathbf{J}(\mathbf{r},t)$ as the sum of the gradient of the difference of chemical potentials of each component $\mu = \mu_A - \mu_B$ (this is the well known Fick's law) plus a random, noise type term to take properly into account thermal fluctuations:

1.8. Heat bath

In the Metropolis algorithm the acceptance probability $h(x|y)$ was determined (with some freedom) once the proposal $g_x(x|y)$ had been specified. In the so called **heat bath algorithm**, which is useful for N-dimensional variables, the proposed value for the variable is always accepted, i.e. one chooses

$$h(x|y) = 1 \tag{1.60}$$

The detailed balance condition becomes

$$g_x(x|y)f_x(y) = g_x(y|x)f_x(x) \tag{1.61}$$

In the 1-variable case, a trivial solution (remember that $g_x(x|y)$ must be a probability density function) is: $g_x(x|y) = f_x(x)$ which is independent of the old value y. In the N-variable case, a solution is found by changing only one of the N variables at a time:

$$g_x(x|y) = \frac{1}{N}\sum_{i=1}^{N} g_x(x_i|y)\prod_{j\neq i}\delta(x_j - y_j) \tag{1.62}$$

where each of the functions $g_x(x_i|y)$ satisfies detailed balance:

$$\begin{aligned} &g_x(x_i|y)f_x(x_1,\ldots,x_{i-1},y_i,x_{i+1},\ldots,x_N) = \\ &g_x(y_i|x)f_x(x_1,\ldots,x_{i-1},x_i,x_{i+1},\ldots,x_N) \end{aligned} \tag{1.63}$$

A solution of this functional equation is obtained by taking $g_x(x_i|y) = g_x(x_i)$, independent of y, as the following conditional probability:

$$g_x(x_i) = f_x(x_i|x_1,\ldots,x_{i-1},x_{i+1},\ldots,x_N) \tag{1.64}$$

It is trivial to verify detailed balance, Eq.(1.63), if one remembers the definition of the conditional probability:

$$f_x(x_i|x_1,\ldots,x_{i-1},x_{i+1},\ldots,x_N) = \frac{f_x(x_1,\ldots,x_{i-1},x_i,x_{i+1},\ldots,x_N)}{f_x(x_1,\ldots,x_{i-1},x_{i+1},\ldots,x_N)} \tag{1.65}$$

Intuitively, what the heat bath method does when updating variable x_i is to select the value of x_i according to the conditional probability given that the rest of the variables is fixed. These fixed variables act a a *heat bath* for variable x_i. In many cases, it turns out that the conditional probability $g_x(x_i) = f_x(x_i|x_1,\ldots,x_{i-1},x_{i+1},\ldots,x_N)$ takes a simple form and can be sampled by any of the 1-variable methods explained in this chapter.

2. ϕ^4 Model

2.1. Introduction and basic definitions

We will illustrate the use of Monte Carlo techniques in field theory with the scalar ϕ^4 model. This model has been used in many different contexts, in such different topics as quantum field theory (Zinn Justin, 1989) or in the study of structural phase transitions (Cowley, 1980; Bruce, 1980; Bruce and Cowley, 1980).

Let us consider a d-dimensional (hyper-cubic) regular lattice Λ, consisting of $N = L^d$ points. Every point $i = 1, \ldots, N$ of this lattice has d coordinates: $i = (j_1, \ldots, j_d)$. Periodic boundary conditions are assumed on this lattice. On every site of the lattice there is a scalar variable ϕ_i. The set of all variables is $[\phi] \equiv (\phi_1, \ldots, \phi_N)$. We also introduce a Hamiltonian function $\mathcal{H}$ given by:

$$\beta\mathcal{H}([\phi]) = \sum_{i=1}^{N} a_0^d \left[\frac{-b}{2}\phi_i^2 + \frac{u}{4}\phi_i^4 + \frac{K}{2}\sum_{\mu=1}^{d}\left(\frac{\phi_{i_\mu} - \phi_i}{a_0}\right)^2 \right] \tag{2.1}$$

The sum over μ runs over d-nearest neighbours of site i, i.e. if the coordinates of i are $(j_1, \ldots, j_d)$ then the coordinates of i_μ are $(j_1, \ldots, j_\mu + 1, \ldots, j_d)$. The continuum limit of the system can be obtained by letting the lattice spacing a_0 tend to 0 and the system size L to ∞. In this limit, the sums are replaced by integrals and the sum over μ tends to a gradient. The continuum Hamiltonian is then:

$$\beta\mathcal{H}([\phi]) = \int dr \left[\frac{-b}{2}\phi(r)^2 + \frac{u}{4}\phi(r)^4 + \frac{K}{2}|\nabla\phi(r)|^2 \right] \tag{2.2}$$

This expression for the Hamiltonian is the preferred one for analytical treatment, such as series expansions or renormalization-group treatments in momentum space (Amit, 1984). The lattice version is the preferred one for numerical studies, besides the fact that it yields a regularization of the Hamiltonian (Parisi, 1988). We will consider from now on only the lattice version of the ϕ^4 model. We can set the lattice spacing $a_0 = 1$, since it can be rescaled in the parameters b, u and K.

The first two terms of the sum appearing in the Hamiltonian (2.1) are local terms (depending only on the field at location i) and can be thought of as local potential terms $V(\phi_i)$:

$$V(\phi_i) = \frac{-b}{2}\phi_i^2 + \frac{u}{4}\phi_i^4 \tag{2.3}$$

For stability of this local potential, the parameter u must be greater than 0. The local potential changes qualitative when the parameter b changes sign (see Fig.3). If $b < 0$ the local potential has only one minimum at $\phi_i = 0$. On the other hand, when $b > 0$ there are two minima of equal depth located at $\phi_i = \pm\sqrt{b/u}$.

The third term in (2.1), the one multiplied by K, is called the interaction term. When $K > 0$, the contribution of this term is always non negative and the ground state of the Hamiltonian $\mathcal{H}$ is reached when the contribution of this term is zero, i.e. when all the fields take the same values $\phi_i = \phi_0, \forall i$. This is the situation considered by the simple mean field theory (Landau and Lifshits,

technique is most successful in reducing critical slowing down. Of course, the example is purely academic, since the Gaussian model can be solved analytically without having to resource to numerical methods.

The Gaussian model is defined by the following Hamiltonian for the scalar fields $[\phi_i]$ (Parisi, 1988):

$$\mathcal{H} = \sum_{i=1}^{N}\left[\frac{\mu}{2}\phi_i^2 + \frac{1}{2}\mid\nabla_L\phi_i\mid^2\right] \tag{4.33}$$

index i runs over the $N = L^d$ sites of a d-dimensional regular lattice Λ, with periodic boundary conditions; ∇_L is the usual lattice discretised version of the gradient operator; μ is a parameter called the *field mass*. Although this model does not show a real phase transition, the critical slowing down occurs for the critical value" $\mu = 0$.

To implement the generalized hybrid Monte Carlo method we choose the number of momenta variables associated to a given field equal to 1 (i.e. $D = 1$ in Eq.(4.28)). The total Hamiltonian $\hat{\mathcal{H}}$, Eq.(4.30), including the kinetic energy terms can be written in terms of the Fourier transform of fields and momenta:

$$\hat{\mathcal{H}} = \sum_{k=1}^{N}\left[\frac{\omega_k^2}{2}|\hat{\phi}_k|^2 + \frac{1}{2}|\hat{Q}_k|^2\right] \tag{4.34}$$

the sum runs over the N points in the reciprocal lattice, $k = (k_1, \ldots, k_d)$. Here $\omega_k^2 = \mu + 4\sum_{j=1}^{d}\sin^2(k_j/2)$ and $\hat{\phi}_k$ and $\hat{Q}_k$ stand for the fields and momenta variables in Fourier space. Notice that the total Hamiltonian is a sum of terms each one depending on a single mode k, such that the modes evolve independently of each other.

According to the discussion above, we implement Fourier acceleration by choosing the matrix $\mathcal{A}$, generating the dynamics, diagonal in Fourier space. Let us denote by $\hat{A}_k$ the diagonal elements of the matrix $\mathcal{A}$ in Fourier space. After n leap-frog steps, the evolution equations (4.31) imply:

$$\begin{bmatrix}\omega_k\hat{\phi}_k(n\delta t)\\ \hat{Q}_k(n\delta t)\end{bmatrix} = M_k^n\begin{bmatrix}\omega_k\hat{\phi}_k(0)\\ \hat{Q}_k(0)\end{bmatrix} \qquad k = 1, \ldots, N \tag{4.35}$$

The dynamical properties of the algorithm are determined by matrices M_k^n, given by:

$$M_k^n = \begin{pmatrix}\cos(n\theta_k) & \sin(n\theta_k)/\cos(\theta_k/2)\\ -\cos(\theta_k/2)\sin(n\theta_k) & \cos(n\theta_k)\end{pmatrix} \tag{4.36}$$

where we have introduced $\theta_k = \cos^{-1}(1 - c_k^2/2)$ and $c_k = \hat{A}_k\omega_k\delta t$. We see explicitly how in this model different modes evolve independently of each other. The fact that the evolution equations are linear greatly simplifies the analysis of this problem (this is similar to the standard hybrid Monte Carlo where $\mathcal{A} = 1$, Kennedy and Pendleton, 1991).

$$\Phi_i(\tau + \delta\tau) = \Phi_i(\tau) + \sum_{j=1}^{N}\left[-\delta\tau\epsilon_{ij}\frac{\delta\mathcal{H}}{\delta\Phi_j} + \sqrt{2\delta\tau}\sqrt{\epsilon}_{ij}u_j\right] \qquad (4.32)$$

Where ϵ_{ij} is an arbitrary matrix and u_j is a Gaussian variable of mean zero and correlations $\langle u_i u_j\rangle = \delta_{ij}$. Comparing with (4.31) we can see that it corresponds exactly to the one step leap-frog approximation of the generalized hybrid Monte Carlo method introduced above taking $D = 1$ and if we identify: $(\delta t)^2/2 = \delta\tau$ and $\mathcal{A}\mathcal{A}^{\top} = \epsilon$. The main difference between the two methods is the presence of an acceptance/rejection step in the generalized hybrid Monte Carlo. In this sense, we can say that the generalized hybrid Monte Carlo method introduced in this section makes exact (in the sense that averages are not biased by the choice of the time step) the numerical integration of the Langevin equation using a matrix time step introduced in reference (Batrouni et al., 1985).

4.5. Fourier acceleration

Near a second order phase transition simulations become very time consuming due to the large correlations which appear in the neighbourhood of the critical point. This enhancement of the time correlations, known as critical slowing down, greatly increases the statistical errors in a Monte Carlo simulation making it necessary to average over a large number of configurations in order to obtain values with an acceptable error. The physical origin of critical slowing down is related to the fact that, near the critical point, fluctuations of all wavelengths are present, each with a characteristic time scale. In a Langevin integration, for example, the integration step has to be small enough to treat correctly the short-wavelength components but, on the other hand, the integration has to proceed for a sufficient number of steps to have the long-wavelengths mode evolve significantly. In the **Fourier acceleration** method (Parisi, 1983; Batrouni et al., 1985), an integration technique is developed such that each mode evolves with its own effective time step, large for long wavelengths and small for small wavelengths. Whether Fourier acceleration is successful in completely overcoming critical slowing down for a particular system depends on to which extent the evolution of the different Fourier modes can be considered indeed independent of each other.

Fourier acceleration has been traditionally framed in the language of Langevin equations. But we know already that numerical solutions of Langevin equations introduce systematic errors due to the finiteness of the time step used in the numerical integration. It is possible to develop exact Fourier acceleration methods in the context of the generalized hybrid Monte Carlo algorithm developed in the previous section. The basic ingredient is the following:

- Use matrices $\mathcal{A}^t$ whose elements are diagonal in Fourier space.

The optimal choice for these matrices depends on the system we are considering. Let us now discuss the example of the Gaussian model, for which the

1980). Since all the fields take the same value, the mean field Hamiltonian reduces to:

$$N^{-1}\beta\mathcal{H}^{MF}(\Phi_0) = \frac{-b}{2}\Phi_0^2 + \frac{u}{4}\Phi_0^4 \qquad (2.4)$$

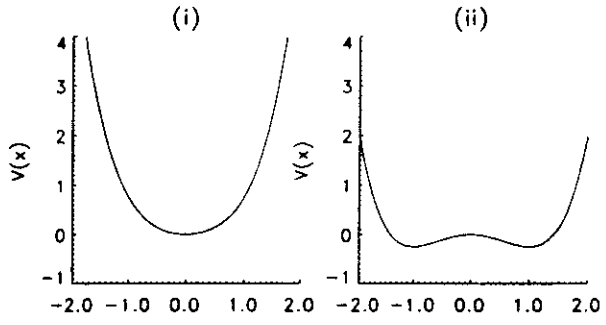

Fig. 3. Local Potential $V(\Phi)$. Eq.(2.3), in the cases (i) $b > 0$ and (ii) $b < 0$

The value of the mean field value Φ_0 depends on the constants b, u and is given by:

$$\Phi_0 = \begin{cases} 0 & \text{if} \quad b < 0 \\ \sqrt{\dfrac{b}{u}} & \text{if} \quad b > 0 \end{cases} \qquad (2.5)$$

(see Fig.4). To go beyond mean field theory one needs to consider fluctuations: the fields Φ_i do not take a constant value, but fluctuate from one lattice site to another. In this case, we need a statistical description which, according to the principles of Statistical Mechanics (Pathria, 1972), is given by the canonical distribution. The probability density function $f([\Phi])$ governing the statistical properties of the fields $[\Phi]$ at inverse temperature β is:

$$f([\Phi]) = \frac{e^{-\beta\mathcal{H}[\Phi]}}{Z(b,u,K)} \qquad (2.6)$$

The denominator of this expression is called the **partition function** and it is the multiple integral of the numerator for all the field values:

$$Z(b,u,K) = \int_{-\infty}^{\infty} d\Phi_1 \ldots \int_{-\infty}^{\infty} d\Phi_N e^{-\beta\mathcal{H}([\Phi])} \equiv \int d\Phi e^{-\beta\mathcal{H}([\Phi])} \qquad (2.7)$$

The magnitudes of interest are computed as averages of field functions, $G([\Phi])$, with the probability density function $f([\Phi])$:

$$\langle G([\phi]) \rangle = Z^{-1} \int d\Phi G([\phi]) e^{-\beta \mathcal{H}([\phi])} \tag{2.8}$$

Example of quantities of interest are the *magnetization*, m defined as:

$$m = \langle \frac{1}{N} \sum_{i=1}^{N} \phi_i \rangle \tag{2.9}$$

the energy, e:

$$e = \left\langle \frac{\mathcal{H}[\phi]}{N} \right\rangle \tag{2.10}$$

the magnetic susceptibility, κ_T:

$$\kappa_T = N \left[\langle \left(\frac{1}{N} \sum_{i=1}^{N} \phi_i \right)^2 \rangle - \langle m \rangle^2 \right] \tag{2.11}$$

the specific heat, C_V:

$$C_V = N \left[\langle \left(\frac{\mathcal{H}[\phi]}{N} \right)^2 \rangle - \langle e \rangle^2 \right] \tag{2.12}$$

and many others.

In general, these quantities differ considerably from the mean field values. In Figure 4 we can see the difference between the magnetization computed from a numerical calculation in two dimensions and the mean field result (which is independent of dimension).

It is known that the ϕ^4 model belongs to the universality class of the Ising model (Amit, 1984). This means that both models share the same critical exponents and scaling functions. Here, however, we want to point out a different relation between the two models, namely, that the Ising model can be obtained as a suitable limit of the ϕ^4 model. The limit is obtained as follows: expanding the square in the "gradient" term and using the periodic boundary conditions, one can rewrite the Hamiltonian in the form:

$$\beta \mathcal{H}([\phi]) = \sum_{i=1}^{N} \left[\left(dK - \frac{b}{2} \right) \phi_i^2 + \frac{u}{4} \phi_i^4 \right] - K \sum_{\langle i,j \rangle} \phi_i \phi_j \tag{2.13}$$

where the sum over $\langle i,j \rangle$ means sum over all the possible pairs of i-j nearest neighbours in the lattice. Introducing a rescaled field variable

$$S_i = \frac{\phi_i}{\sqrt{\frac{b - 2dK}{u}}} \tag{2.14}$$

one can write:

$$\beta \mathcal{H}([S]) = \alpha \sum_{i=1}^{N} \left[-\frac{1}{2} S_i^2 + \frac{1}{4} S_i^4 \right] - \beta J \sum_{\langle i,j \rangle} S_i S_j \tag{2.15}$$

or, written in more compact vector notation:

$$\begin{aligned} \frac{d\Phi}{dt} &= \sum_{s=1}^{D} \mathcal{A}^s Q^s \\ \frac{dQ^s}{dt} &= (\mathcal{A}^s)^{\mathsf{T}} F \qquad\qquad s = 1, \ldots, D \end{aligned} \tag{4.29}$$

where the $\mathcal{A}^s$ are some linear operators which can be represented as a matrix, and F_j represents the force as computed from the Hamiltonian $-\frac{\partial}{\partial \Phi_j} \mathcal{H}$. We also introduce a total Hamiltonian $\hat{\mathcal{H}}$, including the kinetic energy terms:

$$\hat{\mathcal{H}}([\Phi, Q]) = \mathcal{H}(\Phi) + \sum_{i=1}^{N} \sum_{s=1}^{D} \frac{(q_i^s)^2}{2} \tag{4.30}$$

The reader can easily verify that the proposed dynamics in Eqs.(4.28) exactly conserves energy, i.e., $d\hat{\mathcal{H}}/dt = 0$. The standard hybrid Monte Carlo can be obtained from the above dynamics setting $D = 1$ and $\mathcal{A}$ equal to the identity operator.

For the approximate integration of the previous equations of motion the leap-frog scheme can be used, introducing a discrete mapping $[\Phi(t), Q(t)] \to [\Phi(t + \delta t), Q(t + \delta t)] = G^{\delta t}([\Phi(t), Q(t)])$, dependent on the time step δt chosen. The leap-frog approximation reads:

$$\begin{aligned} \Phi' &= \Phi + \delta t \sum_{s=1}^{D} \mathcal{A}^s Q^s + \frac{(\delta t)^2}{2} \sum_{s=1}^{D} \mathcal{A}^s (\mathcal{A}^s)^{\mathsf{T}} F([\Phi]) \\ Q'' &= Q^s + \frac{\delta t}{2} (\mathcal{A}^s)^{\mathsf{T}} (F([\Phi]) + F([\Phi'])) \end{aligned} \tag{4.31}$$

It can be shown that this leap-frog approximation for arbritrary matrices $\mathcal{A}^s$ satisfies the properties of time reversibility and area preserving. However, again as a result of the time discretization used in the leap-frog scheme, the total energy is no longer conserved although its variation can be controlled by varying δt. We define yet another mapping obtained iterating n times the previous mapping, i.e. $\mathcal{G} = (G^{\delta t})^n$. To satisfy detailed balance the configuration obtained when one applies $\mathcal{G}$ is accepted with probability $\min[1, \exp(-\Delta \hat{\mathcal{H}})]$, where $\Delta \hat{\mathcal{H}} = \hat{\mathcal{H}}(\mathcal{G}([\Phi, Q])) - \hat{\mathcal{H}}([\Phi, Q])$. As in the standard hybrid Monte Carlo, the momenta variables are refreshed after every acceptance/rejection step according to a Gaussian distribution of independent variables.

We have defined a general class of hybrid Monte Carlo-type methods characterized by a particular choice of matrices $\mathcal{A}^s$. One can choose the matrices $\mathcal{A}^s$ that better suit a particular problem. This generalized hybrid Monte Carlo method turns out to be related to the method introduced in reference (Batrouni et al., 1985) using the numerical integration of a Langevin equation with a matrix time-step. This method is based upon the observation that the stationary solution of the Langevin equation (4.25) can be obtained approximately by the recursion relation:

(iii) Compute $\Delta\tilde{\mathcal{H}} = \tilde{\mathcal{H}}(t + \Delta t) - \tilde{\mathcal{H}}(t)$

(iv) Accept configuration $\Phi' = \Phi(t + \Delta t)$ with probability $\min(1, e^{-\Delta\tilde{\mathcal{H}}})$

Hybrid Monte Carlo constitutes an important tool for the simulation of field theories and it has been applied successfully to $SU(n)$ field theory (Sexton and Weingarten, 1992), Lennard-Jones systems (Mehlig et al., 1992a), Φ^4 scalar field (Mehlig et al., 1992b), $X-Y$ model (Gupta, 1992), polymer systems (Forrest and Toral, 1994; Irbeck, 1994), etc. and it is today a routine tool of great applicability.

There is another important aspect of the Hybrid Monte Carlo algorithm, namely its relation with Langevin dynamics. Remember the Langevin equation defining model A Eq (3.1):

$$\frac{\partial\Phi_i}{\partial\tau} = -\frac{\delta\mathcal{H}}{\delta\Phi_i} + \eta_i(\tau) = F_i(\tau) + \eta_i(\tau) \tag{4.25}$$

where the noise terms satisfies:

$$< \eta_i(\tau)\eta_j(\tau') >= 2\delta_{i,j}\delta(\tau - \tau') \tag{4.26}$$

The numerical solution using the Euler algorithm proceeds via the following recursion relation:

$$\Phi_i(\tau + \delta\tau) = \Phi_i(\tau) + \delta\tau F_i(\tau) + \sqrt{2\delta\tau}u_i(\tau) \tag{4.27}$$

where $u_i(\tau)$ are Gaussian variables of mean 0 and correlations $\langle u_i(\tau)u_j(\tau)\rangle = \delta_{ij}$. This is exactly the same evolution scheme of the leap-frog algorithm, Eq (4.15), if we make the following relation between the time steps of the two methods $\delta\tau = \delta t^2/2$. We conclude that Hybrid Monte Carlo uses the same updating scheme than Langevin (with a different unit of time), but the presence of the acceptance/rejection step makes the method independent of the time step used in the Langevin integration, so avoiding the systematic errors so difficult to deal with in the Langevin method.

4.4. Generalized hybrid Monte Carlo

It is clear that Hybrid Monte Carlo relies upon a numerical integration of the differential equations for a dynamical system in which the energy is conserved. We will now introduce a general class of dynamical equations that also conserve energy. This will give rise to a generalization of the hybrid Monte Carlo method (Ferreira and Toral, 1993; Toral and Ferreira, 1994).

The generalization goes as follow: to each field Φ_i we assign a vector momenta variable $Q_i = (q_i^1, \ldots, q_i^D)$ of arbitrary dimension D. We introduce the following equations of motion:

$$\begin{aligned} \frac{d\Phi_i}{dt} &= \sum_{s=1}^{D}\sum_{j=1}^{N}(\mathcal{A}^s)_{i,j}Q_j^s \\ \frac{dq_i^s}{dt} &= \sum_{j=1}^{N}(\mathcal{A}^s)_{j,i}F_j \qquad\qquad s = 1, \ldots, D \end{aligned} \tag{4.28}$$

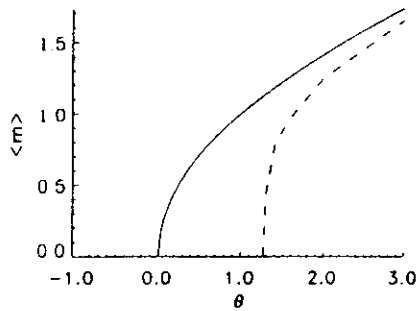

Fig. 4. Mean field magnetisation, Eq.(2.5) (solid line) and the result of a numerical calculation using Monte Carlo techniques in the two-dimensional system (dashed line). In this plot we use the value $\chi = 1$ (see Eq.(2.21) for a definition of the parameters).

with

$$\alpha = \frac{(-b + 2dK)^2}{u}, \qquad \beta J = \frac{K(b - 2dK)}{u} \tag{2.16}$$

The Gibbs factor is

$$e^{-\beta\mathcal{H}(\{S\})} = \prod_{i=1}^{N}\left\{\exp\left[-\alpha(-\frac{1}{2}S_i^2 + \frac{1}{4}S_i^4)\right]\exp\left[\beta J\sum_{<i,j>}S_iS_j\right]\right\} \tag{2.17}$$

The local factor of this distribution is always double peaked centered around the values ± 1 (see Fig.5). Now we can think of the parameter α as controlling the width of the local field distribution around these two maxima. A large value for α implies that the field is bound to take essentially the values ± 1, and S_i becomes what is called a *spin variable*. In the limit $\alpha \to \infty$ with J kept constant we recover the Ising model. This limit is obtained in the original Φ^4 model by taking

$$\begin{aligned} &b \to \infty \\ &u \to \infty \\ &\frac{b}{u} \to \text{constant} \qquad\qquad \beta J = K\frac{b}{u} \end{aligned} \tag{2.18}$$

In this limit, one obtains for the Gibbs factor:

$$e^{-\beta\mathcal{H}(\{S\})} = \prod_{i=1}^{N}\left[\delta(S_i^2 - 1)\right]\exp\left[\beta J\sum_{<i,j>}S_iS_j\right] \tag{2.19}$$

This is equivalent to writing:

$$\mathcal{H}([S]) = -J \sum_{<i,j>} S_i S_j \qquad S_i = \pm 1 \tag{2.20}$$

Which is nothing but the Hamiltonian of the Ising model. For smaller values of α, the field can fluctuate around the two maxima, hence the name of *soft spins model* that sometimes is given to the ϕ^4 model in this situation (Cowley, 1980; Bruce, 1980; Bruce and Cowley, 1980).

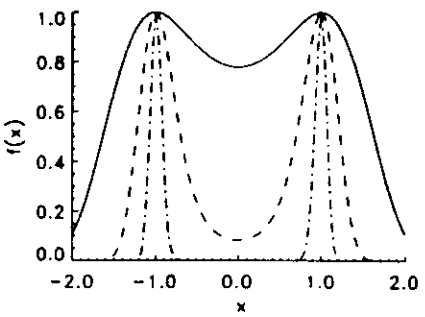

Fig. 5. Function $f(x) = \exp\left[-\alpha(-\frac{1}{2}S_i^2 + \frac{1}{4}S_i^4)\right]$ appearing in Eq.(2.17), in the cases $\alpha = 1$ (solid line), $\alpha = 10$ (dashed line), $\alpha = 100$ (dotted–dashed line). When $\alpha \to \infty$, the function $f_\delta(x)$ tends to the sum of two delta functions located at $x = \pm 1$.

2.2. Monte Carlo methods

Before we proceed further and show how one can obtain numerically the quantities of interest in the ϕ^4 model, we notice that one of the three parameters of the model, u, b, K, is redundant since it can be absorbed in the field scale. Many ways of redefining parameters have been used in the literature (see (Toral and Chakrabarti, 1990) for a review). We will use here a simple reparametrization in which the field is rescaled by a factor $K^{1/2}$ hence yielding a parameter independent interaction term (this rescaling is obviously valid only in the ferromagnetic case $K > 0$). Specifically, we introduce a new field ϕ, and two new parameters θ and χ by the definitions:

$$\begin{aligned} \phi &= K^{1/2}\Phi \\ \theta &= \frac{b}{K} \\ \chi &= \frac{u}{K^2} \end{aligned} \tag{2.21}$$

The Hamiltonian, in terms of these new variables, can be written as:

$$e^{-\mathcal{H}([\Phi])} g_\delta(\Phi'|\Phi) h(\Phi'|\Phi) = e^{-\mathcal{H}([\Phi'])} g_\delta(\Phi|\Phi') h(\Phi|\Phi') \tag{4.17}$$

The proposal $g_\delta(\Phi|\Phi')$ is given again by integration of Hamilton equations with a suitable value for the momenta, $[Q'']$:

$$\begin{pmatrix} \Phi' \\ Q'' \end{pmatrix} \overset{\delta t}{\to} \begin{pmatrix} \Phi \\ Q''' \end{pmatrix} \tag{4.18}$$

from where one gets for $g_\delta(\Phi|\Phi')$:

$$g_\delta(\Phi|\Phi')d\Phi = dQ'' e^{-\beta \frac{Q''^2}{2}} \tag{4.19}$$

being Q'' the value of the momenta necessary to go from Φ' to Φ. The detailed balance condition becomes:

$$e^{-\frac{Q^2}{2}} e^{-\mathcal{H}(\Phi)} h(\Phi'|\Phi) d\Phi dQ = e^{-\frac{Q''^2}{2}} e^{-\mathcal{H}(\Phi')} h(\Phi|\Phi') d\Phi' dQ'' \tag{4.20}$$

Now the following properties apply:

(i) If the numerical integration satisfies time reversal, $Q'' = -Q'$ hence the Jacobian dQ''/dQ' is equal to 1.

$$e^{-\frac{Q^2}{2}} e^{-\mathcal{H}(\Phi)} h(\Phi'|\Phi) d\Phi dQ = e^{-\frac{Q'^2}{2}} e^{-\mathcal{H}(\Phi')} h(\Phi|\Phi') d\Phi' dQ' \tag{4.21}$$

(ii) If it satisfies the area conserving property $dQd\Phi = dQ'd\Phi'$

$$e^{-\frac{Q^2}{2}} e^{-\mathcal{H}(\Phi)} h(\Phi'|\Phi) = e^{-\frac{Q'^2}{2}} e^{-\mathcal{H}(\Phi')} h(\Phi|\Phi') \tag{4.22}$$

Which, using Eq.(4.13), can be written as:

$$e^{-\hat{\mathcal{H}}(\Phi,Q)} h(\Phi'|\Phi) = e^{-\hat{\mathcal{H}}(\Phi',Q')} h(\Phi|\Phi') \tag{4.23}$$

We already know a possible solution to this equation, the Metropolis solution:

$$h(\Phi'|\Phi) = \min(1, e^{-\delta\hat{\mathcal{H}}}) \tag{4.24}$$

where $\delta\hat{\mathcal{H}} = \hat{\mathcal{H}}(t+\delta t) - \hat{\mathcal{H}}(t))$ is the change of total energy produced in the evolution by time step δt. Notice that, although we have made a global change by updating all the variables Φ_i at once, $\delta\hat{\mathcal{H}}$ is controllable and the acceptance probability can be made to stay within reasonable limits (close to 50%). It is not necessary to make the acceptance/rejection decision every time step δt. Instead, usually one integrates during n time steps before acceptance/rejection.

We give now an explicit implementation of the *Hybrid Monte Carlo method*:

(i) Generate independent Gaussian momenta $[Q]$.

(ii) Update the system $[\Phi, Q]$ using leap-frog (or any other time reversible, area preserving method) during a time $\Delta t = n\delta t$

$$\begin{pmatrix} \Phi(t) \\ Q(t) \end{pmatrix} \overset{\delta t}{\to} \begin{pmatrix} \Phi(t+\delta t) \\ Q(t+\delta t) \end{pmatrix} \overset{\delta t}{\to} \cdots \overset{\delta t}{\to} \begin{pmatrix} \Phi(t+\Delta t) \\ Q(t+\Delta t) \end{pmatrix}$$

space to another point with some error in the conservation of energy or, in other words, leap-frog defines a global change of variables that almost conserves energy. The idea naturally appears to combine this mapping with the acceptance/rejection technique typical of the Monte Carlo method. This is the main idea behind the hybrid Monte Carlo method introduced by Duane et al. (1987) that we now develop in more detail.

4.3. Hybrid Monte Carlo

Let us consider a scalar field $\Phi = (\Phi_1, \ldots, \Phi_N)$ on the regular hypercubic lattice Λ. The statistical properties of the system are given by the Gibbs factor $\exp[-\mathcal{H}([\Phi])]$ (we take $\beta = 1$ to simplify notation), with a Hamiltonian $\mathcal{H}([\Phi])$. In order to define a Hamiltonian dynamics we introduce some **fictitious** momenta fields $[Q] = (Q_1, \ldots, Q_N)$ and a new Hamiltonian function

$$\hat{\mathcal{H}}([\Phi, Q]) = \mathcal{H}([\Phi]) + \frac{Q^2}{2} = \mathcal{H}(\Phi) + \sum_{i=1}^{N} \frac{Q_i^2}{2} \tag{4.12}$$

Since

$$\exp\left[-\hat{\mathcal{H}}([\Phi, Q])\right] = \exp[-\mathcal{H}([\Phi])] \exp\left[-\frac{Q^2}{2}\right] \tag{4.13}$$

from the statistical point of view, the momenta variables $(Q_1, \ldots, Q_N)$ are simply Gaussian distributed independent variables. By independent we imply not just independent of each other but also of the fields $[\Phi]$.

According to our plan, we want to make a proposal $g_{\mathbf{x}}(\Phi'|\Phi)$ by using the numerical solution of Hamilton equations. We specify some initial values for the momenta $[Q]$ according to the Gaussian distribution $\exp\left[-\frac{Q^2}{2}\right]$ and then integrate numerically, obtaining new values for the field:

$$\begin{pmatrix} \Phi \\ Q \end{pmatrix} \overset{\delta t}{\rightarrow} \begin{pmatrix} \Phi' \\ Q' \end{pmatrix} \tag{4.14}$$

This mapping can be done, for instance, by using the leap-frog algorithm, Eqs.(4.7):

$$\begin{aligned} \Phi_i' &= \Phi_i + \frac{\delta t^2}{2} F_i + \delta t Q_i \\ Q_i' &= Q_i + \frac{\delta t}{2}(F_i + F_i') \end{aligned} \tag{4.15}$$

We use this mapping to construct the proposal probability $g_{\mathbf{x}}(\Phi'|\Phi)$. More specifically, since the probability distribution function of the Q variables is $\exp(-Q^2/2)$ we can write out the probability density function $g_{\mathbf{x}}(\Phi'|\Phi)$ as:

$$g_{\mathbf{x}}(\Phi'|\Phi)d\Phi' = dQ e^{-\frac{Q^2}{2}} \tag{4.16}$$

being Q the value of the momenta necessary to go from Φ to Φ'. The key point now is to choose an acceptance probability such that detailed balance is satisfied with the hamiltonian $\mathcal{H}([\Phi])$:

$$\begin{aligned} \beta\mathcal{H}([\phi]) &= \sum_{i=1}^{N} \left[\frac{-\theta}{2}\phi_i^2 + \frac{\chi}{4}\phi_i^4 + \frac{1}{2}\sum_{\mu=1}^{d} (\phi_{i_\mu} - \phi_i)^2 \right] \\ &= \sum_{i=1}^{N} \left[\frac{\tilde{\theta}}{2}\phi_i^2 + \frac{\chi}{4}\phi_i^4 - \sum_{\mu=1}^{2d} \phi_i \phi_{i_\mu} \right] \end{aligned} \tag{2.22}$$

(the sum over μ runs over the $2d$ nearest neighbours of site i). Here we have introduced

$$\tilde{\theta} = 2d - \theta \tag{2.23}$$

This Hamiltonian can be explicitly separated into the local part and the interaction part, $\beta\mathcal{H} = \beta\mathcal{H}_0 + \beta\mathcal{H}_I$ with

$$\beta\mathcal{H}_0 = \sum_{i=1}^{N} \left[\frac{\tilde{\theta}}{2}\phi_i^2 + \frac{\chi}{4}\phi_i^4 \right] \tag{2.24}$$

$$\beta\mathcal{H}_I = -\sum_{<i,j>} \phi_i \phi_j \tag{2.25}$$

Now it is about time we start applying what we learnt in the previous chapter about Monte Carlo techniques! To implement the Metropolis algorithm we need to take the following steps:

(i) Select (randomly or sequentially) one of the N field variables, ϕ_i.
(ii) Propose a change to another close value, ϕ_i', chosen randomly in the interval $\phi_i - \Delta, \phi_i + \Delta$, with Δ a suitable value selected such that the acceptance probability is around 0.5.
(iii) Compute the change in energy, $\Delta\mathcal{H}$ that this proposed change produces.
(iv) Accept the proposed value ϕ_i' with probability $\min(1, e^{-\beta\Delta\mathcal{H}})$.

In computing the change of energy one does not have to use the full expression (2.22), but rather notice that most of the terms disappear when subtracting the old and the new energy, such that the change in energy is simply:

$$\beta\Delta\mathcal{H} = \frac{\tilde{\theta}}{2}(\phi_i'^2 - \phi_i^2) + \frac{\chi}{4}(\phi_i'^4 - \phi_i^4) + (\phi_i' - \phi_i)\sum_{\mu=1}^{2d} \phi_{i_\mu} \tag{2.26}$$

This simple Metropolis algorithm has some convergence problems due to the fact that most of the trials belong to a small probability region. This is particularly true in the vicinities of the Ising limit in which the values around 0 have a very small probability (see again Fig.5). Several methods have been proposed as an alternative to the Metropolis algorithm and all of these methods fit into the proposal/acceptance scheme developed in the previous chapter: use a proposal probability density function $g_{\mathbf{x}}(x|y)$ (where $x \equiv (\phi_1', \ldots, \phi_N')$ and $y \equiv (\phi_1, \ldots, \phi_N)$ stand for the complete field configuration after and before the proposal, respectively) and an acceptance probability $h(x|y)$, satisfying detailed balance:

$$g_{\mathbf{x}}(x|y)h(x|y)\frac{e^{-\beta\mathcal{H}(y)}}{Z} = g_{\mathbf{x}}(y|x)h(y|x)\frac{e^{-\beta\mathcal{H}(x)}}{Z} \tag{2.27}$$

As usual, only one variable will be updated at a time, what makes the proposal $g_x(x|y)$ become a function $g_x(\phi'_i|y)$. In the approach of reference (Milchev et al., 1986) the proposal $g_x(\phi'_i|y)$ is chosen independent of y and proportional to the Gibbs factor of the local term of the Hamiltonian:

$$g_x(\phi'_i) = C\exp(-\frac{\tilde{\theta}}{2}\phi'^2_i - \frac{\chi}{4}\phi'^4_i) \tag{2.28}$$

this is a one-variable probability density function that can be sampled by any of the methods explained in chapter 1. The authors in reference (Milchev et al., 1986) chose a numerical inversion method. Once this proposal has been taken, in the detailed balance condition only the interaction part of the Hamiltonian appears explicitly,

$$h(x|y)e^{-\beta\mathcal{H}_I[y]} = h(y|x)e^{-\beta\mathcal{H}_I[x]} \tag{2.29}$$

For this equation we can use the Metropolis solution:

$$h(x|y) = \min(1, e^{-\beta\Delta\mathcal{H}_I}) \tag{2.30}$$

where the novel feature is that only the change of the interaction energy appears in the exponential. This adopts a very simple form:

$$\beta\Delta\mathcal{H}_I = (\phi'_i - \phi_i)\sum_{\mu=1}^{2d}\phi_{i,\mu} \tag{2.31}$$

In general, this procedure can be used when the Hamiltonian can be splitted in a sum of local terms plus an interaction term. One can chose the new value of the variable, independently of the old value, according to the distribution dictated by the local term. This proposal is then accepted with the Metropolis probability using only the interaction term.

The heat-bath algorithm has also been used for this model (Toral and Chakrabarti, 1990). Let us remember than in the heat-bath algorithm, the acceptance probability is equal to 1 (i.e. the proposal is always accepted), one variable ϕ'_i is changed at a time, and the proposal probability density function $g_x(\phi'_i)$ is obtained from a distribution in which all the other variables remain constant, i.e. we need to identify exactly where does the variable ϕ'_i appears, all the other terms will be considered constants. From Eq.(2.22) it is very easy to find out the expression for $g_x(\phi'_i)$:

$$g_x(\phi'_i) = A\exp\left(-\frac{\tilde{\theta}}{2}\phi'^2_i - \frac{\chi}{4}\phi'^4_i + \phi'_i\sum_{\mu=1}^{2d}\phi_{i,\mu}\right) \tag{2.32}$$

A is some normalisation factor depending on the values of the other fields (which are considered to be constant in the heat-bath method). To sample this one-variable probability density function it will not be useful to use a numerical inversion method, because this function depends of the sum of the $2d$ neighbours of site i, which vary from trial to trial. To sample this distribution we can use

$$\left.\begin{aligned}\frac{x_i(t+\delta t) - x_i(t)}{\delta t} + O(\delta t) &= p_i(t)\\ \frac{p_i(t+\delta t) - p_i(t)}{\delta t} + O(\delta t) &= F_i(t)\end{aligned}\right\} \tag{4.5}$$

From where one gets the following recursive relations:

$$\left.\begin{aligned}x_i(t+\delta t) &= x_i(t) + \delta t p_i(t) + O(\delta t)^2\\ p_i(t+\delta t) &= p_i(t) + \delta t F_i(t) + O(\delta t)^2\end{aligned}\right\} \tag{4.6}$$

The local integration error is of order $o(\delta t)^2$. After n integration steps, $n\delta t = t$ the integration error is $\epsilon = O(n(\delta t)^2) = O(t\delta t) = O(\delta t)$. This error is usually too large and demands choosing a very small time step for accuracy and numerical stability. Of course, there are many other higher-order integration methods. Amongst all of them the *leap frog* algorithm will be particularly suited to our needs. The algorithm is:

$$\begin{aligned}x_i(t+\delta t) &= x_i(t) + \delta t\left(p_i(t) + \frac{\delta t}{2}F_i(t)\right)\\ p_i(t+\delta t) &= p_i(t) + \frac{\delta t}{2}\left(F_i(t) + F_i(t+\delta t)\right), \qquad i = 1, \ldots, N\end{aligned} \tag{4.7}$$

and has a local error of order $o(\delta t)^3$. Although this is an improvement over the Euler method, still discretization errors show up, for instance, in the fact that the energy is not exactly conserved. These energy fluctuations (of numerical origin) imply that the microcanonical ensemble is not sampled exactly.

Other properties of the Hamiltonian dynamics are, however, preserved by this algorithm. In particular leap frog satisfies:
(i) Time reversal. If:

$$\begin{pmatrix}X(t)\\ P(t)\end{pmatrix}\delta t \to \begin{pmatrix}X(t+\delta t)\\ P(t+\delta t)\end{pmatrix} \tag{4.8}$$

then reversal of the momenta will take us back to the original value for $[X]$ and the reversed value for the momenta $[P]$:

$$\begin{pmatrix}X(t+\delta t)\\ -P(t+\delta t)\end{pmatrix}\delta t \to \begin{pmatrix}X(t+2\delta t)\\ P(t+2\delta t)\end{pmatrix} = \begin{pmatrix}X(t)\\ -P(t)\end{pmatrix} \tag{4.9}$$

(ii) Area preserving. The Jacobian of the change of variables induced during the time evolution is equal to one:

$$J\left(\frac{X(t+\delta t), P(t+\delta t)}{X(t), P(t)}\right) = 1 \tag{4.10}$$

But, let us repeat it once again, it does not conserve energy:

$$\delta\mathcal{H} = \mathcal{H}(t+\delta t) - \mathcal{H}(t) = O[(\delta t)^m] \neq 0 \tag{4.11}$$

Summarising, the numerical integration by the leap-frog method induces a mapping given by Eq.(4.7) that evolves the whole system from one point of phase

equation produces systematic errors due to the finiteness of the time step used in the integration. These systematic errors are much more cumbersome, since their numerical importance is not known a priori. A recent idea aims to combine the best of both worlds. In the so called *Hybrid Monte Carlo* algorithm (Duane et al., 1987) the numerical integration of the stochastic differential equation is used as the proposal to which an acceptance/rejection step is applied. Before we develop this beautiful idea, we need to develop some concepts related to the microcanonical ensemble.

4.2. Molecular Dynamics

Molecular dynamics (Allen and Tildesley, 1987) offers a direct numerical approach to the behavior of a system with many degrees of freedom. Let $[X] = (x_1, x_2, \ldots, x_N)$ be microscopic variables and $[P] \equiv (p_1, p_2, \ldots, p_N)$ their conjugate momenta. The Hamiltonian function is:

$$\mathcal{H}(X,P) = \mathcal{V}(X) + \mathcal{T}(P) = \mathcal{V}(X) + \frac{P^2}{2} = \mathcal{V}(X) + \sum_{i=1}^{N} \frac{p_i^2}{2} \tag{4.1}$$

The representative point of the system $[x,p]$ evolves in phase space according to Hamilton equations

$$\begin{aligned} \frac{dx_i}{dt} &= p_i \\ \frac{dp_i}{dt} &= F_i = -\frac{\partial \mathcal{H}}{\partial x_i} \end{aligned} \tag{4.2}$$

and the movement is confined to the hypersurface of constant energy, $\mathcal{H}(X,P) = E$. This property can be used to perform averages on the microcanonical ensemble according to the ergodic principle that allows substitution of ensemble averages $\{G\}$ by time averages $\bar{G}$:

$$\bar{G} = \lim_{T\to\infty} \frac{1}{T-t_0} \int_{t_0}^{T} dt G(x(t), p(t)) \tag{4.3}$$

To perform this time average we can integrate numerically Hamilton equations. In this way we can obtain equilibrium properties as well as dynamical (transitory) properties. However, similarly to what happened when using the numerical integration of Langevin equations to sample the canonical distribution, two kinds of errors are present: (i) statistical errors due to the finite number of samplings and (ii) systematic errors due to the time discretization used in the numerical solution.

The simplest integration scheme is the Euler method in which the derivative of a function $b(t)$ is approximated by:

$$\frac{db(t)}{dt} = \frac{b(t+\delta t) - b(t)}{\delta t} + O(\delta t) \tag{4.4}$$

Using this approximation, Hamilton equations become:

instead a rejection technique. If we introduce $c = \sum_{\mu=1}^{2d} \phi_{i,\mu}$, we can write the above function as.

$$g_{\mathbf{x}}(\phi'_i) = B\left[\exp\left(-\frac{\lambda}{4}\phi'^4_i\right)\right]\left[\frac{1}{\tilde{\theta}^{-1/2}\sqrt{2\pi}} \exp\left(-\frac{(\phi'_i - c/\tilde{\theta})^2}{2\tilde{\theta}^{-1}}\right)\right] \tag{2.33}$$

B is another normalization constant. This is the product of the function $\exp(-\frac{\lambda}{4}\phi'^4_i)$ and a Gaussian distribution of mean $c/\tilde{\theta}$ and variance $\tilde{\theta}^{-1}$ (for this we require $\tilde{\theta} > 0$). This Gaussian distribution can be generated by the relation $\phi'_i = c/\tilde{\theta} + \tilde{\theta}^{-1/2}$ran_g() where ran_g() is a Gaussian distributed random variable of mean 0 and variance 1. Finally, the value ϕ'_i is accepted with a probability $\exp(-\frac{\lambda}{4}\phi'^4_i)$.

Another elegant way of implementing a Monte Carlo method for the ϕ^4 model is that of Bruce (Bruce, 1985) in his study of the *border model* (this is nothing but the ϕ^4 model in the case $\tilde{\theta} = 0$). In his approach, the proposal $g_{\mathbf{x}}(x|y) \equiv g_{\mathbf{x}}(\phi'_i)$ is also independent of the old configuration y (in the same vein than heat-bath), but $g_{\mathbf{x}}(\phi'_i)$ is chosen to be the sum of two Gaussians which best approximate the actual local distribution of the field ϕ'_i:

$$\begin{aligned} g_{\mathbf{x}}(\phi'_i) = \frac{1}{2}\Bigg[&\frac{1}{\sigma_1\sqrt{2\pi}} \exp\left(-\frac{(\phi'_i - \mu_1)^2}{2\sigma_1^2}\right) \\ &+ \frac{1}{\sigma_2\sqrt{2\pi}} \exp\left(-\frac{(\phi'_i - \mu_2)^2}{2\sigma_2^2}\right)\Bigg] \end{aligned} \tag{2.34}$$

To sample this distribution one generates a Gaussian number, ran_g() of mean 0 and variance 1 and a uniform number, ξ, in $(0,1)$. If $\xi < 0.5$ then one chooses the field from the first Gaussian distribution, i.e. $\phi'_i = \mu_1 + \sigma_1$ran_g(), else, if $\xi \geq 0.5$, one chooses from the second, $\phi'_i = \mu_2 + \sigma_2$ran_g(). An initial guess of the parameters μ_1, μ_2, σ_1 and σ_2 is later refined with the information coming from the computed local distribution. The acceptance probability must satisfy detailed balance:

$$g_{\mathbf{x}}(\phi'_i)h(x|y)\frac{e^{-\beta\mathcal{H}(y)}}{\mathcal{Z}} = g_{\mathbf{x}}(\phi_i)h(y|x)\frac{e^{-\beta\mathcal{H}(x)}}{\mathcal{Z}} \tag{2.35}$$

introducing the *effective* interaction Hamiltonian, $\tilde{\mathcal{H}}([\phi])$:

$$\beta\tilde{\mathcal{H}}([\phi]) = \beta\mathcal{H}([\phi]) + \sum_{i=1}^{N} \ln g_{\mathbf{x}}(\phi_i) \tag{2.36}$$

the detailed balance condition becomes:

$$h(x|y)e^{-\beta\tilde{\mathcal{H}}(y)} = h(y|x)e^{-\beta\tilde{\mathcal{H}}(x)} \tag{2.37}$$

from which it is clear that a possible solution for the acceptance probability is the Metropolis solution in terms of the function $\tilde{\mathcal{H}}$:

$$h(x|y) = \min\left(1, e^{-\beta\Delta\tilde{\mathcal{H}}}\right) \tag{2.38}$$

2.3. Histogram extrapolation

We have now developed some tools to study numerically the ϕ^4 model. We shall next apply them to the computation of some magnitudes of interest. Let us focus first on the magnetization m (see Fig.4). This is a function of the parameters θ and χ. If we are interested, say, in the variation of m with θ for a fixed value of χ, we have to run our numerical algorithm for several values of θ. For each run, we have to make sure that the system has reached equilibrium (thermalization) and then produce a sufficient number of independent configurations such that the errors are kept under reasonable limits. Repeating this procedure for a large number of θ values in order to have smooth curves for the magnetization is a painful and slow procedure. There is a way of improving somehow this process by using information from simulations at a given value of the parameter θ to obtain results for another value θ'. The idea, which is extremely simple (and clever!), has been obtained and reobtained many times, but were Ferrenberg and Swendsen (see Ferrenberg and Swendsen (1989) and references therein) who dramatically demonstrated its utility in the case of the Ising model. We now describe this *histogram extrapolation technique* for the ϕ^4 model.

The configurations obtained in a numerical simulation using the Monte Carlo method follow the Gibbs probability distribution which depend on the parameters θ and χ, that we now write out explicitly:

$$f([\phi];\theta,\chi) = \frac{e^{-\beta\mathcal{H}([\phi];\theta,\chi)}}{Z(\theta,\chi)} \tag{2.39}$$

The type of averages one is interested on usually involve only the following functions:

$$\begin{aligned} m_0 &= \sum_{i=1}^{N} \phi_i \\ m_1 &= \sum_{i=1}^{N} \phi_i^2 \\ m_2 &= \sum_{i=1}^{N} \phi_i^4 \\ m_3 &= \sum_{i=1}^{N} \sum_{\mu=1}^{d} (\phi_{i_\mu} - \phi_i)^2 \end{aligned} \tag{2.40}$$

other functions m_i can be incorporated into what follows, but we restrict to these for simplicity. Since the Hamiltonian depends only on linear combinations of m_1, m_2 and m_3, the probability distribution function in terms of m_0, m_1, m_2 and m_3 is:

$$f(m_0,m_1,m_2,m_3;\theta,\chi) = \frac{N(m_0,m_1,m_2,m_3)\exp\left(\frac{\theta}{2}m_1 - \frac{\chi}{4}m_2 - \frac{1}{2}m_3\right)}{Z(\theta,\chi)} \tag{2.41}$$

$$\begin{aligned} x_i^{(n+1)} = x_i^{(n)} &+ h\left[F_i^{(n)} + \frac{D}{2}\sum_{j=1}^{N}\sum_{k=1}^{N} G_{j,k}^{(n)} \left.\frac{\partial G_{i,k}}{\partial x_j}\right|^{(n)}\right] \\ &+ \sqrt{Dh}\sum_{j=1}^{N} G_{i,j}^{(n)} u_j^{(n)} \end{aligned} \tag{3.40}$$

where the $u_i^{(n)}$ are independent Gaussian variables of mean 0 and variance 1:

$$\langle u_i^{(n)} u_{i'}^{(n')} \rangle = \delta_{n,n'}\delta_{i,i'} \tag{3.41}$$

In the case of *diagonal* noise, (Kloeden and Platen, 1992), i.e. one in which the noise terms do not couple variable at different lattice locations:

$$G_{i,j}(x_1,\ldots,x_N) = G_i(x_i)\delta_{i,j} \tag{3.42}$$

one can generalize the Milshtein algorithm to:

$$x_i^{(n+1)} = x_i^{(n)} + hF_i^{(n)} + \sqrt{Dh}u_i^{(n)} + \frac{1}{2}G_i^{(n)}\left.\frac{dG_i}{dx_i}\right|^{(n)} Dh[u_i^{(n)}]^2 \tag{3.43}$$

In next chapters we will show some applications of the numerical integration of Langevin field equations. In Chapter 4 the Langevin equation will be combined with Monte Carlo techniques to yield a very useful tool to study equilibrium properties: the *hybrid Monte Carlo algorithm*. In Chapter 5 we will be concerned with the dynamics of growth in two very different situations: phase separation and growth of random surfaces.

4. Hybrid Monte Carlo

4.1. Introduction

The numerical integration of Langevin equations described in the previous chapter has been used extensively as an alternative to Monte Carlo methods to sample the canonical distribution. The idea is to run the Langevin equation up to the stationary state (a process similar to thermalization for Monte Carlo) and then average the different field configurations produced over time. An advantage of this procedure as compared to Monte Carlo is that it is not necessary to compute the change in energy every time a single variable is updated. This is important when the computation of the Hamiltonian is extremely time consuming. Such situation arises in lattice gauge theories that include dynamical fermions (Zinn Justin, 1989). The effective Hamiltonian is so complicated for those systems that it is prohibitive having to compute $\mathcal{H}$ N times per Monte Carlo step.

An advantage of Monte Carlo methods over the Langevin integration is that the only errors in Monte Carlo are of statistical origin due to the limited number of configurations in the sample (and also to the correlations amongst them) and are known to behave as the inverse square root of the number of configurations. On top of the statistical errors, the numerical integration of the Langevin

The Milshtein method is an algorithm correct to order h and can then be considered as the stochastic equivalent of the Euler method to solve numerically ordinary differential equations. Sometimes in the literature (Greiner et al., 1988) the name Euler method for stochastic differential equations (in the Stratonovich sense) is given to the above expression in which the term $[u^{(n)}]^2$ is replaced by its mean value $\langle [u^{(n)}]^2 \rangle = 1$:

$$x^{(n+1)} = x^{(n)} + h\left[F^{(n)} + \frac{D}{2}G^{(n)}\left.\frac{dG}{dx}\right|^{(n)}\right] + \sqrt{Dh}u^{(n)} \qquad (3.38)$$

This is an algorithm with a worst convergence that the Milshtein algorithm. However, if one is interested only on computing the moments $\langle x(t)^k \rangle$ of the variable $x(t)$ one can prove that this Euler algorithm has the same accuracy than the Milshtein algorithm. Given that both algorithms have approximately the same computational complexity, it does not seem justified to use the poorer Euler algorithm instead of the Milshtein algorithm.

It is possible but very tedious to develop higher order algorithms. The good news is that very rarely one really needs them. This is so because, in general, one has to solve numerically the Langevin equations and average the results for different realizations of the noise (and maybe initial conditions). This generates a source of statistical errors coming from the averages which are, in many occasions, greater than the systematic errors due to the order of convergence of the numerical method. So it is usually better to spend the computer time in reducing the statistical errors by increasing the number of samples in the average rather than using a more complicated, higher order, algorithm. However, we would like to mention briefly the stochastic Runge-Kutta type methods because, although they do not yield better results than the Milshtein method for the convergence of the stochastic terms, they do treat better the deterministic terms, increasing in many cases the numerical stability. The simplest stochastic Runge-Kutta type method is the Heun method which, for Eq.(3.32) reads:

$$\begin{aligned} k &= hF(x(0)) \\ l &= \sqrt{Dh}u^{(0)}G(x(0)) \\ y &= x(0) + k + l \\ x(h) &= x(0) + \frac{h}{2}\left[F(x(0)) + F(y)\right] + \frac{\sqrt{Dh}u^{(0)}}{2}\left[G(x(0)) + G(y)\right] \end{aligned} \qquad (3.39)$$

One can prove by Taylor expanding the functions $F(x)$ and $G(x)$ that the Heun method reproduces, to order h, the stochastic part of the Milshtein method (Gard, 1987). For the purely deterministic case, $D = 0$, the Heun algorithm reduces to the standard 2^{nd} order Runge-Kutta method.

So far, we have only considered one-variable equations. It is very complicated to develop algorithms for the general N-variable case of Eq.(3.20). The interested reader can find in (Kloeden and Platen, 1992) an extensive account of these general methods. One can always use the following extension of the Euler method:

Here $N(m_0, m_1, m_2, m_3)dm_0dm_1dm_2dm_3$ is the number of configurations with values of m_i in the interval $(m_i, m_i + dm_i)$, $i = 0, 1, 2, 3$. These values of $N(m_0, m_1, m_2, m_3) \equiv N([m_i])$ are recorded during the simulation forming a histogram (hence the name of histogram extrapolation). The partition function can be expressed in terms of $N([m_i])$ as:

$$Z(\theta, \chi) = \int \prod_i dm_i N([m_i]) \exp\left(\frac{\theta}{2}m_1 - \frac{\chi}{4}m_2 - \frac{1}{2}m_3\right) \qquad (2.42)$$

The average value of any function $G([m_i])$ can be computed as:

$$\langle G([m_i]) \rangle = \int \prod_i dm_i f([m_i]; \theta, \chi) G([m_i]) \qquad (2.43)$$

The extrapolation scheme allows one to compute the probability density function $f([m_i]; \theta', \chi')$, for values θ', χ' of the model parameters, if $f([m_i]; \theta, \chi)$ is known. For our particular model, the method is based on the exact relation:

$$f([m_i]; \theta', \chi') = \frac{f([m_i]; \theta, \chi) \exp\left(\frac{\theta'-\theta}{2}m_1 - \frac{\chi'-\chi}{4}m_2\right)}{\int \prod_i dm_i f([m_i]; \theta, \chi) \exp\left(\frac{\theta'-\theta}{2}m_1 - \frac{\chi'-\chi}{4}m_2\right)} \qquad (2.44)$$

Let us, in order to discuss the implication of this relation, consider the simpler case $\chi' = \chi$ for which the above formula reduces to:

$$f([m_i]; \theta', \chi) = \frac{f([m_i]; \theta, \chi) \exp\left(\frac{\theta'-\theta}{2}m_1\right)}{\int \prod_i dm_i f([m_i]; \theta, \chi) \exp\left(\frac{\theta'-\theta}{2}m_1\right)} \qquad (2.45)$$

This identity is telling us that if we know the probability distribution function of the m_i's at a given value of the parameter θ then we know it for any other value θ'. This is wonderful! Only one simulation at a selected value of θ is required! Once we have computed the probability density function $f([m_i]; \theta, \chi)$ we can obtain, by means of the previous formula, the probability density function $f([m_i]; \theta', \chi)$ and from the knowledge of $f([m_i]; \theta, \chi)$ we can compute any average we need using Eq.(2.43).

In practice, alas!, things are not so easy. Relation (2.45) is indeed exact, but what it is telling us is that the information contained in the tail of the distribution of $f([m_i]; \theta, \chi)$ is used to compute the distribution $f([m_i]; \theta', \chi)$, see Fig. 6. The only problem is that the errors in the tail of the distribution usually are very large, so making infeasible to extrapolate to a value of θ' very far from θ.

Of course, the width of the distribution $f([m_i]; \theta, \chi)$ will be very important to determine the extrapolation range $\Delta\theta$. If the distribution is very wide, one can extrapolate to farther away values than for a very narrow distribution. This is the reason why this histogram extrapolation technique is useful near the critical point where the distributions are wider.

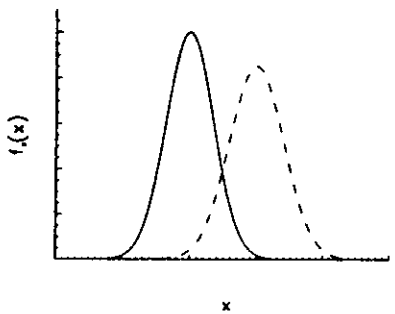

Fig. 6. Probability distribution functions $f([m_i];\theta,\chi)$ at two different values of θ using Eq.(2.43). According to Eq (2.45) the region around the maximum of the function given by the dashed line is obtained from the tail of the function given by the solid line, where statistical errors are larger.

2.4. Finite size scaling

In Figures 7 to 10 we have plotted, for different system sizes and using the histogram extrapolation scheme, results for several quantities of interest: magnetization, energy, specific heat and susceptibility. Each of these figures has been produced by just two simulations whose location is marked with points in the figures. The rest of the curves have been obtained using the extrapolation scheme detailed above.

These figures show what is called *finite size effects* (Barber, 1983). Let us compare Fig. 7 for the magnetization with Fig.4 which depicts the mean field behavior and the expected true behavior. The theory predicts that there should be a value of $\theta = \theta_c$ below which the spontaneous magnetisation is strictly zero. In fact, the magnetization behaviour near θ_c can be characterised by a critical exponent, β such that:

$$m(\theta) = \begin{cases} 0 & \text{if} \quad \theta < \theta_c \\ a\epsilon^{\beta} & \text{if} \quad \theta > \theta_c \end{cases} \tag{2.46}$$

Here $\epsilon = 1 - \frac{\theta}{\theta_c}$. This is a non-analytical behaviour which, strictly speaking, can only appear in a system of infinite size. For a finite system, the number of integrations appearing in the definition of the partition function and the calculation of averages is always finite, thus leading necessarily to an analytical result. We can understand intuitively why finite size effects will be more important near a second order phase transition. In this situation the correlation length which measures the linear range over which fields at different sites of the lattice are correlated, diverges (in an infinite system) with a power-law singularity:

where $u^{(n)}$ are independent Gaussian variables of mean zero and variance unity which can be generated, for instance, by the Box-Muller-Wiener method. The final recursion relation reads:

$$\begin{aligned} x^{(0)} &= x_0 \\ x^{(n+1)} &= x^{(n)} + hF^{(n)} + \sqrt{Dh}u^{(n)} \end{aligned} \tag{3.31}$$

with the obvious notation $x^{(n)} = x(t_0 + nh)$, $F^{(n)} = F(x(t_0 + nh))$, etc. This simple example has taught us that the stochastic contribution is of order $h^{1/2}$ whereas the deterministic contribution is of order h. This singular expansion is the main reason for the failure of algorithms based on a naïve Taylor series on integer powers of h. Let us now consider another example:

$$\frac{dx(t)}{dt} = F(x) + G(x)\eta(t) \tag{3.32}$$

Integration of this equation leads to (we have taken $t_0 = 0$ to simplify notation):

$$x(h) = x(0) + \int_0^h ds F(x(s)) + \int_0^h ds G(x(s))\eta(s) \tag{3.33}$$

To proceed, we Taylor expand the functions $F(x)$ and $G(x)$:

$$\begin{aligned} F(x(s)) &= F(x(0)) + \left.\frac{dF}{dx}\right|_{x=x(0)} (x(s) - x(0)) + o(x(s) - x(0))^2 \\ G(x(s)) &= G(x(0)) + \left.\frac{dG}{dx}\right|_{x=x(0)} (x(s) - x(0)) + o(x(s) - x(0))^2 \end{aligned} \tag{3.34}$$

By substituting these expansions in (3.33) we notice is that at lowest order, $h^{1/2}$, we have

$$x(s) - x(0) = G(x(0)) \int_0^s du\eta(u) \tag{3.35}$$

and hence, to have an algorithm correct to $o(h)$ it suffices to consider the following terms in the expansion:

$$\begin{aligned} x(h) =& x(0) + F(x(0))h + G(x(0))\omega_h(0) + \\ & G(x(0)) \left.\frac{dG}{dx}\right|_{x=x(0)} \int_0^h ds \int_0^s du\eta(s)\eta(u) + o(h^{3/2}) \end{aligned} \tag{3.36}$$

The double integral gives $\omega_h(0)^2/2$. Replacing ω_h by $\sqrt{Dh}u$, see Eq.(3.30), we arrive at the following recursion relation, known as the Milshtein algorithm (Milshtein, 1974):

$$\begin{aligned} x^{(0)} &= x_0 \\ x^{(n+1)} &= x^{(n)} + hF^{(n)} + \sqrt{Dh}u^{(n)} + \frac{1}{2}G^{(n)} \left.\frac{dG}{dx}\right|^{(n)} Dh[u^{(n)}]^2 \end{aligned} \tag{3.37}$$

where $F(t)$ is a sufficiently smooth (differentiable) function and $\eta(t)$ is a Gaussian distributed variable of mean zero and correlations:

$$\langle \eta(t)\eta(t')\rangle = D\delta(t-t') \tag{3.23}$$

In fact, this equation is so simple that we can solve it exactly. However, let us develop a numerical algorithm to solve it. The algorithm generates a recursion relation that will allow us to compute $x(t+h)$ given $x(t)$, h is the integration step. This is the same structure than in ordinary differential equations in which numerical methods do not give the solution for every value of time t but only at regular intervals $t_n = t_0 + nh$, $n = 0, 1, \ldots$ separated by a integration step h. In order to find the recursion relation we integrate (3.22) between t_n and $t_n + h$ to obtain:

$$\int_{t_n}^{t_n+h} dt \frac{dx(t)}{dt} = x(t_n+h) - x(t_n) = \int_{t_n}^{t_n+h} dsF(s) + \int_{t_n}^{t_n+h} ds\eta(s) \tag{3.24}$$

the first term of the right hand side of this equation can be approximated by

$$\int_{t_n}^{t_n+h} dsF(s) = hF(t_n) + o(h^2) \tag{3.25}$$

The second term is a Gaussian variable since it is the integral of a Gaussian variable. Hence, its statistical properties are completely determined by the mean value and the correlations. Let us define the random variable:

$$\omega_h(t) = \int_t^{t+h} ds\eta(s) \tag{3.26}$$

whose mean value is:

$$\langle \omega_h(t)\rangle = \int_t^{t+h} ds\langle \eta(s)\rangle = 0 \tag{3.27}$$

and whose correlations are given by:

$$\langle \omega_h(t)\omega_h(t')\rangle = \int_t^{t+h} ds \int_{t'}^{t'+h} du\langle \eta(s)\eta(u)\rangle = \int_t^{t+h} ds \int_{t'}^{t'+h} duD\delta(s-u) \tag{3.28}$$

This integral is an easy exercise on delta-function integration. The result is:

$$\langle \omega_h(t)\omega_h(t')\rangle = \begin{cases} D(h-|t-t'|) & |t-t'| \le h \\ 0 & |t-t'| \ge h \end{cases} \tag{3.29}$$

The important thing to notice is that for the times t_n that appear in the recursion relation (3.24), one has $\langle \omega_h(t_n)\omega_h(t_{n'})\rangle = Dh\delta_{n,n'}$, so that the variables $\omega_h(t_n)$ are independent, Gaussian, random variables of zero mean and variance $\langle \omega_h(t_n)^2\rangle = Dh$. Hence they can be written as

$$\omega_h(t_n) = \sqrt{Dh}u^{(n)} \tag{3.30}$$

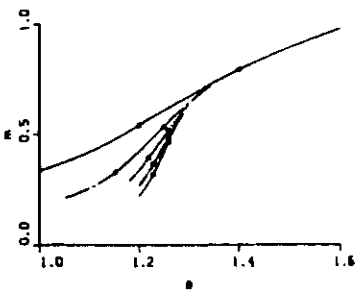

Fig. 7. Magnetization m for the two-dimensional ϕ^4 model for $\chi = 1$ and different values of the system side $L = 8, 16, 24, 32, 40$ (from bottom to top lines). For each value of L a continuous line has been drawn by running two simulations at the points marked with a dot and extrapolating to other values of θ using Eq (2.45).

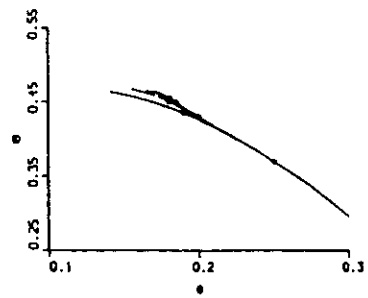

Fig. 8. Same than figure 7 for the energy e and $\chi = 0.1$.

$$\xi(\theta) \sim |c|^{-\nu} \tag{2.47}$$

For a finite system, the fields can not be correlated longer that the system side and we must have $\xi \sim L$. The theory of finite size tells us exactly how (and why!) the averages of interest behave (Cardy, 1988). The basic idea is that now the magnetization, say, becomes a *homogeneous* function of ξ and the system side L, $m(\xi, L) = \xi^{\kappa}\bar{m}(\xi/L)$. The unknown exponent κ is obtained by demanding that in the infinite system, and close enough to the critical point, one recovers the known behaviour given by Eq (2.46). This implies that the function $\bar{m}(x)$ takes

a finite limit when $z \to 0$ and then:

$$m(\theta) = \lim_{L\to\infty} m(\theta, L) = \xi^x \tilde{m}(0) \sim \left[\epsilon^{-\nu}\right]^x \sim \epsilon^{-x\nu} \tag{2.48}$$

compared to (2.46) one concludes $\beta = -x\nu$ and then the prediction for the magnetization near the critical point for a finite system is:

$$m(\theta, L) = \xi^{-\beta/\nu}\tilde{m}(\xi/L) = L^{-\beta/\nu}\tilde{\tilde{m}}[(1-\theta/\theta_c)L^{-1/\nu}] \tag{2.49}$$

The typical way of checking this scaling behavior is to plot $m(\theta, L)L^{\beta/\nu}$ *vs* the rescaled variable $(1-\theta/\theta_c)L^{-1/\nu}$. If, as it is usually the case, the critical value θ_c and the critical exponents ν, β are not known, this procedure implies a three-parameter fit which is very difficult to do in practice. One can use the equivalent scaling relations for the specific heat and the susceptibility:

$$\begin{aligned} C(\theta, L) &= L^{\alpha/\nu}\tilde{C}[(1-\theta/\theta_c)L^{-1/\nu}] \\ \kappa(\theta, L) &= L^{\gamma/\nu}\tilde{\kappa}[(1-\theta/\theta_c)L^{-1/\nu}] \end{aligned} \tag{2.50}$$

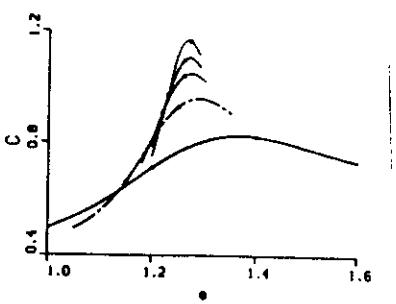

Fig. 9. Specific heat for the two-dimensional ϕ^4 model for $\chi = 1$. Same symbols and meanings than in figure 7.

From Figures 9 and 10 we see that both $C(\theta, L)$ and $\kappa(\theta, L)$ develop maxima at locations $\theta_c^1(L)$ and $\theta_c^2(L)$, respectively. By using the above expressions for the specific heat and the susceptibility one can see that these values behave as:

$$\begin{aligned} \theta_c^1(L) &= \theta_c + a_1 L^{-1/\nu} \\ \theta_c^2(L) &= \theta_c + a_2 L^{-1/\nu} \end{aligned} \tag{2.51}$$

From where we deduce that a plot of $\theta_c^1(L)$ and $\theta_c^2(L)$ *vs* $L^{-1/\nu}$ must yield a straight line whose interception at the origin is precisely θ_c. This can be seen in Fig.11 for which the critical value $\theta_c = 1.265 \pm 0.010$ for $\chi = 1$ is deduced.

Again, in order to ensure that the correct equilibrium distribution is obtained, one needs to tune the correct value for D. The Fokker-Planck equation is now:

$$\begin{aligned} \frac{\partial P([\phi];t)}{\partial t} &= \sum_{i=1}^{N} \frac{\partial}{\partial \Phi_i}\left[-\Gamma\nabla_L^2\left(\frac{\partial \mathcal{H}}{\partial \Phi_i}\right)P + \frac{D}{2}\sum_{j=1}^{N}\frac{\partial}{\partial \Phi_j}\left(-\nabla_L^2\delta_{i,j}P\right)\right] \\ &= -\sum_{i=1}^{N}\frac{\partial}{\partial \Phi_i}\nabla_L^2\left[\Gamma\frac{\partial \mathcal{H}}{\partial \Phi_i}P + \frac{D}{2}\frac{\partial P}{\partial \Phi_i}\right] \end{aligned} \tag{3.19}$$

The equilibrium distribution is given by $\exp\left[-\frac{2\Gamma}{D}\mathcal{H}([\Phi])\right]$ and we are led to identify $D = 2\Gamma k_B T$ as in model A.

3.3. Numerical solution of stochastic differential equations

The Langevin equations for models A and B that we considered in the previous section can not be solved exactly. A great deal of what we know about the behavior of the solution of these equations comes from numerical simulations. In this section we want to study how to handle numerically Langevin equations of the general form:

$$\frac{dx_i(t)}{dt} = F_i(t) + \sum_{j=1}^{N} G_{ij}\eta_i(t) \qquad i = 1, \ldots, N \tag{3.20}$$

F_i are functions that depend on the set of variables $x_1, \ldots, x_N$. If $G_{i,j}$ also depend on $x_1, \ldots, x_N$, one talks of *multiplicative* noise and the resulting stochastic differential equations will be considered in the Stratonovich sense (van Kampen, 1981). If, on the other hand, $G_{i,j}$ are constant functions, one talks of *additive* noise. The noise variables $\eta_i(t)$ are Gaussian distributed, independent random variables of mean zero and correlations given by:

$$\langle \eta_i(t)\eta_j(t')\rangle = D\delta_{i,j}\delta(t-t') \tag{3.21}$$

Of course, the appearance of the Dirac-delta functions tells us that we might have some problems of mathematical rigor in we insist in considering the noise variables η_i as simple functions. They should be considered as distributions, but most of the results we can get with more mathematical rigor are also obtained with the usual function formalism ... and some care. In particular, since the noise variables are not differentiable, we can not use the standard Taylor expansions that help so much in developing algorithms for numerically solving ordinary (not stochastic) differential equations (Press et al., 1986). Instead, we must use integration expansions (Kloeden and Platen, 1992). We can express these ideas more clearly with a simple example.

Let us consider a one variable stochastic differential equation:

$$\frac{dx(t)}{dt} = F(t) + \eta(t) \tag{3.22}$$

$$\frac{2\Gamma}{D} = \beta \Longrightarrow D = 2k_B T\Gamma \tag{3.10}$$

D is then proportional to temperature, as we had anticipated. By using the expression for the lattice Hamiltonian equation (2.1) we arrive at the following equation:

$$\frac{d\Phi_i(t)}{dt} = \Gamma k_B T\left(b\Phi_i - u\Phi_i^3 + K\nabla_L^2\Phi_i\right) + \eta_i(t) \tag{3.11}$$

∇_L^2 is the lattice laplacian operator defined by:

$$\nabla_L^2\Phi_i = \sum_{\mu=1}^{2d}(\Phi_{i_\mu} - \Phi_i) \tag{3.12}$$

here the sum over μ runs over the $2d$ nearest neighbours of site i. By redefining time $t \to t\Gamma K k_B T$ and by introducing the same field rescaling and parameters than in the equilibrium case, Eq. (2.21), we arrive at the somewhat simpler equation:

$$\frac{d\phi_i(t)}{dt} = \theta\phi_i - \chi\phi_i^3 + \nabla_L^2\phi_i + \xi_i(t) \tag{3.13}$$

where the new noise variables ξ_i satisfy:

$$\langle\eta_i(t)\eta_j(t')\rangle = 2\delta_{i,j}\delta(t-t') \tag{3.14}$$

The Langevin equation we have considered so far is the simplest dynamical model than can be written for a scalar field and in the famous taxonomy of Hohenberg and Halperin (Hohenberg and Halperin, 1977) is simply called *model A*. Langevin-type equations can describe more complex systems, such as *model B* which is obtained formally by replacing the constant coefficient Γ in Eq.(3.1) defining model A by $-\Gamma\nabla^2$. The resulting equation of motion is:

$$\frac{\partial\Phi(\mathbf{r},t)}{\partial t} = \nabla^2\left(\Gamma\frac{\delta\mathcal{H}([\Phi])}{\delta\Phi(\mathbf{r},t)}\right) + \eta(\mathbf{r},t) \tag{3.15}$$

where $\eta(\mathbf{r},t)$ are Gaussian distributed random variables of mean zero and correlations:

$$\langle\eta(\mathbf{r},t)\eta(\mathbf{r}',t')\rangle = -D\delta(t-t')\nabla^2\delta(t-t') \tag{3.16}$$

We let the physical interpretation of this model to the next chapter. Here we will mention that model B is suitable to describe the relaxational evolution of a *conserved* field, i.e. one for which the spatial integral of the field is time independent:

$$m \equiv \int d\mathbf{r}\Phi(\mathbf{r},t) \longrightarrow \frac{dm}{dt} = 0 \tag{3.17}$$

The lattice discretization of model B equation leads to:

$$\frac{d\Phi_i(t)}{dt} = \nabla_L^2\left(\Gamma\frac{\partial\mathcal{H}([\Phi])}{\partial\Phi(\mathbf{r},t)}\right) + \eta_i(t) \tag{3.18}$$

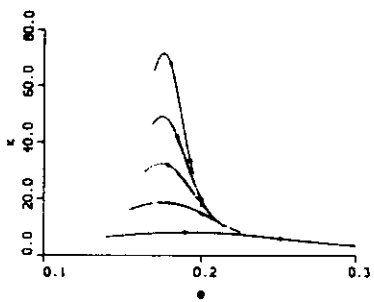

Fig. 10. Magnetic susceptibility for the two-dimensional ϕ^4 model for $\chi = 0.1$. Same symbols and meanings than in figure 7.

In this figure we have used the known value $\nu = 1$ for the $2-d$ ϕ^4 model. When the value of ν is not known one could use directly the three parameter fit $\theta_c^L(L) = \theta_c + a_i L^{-1/\nu}$ to obtain θ_c although the quality of the fit usually is not good enough to allow also for a very accurate measurement of ν. Once the value of θ_c is known one can use the remaining finite size scaling relations to obtain the critical exponents.

3. Field Dynamics

3.1. Introduction

Up to now we have focused only on the equilibrium properties of the scalar Φ^4 model. If one wants to write dynamical equations for the fields one finds the difficulty that the Φ^4 Hamiltonian, so successful for equilibrium properties, does not contain enough information (e.g. kinetic energy terms) to determine the dynamics of the model. Instead of adding more terms to the Hamiltonian, the usual approach to study dynamical properties is to consider that the field variables follow some phenomenological equations of motion. These equations of motion will be stochastic in nature to reflect our ignorance of the detailed effect of the microscopic variables in the field variables (Gunton et al., 1983b). In addition, they must respect the basic symmetries of the system and lead, in the limit of infinite time, to the equilibrium canonical distribution given by the Gibbs factor.

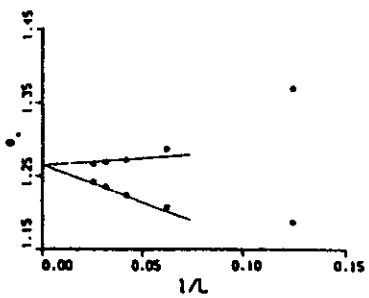

Fig. 11. Pseudo critical parameters $\theta_c^1(L)$ (open dots) and $\theta_c^2(L)$ (black dots) defined as the location of the maxima of the specific heat and susceptibility, respectively, plotted vs. L^{-1}. The extrapolation to the origin, according to Eq.(2.51) yields the critical value $\theta_c = 1.265 \pm 0.010$.

3.2. The Langevin equation

As discussed before, one writes down semi-phenomenological stochastic equations (Langevin equations) to model the time evolution of the field. For the simplest case of the ϕ^4 model without any further symmetry (remember than the main symmetry of the model is the $\phi \to -\phi$), one is guided by the fact that at sufficiently low temperatures the final configuration must be a minimum of the Hamiltonian. Then, the time evolution is defined by a purely relaxational model such that the speed of approaching the ground state is proportional to the gradient of the Hamiltonian. One adds a stochastic contribution (usually called the noise term) that ensures the correct thermal fluctuations in the stationary (equilibrium) state. The resulting Langevin equation is:

$$\frac{\partial \Phi(\mathbf{r},t)}{\partial t} = -\Gamma \frac{\delta \mathcal{H}}{\delta \Phi(\mathbf{r},t)} + \eta(\mathbf{r},t) \tag{3.1}$$

Here Γ is a positive coefficient usually assumed to be constant, although in some cases one also studies the effect of the dependence of Γ on the field Φ (Langer et al., 1975; Lacasta et al., 1992, 1993). As in the equilibrium case, one assumes a lattice discretization in which, instead of a real variable in every point of the space, only points on a d-dimensional lattice Λ are considered. In the lattice case, the functional derivative $\delta\mathcal{H}/\delta\Phi(\mathbf{r},t)$ becomes a partial derivative:

$$\frac{d\Phi_i(t)}{dt} = -\Gamma a_0^{-d} \frac{\partial \mathcal{H}}{\partial \Phi_i(t)} + \eta_i(t) \tag{3.2}$$

In the absence of the noise term, it is easy to show that the system evolves towards a minimum of the Hamiltonian. We have:

$$\frac{d\mathcal{H}}{dt} = \sum_{i=1}^{N} \frac{\partial \mathcal{H}}{\partial \Phi_i} \frac{d\Phi_i}{dt} = -\Gamma a_0^{-d} \sum_{i=1}^{N} \left(\frac{\partial \mathcal{H}}{\partial \Phi_i} \right)^2 \leq 0 \tag{3.3}$$

The statistical properties of the noise terms, $\eta_i(t)$, have to be determined in order to obtain the correct equilibrium distribution. They are supposed to be Gaussian distributed of mean zero and correlations given by:

$$\langle \eta_i(t) \eta_j(t') \rangle = D a_0^{-d} \delta_{i,j} \delta(t - t') \tag{3.4}$$

characteristic of the so called *white noise* (Gardiner, 1985). D is a parameter, to be determined, representing the intensity of the noise and, consequently, D must increase with temperature. In the limit of the lattice spacing a_0 going to 0, the Kronecker-delta becomes a Dirac-delta function:

$$\langle \eta(\mathbf{r},t) \eta(\mathbf{r}',t') \rangle = D \delta(\mathbf{r} - \mathbf{r}') \delta(t - t') \tag{3.5}$$

From now on, we will take the lattice spacing as unit of length $a_0 = 1$. Since η_i is Gaussian, these correlation functions completely determine its statistical properties. We now relate the noise intensity D to temperature T. For later reference, we will be more general and consider the set of stochastic differential equations:

$$\frac{d\Phi_i(t)}{dt} = F_i(t) + \sum_{j=1}^{N} G_{ij} \eta_i(t) \tag{3.6}$$

With the same statistical properties for the noise term than before, Eq.(3.4). G_{ij} is a constant matrix. The complete statistical description of the fields $[\Phi]$ is given by the joint probability density function $P([\Phi];t)$, which satisfies the Fokker-Planck equation (Gardiner, 1985). The description given by the Langevin equations is equivalent to the one given by the Fokker-Planck equation:

$$\frac{\partial P([\phi];t)}{\partial t} = \sum_{i=1}^{N} \frac{\partial}{\partial \Phi_i} \left[-F_i P + \frac{D}{2} \sum_{j=1}^{N} H_{ij} \frac{\partial P}{\partial \Phi_j} \right] \tag{3.7}$$

The matrix H is $H = GG^T$. In the case we are concerned with, Eq.(3.2), $H = \mathrm{I}$, unity matrix, and F_i is related to the partial derivative of the Hamiltonian:

$$\frac{\partial P([\phi];t)}{\partial t} = \sum_{i=1}^{N} \frac{\partial}{\partial \Phi_i} \left[\Gamma \frac{\partial \mathcal{H}}{\partial \Phi_i} P + \frac{D}{2} \frac{\partial P}{\partial \Phi_i} \right] \tag{3.8}$$

It is easy to verify that the stationary solution of this equation is:

$$P_{st}([\Phi]) \propto \exp\left[-\frac{2\Gamma}{D} \mathcal{H}([\Phi]) \right] \tag{3.9}$$

Since we want the statistical stationary properties of $[\Phi]$ to be determined by the Gibbs distribution, $\exp[-\beta\mathcal{H}([\Phi])]$ we are led to identify

Effect of Color in Nonequilibrium Phase Transitions Induced by Multiplicative Noise

S. Mangioni* and R. Deza
Departamento de Física, Facultad de Ciencias Exactas y Naturales
Universidad Nacional de Mar del Plata
Deán Funes 3350, 7600 Mar del Plata, Argentina.

H. S. Wio*†
Centro Atómico Bariloche (CNEA) and Instituto Balseiro (U.N. de Cuyo)
8400 S.C. de Bariloche, Argentina.

R. Toral ‡
Departament de Física, Universitat de les Illes Balears and
Instituto Mediterráneo de Estudios Avanzados, IMEDEA (CSIC-UIB)
E-07071 Palma de Mallorca, Spain

The model introduced by C. van den Broeck et al [Phys. Rev. Lett. **73**, 3395 (1994)] -leading to a noise–induced second–order phase transition which shows reentrance as a function of the (multiplicative) noise intensity σ- is studied under the presence of colored noise. By using a Markovian approximation and a mean field treatment, it is found that the variation of the noise self–correlation time, τ, can either induce order or destroy an ordered state according to the values of σ and the spatial coupling D. It is also found that the transition is reentrant with respect to D, i.e. that a large enough value for the spatial coupling leads for $\tau \neq 0$ to a disordered state, at variance with the usual behavior for equilibrium phase transitions. These effects are supported by numerical simulations.

Too often do we resort -in studying nonequilibrium systems- to the paradigmatic body we have inherited from equilibrium thermodynamics. Though most times this way of reasoning is of valuable help for us to interpret the results, we should be more aware of the fact that sometimes it can be seriously misleading. An archetypical example is the intuitive image we have developed of a close relationship between *noise* and *disorder*: it is true that studies on e.g. Ginzburg–Landau models subject to *additive* noise seem to reinforce this "rule" [1–3]; however, in the last decade we have also witnessed examples of exactly the opposite trend, namely, dynamical systems in which a *multiplicative* noise couples to the system's nonlinearities in such a way that it generates a transition to an *ordered* state. In fact, it is by now well known that in some zero–dimensional models, noise can induce a unimodal–bimodal transition [4]; nevertheless, this result can still be argued to be somewhat restricted since in this case there cannot be breakdown of ergodicity, which is required for a (nonequilibrium, noise–induced) *phase* transition.

Recently, a model was introduced (perhaps the simplest one displaying such a behavior) whereby an *extended* system subject to a Gaussian -white both in space and time- multiplicative noise, can undergo a noise–induced symmetry–breaking transition towards an ordered state: this became the first example of a *purely* noise–induced, nonequilibrium, ordering *phase* transition [5]. This result was obtained within a Curie–Weiss–like mean–field approximation, extended to consider the simplest correlation–function approach. In this case, and at variance with the case of order–disorder transitions at equilibrium -induced as we know by the spatial coupling constant D and the bistability of the local potential- it is the combined effects of the multiplicative noise intensity σ and the spatial coupling D which induce the transition. The remarkable feature is that neither the 0–dimensional system ($D = 0$) nor the deterministic one ($\sigma = 0$) show any transition. Such a noise–induced phase transition -besides being of a second order type as a function of noise intensity- has the noteworthy feature of being *reentrant*: the ordered state can be found only inside a window determined by two values of the noise intensity σ. A similar reentrant effect has been observed in the Ginzburg–Landau model with multiplicative and additive noises [6].

Whereas it is known that a correlated (or "colored") *additive* noise can (at least in the "adiabatic approximation") be accounted for by introducing an effective *white* multiplicative noise as an accounting device, one can question whether it is realistic enough to consider a genuine multiplicative noise as white. It appears more likely that the kind of fluctuations leading to multiplicative noise will show some degree of correlation. [4,7–9] One might expect new non–trivial effects as a function of the self–correlation ("color") of the multiplicative noise. After all, it was shown in Refs. [2,3] that an *ordering* non–equilibrium phase transition can be induced in a Ginzburg–Landau model by varying the correlation time τ of the *additive* noise. Moreover, for zero–dimensional systems, a reentrant behavior has been found in a noise–induced transition as a consequence of color [10].

It is our aim in this work to investigate the effects of the self–correlation time τ of the multiplicative noise on the model of Ref. [5]. To that end we pick a specific form for this correlation (an Ornstein–Uhlenbeck one) and apply -in the framework of the mean–field treatment of Ref. [5]- a "unified colored noise approximation" (UCNA)–like approxima-

tion [11,12]. Our main finding is that color can have both a constructive or destructive effect for ordered states, according to the values of the noise intensity σ and coupling constant D. The most widespread effect is that an ordered phase is destroyed by increasing the noise correlation time τ. A more subtle effect that appears for a limited range of σ and D is that an ordered state can appear by increasing τ. Another important result is that a large coupling constant D leads invariably for $\tau > 0$ to a disordered state at variance with the usual behavior in other models of equilibrium statistical mechanics.

As in Ref. [5] we shall resort to a lattice version of the extended system, whereas we still regard time as a continuous variable. The state of the system at time t will then be given by the set of stochastic variables $\{x_i(t)\}$ $(i = 1, \ldots, N)$ defined at the sites $\mathbf{r}_i$ of a hyper–cubic d–dimensional lattice of side L (hence $N = L^d$). The variables $\{x_i\}$ obey the following system of ordinary *stochastic differential equation* (SDE):

$$\dot{x}_i = f(x_i) + g(x_i)\eta_i + \frac{D}{2d}\sum_{j\in n(i)}(x_j - x_i) \qquad (1)$$

where D is the diffusion coefficient (which acts as the coupling constant between nearest–neighbor lattice sites), $n(i)$ stands for the set of $2d$ sites which form the neighborhood of site $\mathbf{r}_i$, and η_i is the *colored multiplicative* noise acting on site $\mathbf{r}_i$. This coupled set of Langevin–like equations is the discrete version of the *partial* SDE which in the continuum would determine the state of the extended system. The last term of the right–hand–side of Eq.(1) will, in the continuum limit, be replaced by the Laplacian operator $\nabla^2 x$. The specific case analyzed in Ref. [5] (which the authors conjecture that could be the simplest example exhibiting such a transition) is

$$f(x) = -x(1 + x^2)^2 \text{ and } g(x) = 1 + x^2 \qquad (2)$$

As in Ref. [2], the noises $\{\eta_i\}$ are taken to be Ornstein–Uhlenbeck noises, i.e. Gaussian distributed stochastic variables of zero mean and the following correlations:

$$\langle \eta_i(t)\eta_j(t')\rangle = \delta_{ij}\frac{\sigma^2}{2\tau}\exp(-\frac{|t-t'|}{\tau}) \qquad (3)$$

They arise as solutions of an uncoupled set of Langevin SDE:

$$\tau\dot{\eta}_i = -\eta_i + \sigma\xi_i \qquad (4)$$

where $\{\xi_i(t)\}$ are white noises, i.e. Gaussian stochastic variables of zero mean and correlations: $\langle \xi_i(t)\xi_j(t')\rangle = \delta_{ij}\delta(t-t')$. In the limit $\tau \to 0$ the Ornstein–Uhlenbeck noise $\eta_i(t)$ tends to the white–noise $\xi_i^W(t)$ with correlations $\langle \xi_i^W(t)\xi_j^W(t')\rangle = \sigma^2\delta_{ij}\delta(t-t')$, i.e. the case studied in reference [5].

The non Markovian character of the process $\{x_i\}$, due to the colored noise $\{\eta_i\}$ makes it difficult to study. However, there are some approximate Markovian techniques that might capture some of the essential features of the complete non Markovian process [9]. Besides, this kind of approximations strongly simplify the treatment of the equations allowing to exploit well known Markovian techniques. Amongst those approximations, the UCNA and related interpolation schemes are very useful since they can reproduce the limit of small and large correlation time τ [11,12].

We now sketch the main lines of our calculation (a more detailed account will be given elsewhere). For our particular problem, the UCNA proceeds by taking the time derivative of Eqs.(1) and after substitution of Eq.(4), set $\ddot{x}_i$ and $(\dot{x}_i)^2$ equal to zero. The former corresponds to an adiabatic elimination procedure, while the latter is necessary in order to recover a proper Fokker–Planck equation description [13]. To the resulting set of Markovian stochastic differential equations we apply another approximation in the spirit of (but not equal to) the Curie–Weiss mean–field type of approach used in [5]. This consists, in essence, in replacing the $2d$ neighbors x_j of variable x_i by a common value y_i, thus reducing the number of SDE's from N to 2. This approximation relies on the hypothesis that the system is homogeneous. ¿From the stationary joint probability density function (pdf) $P^{st}(x, y)$ (we have dropped the subindex i for the sake of clarity) one derives an effective pdf $P^{st}(x)$ by setting $y = \langle x\rangle$, the average value of x. The value of $\langle x\rangle$ follows from a self–consistency relation:

$$\langle x\rangle = \int_{-\infty}^{\infty} dx\, x P^{st}(x) \qquad (5)$$

This equation can be shown to have always the trivial solution $\langle x\rangle = 0$ corresponding to a disordered phase. When other stable non–trivial, $\langle x\rangle \neq 0$, solutions appear, the system develops order through a genuine phase transition and $m \equiv |\langle x\rangle|$ can be considered as the order parameter (notice that, due to the symmetry of the problem, $\langle x\rangle$ and $-\langle x\rangle$ are both solutions of the previous equation). In the white noise limit $\tau = 0$ this is known to be the case for sufficiently large values of the coupling D and for a window of values for the noise intensity $\sigma \in [\sigma_1, \sigma_2]$. We discuss now how the presence of ordered states is altered by non–zero values of τ.

In Figs.(1) and (2) we plot, respectively, the curves σ vs. τ and D vs. σ for different values of the parameters, separating the regions corresponding to the ordered and disordered phases. The noteworthy aspects of these curves are as follows:

(a) For fixed values of σ and D (D large enough), there exists a value of the correlation time τ beyond which the system becomes disordered, as indicated by the continuous arrowed line in Fig.(1). Furthermore, there exists a value of τ for which order is impossible whatever the values of D and σ.

(b) For some values of D and σ that would correspond to a disordered phase in the case $\tau = 0$, an increase in τ induces an ordered phase inside a window of values for τ, as indicated by the dashed arrowed line in Fig.(1) i.e. the transition can also be reentrant with respect to τ.

(c) For fixed values of σ and $\tau \neq 0$ the ordered states exist only within a window of values for D. This predicts that reentrance appears not only with respect to σ, as in the case $\tau = 0$, but also with respect to D.

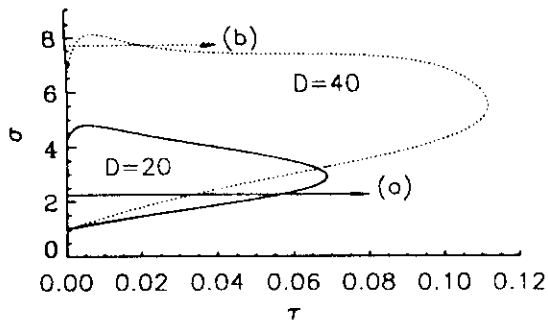

FIG. 1. Noise intensity σ vs. self–correlation time τ, for values of the spatial coupling $D = 20$ (continuous line) and $D = 40$ dotted line. The ordered regions are the ones inside the curves (marked "D=20" and "D=40", respectively). The continuous arrowed line (a) indicates the destruction of an ordered state by increasing the correlation time τ, whereas the dashed arrowed line (b) shows the creation and further destruction of order.

The reentrant nature with respect to the coupling constant D is a surprising effect that can be best observed in Fig.(2) where we plot the D vs. σ curves. It can be seen that -as τ increases from zero- the maximum value of D compatible with the ordered phase reaches a *constant* for σ large enough, and this "plateau" is a decreasing function of τ. At the same time, the branch that at $\tau = 0$ increased linearly with σ tends also to a constant (increasing with τ) for σ large enough, until the window available for the ordered phase virtually disappears.

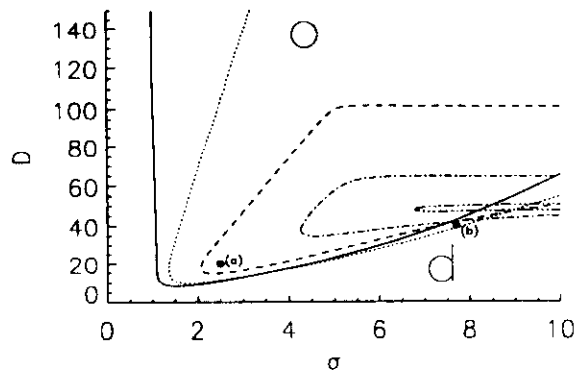

FIG. 2. Spatial coupling D vs. noise intensity σ for $\tau = 0$ (continous line), $\tau_1 = 0.015$ (dotted line), $\tau_3 = 0.05$ (dashed line), $\tau_6 = 0.1$ (dotted-dashed line), and $\tau_8 = 0.123$ (triple dotted-dashed line). For each curve, the ordered zone is the area inside the curve (for $\tau = 0$ we have marked the ordered and disorderd regions with "o" and "d", respectively). Points (a) and (b) correspond to the transitions indicated in Fig.(1).

In Fig.(2) we have also marked two possible points exhibiting the phenomena (a) and (b) described above: the point (a) corresponds to the destruction of order induced by increasing the correlation time τ in a state that is ordered for $\tau = 0$; the point (b) corresponds to a state which, being disordered for $\tau = 0$, becomes first ordered and then again disordered as τ increases. We stress again the fact that these effects of a colored multiplicative noise on an extended dynamical system (unable to undergo any phase transition in the absence of noise) are *qualitatively* different to the ones observed in (nonequilibrium) phase transitions driven by a colored additive noise on a prototypic model for equilibrium phase transitions [2,3]. Whereas in the last case the role of the correlation time is to stabilize the ordered phase and/or induce order in systems that are disordered for $\tau = 0$, the main effect of color in our case is to destroy order.

The previous features can also be seen in the phase diagrams. In Fig.(3) we plot the order parameter m vs. noise intensity σ showing, for fixed value of $D = 20$ and different values of τ, the curves separating ordered and disordered phases. The window of σ values where the ordered phases appears has the following behavior: the lower limit systematically increases with increasing τ, while the upper limit first increases and finally bounces back until, for some value of τ, the window disappears. This is, of course, consistent to what was shown in Fig.(1).

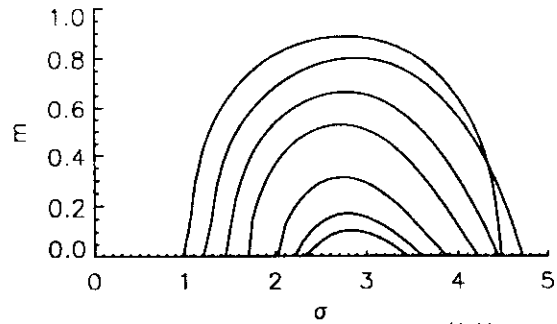

FIG. 3. Figure 3: Average value $m = |\langle x \rangle|$, obtained as a solution of the consistency equation (5), as a function of the noise intensity σ, for several values of the self–correlation time τ, and for $D = 20$. Values of τ from top to bottom are: $\tau = 0$, 0.01, 0.02, 0.03, 0.045, 0.055, 0.06.

Since the previous results have been obtained in the mean–field approximation, we have also performed numerical simulations in order to have an independent check of the predictions. As a representative example, corresponding to the phenomenon (c) above, namely: the destruction of the ordered phase by an increasing coupling constant D, we plot in Fig.(4) the phase diagram predicted by our mean–field theory and results coming from a numerical integration of the stochastic differential equations. Although the numerical results are affected by finite size effects as one would expect in a phase transition, one can see unambigously the decrease of the order parameter m with incresing coupling constant D. The mean field results agree only qualitatively with the simulation results and, in particular, they differ in the fact that mean–field predicts a much sharper decay to zero or the order parameter.

In order to understand this sudden change in behavior as soon as a tiny self–correlation is present, we have studied the time evolution equation for $\langle x \rangle$ within the mean–field approx-

imation as $\frac{D}{\sigma} \to \infty$. In Ref. [14] this simple linear criterion of stabilisation of the disordered phase was introduced as a way of determining the region of appearance of ordered phases. Up to first–order both in τ and in $\langle x \rangle$, it reads

$$\langle \dot{x} \rangle = -\alpha \langle x \rangle, \quad \text{with} \quad \alpha = \frac{1 + \tau D - \sigma^2}{1 + \tau D} \tag{6}$$

When $\tau D + 1 > \sigma^2$, it is $\alpha > 0$ and hence the disordered phase ($\langle x \rangle = 0$) is stable. On the other hand, if $\tau D + 1 < \sigma^2$ it is $\alpha < 0$, destabilizing the disordered phase in favor of the ordered one ($\langle x \rangle \neq 0$). In summary, whereas the noise intensity σ has a destabilizing effect on the disordered phase, as soon as $\tau \neq 0$ the spatial coupling D tends to *stabilize* it. For $\tau = 0$ the last effect is not present, being then the condition for ordering that $\sigma > 1$ (this is the effect that was reported in Refs. [5,14]). Considering that the effect of even a tiny correlation is enhanced by D, we can understand the abrupt change shown in Fig.(2) as soon as $\tau \neq 0$.

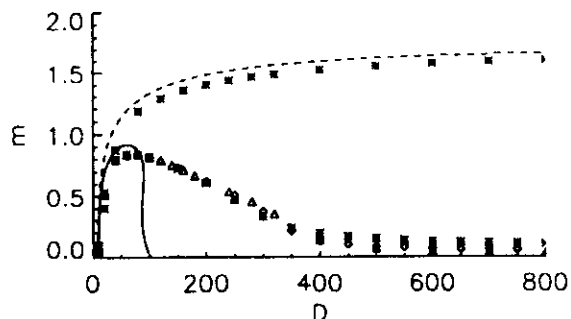

FIG. 4. Figure 4: Mean–field prediction for the order parameter m as a function of the spatial coupling D, for noise intensity $\sigma = 2$ and self–correlation times $\tau = 0$ (dashed line) and $\tau = 0.01$ (continuous line). Notice that for $\tau = 0$ the curve tend to the asymptotic value $(\sigma^2 - 1)^{1/2} = 1.73$, whereas for $\tau = 0.01$ the order parameter decays to zero for a critical value, D_c of the coupling. Simulation results for different system sizes $L = 16$ (asterisks), $L = 32$ (rombhi) and $L = 64$ (triangles) are also included.

This work has focused on the effects of a self–correlation in the multiplicative noise on the reentrant noise–induced phase transition reported in Ref. [5]. It appears that for $\tau \neq 0$, a strong enough spatial coupling is capable of destroying the order established as a consequence of the multiplicative character of the noise. The maximum value of D which holds the ordered phase reaches rapidly a "plateau" as the noise intensity is increased (note the approximately inverse relation between τ and the plateau value for D in Fig.(2), even when eq.(6) is only valid for $\frac{D}{\sigma} \to \infty$). Simultaneously, the lower branch decreases its slope as τ increases.

In order to understand the foregoing result, we stress the fact that the ordered phase arises as a consequence of the collaboration between the multiplicative character of the noise and the presence of spatial coupling. When no self–correlation is present, the disordering effect of D cannot be felt. This explains the results in Ref. [14], which have been rightly interpreted in terms of a "freezing" of the short–time behavior by a strong enough spatial coupling. As τ increases, the minimum value of D required to stabilize the disordered phase becomes lower and lower. In this way, the region in parameter space available to the ordered phase shrinks further and further until it vanishes.

The main lesson that we can draw from this work is that the conceptual inheritance from equilibrium thermodynamics (though often useful) is not always applicable. By following the equilibrium–thermodynamic lore, one should tend to think that as $D \to \infty$ an ordered situation is favored. This is certainly true for the Curie–Weiss–type models, since in that case the deterministic potential is itself bistable and an increase of spatial coupling has the effect of rising the potential barrier between the stable states. In the case we are dealing with, the deterministic potential is monostable and it is the combined effects of the multiplicative noise and the spatial coupling that induce the transition.

R. Toral acknowledges financial support from DGICyT, projects number PB94-1167 and PB94-1172 and H.S. Wio from Fundacion Antorchas project A-13396/1.

[1] R. Toral and A. Chakrabarti, Phys. Rev. B **42**, 2445 (1990) and references therein.
[2] J. García-Ojalvo, J.M. Sancho and L. Ramírez–Piscina, Phys. Lett. A **168**, 35 (1992).
[3] J. García-Ojalvo, J.M. Sancho, Phys. Rev. E **49**, 2769 (1994).
[4] W. Horsthemke and M. Malek–Mansour, Z. Phys. B **24**, 307 (1976);
L. Arnold, W. Horsthemke and R. Lefever, Z. Phys. B **29**, 367 (1978);
W. Horsthemke and R. Lefever, *Noise–Induced Transitions: Theory and Applications in Physics, Chemistry and Biology* (Springer, 1984).
[5] C. Van den Broeck, J. M. R. Parrondo and R. Toral, Phys. Rev. Lett. **73**, 3395 (1994).
[6] J. García–Ojalvo, J.M.R. Parrondo, J.M. Sancho, C. van den Broeck, to be published in Phys. Rev. E.
[7] A. V. Soldatov, Mod. Phys. Lett. B **7**, 1253 (1993).
[8] I. L'Heureux and R. Kapral, J. Chem. Phys. **90**, 2453 (1988).
[9] J.M. Sancho, M. San Miguel, in "Noise in Nonlinear Dynamical Systems", p.72, F. Moss and P.V.E. McClintock, eds. Cambridge University Press (1989).
[10] F. Castro, A. D. Sánchez and H. S. Wio, Phys. Rev. Lett. **75**, 1691 (1995).
[11] P. Jung and P. Hänggi, Phys. Rev. A **35**, 4464 (1987);
L. H'walisz, P. Jung, P. Hänggi, P. Talkner and L. Schimansky–Geier, Z. Phys. B **77**, 471 (1989);
P. Hänggi, Chem. Phys. **180**, 157 (1994).
[12] F. Castro, H. S. Wio and G. Abramson, Phys. Rev. E **51**, (1995).
[13] H.S. Wio, P. Colet, M. San Miguel, L. Pesquera and M. Rodriguez, Phys. Rev. A **40**, 7312 (1989).
[14] C. Van den Broeck, J. M. R. Parrondo, R. Toral and R. Kawai, Limburgs Universitair Centrum preprint (1996).

*Member, CONICET
†e–mail: wio@cab.cnea.edu.ar
‡e–mail: dfsrtg0@ps.uib.es, WWW http://www.imedea.uib.es/~raul

Phase Separation Driven by External Fluctuations

J. García-Ojalvo
Departament de Física i Enginyeria Nuclear, Universitat Politècnica de Catalunya, Colom 11, E-08222 Terrassa, Spain

A.M. Lacasta
Departament de Física Aplicada, Universitat Politècnica de Catalunya, Av. Dr. Gregorio Marañón, 50, E-08028 Barcelona, Spain

J.M. Sancho
Institute for Nonlinear Science, Department 0407, University of California, San Diego, 9500 Gilman Drive, La Jolla, California 92093-0407 and Departament d'Estructura i Constituents de la Matèria, Universitat de Barcelona, Av. Diagonal 647, E-08028 Barcelona, Spain

R. Toral
Departament de Física, Universitat de les Illes Balears and Instituto Mediterráneo de Estudios Avanzados (UIB-CSIC), E-07071 Palma de Mallorca, Spain

The influence of external fluctuations in phase separation processes is analysed. These fluctuations arise from random variations of an external control parameter. A linear stability analysis of the homogeneous state shows that phase separation dynamics can be induced by external noise. The spatial structure of the noise is found to have a relevant role in this phenomenon. Numerical simulations confirm these results. A comparison with order-disorder noise induced phase transitions is also made.

PACS numbers: 05.40+j, 47.20.Ky, 47.20.Hw

The role of noise as an ordering agent has been broadly studied in recent years in the context of both temporal and spatiotemporal dynamics. In the temporal case, which was the one to be addressed earlier, external fluctuations were found to produce and control transitions (known as *noise-induced transitions*) from monostable to bistable stationary distributions in a large variety of physical, chemical and biological systems [1]. Spatiotemporal systems have been faced much more recently. In these cases, the combined effects of the spatial coupling and the noise terms acting upon the system variables may produce an ergodicity breaking of a bistable state, leading to phase transitions between spatially homogeneous and inhomogeneous phases. Results obtained in this field include critical-point shifts in standard models of phase transitions [2, 3, 4], pure *noise-induced phase transitions* [5, 6, 7], stabilization of propagating fronts [8], and noise-driven structures in pattern-formation processes [9, 10, 11, 12]. In all these cases, the qualitative (and somewhat counterintuitive) effect of noise is to enlarge the domain of existence of the ordered phase in parameter space. It is the purpose of this Letter to analyse the role of fluctuations in a radically different type of spatiotemporal process, namely in phase separation dynamics. It will be shown that external noise can induce the phase separation process and that this effect is determined by the spatial correlation of the noise terms. An important conclusion is that phase separation does not occur, necessarily, for the same range of parameters for which the system presents a phase ordering process.

The dynamics of a large class of spatially-extended systems can be described in a general way by the following standard model[13]:

$$\frac{\partial \psi(\vec{x},t)}{\partial t} = -\mathcal{L}(\nabla)\left(\frac{\delta \mathcal{F}}{\delta \psi}\right) + \xi(\vec{x},t) \qquad (1)$$

where $\psi(\vec{x},t)$ is a dynamical field that describes the state of the system, $\mathcal{F}$ is a free energy functional, and $\xi(\vec{x},t)$ is a space-dependent stochastic process that accounts for thermal fluctuations. Thermal equilibrium at temperature T is reached at long times if the fluctuation-dissipation relation holds:

$$\langle \xi(\vec{x},t)\xi(\vec{x}',t')\rangle = 2\varepsilon \mathcal{L}(\nabla)\delta(t-t')\delta(\vec{x}-\vec{x}') \qquad (2)$$

with $\varepsilon = k_B T$. The system is usually characterised by the behavior of the spatial average of the field ψ, which plays the role of an order parameter. The operator $\mathcal{L}(\nabla)$ does not alter the equilibrium state of the system ($\sim \exp(-\mathcal{F}/k_B T)$), but only its transient dynamics. Two forms of $\mathcal{L}$ are usually adopted: for $\mathcal{L} = 1$ (the so-called *model A*) the system evolves towards its equilibrium state without any constraint on the value of the order parameter; for $\mathcal{L}(\nabla) = -\nabla^2$ (*model B*) the order

parameter is conserved throughout the dynamical evolution. Model A is a prototype of ferromagnetic ordering, and model B of phase separation dynamics following a quench from a high temperature homogeneous phase to a low temperature state. In this latter case, according to the value of the order parameter and the quench location, the evolution might proceed either by spinodal decomposition or by nucleation[14].

Far from the critical point, the dynamics is not qualitatively affected by the presence of the thermal noise term $\xi(\vec{x},t)$. Instead, we will consider the situation in which there is an additional source of noise, $\eta(\vec{x},t)$. This happens, for instance, when one of the externally controlled system parameters is subjected to fluctuations. As these fluctuations are external, they do not usually verify the fluctuation-dissipation relation (2) and the system is no longer at equilibrium. We will show that, in the case of model B, these external fluctuations can induce a phase separation in the system. Although this is a reminiscence of noise-induced phase transitions reported earlier for model A [2, 4, 15] (and, in what follows, we will make a comparison between the effect of external noise in both models), an unexpected and notorious feature is that the nature of the destabilizing terms due to the noise is intrinsically different for model A and model B. We conclude that phase separation does not necessarily occur in the conserved order-parameter model B at the same values for which model A shows a noise-induced phase transition. It follows that, in contrast with what happens at equilibrium, both models have now different stationary distributions. Furthermore, a relevant result of our analysis is that the spatial structure of the noise plays an important and distinct role for both models. We assume the following correlation for the external noise with a characteristic correlation length λ:

$$\langle \eta(\vec{x},t)\eta(\vec{x}\,',t')\rangle = 2\sigma^2\delta(t-t')g(|\vec{x}-\vec{x}\,'|/\lambda) \qquad (3)$$

where g is a (short-ranged) spatial correlation function. It is expected, and will be confirmed in what follows, that since model B represents a domain-growth process, this correlation length will play a role far beyond the intuitive intensity-reduction effect of space-time noise correlation [3]. Correlation time of the noise should not have a parallel influence, since all time scales of the system are larger than those of the noise. Therefore, it seems that a finite (non-zero) correlation time of the noise would not differentiate between models A and B, and will not be considered here (the time dependence of the correlation of $\eta(\vec{x},t)$ will be assumed to be a Dirac delta, as shown in Eq.(3)).

Although our results are quite general, we shall work, for the sake of clarity, with the well known Ginzburg-Landau free energy

$$\mathcal{F} = \int d\vec{x}\left[\frac{r}{2}\psi^2 + \frac{1}{4}\psi^4 + \frac{K}{2}|\vec{\nabla}\psi|^2\right] \qquad (4)$$

In the absence of additive (thermal) noise, phase separation occurs for $r < r_c = 0$. If additive noise is present, the transition occurs at $r_c < 0$. We will consider $r > 0$, so that order will not appear spontaneously. The control parameter r will be assumed to be subjected to external fluctuations, *i.e.* $r \to r + \eta(\vec{x},t)$. The spatial correlation function g is chosen to be a Gaussian of width λ:

$$g\left(\frac{|\vec{x}-\vec{x}\,'|}{\lambda}\right) = \frac{1}{(\lambda\sqrt{2\pi})^d}\,\exp\left(-\frac{|\vec{x}-\vec{x}\,'|^2}{2\lambda^2}\right), \qquad (5)$$

(d is the $\vec{x}$-space dimension) which becomes a delta function in the limit $\lambda \to 0$. It is simpler to analyze the role of noise by using a lattice discretization in which the space vectors $\vec{x}$ take values x_i $(i = 1,\ldots,N)$, defined on regular lattice of linear cell size $\Delta x = 1$. The field $\psi(\vec{x},t)$ then becomes a discrete set of variables $\psi_i(t)$ and similar notation is used for the random fields $\eta_i(t)$ and $\xi_i(t)$. Under these considerations, the lattice version of model (1) with the Ginzburg-Landau free energy (4) is:

$$\dot{\psi}_i = -\mathcal{L}_L(r\psi_i + \eta_i\psi_i + \psi_i^3 - K\nabla_L^2\psi_i) + \xi_i\,, \qquad (6)$$

where $\mathcal{L}_L = 1$ for model A and $\mathcal{L}_L = -\nabla_L^2$ for model B. ∇_L^2 is the lattice Laplacian operator. Finally, in this version, the external noise has a correlation function $g_{|i-j|}$ which is the discrete inverse Fourier transform of $\hat{g}_k$, the corresponding lattice version of the Fourier transform of (5), namely (in two dimensions):

$$\hat{g}_k = \exp\left(-\frac{\lambda^2}{2}\left(\sin(k_x/2)^2 + \sin(k_y/2)^2\right)\right) \qquad (7)$$

There is no closed analytical form for $g_{|i-j|}$ and the desired values g_0 and g_1 (see later) must be obtained numerically.

The transition towards an ordered state can be analyzed by studying the stability of the homogeneous phase $\psi_i = 0$. The early time evolution of the statistical moments of ψ_i in Fourier space can be obtained in a linear approximation. For example, the second moment (structure function) is defined as $S_k(t) = \frac{1}{N}\langle\hat{\psi}_k\hat{\psi}_{-k}\rangle$, where N is the number of points of the system. Making use of the Stratonovich calculus and Novikov's theorem, its evolution equation is [11]:

$$\frac{dS_k(t)}{dt} = -2\,\omega(k)S_k(t) + \frac{1}{N}\,f(k)\sum_k \hat{g}_k S_k(t) + 2\varepsilon \qquad (8)$$

Hence the second moment equation contains a term which globally couples Fourier modes and a constant term due to thermal noise. The particular values of the dispersion relation $\omega(k)$ and of the mode-coupling coefficient $f(k)$ differ for models A and B. For model A, the result is well known [4]

$$\omega^A(k) = r_{eff}^A + Kk^2, \qquad f^A(k) = 1 \qquad (9)$$

with an effective control parameter $r^A_{eff} = r - \sigma^2 g_0$. For model B the situation is drastically different:

$$\omega^B(k) = r^B_{eff} k^2 + K^B_{eff} k^4, \qquad f^B(k) = k^2 \qquad (10)$$

with effective control parameter $r^B_{eff} = r + \sigma^2 \nabla^2_L g_0$ and effective diffusion coefficient $K^B_{eff} = K - \sigma^2 g_1$. Two main differences are observed with respect to model A: the diffusion coefficient K is also renormalized by the correlated external noise, and the noise-induced shift of the control parameter r depends now, through the Laplace operator ∇^2_L, on the spatial structure of the noise correlation, i.e. not only on the same–site correlation g_0, but also on the nearest–neighbor correlation g_1. These differences will reveal itself in the position of the transition point where the homogeneous state loses stability and phase separation appears.

When neglecting the mode–coupling terms in Eq.(8), it is readily seen that perturbations grow when $\omega(k)^{A,B} < 0$ for some interval of k values. We have checked, by means of a numerical integration of Eq. (8), that mode-coupling terms hardly influence the position of the transition curves. Hence the transition point is characterised by $r_{eff} = 0$ for both model A and model B. The critical value of the control parameter r and its dependence on the spatial structure of the noise is, however, different in the two cases:

$$\begin{aligned} &\text{model } A: \quad r_c = \sigma^2 g_0 \\ &\text{model } B: \quad r_c = -\sigma^2 \nabla^2_L g_0 = \sigma^2 2d(g_0 - g_1) \end{aligned} \qquad (11)$$

Figure 1 shows the transition curves between homogenous and inhomogeneous states in the (λ, σ^2) plane for models A and B for a fixed value, $r = 0.2$, of the control parameter and spatial dimension $d = 2$. All points located above the curves shown in this phase diagram are in an inhomogeneous state, which corresponds to an ordered phase in model A (solid curve) and to phase separation in model B (dashed curve). The λ–dependence of the model-A curve is merely due to the natural "softening" effect of noise correlation [3, 11]. In the case of model B, on the other hand, additional, non-trivial dependence on the correlation length is introduced via the Laplace operator. As a consequence, for small λ, the transition in model B occurs *sooner* in model B than in model A, whereas the situation is the opposite for large values of λ. A crossing of the two transition curves occurs for an intermediate value of $\lambda \approx 1.8$. We stress again that the presence of ordered regions in the phase diagram of figure 1 is due to the presence of a multiplicative noise on the model, since we are taking $r = 0.2$ which is larger than the mean–field critical value $r_c = 0$.

The lines drawn in the phase diagram of Fig. 1 have been obtained in a linear approximation (11). It is presumable that this linear stability analysis will provide the position of the transition points up to leading order of approximation [4]. In order to corroborate the results obtained by means of the linear stability analysis, equations (6) have been integrated numerically for models A and B in dimension $d = 2$. A standard stochastic algorithm is used in order to handle both the additive and multiplicative noise terms [16]. Gaussianly-distributed random vectors are generated by means of a numerical inversion method, optimised to efficiently produce large quantities of Gaussian random numbers [17]. According to the previous discussion, the spatially correlated external noise is generated in Fourier space with the desired correlation function (7), and transformed back to real space at each integration time step [11].

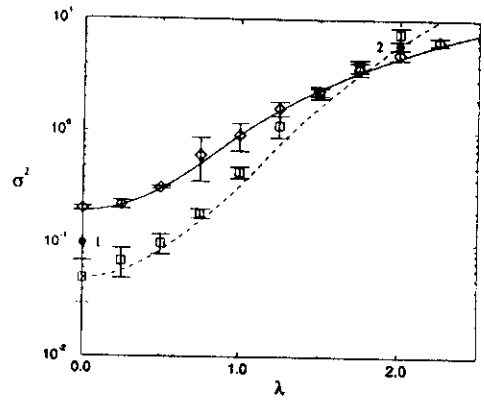

FIG. 1. Phase diagram in the (λ, σ^2) plane for model A (solid line) and model B (dashed line), obtained from a linear stability analysis (8). Points correspond to numerical simulations of the full model (6), (diamonds: model A, squares: model B) ($r = 0.2$, $K = 1$, and $\epsilon = 10^{-4}$).

A unified criterion for the existence of an ordered phase in model A and of phase separation in model B is the growth of the averaged second moment of ψ in real space (the averaged first moment is not useful for model B because this model conserves the order parameter). We define this quantity as $J(t) = \frac{1}{N}\langle \sum_i \psi_i^2(t) \rangle$ or, alternatively, as $J(t) = \sum_k S_k(t)$. The instability point is thus defined so that, below it, $J(t)$ decays to a thermal-noise background at large times and, above it, it grows to a non-zero steady-state value J_{st}. In this way, one can determine numerically the phase diagram of the system. The numerical results are represented in Fig. 1 as diamonds (model A) and squares (model B). It can be observed that the simulations of the full nonlinear models reasonably adjust to the predictions of the linear analysis. The agreement starts to fail at high values of λ and σ^2. In fact, according to previous observations in model A [15] and other models [5, 6], the transition curves might be expected to exhibit, for higher values of the noise intensity, a reentrant branch towards the $\lambda = 0$ axis. These reentrant transitions are hard to observe numerically be-

cause of the large noise intensities involved.

Fig. 2 shows two patterns of a system evolving according to model B, for point 1 in the phase diagram of Fig. 1. Depending on the initial conditions we get spinodal decomposition (Fig. 2a, with $\langle\psi(\vec{x},0)\rangle = 0$), or nucleation (Fig. 2b, with $\langle\psi(\vec{x},0)\rangle = 0.1$). For the same values of the noise parameters a homogeneous phase is obtained for model A.

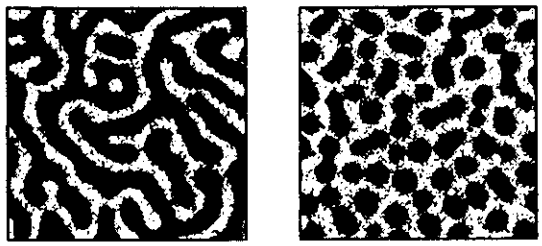

(a) (b)

FIG. 2. Spatial patterns of model B: a) Spinodal decomposition and b) Nucleation. ($t = 2500$, $\lambda = 0$, $\sigma^2 = 0.1$ and $\epsilon = 10^{-4}$)

For larger values of the noise parameters a reverse situation is found. Fig. 3 shows a spatial pattern of model A for point 2 in the phase diagram of Fig. 1. Now the homogeneous phase corresponds to model B.

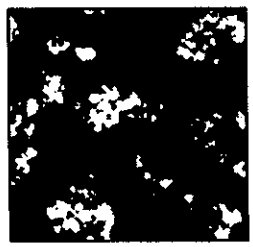

FIG. 3. Spatial pattern of model A. ($t = 100$, $\lambda = 2$, $\sigma^2 = 6$ and $\epsilon = 10^{-4}$.)

In conclusion, we have demonstrated for the first time the ordering role of external noise in processes of phase separation. The study has concentrated on the conserved time-dependent Ginzburg-Landau model, although our results are not restricted to this particular model. External noise is found to enhance the phase separation process, and this effect is observed to be modified by spatial correlation of the noise, which increases the efficiency of fluctuations for small correlation lengths and decreases it for large correlation lengths. Future work on this issue should analyse the important effect of external noise on the dynamical scaling of the phase separation process. Additional theoretical analysis such as a mean-field approach [2, 5, 6] could be useful in determining whether a reentrant transition should be expected in this model.

We acknowledge financial support from the Dirección General de Investigación Científica y Técnica (Spain), under projects PB96-0421, PB94-1167 and PB94-1172), and computing support from Fundació Catalana per a la Recerca.

[1] W. Horsthemke and R. Lefever, *Noise-Induced Transitions* (Springer-Verlag, Berlin, 1984).
[2] C. Van den Broeck, J.M.R. Parrondo, J. Armero, and A. Hernández-Machado, Phys. Rev. E **49**, 2639 (1994).
[3] J. García-Ojalvo and J.M. Sancho, Phys. Rev. E **49**, 2769 (1994).
[4] A. Becker and L. Kramer, Phys. Rev. Lett. **73**, 955 (1994); Physica D **90**, 408 (1995).
[5] C. Van den Broeck, J.M.R. Parrondo, and R. Toral, Phys. Rev. Lett. **73**, 3395 (1994).
[6] C. Van den Broeck, J.M.R. Parrondo, R. Toral, and R. Kawai, Phys. Rev. E **55**, 4084 (1997).
[7] S.H. Park and S. Kim, Phys. Rev. E **53**, 3425 (1996).
[8] J. Armero, J.M. Sancho, J. Casademunt, A.M. Lacasta, L. Ramírez-Piscina, and F. Sagués, Phys. Rev. Lett. **76**, 3045 (1996).
[9] J. García-Ojalvo, A. Hernández-Machado, and J.M. Sancho, Phys. Rev. Lett. **71**, 1542 (1993).
[10] J.M.R. Parrondo, C. Van den Broeck, J. Buceta, and F.J. de la Rubia, Physica A **224**, 153 (1996).
[11] J. García-Ojalvo and J.M. Sancho, Phys. Rev. E **53**, 5680 (1996).
[12] G.D. Lythe, Phys, Rev. E **53**, R4271 (1996).
[13] P.C. Hohenberg and B.I. Halperin, Rev. Mod. Phys. **49**,435 (1977).
[14] J.D. Gunton, M. San Miguel and P. Sahni, in *Phase Transitions and Critical Phenomena*, vol. 8, edited by C. Domb and J.L. Lebowitz, Academic, New York (1983).
[15] J. García-Ojalvo, J.M.R. Parrondo, J.M Sancho, and C. Van den Broeck, Phys. Rev. E **54**, 6918 (1996).
[16] T.C. Gard, *Introduction to Stochastic Differential Equations* (Marcel Dekker, New York, 1987).
[17] R. Toral and A. Chakrabarti, Comp. Phys. Commun. **74**, 327 (1993).

Nonequilibrium phase transitions induced by multiplicative noise

C. Van den Broeck
Limburgs Universitair Centrum, B-3590 Diepenbeek, Belgium

J. M. R. Parrondo
Departamento de Física Aplicada I, Universidad Complutense Madrid, E-28040 Madrid, Spain

R. Toral
Departament de Física, Universitat de les Illes Balears, and Instituto Mediterráneo de Estudios Avanzados, IMEDEA (CSIC-UIB), E-07071 Palma de Mallorca, Spain

R. Kawai
Department of Physics, University of Alabama at Birmingham, Birmingham, Alabama 35294
(Received 15 July 1996)

We review a mean-field analysis and give the details of a correlation function approach for spatially distributed systems subject to multiplicative noise, white in space and time. We confirm the existence of a pure noise-induced reentrant nonequilibrium phase transition in the model introduced in [C. Van den Broeck *et al.*, Phys. Rev. Lett. **73**, 3395 (1994)], give an intuitive explanation of its origin, and present extensive simulations in dimension $d=2$. The observed critical properties are compatible with those of the Ising universality class. [S1063-651X(97)08704-7]

PACS number(s): 05.40.+j

I. INTRODUCTION

Noise is usually thought of as a phenomenon which perturbs the observation and creates disorder. This idea is based mainly on our day to day experience and, in the context of physical theories, on the study of equilibrium systems. The effect of noise can, however, be quite different in nonlinear nonequilibrium systems. Several situations have been documented in the literature, in which the noise actually participates in the creation of ordered states or is responsible for surprising phenomena through its interaction with the nonlinearities of the system [1–10]. Recently [11], a quite spectacular phenomenon was discovered in a specific model of a spatially distributed system with multiplicative noise, white in space and time. It was found that the noise generates an ordered symmetry-breaking state through a genuine second-order phase transition, whereas no such transition is observed in the absence of noise. The purpose of this paper is to present a more detailed investigation of this phenomenon. First, we will give an intuitive explanation of why the transition occurs in this particular model and not in others. This explanation also sheds light on why phase transitions were not discovered in the related context of noise-induced transitions [1]. Second, after reviewing the mean-field analysis which was introduced in [12], we present the details of a more sophisticated approach, which involves the approximate calculation of the spatial correlation function. Third, we include extensive simulations of the model in spatial dimension $d=2$, and present a finite-size scaling analysis showing that the critical properties of the phase transition are compatible with those of the dynamical Landau-Ginzburg model or the Ising model.

II. ZERO-DIMENSIONAL MODELS: SHORT-TIME VS LONG-TIME BEHAVIOR

Consider the stochastic differential equation

$$\dot{x}=f(x)+g(x)\xi, \tag{1}$$

where ξ stands for Gaussian white noise with first two moments

$$\langle\xi(t)\rangle=0,$$
$$\langle\xi(t)\xi(t')\rangle=\sigma^2\delta(t-t'). \tag{2}$$

Equation (1) is interpreted according to the Stratonovitch interpretation [13]. Hence the probability density $P(x,t)$ for the variable $x(t)$ obeys the Fokker-Planck equation [1,14]

$$\partial_t P(x,t)=-\partial_x[f(x)P(x,t)]+\frac{\sigma^2}{2}\partial_x\{g(x)\partial_x[g(x)P(x,t)]\}, \tag{3}$$

and the steady-state solution is given by

$$P^{\rm st}(x)=N\exp\left\{\int_0^x\frac{f(y)-\frac{\sigma^2}{2}g(y)g'(y)}{\frac{\sigma^2}{2}g^2(y)}dy\right\}, \tag{4}$$

where N is a normalization constant and $g'(x)$ stands for the derivative of $g(x)$ with respect to its argument. The extrema $\bar{x}$ of the steady-state density obey the following equation:

$$f(\bar{x})-\frac{\sigma^2}{2}g(\bar{x})g'(\bar{x})=0. \tag{5}$$

One notes that this equation is not identical to the equation $f(\bar{x})=0$ for the steady states in the absence of multiplicative noise. As a result, the most probable states need not coincide with the deterministic stationary states. More importantly, solutions can appear or existing solutions can be "destabilized" by the noise. These changes in the asymptotic behavior of the system have been generally named noise-induced transitions [1].

To illustrate this phenomenon, consider the case of a deterministically stable steady state at $x=0$, e.g., $f(x)=-x+o(x)$, perturbed by a multiplicative noise. As is clear from Eqs. (4) and (5), a noise term of the form $g(x)=1+x^2+o(x^2)$ will have a stabilizing effect, since $-(\sigma^2/2)g(\bar{x})g'(\bar{x})=-\sigma^2\bar{x}+o(\bar{x})$, and it makes the coefficient of x more negative. On the other hand, noise of the form $g(x)=1-x^2+o(x^2)$, i.e., with maximal amplitude at the reference state $x=0$, has the tendency to "destabilize" the reference state. In fact, above a critical intensity $\sigma^2>\sigma_c^2=1$, the stationary probability density will no longer have a maximum at $\bar{x}=0$, and "noise-induced" maxima can appear. This phenomenon remains possible even if the deterministic steady-state equation, obtained by fixing the random value of the noise to a constant value λ, namely, $f(\bar{x})+\lambda g(\bar{x})=0$, has a unique solution for all λ. Hongler's model [17], with $f(x)=-\tanh x=-x+o(x)$ and $g(x)=\mathrm{sech}x=1-x^2/2+o(x^2)$, is a concrete example of this situation: for $\sigma^2>\sigma_c^2=2$, two noise-induced maxima arise on both sides of the deterministic reference state $\bar{x}=0$. One has coined the term "pure noise-induced transition" for this type of transitions.

Following the formalism for equilibrium states, it is tempting to introduce the notion of a "stochastic potential" $U_{st}(x)$ by writing: $P^{st}(x)\sim\exp[-U_{st}(x)]$. One concludes that for a system undergoing a noise-induced transition, e.g., for $g(x)=1-x^2+o(x^2)$, and for $\sigma^2>\sigma_c^2$, the stochastic potential has two minima. Consider now a spatially extended system obtained by coupling such units. The coupling is such that it favors the nearest-neighbor units, to stay at the same maximum of the probability density (minimum of the stochastic potential). In analogy to what happens for equilibrium models, such as the Landau-Ginzburg model [18,19], one expects that this system will undergo a phase transition for some critical value of the "temperature" (noise intensity) σ^2. However, it turns out that this is not the case. In fact, we will show in the next sections that one needs a noise of precisely the other type, namely $g(x)=1+x^2+o(x^2)$, to generate a genuine phase transition. The reason for this counterintuitive result can be clarified by focusing on the short-time behavior.

From Eq. (3), we obtain the following exact equation for the time evolution of the first moment of the probability density:

$$\langle\dot{x}\rangle=\langle f(x)\rangle+\frac{\sigma^2}{2}\langle g(x)g'(x)\rangle. \tag{6}$$

When f and/or g are nonlinear, the evolution of the first moment is coupled to higher-order moments. Suppose, however, that we start with an initial Dirac δ probability density, and follow it for a short time, such that fluctuations are small and the probability density is well approximated by a Gaussian. The equation for the maximum of the probability, which is also the average value in this approximation $\bar{x}=\langle x\rangle$, takes on the following form [valid if $f(\langle x\rangle)\gg\langle\delta x^2\rangle f''(\langle x\rangle)$, and a similar condition for the term involving $g(x)$]:

$$\dot{\bar{x}}=f(\bar{x})+\frac{\sigma^2}{2}g(\bar{x})g'(\bar{x}). \tag{7}$$

The important observation to make is that the sign of the multiplicative noise term is *opposite* to that appearing in the long-time result, cf. Eq. (5). Hence it predicts an opposite effect of the multiplicative noise at early times. In particular, if we were to probe the "stability" of the reference state $\bar{x}=0$, we would conclude from Eq. (7) that a noise of the form $g(x)=1+x^2+o(x^2)$ now has the tendency to destabilize the reference state $\bar{x}=0$, favoring initially non-null values of the variable x.

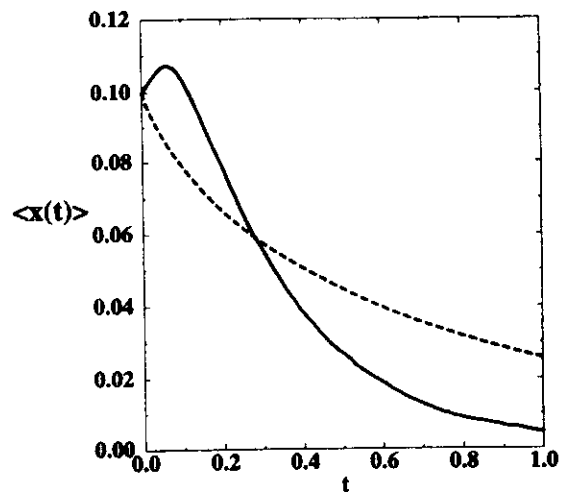

FIG. 1. Time-dependent evolution of the first moment $\langle x(t)\rangle$, starting from an initial state $P(x,t=0)=\delta(x-0.1)$, of a stochastic variable satisfying Eq. (1), for Hongler's model (dashed line), $f(x)=-\tanh x$ and $g(x)x=\mathrm{sech}x\sim 1-x^2/2$, and for the model introduced in [11] (full line), $f(x)=-x(1+x^2)^2$ and $g(x)=1+x^2$. Notice that, for Hongler's model, the decay is monotonic, whereas for the other model there is a tendency to initially destabilize small values of x.

To illustrate this point further, in Fig. 1 we have represented the time-dependent evolution of the first moment $\langle x(t)\rangle$, starting from an initial state $P(x,t=0)=\delta(x-0.1)$, for Hongler's model, $f(x)=-\tanh x$ and $g(x)=\mathrm{sech}x$, and for the model introduced in Ref. [11], $f(x)=-x(1+x^2)^2$ and $g(x)=1+x^2$. For Hongler's model, the analytic result is available. For the other model, $\langle x(t)\rangle$ was obtained through a numerical integration of the corresponding Langevin equation. If one would like to interpret these results again in terms of an equilibrium picture with a Brownian particle in an effective potential $U_{\mathrm{eff}}(x)$, one finds that the short-time behavior corresponds to an effective potential with a single minimum at $x=0$ for Hongler's model, while it it bistable for the other model. In other words, the picture is just the reverse of the one suggested by the consideration of the steady-state probability and the stochastic potential $U_{st}(x)$.

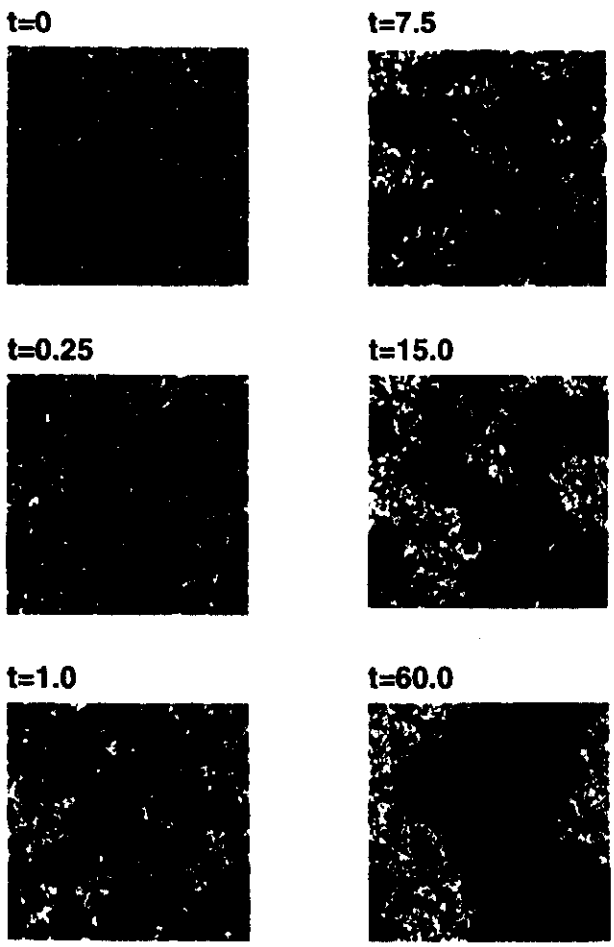

FIG. 2. Time evolution of domains starting in a completely random initial configuration toward an ordered phase for the spatially extended model given by Eqs. (8) and (29) on a square lattice, ($L=128$, $\sigma^2=4.00$, and $D=20$). Dark areas correspond to positive values of the field $x_{\mathbf{r}}$, and light areas to negative values. Notice the initial development of small ordered regions which subsequently grow.

We can now understand a possible mechanism for the presence of a phase transition when coupling such scalar variables. Imagine that the short-time behavior can be described by a bistable potential $U_{\text{eff}}(x)$ according to the discussion in the previous paragraph and, hence, non-null symmetric states develop initially. Then, if the spatial coupling is sufficiently strong, it is possible that these non-null states couple to form local ordered regions which might subsequently coarsen and grow (see Fig. 2). This mechanism is the physical explanation of the existence of a phase transition in the spatially extended version of the system.

III. MEAN-FIELD THEORY FOR SPATIALLY EXTENDED SYSTEMS

We now consider spatially extended systems with multiplicative noise [11,12,20–23]. For simplicity, and in order to keep a clear connection with the zero-dimensional models discussed in Sec. II, we consider a lattice model with one spatially distributed scalar variable $x_{\mathbf{r}}$, with $\mathbf{r}$ determining the location of the lattice point under consideration. The time evolution of $x_{\mathbf{r}}$ is described by the following set of stochastic differential equations (we consider a hypercubic lattice in dimension d with lattice spacing $a_0=1$):

$$\dot{x}_{\mathbf{r}}=f(x_{\mathbf{r}})+g(x_{\mathbf{r}})\xi_{\mathbf{r}}+\frac{D}{2d}\sum_{\mathbf{r}'\in n(\mathbf{r})}(x_{\mathbf{r}'}-x_{\mathbf{r}}), \tag{8}$$

where $n(\mathbf{r})$ denotes the set of $2d$ sites neighbor to $\mathbf{r}$, and $\{\xi_{\mathbf{r}}(t)\}$ are Gaussian noises, white in time and space, with zero mean and an autocorrelation function given by

$$\langle\xi_{\mathbf{r}}(t)\xi_{\mathbf{r}'}(t')\rangle=\sigma^2\delta_{\mathbf{r},\mathbf{r}'}\delta(t-t'). \tag{9}$$

($\delta_{\mathbf{r},\mathbf{r}'}$ stands for a Kronecker δ function.) The last sum of Eq. (8) is, in the continuum limit, nothing but the usual diffusive Laplacian term $\nabla^2 x_{\mathbf{r}}$. Equations of this kind are very general, and cover a multitude of different physical phenomena both in equilibrium and nonequilibrium problems. We focus in this paper on the steady-state properties of this system. However, the presence of multiplicative noise terms complicates matters significantly and, in fact, the multivariate steady-state probability $P^{\text{st}}(\{x_{\mathbf{r}}\})$ is only known in general for the case of additive noise, i.e., when $g(x)$ is a constant function.

The set of Eqs. (8) and (9) are equivalent to the following Fokker-Planck equation:

$$\begin{aligned}\partial_t P(\{x_{\mathbf{r}}\},t)&=\sum_{\mathbf{r}}\left[\frac{\partial}{\partial x_{\mathbf{r}}}\left\{\left[-f(x_{\mathbf{r}})+\frac{D}{2d}\sum_{\mathbf{r}'\in n(\mathbf{r})}(x_{\mathbf{r}}-x_{\mathbf{r}'})\right]P(\{x_{\mathbf{r}}\},t)\right\}\right.\\&\left.+\frac{\sigma^2}{2}\frac{\partial}{\partial x_{\mathbf{r}}}\left\{g(x_{\mathbf{r}})\frac{\partial}{\partial x_{\mathbf{r}}}[g(x_{\mathbf{r}})P(\{x_{\mathbf{r}}\},t)]\right\}\right].\end{aligned} \tag{10}$$

By integrating Eq. (10) over all variables with the exception of $x_{\mathbf{r}}$ (and assuming that the steady-state properties are uniform), one obtains the following exact steady-state equation for the one-site probability:

$$\begin{aligned}0=\frac{\partial}{\partial x_{\mathbf{r}}}\Bigg[&-f(x_{\mathbf{r}})+D[x_{\mathbf{r}}-E(x_{\mathbf{r}})]\\&+\frac{\sigma^2}{2}g(x_{\mathbf{r}})\frac{\partial}{\partial x_{\mathbf{r}}}g(x_{\mathbf{r}})\Bigg]P^{\text{st}}(x_{\mathbf{r}}),\end{aligned} \tag{11}$$

where

$$E(y)=\langle x_{\mathbf{r}'}|x_{\mathbf{r}}=y\rangle=\int dx_{\mathbf{r}'}x_{\mathbf{r}'}P^{\text{st}}(x_{\mathbf{r}'}|x_{\mathbf{r}}=y),\quad \mathbf{r}'\in n(\mathbf{r}) \tag{12}$$

represents the steady-state conditional average of $x_{\mathbf{r}'}$ at a neighboring site $\mathbf{r}'\in n(\mathbf{r})$, given that $x_{\mathbf{r}}$ at site $\mathbf{r}$ takes the value $x_{\mathbf{r}}=y$. The solution to Eq. (11) is readily found (we drop the subscript $\mathbf{r}$ for simplicity of notation),

$$P^{st}(x) = Z^{-1}\exp\left\{\int_0^x dy \frac{f(y)-\frac{\sigma^2}{2}g(y)g'(y)-D[y-E(y)]}{\frac{\sigma^2}{2}g^2(y)}\right\}, \tag{13}$$

where Z is a normalization constant. This result is exact, but we still have to determine the unknown function $E(y)$.

We start by considering in this section the simplest approximation [12], which is analogous to the traditional Weiss mean-field approach from the theory of equilibrium critical phenomena and which has also been applied successfully in several other stochastic problems [24–35]. In this approximation, one neglects the correlation between neighboring sites so that $E(y)=\langle x\rangle$, independent of y. Note that, the steady-state probability is now a function of $\langle x\rangle$, cf. Eq. (13). The value of $\langle x\rangle$ follows from a self-consistent relation arising from its very definition,

$$\langle x\rangle = \int_{-\infty}^{+\infty} dx x P^{st}(x) \equiv F(\langle x\rangle). \tag{14}$$

Since this is a complicated nonlinear equation in $\langle x\rangle$, the appearance of multiple solutions cannot be excluded, thus suggesting the possibility of breaking the ergodicity associated with the presence of a phase transition in the model.

Even though an exact analysis of Eq. (14) is difficult without specifying the explicit form of the functions f and g, one can extract precious information by considering the strong-coupling limit $D\to\infty$. Using the saddle-point approximation, one finds that Eq. (14) reduces to the following simple equation for $\langle x\rangle$:

$$f(\langle x\rangle)+\frac{\sigma^2}{2}g(\langle x\rangle)g'(\langle x\rangle)=0. \tag{15}$$

It is instructive to derive this result in a different way. One easily verifies that the evolution equation for the first moment $\langle x_{\mathbf{r}}(t)\rangle=\langle x(t)\rangle$ is identical in form to that for the zero-dimensional system, i.e., it is given by Eq. (6). At the steady-state and considering the limit $D\to\infty$, one can neglect the fluctuations of the variable x around its average value, and concludes that the steady-state equation for the first moment reduces to Eq. (15), which is thus exact in this limit.

Referring to the discussion in Sec. II, we conclude that in the limit $D\to\infty$ the system will undergo a second-order phase transition if the corresponding zero-dimensional model displays a linear instability in its short-time dynamics. The physical content of this conclusion is clear: when the system is strongly coupled, the short-time instability of the trajectory is the driving force behind the nonequilibrium phase transition. The criterion of short-time linear instability has been mentioned in other theoretical [22] and numerical [34] findings. However, we stress that it only holds as an approximation for finite values of D, and that it can completely break down for small values of D, cf. the example in Sec. V. As an interesting corollary, we return to the discussion of Sec. II to conclude that we expect pure noise-induced *phase* transitions in models for which the noise intensity has a minimum at the reference state and precisely *not* in models whose zero-dimensional version displays a noise-induced transition (e.g., not in Hongler's model). This probably explains why the existence of noise-induced *phase* transitions was not discovered earlier (see also Ref. [36]).

IV. CORRELATION FUNCTION APPROACH

We now present a more sophisticated approach, which involves the approximate calculation of the spatial correlation function. The method is an adaptation to multivariate Fokker-Planck equations of a technique developed in the context of multivariate Master equations [37,38]. The starting point is the following ansatz for the conditional average:

$$\langle x_{\mathbf{r}'}|x_{\mathbf{r}}=y\rangle = \int dx_{\mathbf{r}'} x_{\mathbf{r}'} P^{st}(x_{\mathbf{r}'}|x_{\mathbf{r}}=y) = \langle x\rangle + c_{\mathbf{r}\mathbf{r}'}(y-\langle x\rangle), \tag{16}$$

where $c_{\mathbf{r}\mathbf{r}'}=\langle \delta x_{\mathbf{r}}\delta x_{\mathbf{r}'}\rangle/\langle \delta x^2\rangle$ ($\delta x = x-\langle x\rangle$) is the spatial correlation coefficient between sites $\mathbf{r}$ and $\mathbf{r}'$. The system is assumed to be statistically homogeneous, so that single-site averages are independent of the specific location (and hence the subscript denoting the location will be dropped). In particular, the ansatz (16) implies that

$$E(y)=\langle x\rangle + c(y-\langle x\rangle) \tag{17}$$

where c is the nearest-neighbor correlation coefficient $c=c_{\mathbf{r}\mathbf{r}'}$ with $\mathbf{r}'\in n(\mathbf{r})$. Note that the mean-field approximation corresponds to the choice $c=0$. The variable c appears as a second unknown in the explicit form of the steady-state probability, cf. Eqs. (13) and (17), and its value can be found self-consistently as follows. The ansatz (16) implies the following property for any function ϕ:

$$\langle x_{\mathbf{r}'}\phi(x_{\mathbf{r}})\rangle = \langle x\rangle\langle\phi(x)\rangle + c_{\mathbf{r}\mathbf{r}'}\langle \delta x \phi(x)\rangle,$$

which, in combination with the Fokker-Planck equation (10), leads to the following closed equation for the correlation function $c_{\mathbf{r}\mathbf{r}'}$ for a cubic lattice in dimension d:

$$\frac{D}{2d}\left[\sum_{\mathbf{r}''\in n(\mathbf{r})}(c_{\mathbf{r}\mathbf{r}'}-c_{\mathbf{r}''\mathbf{r}'})+\sum_{\mathbf{r}''\in n(\mathbf{r}')}(c_{\mathbf{r}\mathbf{r}'}-c_{\mathbf{r}\mathbf{r}''})\right] = \beta\delta_{\mathbf{r},\mathbf{r}'}-2\gamma c_{\mathbf{r}\mathbf{r}'}, \tag{18}$$

with β and γ given by

$$\beta=\frac{\sigma^2\langle g^2(x)\rangle}{\langle \delta x^2\rangle}, \tag{19}$$

$$\gamma=-\frac{\left\langle \delta x\left[f(x)+\frac{\sigma^2}{2}g(x)g'(x)\right]\right\rangle}{\langle \delta x^2\rangle}.$$

In deriving Eq. (18), we have used the fact that $\langle f(x)\rangle+(\sigma^2/2)\langle g(x)g'(x)\rangle=0$ at the steady-state, cf. Eq. (6). Obviously, $\beta>0$, and it can be also proved that $\gamma>0$ if $c<1$.

Since the system is space-translational invariant at the steady-state, the correlation function can be written in terms of relative coordinates, i.e., $c_{\mathbf{r}\mathbf{r}'}=c(\mathbf{r}-\mathbf{r}')=c(\mathbf{r}'-\mathbf{r})$. Using this property, Eq. (18) can be rewritten as

$$\frac{D}{d}\sum_{\mathbf{r}'\in n(\mathbf{r})}[c(\mathbf{r}')-c(\mathbf{r})]=2\gamma c(\mathbf{r})-\beta\delta_{\mathbf{r},\mathbf{0}}. \tag{20}$$

A closed expression for the correlation function $c(\mathbf{r})$ can be obtained in the case of a square lattice, $d=2$. By taking the Fourier transform of Eq. (20) one finds

$$D[\cos(k_x)+\cos(k_y)-2]\tilde{c}(\mathbf{k})=2\gamma\tilde{c}(\mathbf{k})-\beta, \tag{21}$$

from which the Fourier transform $\tilde{c}(\mathbf{k})$ of the correlation function is readily obtained. In order to perform the inverse Fourier transform, the following identity is helpful:

$$\int_0^\infty dz e^{-zt}I_l(z)I_m(z)=\frac{1}{\pi^2}\int_0^\pi dk_x \times\int_0^\pi dk_y\frac{\cos(lk_x)\cos(mk_y)}{t-\cos(k_x)-\cos(k_y)},$$

where $I_l(z)$ is the modified Bessel function. One concludes that

$$c(\mathbf{r})=\frac{\beta}{D}\int_0^\infty dz e^{-2z(1+\gamma/D)}I_l(z)I_m(z)\quad\text{for }\mathbf{r}=l\mathbf{e}_x+m\mathbf{e}_y, \tag{22}$$

where $(\mathbf{e}_x,\mathbf{e}_y)$ is the unit cell of the square lattice.

A nearest neighbor in the square lattice has coordinates $l=1$ and $m=0$ (or, equivalently, $l=0$ and $m=1$), and one can perform the Laplace transform appearing in Eq. (22) explicitly (formula 12.9 in Ref. [39]) obtaining the following result for the quantity c:

$$c=-\frac{\beta}{2D}+\frac{\beta}{\pi D}K\left[\left(\frac{D}{\gamma+D}\right)^2\right], \tag{23}$$

where K is the complete elliptic integral of the first kind. This expression can be further simplified by noting that $c=1-\beta/2D+\gamma/D$ which follows directly from Eq. (18) for the choice $\mathbf{r}=\mathbf{r}'$. By elimination of β, one obtains the following final result for c:

$$c=\frac{\gamma+D}{D}\frac{K\left[\left(\frac{D}{\gamma+D}\right)^2\right]-\frac{\pi}{2}}{K\left[\left(\frac{D}{\gamma+D}\right)^2\right]}. \tag{24}$$

The averages appearing in the definition of γ, cf. Eq. (19), have to be calculated with respect to the steady-state probability given by Eq. (13), which itself depends on $\langle x\rangle$ and c. As a result, Eqs. (14) and (24) form a set of two nonlinear self-consistent relations determining the values of $\langle x\rangle$ and c. When multiple solutions to these equations are found, one again expects that the system undergoes a phase transition.

We also mention the following result for the spatial correlation function along the axis of the square lattice:

$$c_l=c(l\mathbf{e}_x)=\frac{\beta}{\pi D}\int_0^\pi dk_x\frac{\cos(lk_x)}{\sqrt{[2(1+\gamma/D)-\cos(k_x)]^2-1}}. \tag{25}$$

Using the relation $1+2\Sigma_{l=1}^{\infty}\cos(lk_x)=\pi\delta(k_x)$, one obtains the following simple result for the spatial correlation length λ:

$$\lambda\equiv\sum_{l=0}^{\infty}c_l=\frac{\beta}{4D}\left[\frac{\gamma}{D}\left(1+\frac{\gamma}{D}\right)\right]^{-1/2}+\frac{1}{2}. \tag{26}$$

At this point, a comment about the limitations of the present approach is in place. As it is clear from the previous result, the divergence of the correlation length requires that $\gamma\to 0$. On the other hand, it is also clear from Eq. (24) that in this limit $c=1$, and in fact $c(\mathbf{r})=1, \forall\mathbf{r}$. The reason of this behavior is that the decay of the spatial correlations is described by a single constant parameter γ, cf. Eq. (18). In a more sophisticated approximation, this would no longer be true and a less trivial appearance of long-range correlations would become possible. In the example that we will treat in Sec. V, we find that the parameter γ never converges to 0, even at a phase transition point. The present method is thus of no use in describing long-range spatial correlations. Its main virtue is to give improved results, when compared to the mean-field theory, for quantities such as the location of the critical point and the local probability density.

Finally, we note that the ansatz in Eq. (16) is exact if $\mathbf{r}$ and $\mathbf{r}'$ are correlated Gaussian variables. This condition is verified for a linear Fokker-Planck equation [$f(x)=-x$ and $g(x)=1$]. The above-derived expressions are therefore *exact* for the linear model. One has in this case that $\langle x\rangle=0$, $\gamma=1$, and $\beta=2[1+(1-c)D]$, with the following final results for c and λ:

$$c=\frac{1+D}{D}\frac{K\left[\left(\frac{D}{1+D}\right)^2\right]-\frac{\pi}{2}}{K\left[\left(\frac{D}{1+D}\right)^2\right]}, \tag{27}$$

$$\lambda=\frac{1}{2}+\frac{1+(1-c)D}{D\sqrt{(1+2/D)^2-1}}. \tag{28}$$

V. PURE NOISE-INDUCED PHASE TRANSITION

The results obtained in Sec. IV are general; they can be applied for any choice of the functions $f(x)$ and $g(x)$. In this paper, however, we want to discuss in detail the case of pure noise-induced phase transitions. We will focus here on the prototype model that was introduced in Ref. [11], namely, the set of Eqs. (8) with the choice

$$f(x)=-x(1+x^2)^2,\quad g(x)=1+x^2. \tag{29}$$

We are inclined to believe that it is the simplest possible model that exhibits such a transition, and possibly corresponds to a kind of "normal form unfolding."

As a first approach to understanding this model, in Fig. 3, we show the phase diagrams as predicted by the mean-field theory and the correlation function approach (CFA) described in Secs. III and IV, respectively. These have been

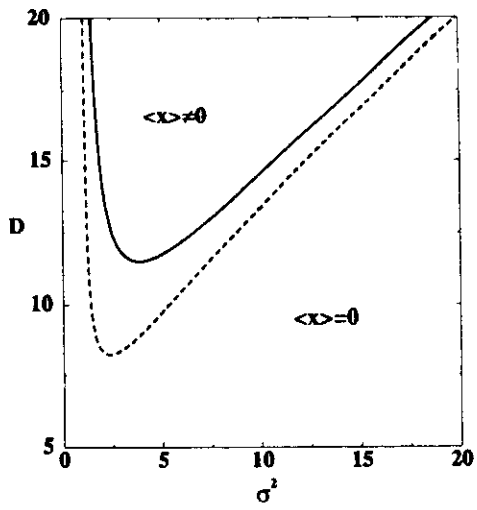

FIG. 3. Phase diagram for the noise-induced phase transition as predicted by the mean-field theory (dashed line), cf. Eq. (14), and the CFA (full line), based on Eqs. (14) and (24) for dimension $d=2$.

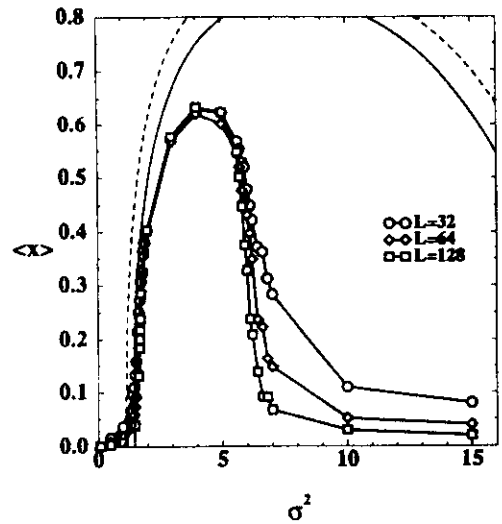

FIG. 4. Order parameter $\langle x\rangle$ vs intensity of the noise for $D=20$, according to the mean-field theory (dashed line), the CFA for $d=2$ (full line), and $2d$ simulations for system sizes 32×32 (circles), 64×64 (diamonds), and 128×128 (squares). Notice that although the general features of mean-field approximations agree with the simulation result, they tend to overestimate the ordered region.

obtained by numerical solution of the self-consistency relations Eqs. (14) and (24). The most important feature shown in Fig. 3 is the prediction of the existence of a symmetry-breaking phase corresponding to a solution of the self-consistent equations with $\langle x\rangle\neq0$. Both the mean-field theory and the CFA predict the appearance of such a phase, although they vary slightly in the region of parameters for which one expects the ordered phase to exist. According to these approximate theories, the ordered phase appears through a second-order phase transition for a sufficiently strong spatial coupling D, and at a finite critical value of the noise intensity σ_c^2. There is no phase transition if the spatial coupling D is less than some critical value. This agrees well with our intuitive explanation of the transition given in Sec. II: if the coupling is not strong enough, and local ordering cannot be induced in the early evolution, the late-time distribution will be governed instead by the maxima $\bar{x}$ of the steady-state probability density, Eq. (5), which in this case is $\bar{x}=0$. If we turn now to the limit of very strong spatial coupling, when $D\to\infty$, the location of the critical point at $\sigma^2=1$ is in agreement with the linear instability criterion mentioned in Sec. II. Another interesting, although certainly not surprising, feature of the transition, is that as one increases further the noise intensity, the ordered phase disappears through another second-order phase transition. This second, reentrant, transition shows that the more "traditional" effect of the noise, namely, the ability to destroy ordered states, is also present in our model.

If we take, for instance, $D=20$, the order parameter $\langle x\rangle$ takes nonzero values only for noise intensity values in the interval $(\sigma_{c_1}^2,\sigma_{c_2}^2)$. The mean-field theory predicts the phase transition points at $\sigma_{c_1}^2\approx1.11$ and $\sigma_{c_2}^2\approx19.1$, while the CFA yields a somewhat narrower region for the ordered phase, namely $1.50<\sigma^2<18.7$. It is expected that the mean-field approach and, to a lesser extent, the CFA, overestimate the size of the ordered region.

In order to check the validity of these mean-field type approximations and also to gain an understanding of this phenomenon of a noise-induced phase transition, we have performed numerical simulations of the model defined by Eqs. (8) and (29) on a square lattice (see the Appendix for details of the simulations). The simulations confirm qualitatively all the predictions of the mean-field approaches, and give us more accurate data about the transition points. In Fig. 4 we plot the order parameter $\langle x\rangle$ as a function of σ^2 for $D=20$ according to the two mean-field-type theories developed earlier together with the simulation results for various system sizes. The simulation data indeed confirm the existence of both phase transitions, but the ordered phase appears in a smaller interval $1.71<\sigma^2<5.8$. The latter values have been obtained on the basis of finite-size scaling analysis, cf. Sec. VI.

VI. CRITICAL PHENOMENA

The pure noise-induced phase transition discussed in Sec. V appears to be an interesting phenomenon. The question therefore arises as to whether this transition shares the usual features of equilibrium phase transitions and, additionally, whether it belongs to any of the existing universality classes. In this sense, a theoretical argument has recently been put forward indicating that the critical properties are those of the Ising universality class [40]. To investigate these points, we have performed extensive computer simulations in the vicinity of both the entrant and reentrant critical points for $D=20$ for two-dimensional systems of size $L\times L$ for values of L ranging in size between $L=10$ and 128. Apart from the order parameter $m=|L^{-2}\Sigma_r x_r|$, and the correlation coefficient, c, we also measure higher-order moments, as well as time and spatial correlations. The results are collected in Figs. 4–11. One clearly recognizes all the trademarks of

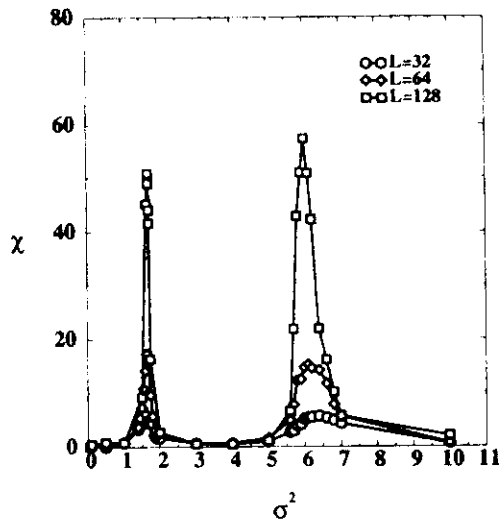

FIG. 5. Susceptibility, $\chi=(L^2/\sigma^2)[\langle m^2\rangle-\langle m\rangle^2]$, as a function of σ^2 for system sizes 32×32 (circles), 64×64 (diamonds), and 128×128 (squares). The peaks clearly show the enhancement of fluctuations around the two critical points.

second-order phase transitions: divergence of fluctuations (Fig. 5), scaling properties (Figs. 7 and 8), long-range spatial correlations (Fig. 9), and critical slowing down (Fig. 10). We now discuss each of these topics in some detail.

In an equilibrium second-order phase transition, the relative fluctuations of the order parameter (susceptibility) and

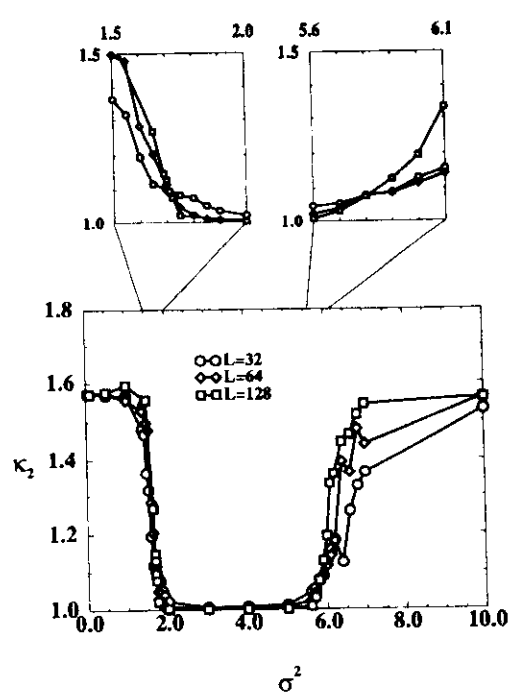

FIG. 6. Second-order cumulant $\kappa_2=\langle m^2\rangle/\langle m\rangle^2$ as a function of σ^2 for system sizes 32×32 (circles), 64×64 (diamonds), and 128×128 (squares). The curves cross at $\sigma^2\approx1.71$ and $\sigma^2\approx5.8$, which, according to the finite-size scaling theory, are identified as the location of the critical points (see the text).

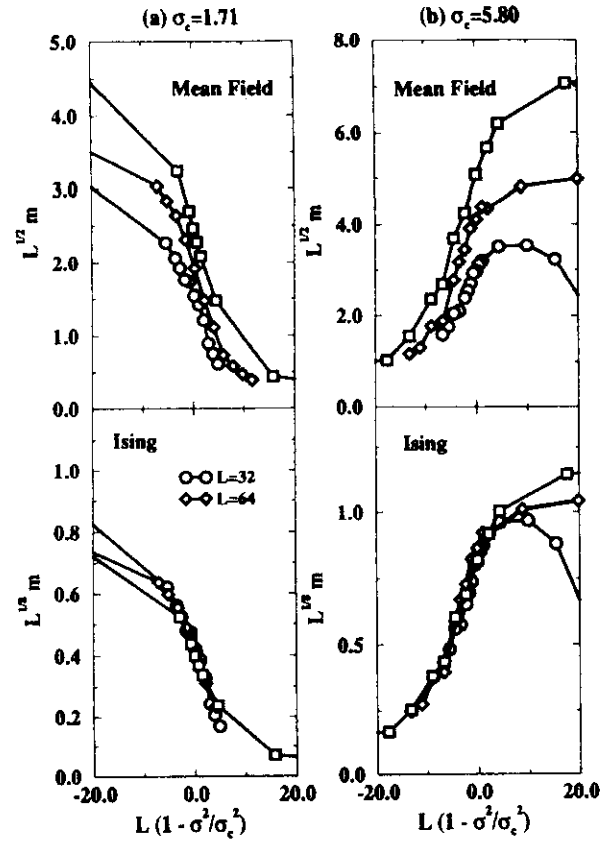

FIG. 7. Plot of $\langle m\rangle L^{v}$ vs $(1-\sigma^2/\sigma_c^2)L^{u}$ in order to check the prediction of finite-size scaling of the order parameter $\langle m\rangle$ for the entrant [plots (a)] and the reentrant [plots (b)] transitions. We use in this figure the Ising ($u=1$, $v=\frac{1}{8}$) and mean-field ($u=1$, $v=\frac{1}{2}$) critical exponents. The quality of the scaling is certainly superior for the Ising exponents than for the mean-field ones.

energy (specific heat) diverge with characteristic critical exponents. In our model, we define a "susceptibility" χ as a suitable measure of the fluctuations of the order parameter

$$\chi\equiv\frac{L^2}{\sigma^2}[\langle m^2\rangle-\langle m\rangle^2]; \tag{30}$$

this definition, and more specifically, the presence of the σ^2 term in the denominator is the equivalent of the usual definition $\chi=L^2[\langle m^2\rangle-\langle m\rangle^2]/k_BT$ for thermal systems. In Fig. 5 we plot χ as a function of noise intensity σ^2 for different system sizes. The enhancement of fluctuations near the two critical points is clear. In the case of equilibrium phase transitions, the susceptibility at the critical point χ_c only diverges in the thermodynamic limit $L\to\infty$. For finite systems, the theory of finite-size scaling [41] tells us that the critical value χ_c increases as a suitable power of the system size, namely, $\chi_c\sim L^{y}$, with the value of y related to the values of the critical exponents. Since in Fig. 5 it is obvious that fluctuations also grow with system size, it is very tempting to try to analyze our data using the standard techniques that have been so successful for equilibrium phase transitions. We now briefly review the main predictions of finite-size scaling theory that are relevant to our study. For a thermal

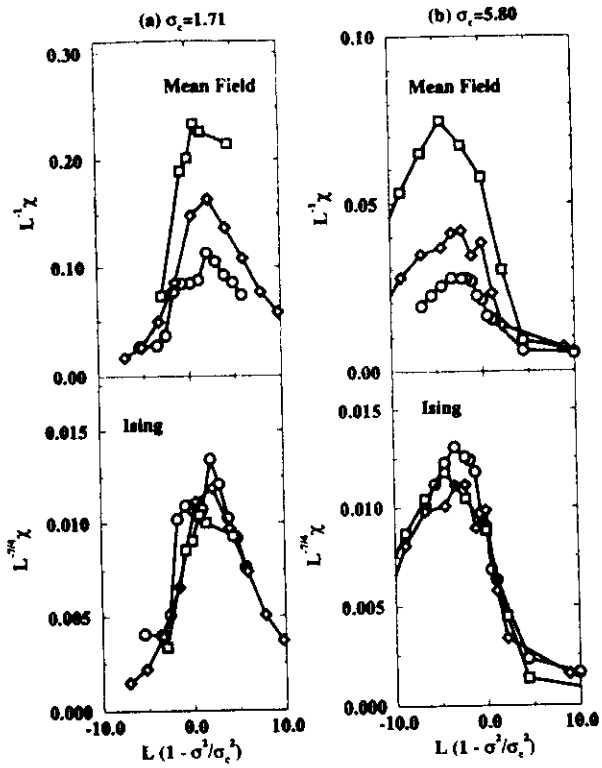

FIG. 8. Plot of $\chi L^{2\upsilon-2}$ vs $(1-\sigma^2/\sigma_c^2)L^u$ in order to check the prediction of finite-size scaling of the "susceptibility" χ for the entrant [plots (a)] and the reentrant [plots (b)] transitions. We use in this figure the Ising ($u=1$, $\upsilon=\frac{1}{8}$) and mean-field ($u=1$, $\upsilon=\frac{1}{2}$) critical exponents. As in the case of the order parameter, Fig. 7, a better scaling is obtained when using the Ising exponents.

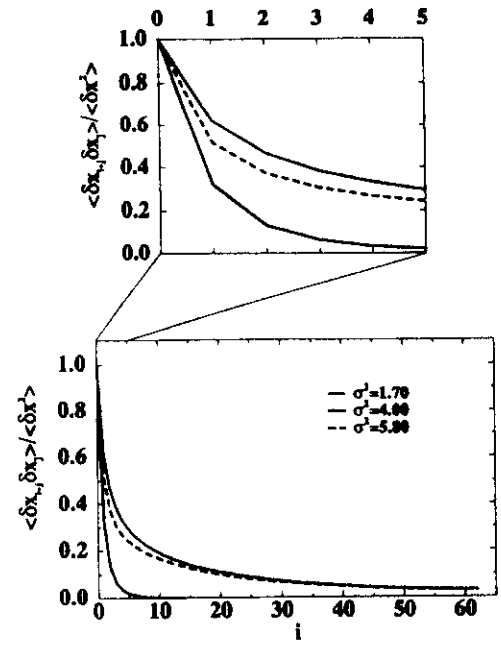

FIG. 9. Plot of the normalized spatial correlation function $c(i)=\langle \delta x_{i+j}\delta x_j\rangle/\langle \delta x^2\rangle$ in the vicinity of the critical points $\sigma_{c_1}^2=1.71$, $\sigma_{c_2}^2=5.8$ and in an intermediate value of σ^2 corresponding to the ordered phase region (we have used in this figure $D=20$, system size $L=128$). Notice the slow decay of the spatial correlation function near the two critical points.

phase transition the order parameter m is a function of temperature T and system size L. Finite-size scaling theory predicts that near a critical point the average of the kth-order moment of m is a homogeneous function of its arguments, namely [42,43],

$$\langle m^k\rangle = L^{-k\upsilon}\tilde{m}_k(\epsilon L^u), \tag{31}$$

where $\epsilon \equiv 1-T/T_c$ is a measure of the distance to the critical point, $\tilde{m}_k$ is a scaling function, and u and υ are critical exponents which take different values according to whether we are below the critical dimension where hyperscaling relations hold ($u=1/\nu$ and $\upsilon=\beta/\nu$) or above the critical dimension where mean-field exponents hold ($u=d/2$, $\upsilon=d/4$). In the following, *we will assume that finite-size scaling also holds for our system* such that equivalent relations are valid with $\epsilon \equiv 1-\sigma^2/\sigma_c^2$ measuring the distance to the transition point. We will use the above expressions in order to locate the critical points σ_c^2 and also to compute the critical exponents u and υ, which in turn, will allow us to obtain the exponents ν and β.

A precise determination of the critical values of the noise intensity is obtained by focusing on the behavior of the second-order cumulant $\kappa_2 \equiv \langle m^2\rangle/\langle m\rangle^2$. According to the previous finite-size scaling relation one finds

$$\kappa_2(\sigma^2,L)=\tilde{\kappa}_2(\epsilon L^{-\upsilon}). \tag{32}$$

For $\sigma^2=\sigma_c^2$, one has $\epsilon=0$ and the prediction is that $\kappa_2(\sigma_c^2,L)=\tilde{\kappa}_2(0)$, i.e., a constant independent of the system size L. As a consequence, by plotting the second-order cumulants for different system sizes, we can determine the critical points as the ones in which the curves for different values of L cross each other. By analyzing the cumulant data in this way (Fig. 6), we are able to locate the entrant critical point quite precisely at $\sigma^2=1.71\pm0.01$, while the reentrant transition is at $\sigma^2=5.8\pm0.1$.

For the order parameter scaling, the prediction is $\langle m\rangle = L^{-\upsilon}\tilde{m}(\epsilon L^u)$, such that a plot of $\langle m\rangle L^{\upsilon}$ versus ϵL^u should yield a curve independent of the system size. This is checked in Fig. 7. Although it is true that the statistical errors of the data do not allow a very precise determination of the critical exponents u and υ, it is shown in the figure that, both for entrant and reentrant transitions, scaling holds better if we use the $2d$ Ising critical exponents $\beta=\frac{1}{8}$ and $\nu=1$ ($u=1$ and $\upsilon=\frac{1}{8}$) than the mean-field ones $u=d/2=1$ and $\upsilon=d/4=\frac{1}{2}$. The same conclusions are reached when analyzing the finite-size scaling behavior of the susceptibility, which, according to its definition Eq. (30), should behave as $\chi=L^{d-2\upsilon}\tilde{\chi}(\epsilon L^u)$. In Fig. 8 we show that properly scaled susceptibility curves fall on top of each other rather well, when using the Ising critical exponents $d-2\upsilon=\frac{7}{4}$ and $u=1$, whereas the quality of scaling is worse when using mean-field exponents $d-2\upsilon=1$ and $u=1$. Note that, in a previous paper [11], we found a good fit at the entrant transition using mean-field exponents for smaller system sizes (up to 48×48). This discrepancy may be due to the fact that the regime of nonclassical behavior is located in a narrow

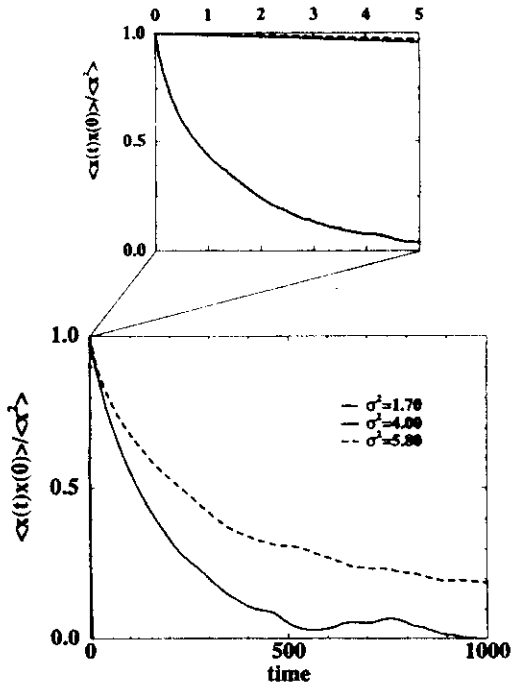

FIG. 10. Similar to Fig. 9 but for the temporal correlation function in the vicinity of the critical points and in the ordered phase region ($D=20$, system size $L=128$).

neighborhood of the critical point that could not be investigated with these system sizes. Further studies will be necessary to determine unambiguously if both transitions (entrant and reentrant) belong to the same universality class of the Ising model.

Finally, the spatial and temporal correlation functions are represented in Figs. 9 and 10 for several values of σ^2. One clearly observes the appearance of long-range correlations in the vicinity of the two critical points, another signature of a phase transition for equilibrium systems. In Fig. 11, we plot the nearest-neighbor correlation coefficient c as a function of σ^2, and compare it with the results obtained through the CFA, cf. Eqs. (24) and (27). As expected, the agreement is only good for small values of the noise intensity.

VII. PERSPECTIVES

We have confirmed the existence of a pure noise-induced phase transition in the model introduced in Ref. [11], explained the role of the short-time instability of the single-site stochastic dynamics in generating the transition, and given evidence that its critical properties are compatible with those of Ising universality class (in $d=2$). These results open a number of perspectives for future research. First, the model that we introduced has been chosen for its mathematical simplicity, but it does not have a direct physical meaning. The intuitive arguments given in Sec. II, however, suggest that the pure noise-induced transitions will arise generically in systems with a multiplicative noise term, whose amplitude has a minimum in the reference state. It remains to be seen whether our model corresponds to a kind of "normal form unfolding" of such phase transitions. Second, we expect

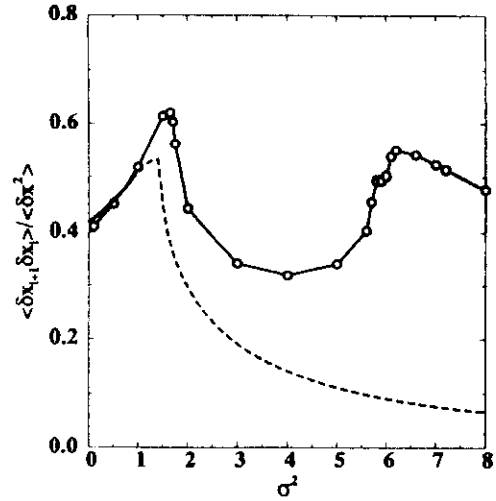

FIG. 11. Nearest-neighbor correlation coefficient c [see Eq. (16)] vs σ^2 from simulations ($L=128$) and theory, cf. Eq. (24). As expected, the agreement is only good for small values of the noise intensity σ^2.

that, even though our model seems to belong to the Ising universality class as far as its critical properties are concerned, the specific noise-induced mechanism by which order appears will reflect itself in the time-dependent properties such as nucleation phenomena or the response to external fields or symmetry-breaking boundary conditions. Third, it is clear that phase transitions of another order (first or higher order) can be generated [44]. In the case of a first-order transition, this would imply that the macroscopic state of the system would change dramatically when the intensity of the noise is varied across a threshold value. Fourth, more complicated pure noise-induced phase transitions, that break temporal symmetry [45], spatial symmetry [46] or both, can be constructed. Finally, we propose to make a search for or reevaluation of experiments in physical systems for which noise-induced shifts [11,20], and pure noise-induced phase transitions may be relevant. Some cases have been documented in the literature of noise-induced shifts in the phase transition or bifurcation point, for example in photosensitive chemical reactions, subject to a fluctuating light intensity [47,48], in liquid crystals [49,50], and in the Raleigh-Benard instability with a fluctuating temperature at the plates [51]. Also, stochastic equations for spatially distributed systems with multiplicative noise have appeared recently in several contexts, including lasers [52], directed percolation [53], and other models for growth [54].

ACKNOWLEDGMENTS

This work was supported by NATO Grant No. CRG 950055. C.V.d.B. also acknowledges support from the Program on Inter-University Attraction Poles, Prime Minister's Office, Belgian Government and NFWO Belgium; J.M.R.P. from Dirección General de Investigación Científica y Técnica (DGICYT) (Spain), Project No. PB94-0388; R.T. from DGICYT Projects No. PB94-1167 and No. PB94-1172; and R.K. from Cray Research Inc. and Alabama Education and Research Network. Most of the computer simulations

were carried out using Cray C90 at Alabama Supercomputer Center and the Connection Machine model 5E at Naval Research Laboratory.

APPENDIX: COMPUTER SIMULATIONS

A Monte Carlo simulation of the stochastic process (8) was performed for two-dimensional square lattices of various sizes up to $L=128$ with periodic boundary conditions. The stochastic differential equation for the variable at the ith site x_i is given by

$$\frac{dx_i}{dt}=F_i(\mathbf{x})+G_i(\mathbf{x})\xi_i(t), \quad i=1,\ldots,N=L^2 \tag{A1}$$

where $\mathbf{x}=(x_1,\ldots,x_N)$, and

$$F_i(\mathbf{x})=f(x_i)-\frac{D}{4}\sum_{j\in n(i)}(x_i-x_j), \tag{A2}$$

$$G_i(\mathbf{x})=g(x_i). \tag{A3}$$

These equations were integrated using two different algorithms, the Milshtein and the Heun methods [55,56].

The Milshtein method allows us to advance forward in time by means of the recursion relations

$$x_i(t+\delta t)=\left[F_i(\mathbf{x}(t))+\frac{\sigma^2}{2}G_i(\mathbf{x}(t))\frac{dG_i(\mathbf{x}(t))}{dx_i}\right]\delta t + G_i(\mathbf{x}(t))\sqrt{\sigma^2\delta t}\,\eta_i(t), \tag{A4}$$

where $\eta_i(t)$ are independent Gaussian random variables of zero mean and variance equal to 1, and the second term is included because Eq. (A1) is interpreted in the Stratonovich sense. The order of numerical error in the Milshtein method is δt. Therefore, a small δt (e.g., $\delta t=1\times10^{-4}$ for $\sigma^2=1$) must be used, while its computational effort per time step is relatively small. For large σ, where fluctuations are rapid and large, a longer integration period and a smaller δt is necessary. The Milshtein method quickly becomes impractical.

The Heun method is based on the second-order Runge-Kutta method, and integrates the stochastic equation by a recursive equation

$$x_i(t+\delta t)=x_i(t)+\frac{\delta t}{2}[F_i(\mathbf{x}(t))+F_i(\mathbf{y}(t))]+\frac{\sqrt{\sigma^2\delta t}}{2}\eta_i(t) \times[G_i(\mathbf{x}(t))+G_i(\mathbf{y}(t))], \tag{A5}$$

where

$$y_i(t)=x_i(t)+F(x_i(t))\delta t+G(x_i(t))\eta_i(t)\sqrt{\sigma^2\delta t}. \tag{A6}$$

This method allows larger δt than the Milshtein method, without a significant increase in computational effort per step. We used this method for $\sigma^2>2$.

The time step δt has been chosen by a stability condition, and also such that averaged magnitudes do not depend on δt within statistical errors. For $D=20$, for example, the necessary values for δt vary between $\delta t=5\times10^{-4}$ for $\sigma^2=1$ and $\delta t=1\times10^{-5}$ for $\sigma^2=15$. The Gaussian random numbers necessary for the simulations were generated either by using the Box-Muller-Wiener algorithm or a very fast numerical inversion method [57]. The time evolution of the average value is carefully monitored until the stationary state is reached.

The order parameter is computed by

$$\langle m\rangle=\left\langle\left\langle\left|\frac{1}{L^2}\sum_{i=1}^{N}x_i\right|\right\rangle_{\text{time}}\right\rangle_{\text{ensemble}}, \tag{A7}$$

where $\langle\ \rangle_{\text{time}}$ and $\langle\ \rangle_{\text{ensemble}}$ indicate time average and ensemble average, respectively. The averaging time T was chosen to be sufficiently longer than the correlation time, for example, $T\approx2\times10^4$ (10^8 steps) near the critical points. The ensemble average was taken over at least ten independent systems. Similarly, the susceptibility is evaluated as

$$\chi=\frac{L^2}{\sigma^2}\left\langle\left\langle\left(\frac{1}{L^2}\sum_{i=1}^{N}x_i\right)^2-\langle m\rangle^2\right\rangle_{\text{time}}\right\rangle_{\text{ensemble}}. \tag{A8}$$

Simulation of large systems (128×128) was too long for Cray C90 despite the code is mostly vectorized. Therefore, we used a massively parallel computer, the connection machine model 5E with 256 processors which appeared to be about ten times faster than Cray C90 for this particular application with the same programs.

[1] W. Horsthemke and R. Lefever, *Noise-Induced Transitions* (Springer-Verlag, Berlin, 1984).

[2] A. Schenzle and H. Brandt, Phys. Rev. A **20**, 1628 (1979).

[3] H. Risken, *The Fokker-Planck Equation* (Springer-Verlag, Berlin, 1984).

[4] R. Graham and A. Schenzle, Phys. Rev. A **25**, 1731 (1982).

[5] *Noise in Nonlinear Dynamical Systems*, edited by F. Moss and P. V. E. McClintock (Cambridge University Press, Cambridge, 1989).

[6] A. S. Mikhailov, Phys. Rep. **184**, 307 (1989).

[7] L. Schimansky-Geier and Ch. Zulicke, Z. Phys. B **82**, 157 (1991).

[8] M. O. Magnasco, Phys. Rev. Lett. **71**, 1477 (1993); see also L. P. Faucheux, L. S. Bourdieu, P. D. Kaplan, and A. J. Libchaber, Phys. Rev. Lett. **74**, 1504 (1995) for more recent references.

[9] *Instabilities and Chaos in Quantum Optics II*, edited by N. B. Abraham, F. T. Arecchi, and L. A. Lugiato (Plenum, New York, 1988).

[10] Ch. Doering and C. Gadoua, Phys. Rev. Lett. **69**, 2138 (1992).

[11] C. Van den Broeck, J. M. R. Parrondo, and R. Toral, Phys. Rev. Lett. **73**, 3395 (1994).

[12] C. Van den Broeck, J. M. R. Parrondo, J. Armero, and A. Hernández-Machado, Phys. Rev. E **49**, 2639 (1994).

[13] There exists an infinity of interpretations of stochastic differential equations with multiplicative noise, with, on one extreme, the mathematically minded Itô rule [corresponding to a diffusion term of the form $\partial_x^2[g^2(x)P(x,t)]$], and on the other

extreme the kinetic definition [corresponding to a diffusion term of the form $\partial_x[g^2(x)\partial_x P(x,t)]$]. Which interpretation is valid depends on the origin of the white noise [14,15] and its interaction with eventual other fast degrees of freedom of the system [16].

[14] N. G. Van Kampen, *Stochastic Processes in Physics and Chemistry* (North-Holland, Amsterdam, 1992).

[15] R. E Mortensen, J. Stat. Phys. **1**, 271 (1969).

[16] R. Graham and A. Schenzle, Phys. Rev. A **26**, 1676 (1982).

[17] M. O. Hongler, Helv. Phys. Acta. **52**, 280 (1979).

[18] D. Amit, *Field Theory, the Renormalization Group and Critical Phenomena* (World Scientific, Singapore, 1984).

[19] R. Toral and A. Chakrabarti, Phys. Rev. B **42**, 2445 (1990).

[20] J. García-Ojalvo, A. Hernández-Machado, and J. M. Sancho, Phys. Rev. Lett. **71**, 1542 (1993).

[21] L. Ramírez-Piscina, J. M. Sancho, and A. Hernández-Machado, Phys. Rev. B **48**, 119 (1993); **48**, 125 (1993).

[22] A. Becker and L. Kramers, Phys. Rev. Lett. **73**, 955 (1994).

[23] G. Grinstein, M. A. Muñoz, and T. Yuhai, Phys. Rev. Lett. **76**, 4376 (1996).

[24] Y. Onodera, Prog. Theor. Phys. **44**, 1477 (1970).

[25] M. Malek Mansour and G. Nicolis, J. Stat. Phys. **13**, 197 (1975).

[26] R. Desai and R. Zwanzig, J. Stat. Phys. **19**, 1 (1978).

[27] A. D. Bruce, Adv. Phys. **29**, 111 (1980).

[28] R. A. Dawson, J. Stat. Phys. **31**, 29 (1983).

[29] M. O. Hongler and R. Desai, J. Stat. Phys. **32**, 585 (1983).

[30] G. Dewel, P. Borckmans, and D. Walgraef, Phys. Rev. A **31**, 1983 (1985).

[31] O. T. Valls and G. F. Mazenko, Phys. Rev. B **34**, 7941 (1986).

[32] M. Shiino, Phys. Rev. A **36**, 2393 (1987).

[33] K. Kaneko, Phys. Rev. Lett. **65**, 1391 (1990).

[34] J. García-Ojalvo, J. M. Sancho, and L. Ramírez-Piscina, Phys. Lett. A **168**, 35 (1992).

[35] P. Jung, U. Behn, E. Pantazelou, and F. Moss, Phys. Rev. A **46**, R1709 (1992).

[36] Ch. Doering, Phys. Lett. A **122**, 133 (1987).

[37] M. Malek Mansour and J. Houard, Phys. Lett. **70A**, 366 (1979).

[38] C. Van den Broeck and M. Malek Mansour, in *Instabilities and Nonequilibrium Structures*, edited by E. Tirapegui and W. Zeller (Kluwer, Dordrecht, 1993), p. 49.

[39] G. E. Roberts and H. Kaufman, *Table of Laplace Transforms* (Saunders, Philadelphia, 1966).

[40] S. Ramaswamy, R. Pandit, and R. Lahiri, Phys. Rev. Lett. **75**, 4786 (1995).

[41] *Finite-Size Scaling*, edited by J. L. Cardy (North-Holland, Amsterdam, 1988).

[42] K. Binder and D. W. Heermann, *Monte Carlo Simulation in Statistical Physics*, (Springer-Verlag, Berlin, 1988).

[43] H.-P. Deutsch, J. Stat. Phys. **67**, 1039 (1992).

[44] R. Muller, K. Lippert, A. Kuhnel and V. Behn (unpublished).

[45] S. H. Park and S. Kim, Phys. Rev. E **53**, 3425 (1996).

[46] J. M. R. Parrondo, C. Van den Broeck, J. Buceta, and F. J. de la Rubia, Physica A **224**, 153 (1996).

[47] J. C. Micheau, W. Horsthemke, and R. Lefever, J. Chem. Phys. **81**, 2450 (1984).

[48] P. de Kepper and W. Horsthemke, in *Synergetics, Far From Equilibrium* (Springer, New York, 1979).

[49] S. Kai, T. Kai, and M. Takata, J. Phys. Soc. Jpn. **47**, 1379 (1979).

[50] M. Wu and C. D. Andereck, Phys. Rev. Lett. **65**, 591 (1990).

[51] C. W. Meyer, G. Ahlers, and D. S. Cannell, Phys. Rev. **44**, 2514 (1991).

[52] J. Martín-Regalado, S. Balle, and N. B. Abraham, IEEE J. Quantum Electron. **32**, 257 (1996).

[53] H. K. Janssen, Z. Phys. B **42**, 151 (1981); P. Grassberger, *ibid.* **47**, 365 (1981); R. Dickman, Phys. Rev. E **50**, 4404 (1994).

[54] T. Vicsek, in *Proceedings of the Workshop on Surface Disordering: Growth, Roughening, and Phase Transitions*, edited by R. Jullien, J. Kertesz, P. Meakin, and D. E. Wolf, Les Houches Series (Nova, New York, 1992) p. 155; A. L. Barabasi and H. E. Stanley, *Fractal Concepts in Surface Growth* (Cambridge University Press, Cambridge, 1995).

[55] P. E. Kloeden and E. Platen, *Numerical Solution of Stochastic Differential Equations* (Springer-Verlag, Berlin, 1992).

[56] R. Toral, in *Third Granada Lectures in Computational Physics*, edited by P. L. Garrido and J. Marro, Lecture Notes in Physics Vol. 448 (Springer, New York, 1995).

[57] R. Toral and A. Chakrabarti, Comput. Phys. Commun. **74**, 327 (1993).